

**Semiconducting Properties of Some μ -Bridged
Phthalocyanines**

by

Nazar A. Hussein, B. Sc., M. Sc.

Thesis submitted to the University of Nottingham for the
degree of Doctor of Philosophy,
January, 1990

To:

My wife **Bushra,**

sister **Zehra, brother Hassan**

and

children **Amir, Ahmed and Assaed**

for their sacrifice

ACKNOWLEDGMENTS

I should like to express my deep gratitude to my supervisor Dr. M. R. Willis for his excellent help and guidance throughout different stages of this work.

My thanks also due to the following people:

Drs. A. J. Dann, M. R. Fahy, D. C. Davies, R. Whitehead and A. Mackie for their excellent help and friendship during this work.

Dr. M. Barker for his help during the thermogravimetric measurements.

Mr. K. Dinsdale for the electron microscope measurements, and Mr. R. Waring for the X-ray diffraction measurements.

Miss. S. M. Critchley, Miss. F. Al-Sagheer, Messrs. R. J. Martin, S. M. Ilett, S. Qureshi, D. M. Petty and K. J. Markland, for their help.

All the technicians especially Mr. N. Barnes and J. A. Heard for all invaluable aid.

My family for their support.

And finally Ministry of higher education and Basrah university /IRAQ for the scholarship.

ABSTRACT

The application of organic materials in electronic devices depends, in part, on the ability to control the electrical properties by structural modification. This thesis explores the possibility of modifying the properties in the cofacially stacked polymeric phthalocyanine, fluoroaluminium phthalocyanine (AlPcF) by copolymerisation with the structurally related fluorogallium phthalocyanine (GaPcF).

Copolymers of AlPcF and GaPcF of composition 2:1, 1:1 and 1:2 were prepared for the first time. The purification, characterisation, and evaluation of the 1:1 copolymer were carried out. It was found that the material could be purified by entrainer sublimation without major change in the composition. The polymeric nature of the material was established through spectroscopic methods, thermogravimetric analysis and X-ray powder diffraction. Evaluation of evaporated copolymer films by XPS, depth profiling by argon ion bombardment, and electron bombardment largely confirmed the expected composition but indicated that a limited amount of fractionation or selective decomposition had occurred.

A detailed study of the properties of compactions and films by a.c. and d.c. show that the copolymer is intermediate between the monomers in its properties, and different from the mixture of the monomers. The a.c. measurements suggest that the films of both pure materials and copolymer have a higher imperfection concentration than the compaction.

Two preliminary studies are also reported. Iodine doping of the copolymer leads to high conductivity which is limited by disorder. The photoconduction response of the copolymer is higher than that of either component, suggesting copolymerisation as a means of enhancing this property.

The successful synthesis of this copolymer offers a route to the copolymerisation of electrically dissimilar materials as a means of enhancing the conductivity in linear chains.

CONTENTS

	<u>page</u>
<u>CHAPTER ONE</u>	
SOME BASIC SOLID STATE CONCEPTS	
1.1) Introduction	1
1.2) Origin of the Band Theory	2
1.3) Fermi Level	5
1.4) The Energy Band	6
1.5) Intrinsic and Extrinsic Conduction	7
1.6) Electrical Conduction in Semiconductors	8
1.7) Conduction in Molecular Crystals	13
1.8) The Potential Box for Molecular Crystals	15
1.8a) Intrinsic Charge Generation	15
1.8b) Extrinsic Charge Generation	16
1.9) Hopping and Tunneling	17
1.10) Band Structure for Amorphous Solids	18
1.11) Effect of Space- Charge Limited Current(SCLC) on the Conductivity	19
1.12) Other Solid state Concepts	21

CHAPTER TWO

PHthalOCYANINES

2.1) Historical Introduction	22
2.2) Structure	23
2.3) Phthalocyanine Bridging	24
2.4) The Polymeric Structure of μ -Bridged Phthalocyanines	25
2.5) Methods of Preparation	26
2.6) General Properties	27
2.7) Applicability of Band Model to Phthalocyanines.	28
2.8) Band Structure of Phthalocyanines	31
2.9) Mobility of Charge Carriers in Phthalocyanines	34
2.10) Electrical Properties of Phthalocyanines	39
2.11) Application of Phthalocyanines in Technology	45
2.12) Objectives of This Research	46

CHAPTER THREE

EXPERIMENTAL TECHNIQUE

3.1) Electrical Conductivity	48
3.1a) Compactions	48
3.1b) Surface Thin Films	49
3.1c) Sandwich Films	49
3.1.1) Purification of Phthalocyanines	51
3.1.2) Film Preparation and Thickness Measurements	53
3.1.3) D.C. Conductivity Measurements	54
3.1.3a) Measurements of Low Resistance Samples	55
3.1.3b) Measurements of High Resistance Samples	56
3.1.4) A.C. Conductivity	57
3.1.4a) Sample Preparation for A.C. Conductivity Measurements	57
3.1.4b) Sample Holder and the A.C. Conductivity Measurement System	57
3.1.4c) Basic Bridge Circuitry	58
3.1.5d) Procedure for A.C. Conductivity Measurements ...	60
3.2) Thermal Analysis	61
3.3) X-Ray Diffraction	62
3.3.1) X-Ray Generation	62
3.3.2) Other Instrumental Specifications	63
3.4) Electron Microscopy	63
3.4.1) Detectors	63
1) Wave Length Dispersive System (WDS)	64
2) Energy Dispersive X-Ray Detector (EDX)	64
3.5) X-ray Photoelectron Spectroscopy (XPS)	65
3.6) Photoconductivity	66
3.7) Spectroscopy	67
3.7.1) U.V-Visible	67
3.7.2) I.R	67
3.7.3) Mass Spectroscopy	67

CHAPTER FOUR

SYNTHESIS AND CHARACTERISATION OF THE MATERIALS

4.1) Synthesis of the Materials	69
4.1.1) Phthalocyaninatoaluminium Fluoride, AlPcF	70
4.1.2) Phthalocyaninatogallium Fluoride, GaPcF	70
4.1.3) The Copolymer(AlPcF-GaPcF) _n	71
4.1.4) Other Materials	72
4.2) Characterisation of the Materials	72
4.2.1) Elemental Analysis	72
4.2.2) U.V-Visible Spectroscopy	74
a) Solution	74

b) Solid-Film	74
4.2.3) I.R. Spectroscopy	75
4.2.4) Mass Spectroscopy	76
4.3) Thermal Analysis	76
4.3.1) Factors affecting Thermogravimetric Analysis	77
a) Instrumental Factors	78
b) Sample Characteristics	80
4.4) Structural Analysis by X-Ray Diffraction	83
4.4.1) Diffraction	83
4.4.2) The Bragg Law	86
4.4.3) Unit Cell	87
4.4.4) The X-Ray Diffraction Technique	88
4.4.5) Factors Affecting Intensities	94
4.4.6) Results and Discussion	97
4.5) The Electron Microscope	101
4.5.1) Quantitative and Qualitative Determination of Al and Ga	102
4.6) X-Ray Spectroscopy	107
4.6.1) X-Ray Photoelectron Spectroscopy(XPS)	107
4.6.2) Auger Electron Spectroscopy	111
4.6.3) Results and Discussion	112

CHAPTER FIVE

D.C. CONDUCTIVITY

5.1) The D.C. Conductivity Results	116
5.1a) Compacted Discs	116
5.1b) Surface Films	118
5.1c) Sandwich Film	118
5.2) Discussion of D.C. Conductivity	119
5.2a) AlPcF	122
5.2b) GaPcF	122
5.2c) The Copolymer	123
5.2d) The Mixture	123
5.2e) Iodine Doped Films	128

CHAPTER SIX

A.C. CONDUCTIVITY

6.1) Introduction	131
6.1.1) Dielectric Properties	131
6.1.2) The Dielectric Relaxation	138
6.1.3) Debye Equations	139
6.1.3a) Cole-Cole Equations	141
6.1.3b) Cole-Davidson Equation	141

6.1.4) Dipolar Loss in Polymeric Solids	142
6.1.5) A.C. Conductivity	143
6.2) Results and Discussion	149
6.2.1) AlPcF	149
6.2.2) GaPcF	157
6.2.3) Copolymer	158
6.2.4) Mixture	160
6.2.5) Conclusion	161

CHAPTER SEVEN

PHOTOCONDUCTIVITY

7.1) Introduction	163
7.2) Examination of photoconduction	165
7.3) External effects on photoconduction	166
7.4) Trapping and recombination	169
7.5) Kinetics of recombination processes	170
7.6) Growth and decay of photocurrents	171
7.7) Results and discussion	173
7.8) Conclusion	176

CHAPTER EIGHT

CONCLUSION AND FURTHER REMARKS FOR FURTHER WORK

.....	178
REFERENCES	180

APPENDIX 1
APPENDIX 2
APPENDIX 3

CHAPTER ONE

SOME BASIC SOLID STATE CONCEPTS

1.1) Introduction:

Solids can be classified into two divisions according to their crystal nature; they are either crystalline or amorphous. They can also be generally classified, according to their electrical conduction, into three main categories; metals, semiconductors and insulators.

Solid state concepts were developed by physicists mainly for the understanding of inorganic semiconductors, but were later extended to solid organic compounds (1.1). The study of the electrical properties of organic solids has therefore made new demands on both physicists and chemists.

The first observation of electrical conductivity in organic solids was at the beginning of this century, whilst detailed studies of this phenomenon started in the late forties. Attention is now focussed on these materials as semiconductors due to their particular properties which may find widespread technological applications. Organic materials have played a very important role in electronics mainly as insulators, e.g., insulation for wiring and protective coating. However, due to developments of a large

range of polymers and crystals with unusual electrical properties, organic materials are starting to enter into fields which are normally reserved for inorganic materials. Some TCNQ compounds exhibit metallic behaviour, e.g., TCNQ-TTF^(1.2). Some other compounds exhibit superconductivity (1.3-4), e.g., (TMTSF)₂PF₆^(1.5). Figure 1.1 shows typical conductivities of some materials.

The study of organic semiconductors has become an increasingly important field of research partly because of their potential for solid state electronic devices and partly because the study of electronic processes in molecular solids can be seen as a step towards the understanding of the behaviour of biological systems^(1.6).

1.2) Origin of the Band Theory:

The initial work on motion of electrons in a solid was carried out by *Drude* and *Lorentz*, who developed the free electron theory of metals. They assumed that a metal is composed of positive ion cores embedded in a perfect gas of freely moving electrons. Using classical equations of motion, they were able to derive the relation,

$$\sigma = n e \mu \quad \dots\dots\dots 1.1$$

where σ is the conductivity, and n , e and μ are the number per unit volume, charge and mobility of the electron respectively. This theory does not provide a very good model for solids in general. For example, it cannot explain the differences between metals, semiconductors and insulators. A satisfactory understanding of characteristic semiconducting behaviour, in which the conductivity increases with temperature, did not emerge until

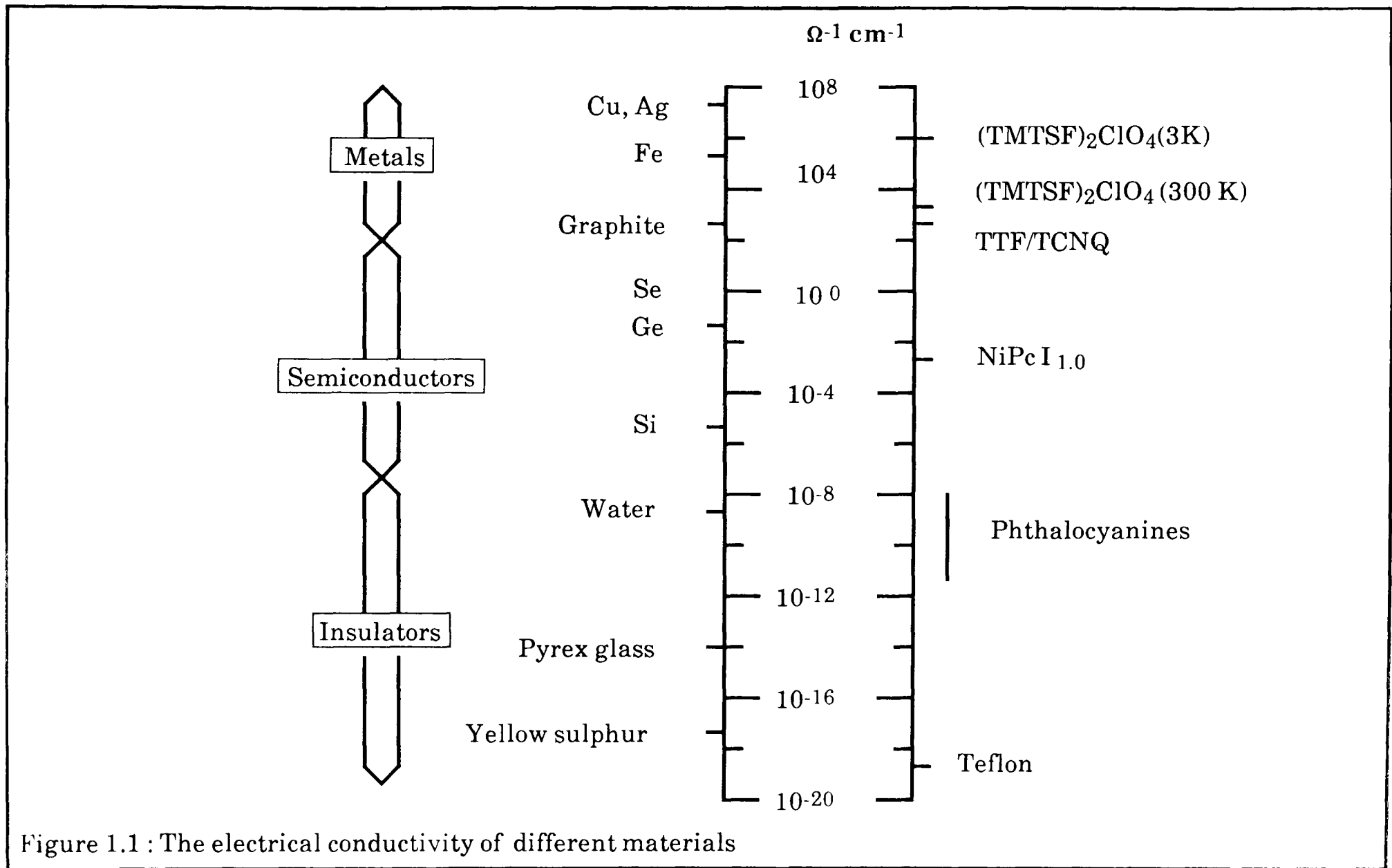


Figure 1.1 : The electrical conductivity of different materials

the development of the quantum mechanical theory of semiconductors in 1931(1.7).

The first application of quantum mechanics to the motion of electrons in solids was carried out by *Sommerfeld* in 1928(1.8) to describe the free electron model. It was assumed that in a metal, the outer electrons(valence electrons) do not belong to individual atoms but are free to move through the solid and cannot escape from the solid. According to the principles of quantum mechanics, this is equivalent to the problem of a particle in a box where the potential energy well is equivalent to the box, in which the electrons move within the solid with potential energy $V=0$, but $V=\infty$ outside the solid. Therefore electrons can move freely within the solid but cannot escape from it, see figure 1.2.

For a one-dimensional case the *Schrodinger equation* is,

$$\frac{d^2\Psi}{dx^2} + \frac{8\pi^2m}{h^2} (E - V) \Psi = 0 \quad \dots\dots\dots 1.2$$

where Ψ is the wave function associated with the electron, E is the total energy, m is the mass of the electron of a potential energy V , h is *Planck's constant*. Since the atom in a crystal lattice occurs periodically the potential energy of the electron within the solid will be periodic due to atomic cores, as is shown in figure 1.3. The wave function for an electron in a linear array of square potential wells, Ψ_B , is,

$$\Psi_B = \Psi_X U(X) \quad \dots\dots\dots 1.3$$



Figure 1.2: Sommerfeld potential well

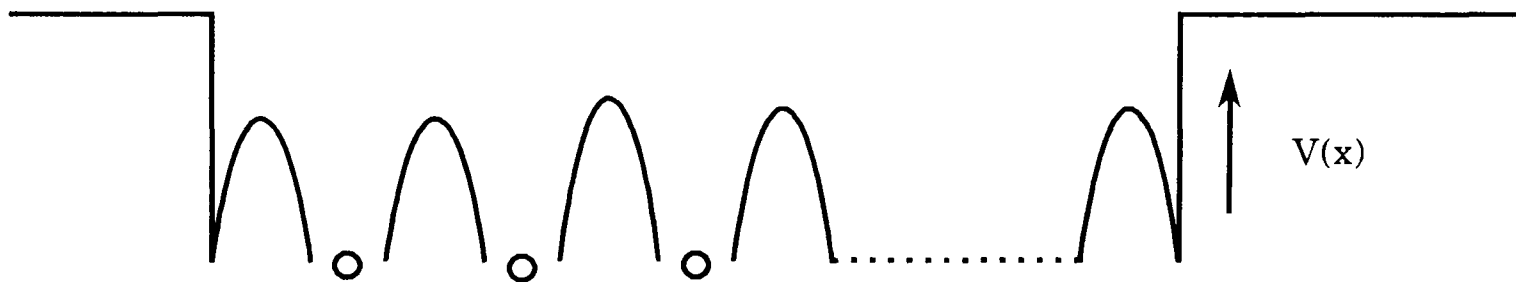


Figure 1.3: Periodic potential due to atomic cores

where Ψ_X is the wave function of a free electron, $U(x)$ is the wave function which has the periodicity of the lattice. These functions are called *Bloch functions*^(1.7,1.9). The *Bloch* solution for equation 1.2 (1.10) is given by,

$$\Psi_B = e^{(i k x)} U(X) \quad \dots\dots\dots 1.4$$

where k is the wave vector $= 2\pi/\lambda$, and λ is the electron wavelength. This equation will give acceptable and well defined solutions only where k is real. Thus, there is an allowed range of energies which give real values of k and a forbidden range of energies which give imaginary values of k . This means that instead of one continuous band of energy, as in the case of an electron in a box, the allowed energy bands are separated by regions of forbidden energy which correspond to certain values of k . Each band consists of many closely spaced levels and may be regarded as a continuum^(1.7), as is shown in figure 1.4. The gaps between allowed energy bands are of significant importance in determining whether a solid is a metal, insulator or semiconductor. The region in k space between $-\pi/a$ and $+\pi/a$ is called the first *Brillouin zone* of this lattice. *Bloch* results are quite general and can be applied to the motion of any electron in a periodic field.

The energy band picture may be explained in another way^(1.11) by considering the overlap of the atomic orbitals of each individual atom in solids. If we consider just one level from each of a pair of atoms at large separation, there will be a single doubly degenerate level. As the two atoms approach each other, this degenerate level will be split into two by the interaction between the atoms. The splitting will increase further as the atoms approach more closely. For n atoms in a crystal, the degeneracy of each level will be n -fold. As the lattice distance decreases, each level will split into n separate levels by the interaction with the other atoms. This

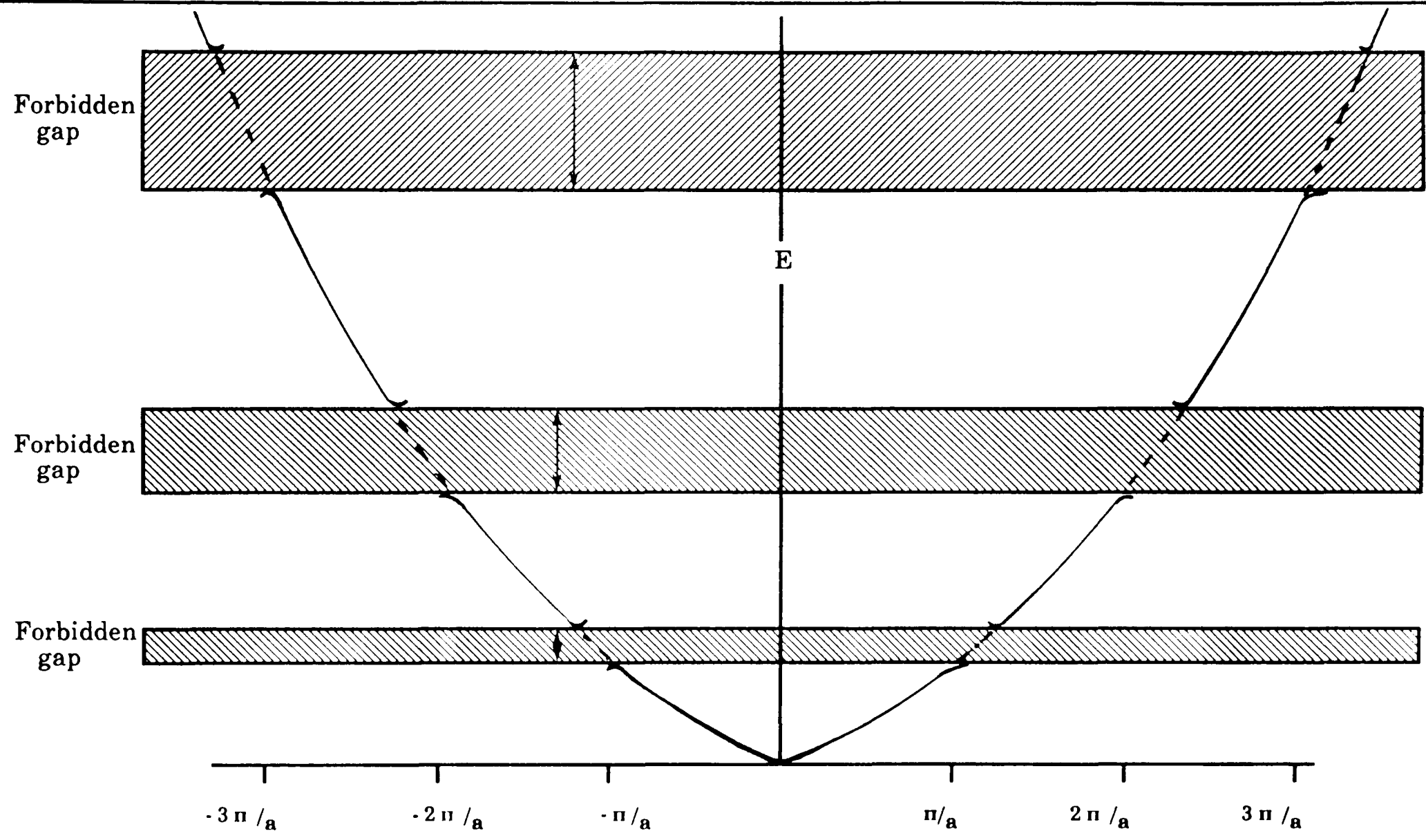


Figure 1.4: The formation of band gaps. The dashed curve is Sommerfeld case; a , is the distance between a given set of parallel lattice planes.

will lead to a band of n closely spaced levels instead of a single degenerate level as is shown in figure 1.5. Electrons are allocated to each level according to the *Pauli exclusion principle*, which allows only two electrons in each energy level. Each atom will have two electrons in each level, so that there are $2n$ electrons to fit into the band. Only bands corresponding to the outer valence electrons may be partially occupied in the ground state.

1.3) Fermi Level:

The population of energy level is determined by a distribution law^(1.12) which takes into account the *Pauli exclusion principle*. The probability of a particular level being occupied is given by the *Fermi-Dirac distribution function* which enables the calculation of the population probability of the energy states as a function of temperature,

$$f(E) = \frac{1}{(1 + e^{\frac{E - E_F}{kT}})} \dots\dots\dots 1.5$$

where $f(E)$ is the probability that the level will be occupied by an electron, k is the *Boltzman constant*, E_F is the energy of *Fermi level*.

Equation 1.5 is plotted in figure 1.6. For $T=0$, $f(E) = 1$ for all values of $E - E_F < 0$, where all the electrons fall into lowest energy levels which means that E_F is the energy associated with the highest occupied state at absolute zero^(1.1,1.13). At higher temperatures the state corresponding to E_F has a population probability of one half which results in an occupation of the higher levels and depopulation of those levels within kT of E_F . When $E - E_F \gg kT$, the exponential term in the denominator of the *Fermi function*

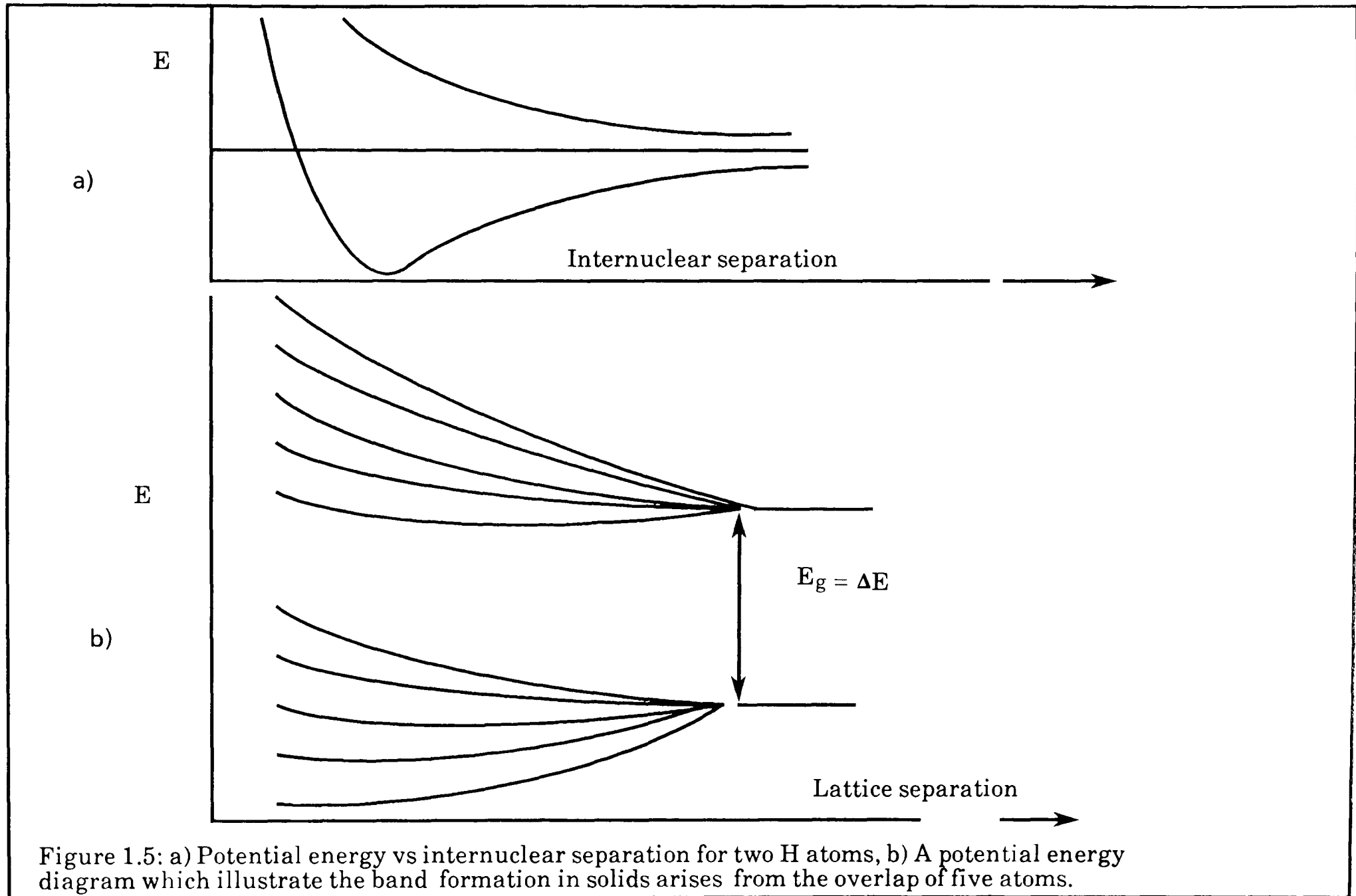


Figure 1.5: a) Potential energy vs internuclear separation for two H atoms, b) A potential energy diagram which illustrate the band formation in solids arises from the overlap of five atoms.

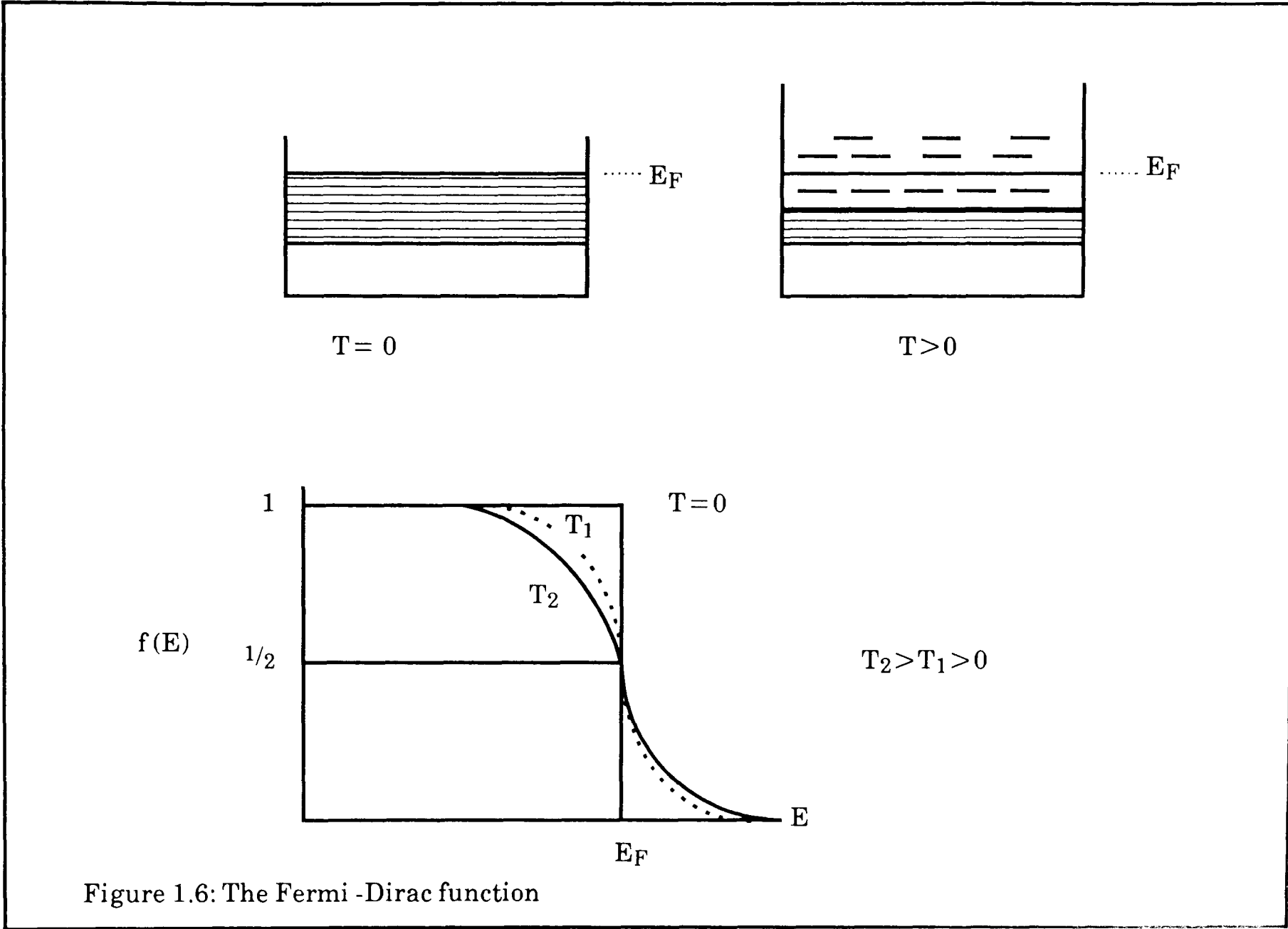


Figure 1.6: The Fermi -Dirac function

becomes very large compared to unity, then the *Fermi-Dirac distribution* approximates to the classical *Boltzmann distribution* given by(1.1,1.14):

$$f(E) = e^{\frac{E_F - E}{kT}} \dots\dots\dots 1.6$$

1.4) The Energy Band:

The highest occupied band is called the valence band, and when fully occupied its electrons are not free to move throughout the solid. Bands of lower energy than the valence band consist of core electrons and are more localised on individual atoms, so they are usually not considered. The highest energy band is generally called the conduction band, and it carries the outermost electrons of the free atoms. Electrons located in this band are free to move throughout the solid. There are, of course, bands of higher energy than the conduction band. The energy separation between the valence and conduction bands is generally called the band gap (E_g), and is usually a forbidden energy region.

The difference between metals, semiconductors and insulators can be described in terms of an energy band diagram, figure 1.7. In insulators, (figure 1.7c) the conduction band is essentially empty at all temperatures. In semiconductors ,(figure 1.7b) the conduction band is partially populated at higher temperatures but it is completely empty at 0 K, whilst in metals , (figure 1.7a) the conduction band is partially filled by electrons at all temperatures.

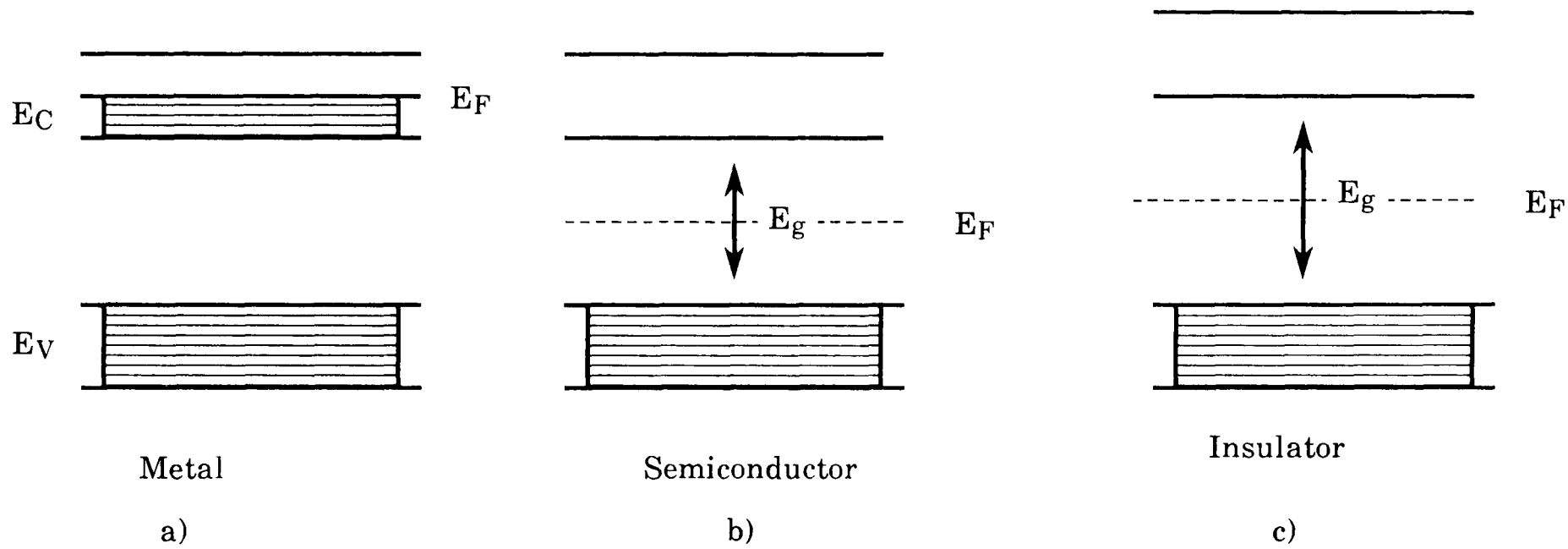


Figure 1.7: Typical band diagram

1.5) Intrinsic and Extrinsic Conduction:

A semiconductor may be either intrinsic or extrinsic. Conductivity shown by the intrinsic semiconductor is due to an electron having sufficient energy to cross the energy band. This energy is supplied thermally (thermal excitation) or by absorption of radiation (photon excitation) or by an electric field (1.1). The electroneutrality condition (1.12) is,

$$n = p = n_i \quad \dots\dots\dots 1.7$$

Where n_i is the concentration of either the electrons (n) or the holes (p).

The position of the *Fermi level* is obtained by,

$$E_F = E_i = \frac{E_C + E_V}{2} + \frac{kT}{2} \ln \frac{N_V}{N_C} \quad \dots\dots\dots 1.8$$

where E_C and E_V are the energies at the bottom and the top of the conduction and valence bands respectively, N_C and N_V are the effective density of states near the bottom of the conduction band and the top of the valence band respectively. Since the effective densities in the valence and conduction bands are approximately equal, the *Fermi level* lies very close to the middle of the band gap. This equation will be derived later. Excitation creates both conduction electrons and holes. If a field is applied they move away in opposite directions, thus giving rise to an electric current. On the other hand extrinsic conduction is caused by donors and acceptors which can form carriers, either by supplying electrons to the conduction band (n-type) or by withdrawing electrons from the valence band (p-type). As a result, new energy levels are introduced in the band gap, and their

positions correspond to the energy which is necessary to either ionize the donor (n-type) or to remove an electron from the valence band to acceptor (p-type). The number of mobile electrons and holes is no longer equal and the *Fermi level* is no longer in the middle of the gap but is displaced towards the valence band (p-type) or the conduction band (n-type).

Generally, in semiconductors the impurities play a very important role for organic and inorganic semiconductors by producing n-type or p-type materials or p-n junctions.

1.6) Electrical Conduction in Semiconductors:

The electronic conductivity of a substance depends mainly on two factors; the number of current carriers per unit volume(carrier density), and the ease of movement of the carriers through the substance(carrier mobility) under an applied electric field.

For conduction to occur in solids there must be a net movement of charge carriers through the lattice due to the presence of an external electric field. This can only happen if the allowed energy bands are only partially filled.

In general there are two types of carriers involved in conduction, electrons and holes. Holes are left behind after electrons have been promoted to a different energy level and move in the lattice under an applied field in the opposite direction to electrons. Holes behave like positively charged particles and are generally referred to as positive holes.

Conductivity can be written,

$$\sigma = n e \mu_e + p e \mu_h \quad \dots\dots\dots 1.9$$

where e is the electronic charge, p and n are the number of holes and electrons per unit volume respectively and μ_e and μ_h are the mobilities of electrons and holes. Thus, electrical conduction in an intrinsic semiconductor consists of motion of electrons in a nearly empty band under the influence of an electric field, and of positive holes in a nearly full band.

According to *Fermi-Dirac statistic* and for temperatures higher than absolute zero, the number of electrons, n , thermally excited into the conduction band is equal to the probability of occupation, $f(E)$, times the density of states (1.15),

$$n = f(E) N_C \quad \dots\dots\dots 1.10$$

substituting equation 1.5 in 1.10, then,

$$n = N_C \left[1 + e^{-\frac{(E_C - E_F)}{kT}} \right]^{-1} \quad \dots\dots\dots 1.11$$

where E_C is the energy at the bottom of the conduction band. If $E_C - E_F \gg kT$, then the term $e^{(E_C - E_F)/kT} > 1$ and equation 1.11 will become,

$$n = N_C e^{-\frac{(E_C - E_F)}{kT}} \quad \dots\dots\dots 1.12$$

For intrinsic or pure materials, every electron in the conduction band has left a hole behind it in the valence band and so the number of holes, p , is obtained by a similar equation,

$$p = N_V e^{-\frac{(E_F - E_V)}{kT}} \dots\dots\dots 1.13$$

where N_V is the density of states for the valence band.

Combining equations 1.12 and 1.13,

$$N_C e^{-\frac{(E_C - E_F)}{kT}} = N_V e^{-\frac{(E_F - E_V)}{kT}} \dots\dots\dots 1.14$$

Then,

$$E_F = \frac{E_C + E_V}{2} + \frac{kT}{2} \ln \frac{N_V}{N_C} \dots\dots\dots 1.15$$

This equation is the same as equation 1.7 which was mentioned earlier.

For $N_C = N_V$, $E_F = (E_C + E_V)/2$. Thus the *Fermi level* will be halfway between the valence and the conduction band in an intrinsic semiconductor.

Multiplying n and p together,

$$np = n_i^2 = N_C N_V e^{-\frac{(E_C - E_V)}{kT}} \dots\dots\dots 1.16$$

$$n_i = \sqrt{N_C N_V} e^{-\frac{(E_C - E_V)}{kT}} \dots\dots\dots 1.17$$

From equation 1.9,

$$\sigma = e(\mu_e + \mu_p) n_i \dots\dots\dots 1.18$$

The temperature dependence of conductivity is given,

$$\sigma = e(\mu_e + \mu_p) \sqrt{N_C N_V} e^{-\frac{(E_C - E_V)}{kT}} \dots 1.19$$

The band gap $E_C - E_V$ is represented by E_g and the term $e(\mu_n + \mu_p) \sqrt{(N_C N_V)}$ is represented by the *pre-exponential factor* (σ_0). Thus the conductivity is given by

$$\sigma = \sigma_0 e^{-\frac{E_g}{2kT}} \dots\dots\dots 1.20$$

This equation shows that in the intrinsic case the conductivity will vary with temperature according to the factor $-E_g/2kT$. Plotting $\ln \sigma$ vs. $1/T$ gives a slope equal to $-E_g/2k$.

If impurities are introduced into the semiconductor, a significant effect on the band structure and the conductivity occurs as illustrated in figure 1.8. Donor impurities may donate an electron to a neighbouring atom or molecule which then enter the conduction band, contributing to the conduction process (n-type). In fact, just in the neighbourhood of the impurity atom the crystal behaves as if its forbidden gap had shrunk from $E_C - E_V$ to a new value $E_C - E_D$ (1.16), where E_D is the energy of the donor level. At temperatures low enough to allow very few electrons to be excited from the valence to the conduction bands, then the only effective source of electrons are the donor impurities, and so then the number of electrons available,

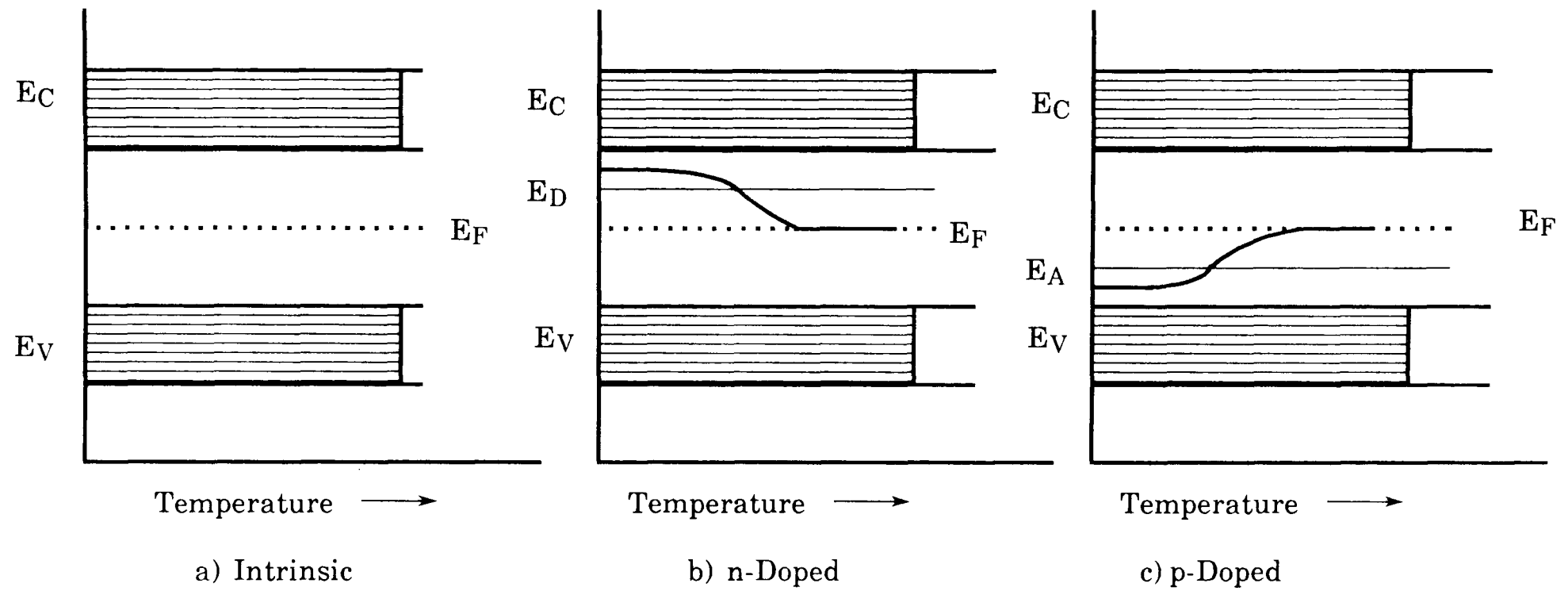


Figure 1. 8 : The variation of Fermi level as a function of temperature for intrinsic, n-doped, and p-doped materials.

$$n^2 = N_C N_D e^{-\frac{(E_C - E_D)}{kT}} \dots\dots\dots 1.21$$

and

$$n = \sqrt{N_C N_D} e^{-\frac{(E_C - E_D)}{2kT}} \dots\dots\dots 1.22$$

where N_D is the density of states for the donor centres.

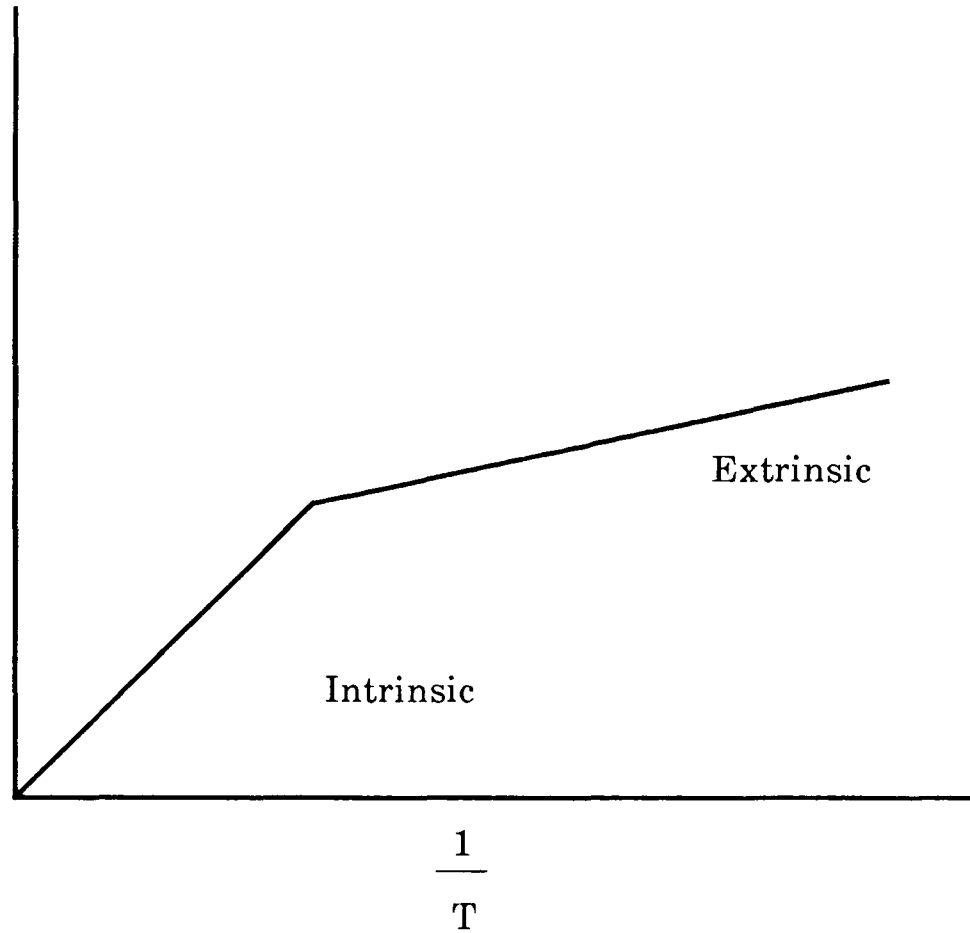
Acceptor impurities will take an electron from a neighbouring atom or molecule (p-type). This will leave a hole in the valence band which will behave as in the case of excitation of an electron from the valence to the conduction band, and the crystal behaves also as if its forbidden gap had shrunk from $E_C - E_V$ to $E_A - E_V$, where E_A is the energy of the acceptor centres. The concentration of holes from the acceptor impurity is given by,

$$p = \sqrt{N_V N_A} e^{-\frac{(E_A - E_V)}{2kT}} \dots\dots\dots 1.23$$

where N_A is the density of the state for the acceptor centres. This behaviour can be illustrated by plotting the natural logarithm of the resistance vs. $1/T$ where the break in the graph at certain temperatures indicates a transition between an intrinsic transport region at high temperatures and an extrinsic one at low temperatures^(1.17) as shown in figure 1.9.

If the temperature is so high that all the impurities(donors or acceptors) contribute to the electrical conduction, then the excitation will be from the

In Resistance



Extrinsic

Intrinsic

$\frac{1}{T}$

Figure 1.9 Temperature dependence showing intrinsic and extrinsic regions

valence to the conduction bands and the forbidden gap appears as if it is expanded again to its normal case, $E_C - E_V$, and the *Fermi level* will be in the middle of the forbidden gap.

For materials containing donor and acceptor centres, it is assumed that electrons from the donors will fall into the acceptors, at low temperatures.

If $N_D = N_A$, then the material behaves as if it is intrinsic because their effects cancel each other out(1.1).

If $N_D > N_A$, then the material behaves as if there is $N_D - N_A$ donors centres present, and so n is given by,

$$n \approx \sqrt{N_C(N_D - N_A)} e^{-\frac{E_D}{2kT}} \dots\dots\dots 1.24$$

If $N_A > N_D$ the material behaves as if $N_A - N_D$ acceptors are present, and p given by,

$$P \approx \sqrt{N_V(N_A - N_D)} e^{-\frac{E_A}{2kT}} \dots\dots\dots 1.25$$

1.7) Conduction in Molecular Crystals:

In contrast to inorganic semiconductors such as selenium, where the bonding is covalent(1.18), the intermolecular interaction in organic molecular crystals is due to weak *van der Waals' forces*. As a consequence the intermolecular orbital overlap is very weak and the bands formed are very narrow. The question arises as to whether band theory applies to such

systems. *Meier* (1.19) has considered the problem and concluded that for broad band theory to apply the mobility should be $\geq 1 \text{ cm}^2 \text{ V}^{-1} \text{ s}^{-1}$. For narrow band theory a value of $0.1 - 1.0 \text{ cm}^2 \text{ V}^{-1} \text{ s}^{-1}$ is acceptable. Since these values are amongst the higher values observed in organic compounds it seems that band theory is, at best, at the limit of its applicability in organics. Nevertheless it remains the most highly developed and convenient way to interpret the electrical properties of these materials (1.6, 1.20-21).

The formation of energy bands in organic solids consisting of conjugated materials can be easily illustrated by taking, as an example, the simple case of ethylene. Because of the sizes of most semiconductor molecules it is often convenient to start from their *Hückel* molecular orbitals. If two p-orbitals are allowed to interact on ethylene, the pair of molecular orbitals which are formed are called the π -bonding and the π^* -antibonding orbitals.

If the π -orbitals of two ethylene molecules stacked directly one above the other are allowed to interact, two sets of two molecular orbitals are formed separated in energy by $2t$, where t is the resonance or transfer integral. If n ethylene molecules are allowed to interact, n states are formed from each π and π^* orbitals. Into each of these states (bands) can be placed $2n$ electrons. In this case the band formed from the highest occupied molecular orbital (*HOMO*) of ethylene is entirely full and the band formed from the lowest unoccupied molecular orbital (*LUMO*) is entirely empty. Band separation will determine whether the molecule is an insulator or a semiconductor. This model is shown in figure 1.10.

Linear polymeric materials such as polyacetylene represent a special case of great importance. The strong intra-molecular bonding and good

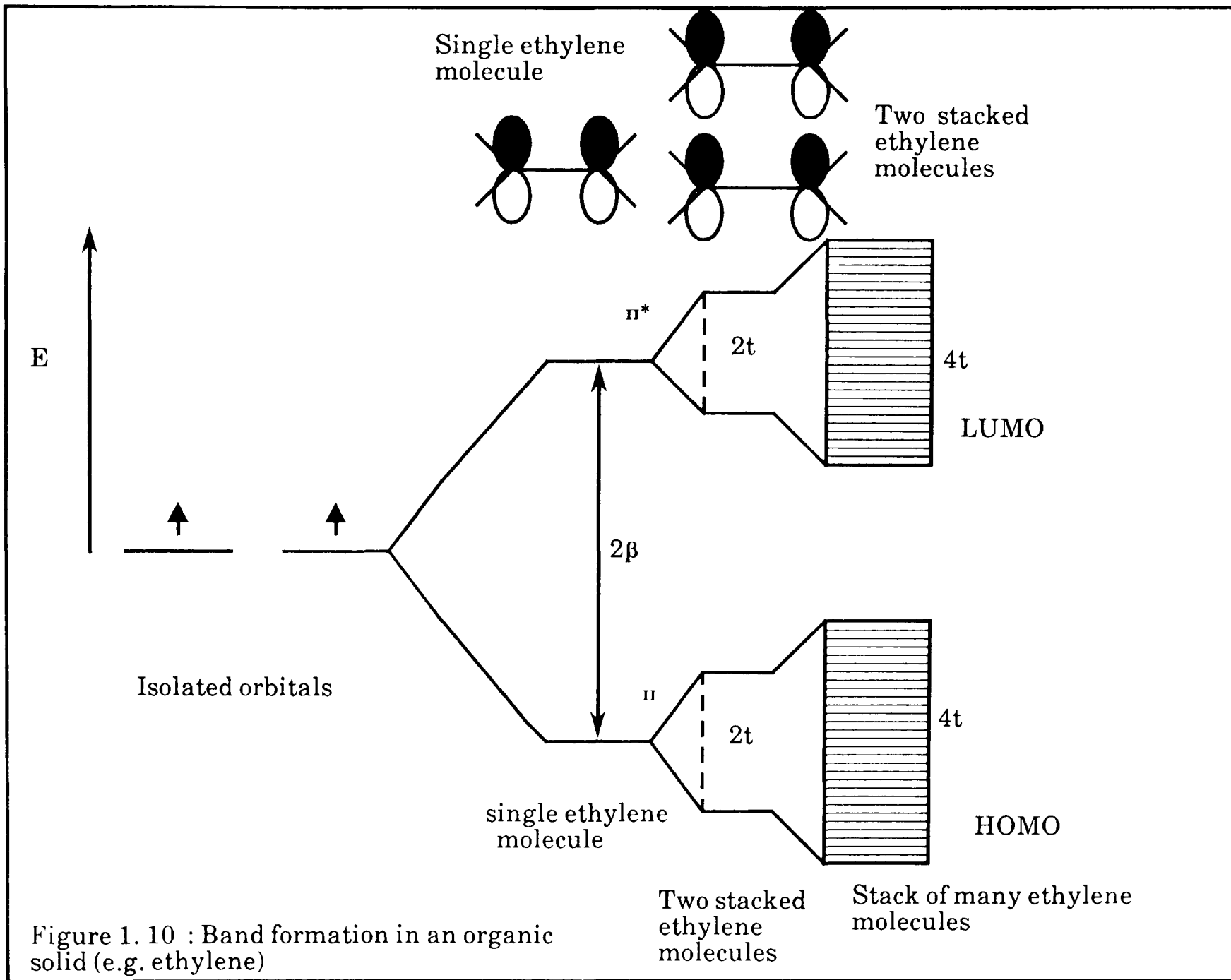


Figure 1. 10 : Band formation in an organic solid (e.g. ethylene)

orbital overlap gives rise to a band structure with broad energy bands^(1.22), and *band theory* is clearly appropriate for intra-molecular charge migration. Movement between molecules, which may be rate determining, suffers from the same limitations as in other molecular crystals.

In those polymers where the band formation is a result of π -orbital overlap between molecules, as in the case of DNA, then the band widths have the same low values as in monomeric materials such as phthalocyanines^(1.19).

1.8) The Potential Box for Molecular Crystals:

An alternative model to the band model introduced by *Eley* ^(1.23-24) is the *Potential Box model*, or *Tunnel model*. This model applies when the band width is narrow and has the advantage of relating electrical behaviour directly to molecular properties. Each molecule is represented by a potential box accommodating the n electrons, and the crystal is represented by an array of such potential boxes.

1.8a) Intrinsic Charge Generation:

In this model an electron and hole can be regarded as free to move independently when the electron has been removed from one molecule to a distant molecule. *Lyons* ^(1.25,1.2) has shown the energy of this process, which is equivalent to the band gap, to be given by,

$$(Eg)_{intrinsic} = I - E_A - P^+ - P^- + \Delta W_f \quad \dots \quad 1.26$$

Where:

I is the ionisation potential of the free molecule,
 E_A is the electron affinity of the free molecule,
 P^+ and P^- are the polarisation energies of the lattice due to the
cores
and

ΔW_f is the stabilisation energy of the ground state in going
from gaseous to crystalline state.

The process is illustrated in figure 1.11a.

1.8b) Extrinsic Charge Generation:

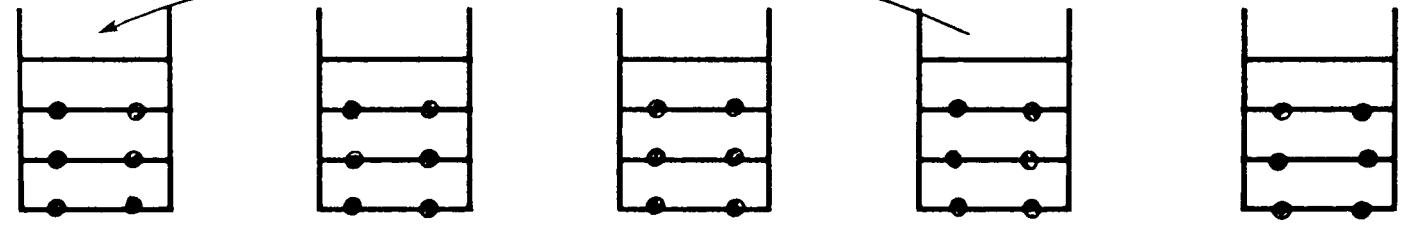
Where the crystal contains impurity molecules with electron acceptor
properties, the process of hole generation occurs with reduced energy, and
the material may be an extrinsic p-type semiconductor. The energetics of
the process, illustrated in figure 1.11c, are,

$$(Eg)_{extrinsic} = I - (E_A)_{impurity} - P^+ - (P^-)_{impurity} + \Delta W_f \quad 1.27$$

Similarly, where the impurity molecules are electron donors
(figure 1.11b), n-type behaviour occurs, the energy of charge generation
being given by

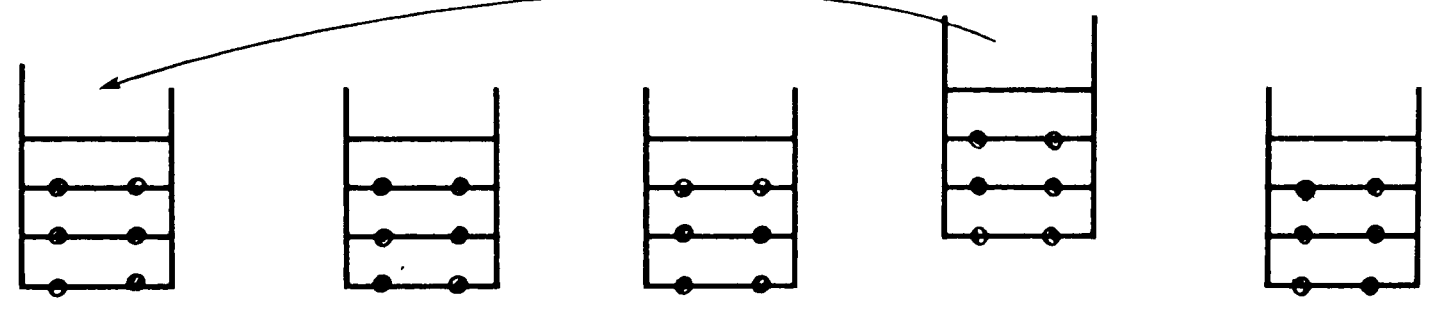
$$(Eg)_{extrinsic} = (I)_{impurity} - E_A - (P^+)_{impurity} - P^- + \Delta W_f \quad ..1.28$$

1.9) Hopping and Tunnelling:



Intrinsic case

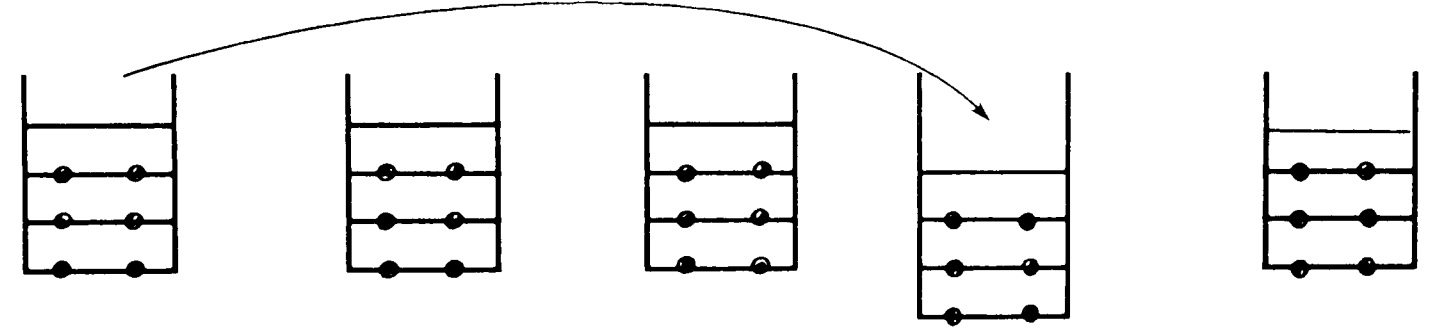
a)



In the presence of donor impurities

Donor impurities

b)



In the presence of acceptor impurities

Acceptor impurities

c)

Figure 1.11 : Effect of doping

In the *Potential Box model Eley* (1.23) proposed that the conducting state is formed via the excited singlet. The electron (or hole) was assumed to move from its parent molecule to a distant site by quantum mechanical tunnelling. The tunnelling probability (W_T) (1.19,1.26) is given by

$$W_T = D'Z = 10^{11} - 10^{14} \text{ s}^{-1} \quad \dots\dots\dots 1.29$$

where D' is the *transition coefficient* and Z is the number of collisions of an electron with the potential barrier. The probability of an excited singlet state returning to the ground state is given by

$$K_R = \frac{1}{\tau_0} = 10^8 \text{ s}^{-1} \quad \dots\dots\dots 1.30$$

where τ_0 is the fluorescence life time. This means that the probability of an excited electron reaching its neighbouring molecule is higher by a factor of 10^3 - 10^6 than its return to the ground state. These calculations suggest that the mechanism is reasonable. However, provided that an equilibrium concentration of carriers is rapidly achieved and maintained, the exact mechanism by which it is achieved does not affect the conductivity.

Of greater significance is the ease of tunnelling of a mobile carrier from molecule to molecule which determines the carrier mobility. In the absence of an applied field the tunnelling probability in either direction. When a field is applied the tunnelling probability in the field direction is enhanced at the expense of movement against the field (1.24).

An important feature of the *Potential Box model* is that the mobility is clearly determined by the barrier height and barrier thickness. In

molecular terms this means that intermolecular distance and orbital overlap are the factors which must be controlled if high mobility is to be achieved.

When the lifetime of the carrier in a molecule is larger than the vibrational relaxation time, the carrier tends to polarise the surrounding lattice. The charge carrier and its associated polarisation form a quasi-particle, called a *polaron*. The *polaron* can migrate by hopping over the potential barrier, a thermally activated process resulting in a temperature dependent mobility (1.12,1.19) ;

$$\mu = \mu_0 e^{-\frac{E'}{kT}} \dots\dots\dots 1.31$$

where μ_0 is temperature dependent varying as T^{-n} with $n = 1-1.5$ (1.2), and E' is the height of the potential barrier.

Hopping and tunnelling models are shown in figure 1.12.

1.10) Band Structure for Amorphous Solids:

The band structure of amorphous semiconductors is complicated by the disorder created by various defects(1.27), but even with the disorder and the decrease in the carrier mobility the energy band model can be applied(1.28).

The density of the energy states displays an exponential tail as the forbidden zone is entered(1.29-30) as shown in figure 1.13. The disorder in the energy states in the forbidden zone may cause the following effects;

- I) The exponential tail of photoconductivity pulses (1.31).
- II) Trapping of holes or electrons and its effect on drift mobility(1.32-33).
- III) Hopping transport between random sites in the a.c conductivity

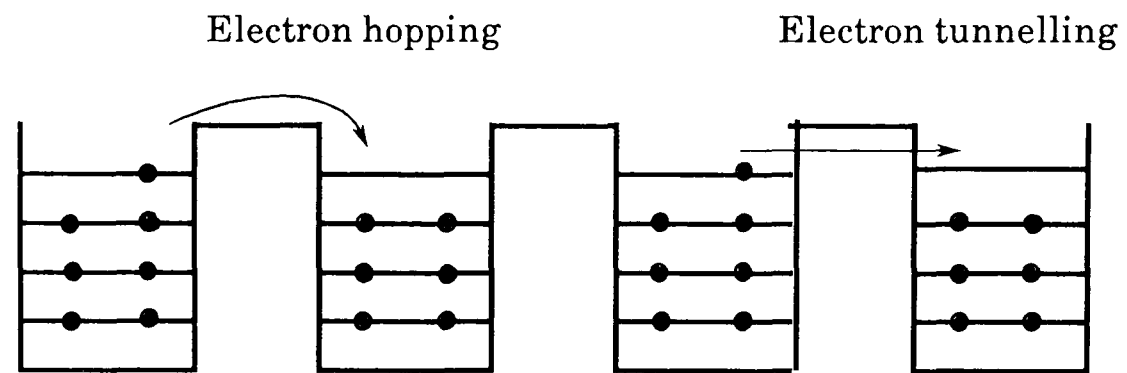
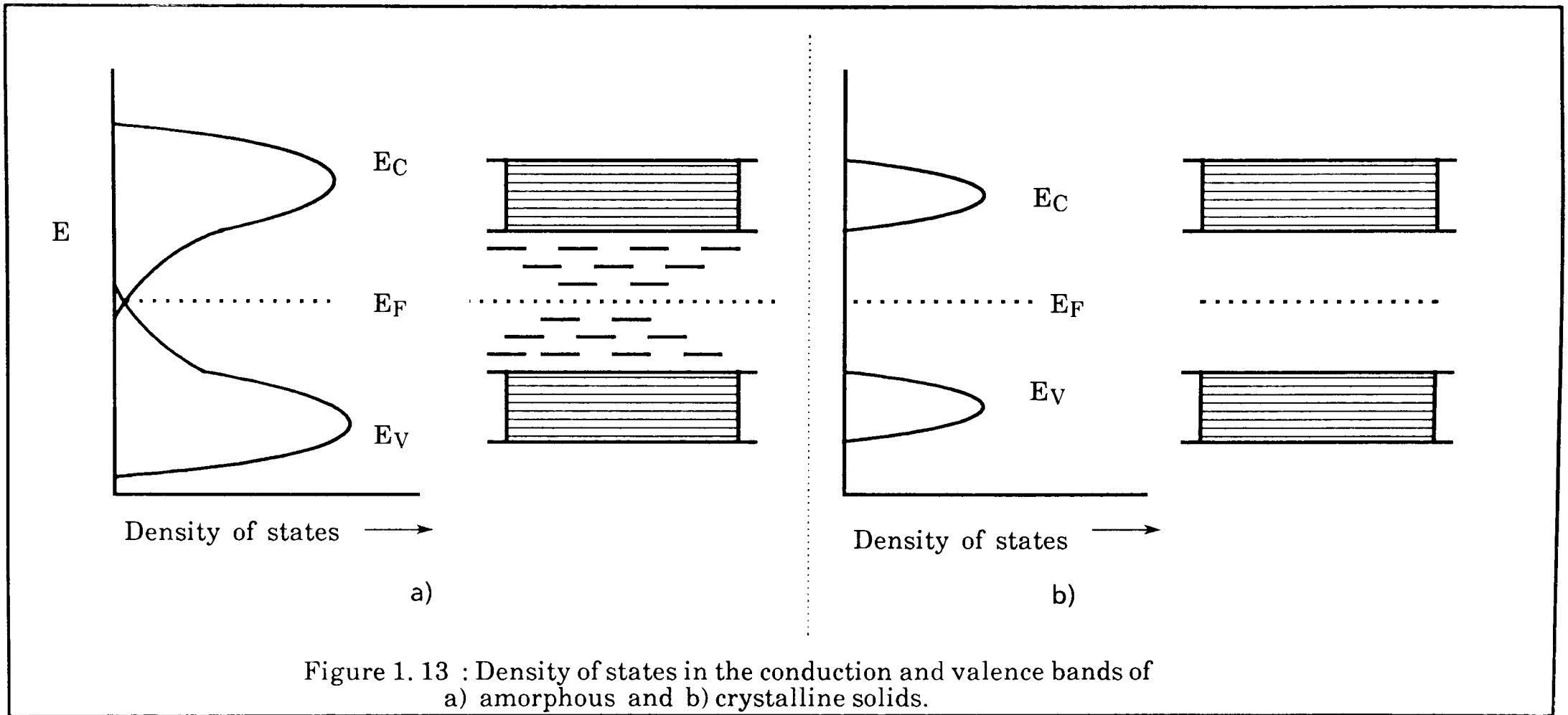


Figure 1.12 : A schematic diagram illustrating the electron hopping across the energy barrier and the electron tunnelling through a square potential barrier.



measurements which is explained by *Mott and Davis* (1.34) as the conduction around a *Fermi level* (See chapter 6).

1.11) Effect of Space-Charge-Limited Current (SCLC) on the Conductivity:

The conductivity, σ , can be described as the relationship between the current density, J , and the applied electric field, E , according to *Ohm's law*,

$$J = \sigma E \quad \dots\dots\dots 1.32$$

The variation of current (I) with the magnitude of the applied Voltage (V) gives the limiting voltage for which *Ohm's law* ($I \propto V$) can be used.

The equilibrium concentration of charge carriers in insulators or semiconductors is very small because of the exponential dependence of carrier density with the band gap^(1.12), so the current transport may be governed by the concentration of charge carriers injected from the contact^(1.6).

At lower voltages the thermal equilibrium density of charge carriers is greater than that injected from the electrodes, so *Ohm's law* will be obeyed.

At higher voltages and with *Ohmic* contact with the metal electrode, the injected carriers near the contact increase and the current voltage curve shows non-*Ohmic* behaviour. This can be attributed to the build-up of *space-charge* within the sample, caused by either excess free carriers or by carrier trapping giving charged regions^(1.29). Reviews of space-charge

limited currents in organic crystals and in polymers are presented in references 1.6, 1.35 and 1.36 respectively.

Figure 1.14 shows the current voltage curve. At low voltages the current obeys *Ohm's law* and follows the region A-B or A-C. If the solid is trap free the current becomes space charged limited at a voltage corresponding to point B at which the concentration of the free carriers injected from the contact becomes greater than the concentration of the thermally generated carriers. At this voltage the current follows the line B-E-F and given by the *Child-Langmuir Law* (1.1, 1.19),

$$I_{SCL} = 10^{-13} A \epsilon \mu \frac{V^2}{L^3} \dots\dots\dots 1.33$$

and the current density,

$$J_{SCL} = 10^{-13} \epsilon \mu \frac{V^2}{L^3} \dots\dots\dots 1.34$$

where A, ϵ , μ , V and L are the electrode surface area *permittivity*, the carrier mobility, voltage applied and the inter-electrode spacing respectively. This law gives a current proportional to the square of the voltage where the current is limited by space charge of the carriers.

In reality, however, samples contain traps. If these traps are shallow a fraction of the carriers will be immobile within the traps, and the others will be free. An equilibrium distribution between the trapped and free carriers is established. The presence of high concentration of traps in the conduction band causes the mobility to drop sharply. Because of trapping the mobility, μ , must be replaced by the *effective mobility*, $\Theta\mu$, then,

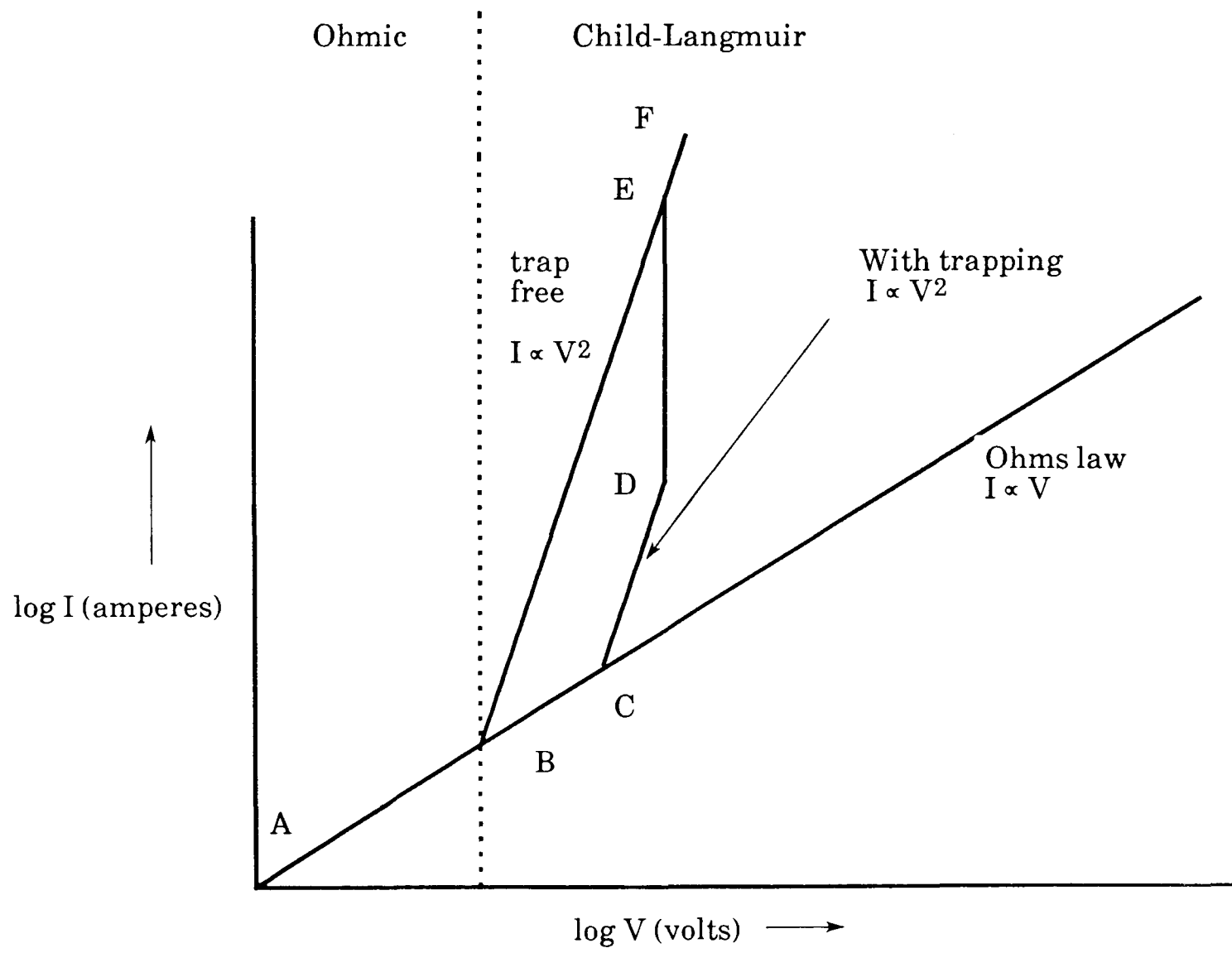


Figure 1.14: Typical current- voltage characteristic curve

$$J_{SCL} = 10^{-13} \epsilon \Theta \mu \frac{V^2}{L^3} \dots\dots\dots 1.35$$

where Θ reflects the extent to which the effective mobility is reduced by traps. Thus the limiting voltage for a trap containing solid is higher than for a trap free solid, the current, however, still obeys the *Child-Langmuir law* and the curve follows the line C-D. When all traps are filled they no longer influence the mobility, μ , and the current rises sharply from D to E. The current again follows the simple *Child-Langmuir law* from E to F since the solid now behaves as if it is trap free. The critical voltage at which the transition from *Ohmic* to non Ohmic occurs in the presence of traps, V_t , can be obtained by substituting equation 1.32 into equation 1.35. Since the current densities for SCLC and Ohmic conductions are equal at the critical voltage (1.2), then,

$$V_t = 10^{13} \sigma \frac{L^2}{\epsilon \Theta \mu} \dots\dots\dots 1.36$$

This permits the calculation of *effective mobility*.

1.12) Other Solid State Concepts:

Solid state concepts related to a.c and photoconductivity are explained in chapters 6 and 7.

CHAPTER TWO

PHTHALOCYANINES

2.1) Historical Introduction:

The word phthalocyanine is derived from the Greek terms for naphtha (rock oil) and cyanine (dark blue). The term phthalocyanine was first used by *Linstead*, of the *Imperial College of Science and Technology* in 1933^(2.1). The compound was first produced accidentally at the *South Metropolitan Gas company* in London in 1907 by *Braun and Techerniac* during a study of the properties of a cyanobenzamide.

In 1928 at Grangemouth, Scotland, traces of a dark blue insoluble impurity were noticed in the iron vessels used to prepare phthalimide from phthalic anhydride and ammonia. This product was iron(II) phthalocyanine. Since then thousands of publications concerning the phthalocyanines have appeared^(2.2).

In 1935, Imperial Chemical Industries began to manufacture copper phthalocyanine. Since the first commercial production of phthalocyanine in the United States, this class of compounds has become an important economic factor in the technology and application of pigments and dyes^(2.1).

Because of their special physical and chemical properties, these compounds have been the subject of great interest to applied and theoretical physicists, chemists and engineers.

2.2) Structure:

The elucidation of the phthalocyanine structure was carried out by *Linstead* and his colleagues in 1933 at *Imperial College*^(2.1-2).

Phthalocyanine (abbreviated Pc) is a macrocyclic compound containing a ring system of four isoindole units linked by aza nitrogen atoms. Its structure therefore is closely related to porphyrins, which have methine corner links rather than aza nitrogen atoms. The phthalocyanine molecule consists of a closed system of carbon and nitrogen atoms in state of double bond single bond resonance. The two central hydrogen atoms are replaceable by a wide range of metals. The central metal atom is attached by covalent bonding to two isoindole nitrogen atoms and is coordinated to the other two nitrogens. Actually, phthalocyanines containing central metal atoms from every group of the periodic table have been prepared. The peripheral hydrogen atoms in the four benzene rings in the phthalocyanine molecule have been replaced by halogen atoms and different organic and inorganic groups^(2.3-4).

X-ray diffraction measurements on phthalocyanine single crystals show that there are three polymorphic forms which are represented by the symbols, α , β and χ ^(2.1,2.5) (Figure 2.1). They differ in their stability, particle size and manner of molecular stacking^(2.6-7). The β -form is the most

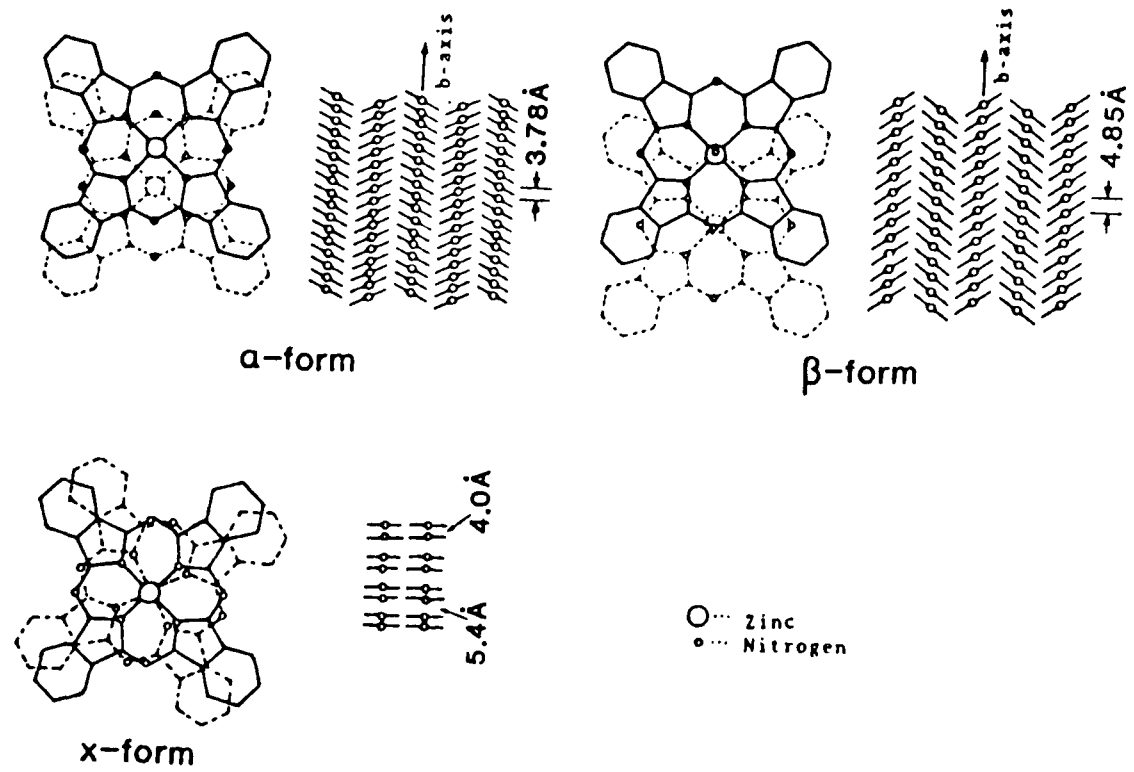


Figure 2.1 : The main molecular stacking for phthalocyanines

stable and tends to form the largest monocrystal. The appearance of such polymorphs is considered to be due to a slight difference in the π -electronic interaction between the stacked planar molecules^(2.8). The three polymorphic forms also differ in their electrical properties^(2.9).

The macrocyclic ring in most metallophthalocyanines is planar to within 0.3 Å^(2.5,2.10), and the polymeric phthalocyanine belong to D_{4h} symmetry. This symmetry will be reduced to D_{2h} for the metal free and monomeric phthalocyanines^(2.5).

2.3) Phthalocyanine Bridging:

Phthalocyanine rings may either be separate units, such as metal free or copper phthalocyanines, or linked with other phthalocyanine rings in the form of dimers, oligomers or polymers. There are three known types of linkages in phthalocyanines.

- ① Dimeric forms have the metal sandwiched between the two phthalocyanine rings. This kind of linkage is found in the phthalocyanine complexes of lanthanides and actinides^(2.11-12).
- ② A two dimensional eka-linked phthalocyanine polymer^(2.13). These materials are usually prepared from tetracyanobenzene where the macrocycles are linked via the peripheral conjugated systems to give a layer type structure^(2.14), with eka-conjugation due to π -electron delocalisation over the entire conjugated chain path.
- ③ μ -Bridged phthalocyanine polymers, where a ligand is used which can act as a bridge between two macrocycles via the central metal atoms. This will give cofacially stacked or face to face phthalocyanine units

with a rigid structure. Several different types of ligands are used to act as bridging units, such as O(μ -oxo)^(2.15), F(μ -fluoro)^(2.16,12.7), CN(μ -cyano)^(2.18), Pyrazine(Pyz)^(2.19) and others^(2.20-21).

The three types of linkages are shown in figures 2.2 and 2.3.

2.4) The Polymeric Structure of μ -Bridged Phthalocyanines:

The μ -oxo bridged phthalocyanines with central metal atoms Si, Ge and Sn have attracted attention because of their stability and conducting properties when oxidized with iodine^(2.22). Other phthalocyanines with μ -fluoro bridging, which have a similar structure to those with μ -oxo bridges, have been prepared more recently with central metal atoms Al, Ga^(2.16) and Fe^(2.17).

The polymeric nature of these compounds, with a linear backbone surrounded by the planar phthalocyanine rings stacked face to face, is suggested from the following information:

- I) The low solubility and low volatility.
- II) The broad band at 500-550 nm, associated with the M-F stretching vibration ^(2.16-17,2.23) indicates that these compounds have a (M-F)_n backbone.
- III) Electron microscopy shows that the planar phthalocyanine molecules are arranged face to face with a constant intermolecular distance. They are stacked such that their projection becomes identical to that of a single molecule ^(2.24).
- IV) High resolution ¹³C n.m.r spectroscopy proves the eclipsed character of

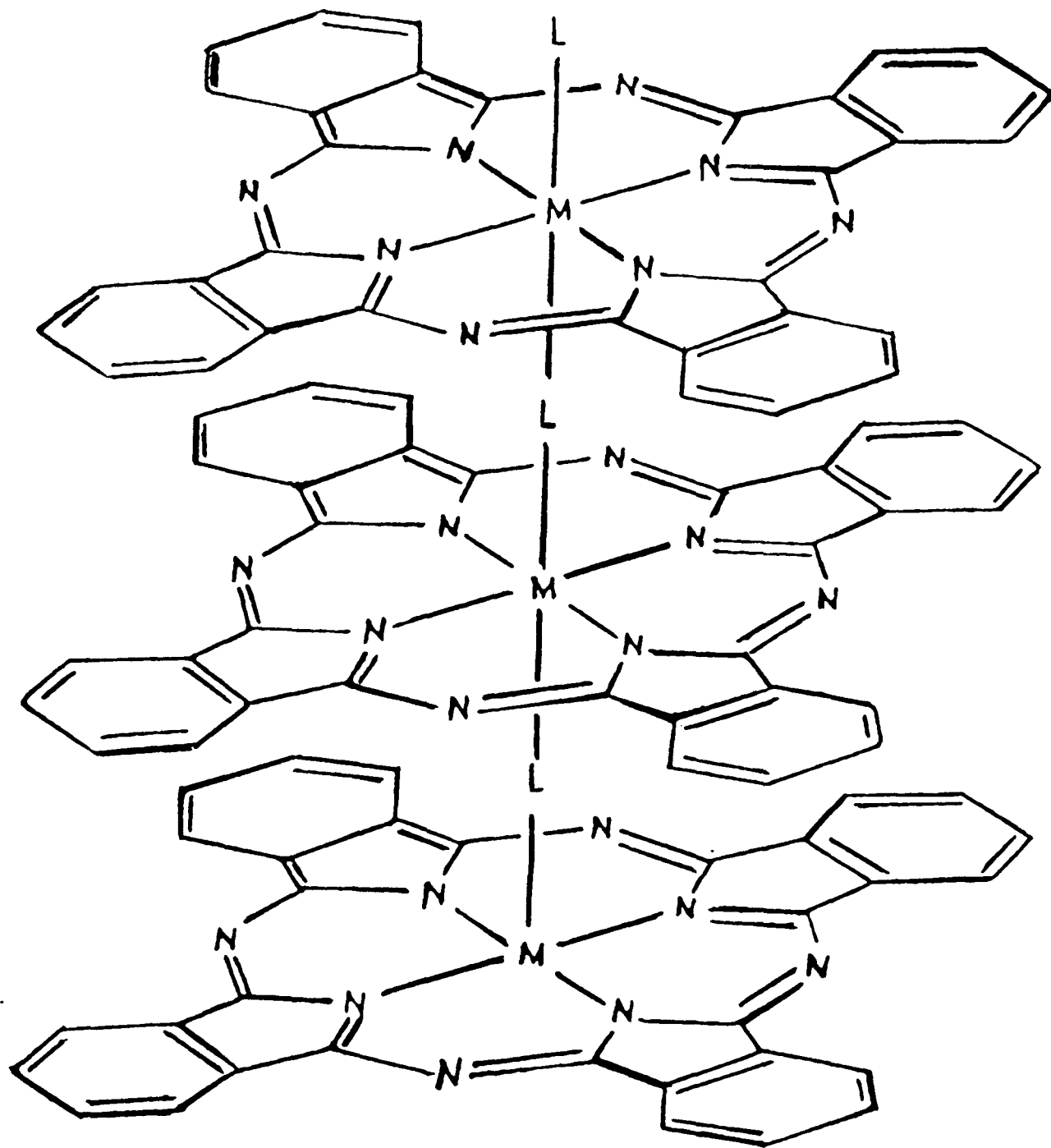


Figure 2.2 : The structure of μ -bridged phthalocyanines.

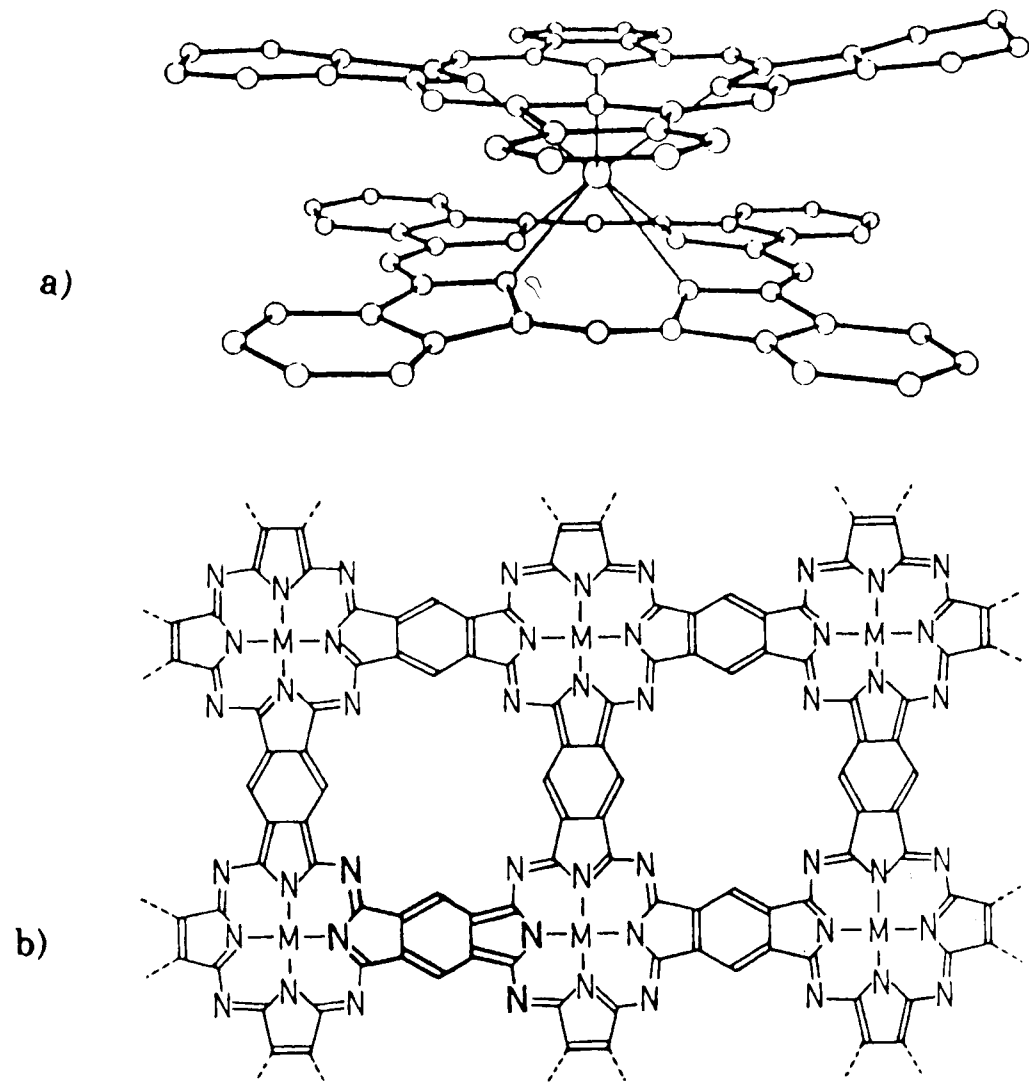


Figure 2.3 : a) The linkage in phthalocyanine complexes of lanthanides , e.g., NdPc₂.
b) eka-linked phthalocyanine polymers.

stacking configuration of Pc rings along the polymeric chain in $(AlPcF)_n$ (2.25).

V) X-ray powder diffraction shows a strong reflection at 3.66 Å and 3.86 Å for AlPcF and GaPcF respectively. This spacing corresponds to the atomic radii Al-F-Al and Ga-F-Ga respectively which indicates that the molecules have a $(M-F)_n$ backbone surrounded by phthalocyanine rings stacked face to face (2.16) as shown in figure 2.2.

VI) Crystallographic studies of AlPcF and GaPcF systems have shown them to be aligned in a cofacial way with M-F bonds having a strong dipole to favour an electrostatic interaction of the type shown below (2.10,2.26).



2.5) Methods of Preparation:

There is no single method which may be used to prepare all metal phthalocyanines, but some methods can be used to prepare several types of such compound. Using various methods, it is possible to prepare metal phthalocyanines from nearly every group in the periodic table.

Apart from the chemical methods of preparation, positive ion bombardment (2.27-28) and electro-synthesis of phthalocyanines (2.29) have been reported. Phthalocyanine free radicals have also been prepared (2.30).

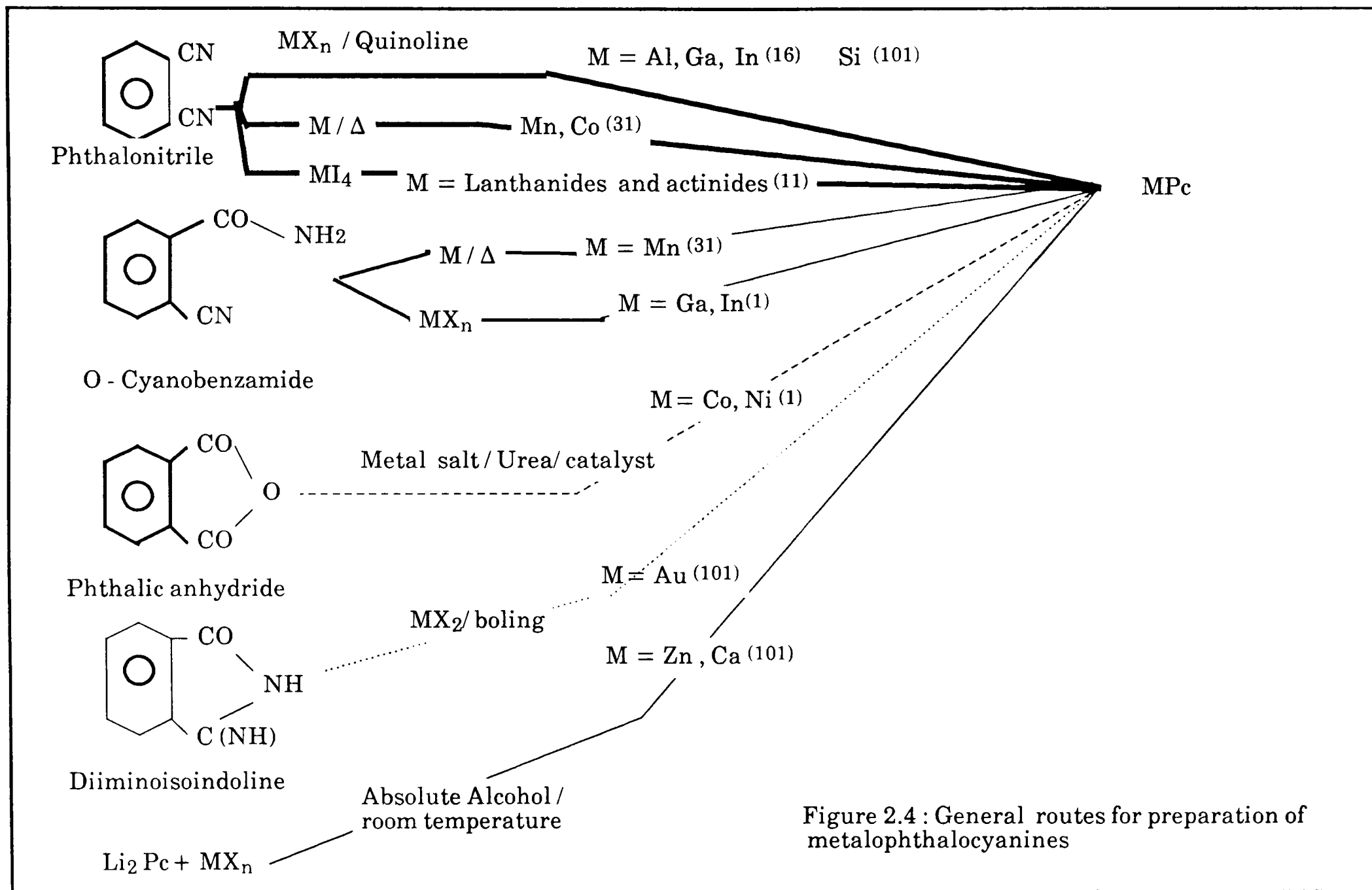


Figure 2.4 : General routes for preparation of metalphthalocyanines

The more general methods of preparation are summarised in figure 2.4 (2.1- 2,2.5,2.31-32).

2.6) General Properties:

- I) Phthalocyanines are solid materials with intense blue or green colouration. This is a result from their delocalised π -system.
- II) They are insoluble in water and most common organic solvents. The best solvents are 1-chloronaphthalene, pyridine and quinoline, but even in these solvents their solubilities vary from insoluble to slightly soluble. Soluble phthalocyanines have been prepared by substituting peripheral hydrogens in the phthalocyanine rings by certain groups such as alkyl or alkoxy groups (2.33). Lithium phthalocyanines are soluble in acetone and ethanol(2.34).
- III) Phthalocyanines are thermally stable with no noticeable degradation up to 400-500 °C, but they decompose below 900 °C under vacuum(2.35). They are also chemically stable. Most of phthalocyanines are soluble in concentrated inorganic acid without decomposition(2.1) and can only be broken down with very strong oxidizing agents such as dichromate(2.36).
- IV) Most of the phthalocyanines are sublimable so they can be purified using different sublimation techniques such as cold finger, entrainment and gradient sublimation. They can be deposited as thin films by vacuum deposition. The molecular beam epitaxy technique has been used to prepare ultra thin film (perfectly smooth films) and to control molecular ordering(2.37).
- V) The nature of the central metal atom(2.21,2.38) and the peripheral substituents on the ring(2.3) have a very large influence on the physical and chemical properties of phthalocyanines.

2.7) Applicability of Band Model to Phthalocyanines:

As in the case of molecular crystals, the question arises as to whether band theory applies to phthalocyanines. Taking into account the *Meier* consideration of applicability of band theory for narrow bands which require mobility values of $0.1-1.0 \text{ cm}^2 \text{ v}^{-1} \text{ s}^{-1}$, the applicability of band theory to phthalocyanines may be questionable.

Heilmeier and Warfield (2.39) concluded that the band model is applicable to phthalocyanines during an attempt to explain the available experimental data on the basis of the known theories of the conduction in organic semiconductors such as anthracene.

Mathur and Ramesh (2.40) investigated the model of charge carrier transport in $\beta\text{-H}_2\text{Pc}$ on the basis of a theory which suggests the possibility of three different modes of transport in organic semiconductors. This depends on the relative magnitudes of the electron-exchange, electron-phonon and phonon-dispersion energies,

① Where:

electron-exchange energies $>$ electron-phonon and phonon-dispersion energies

The calculation of the conventional carrier band structure is only valid in this case.

② Where:

phonon-dispersion energies $<$ electron-exchange energies $<$ electron-phonon energies

③ Where:

electron-exchange $<$ electron-phonon and phonon-dispersion energies

From the experimental findings, *Mathur* and *Ramesh* show that case ① is applicable only for electron transport in the crystallographic b^{-1} direction, while the electron and hole transport along a^{-1} and c^{-1} are indicated by case ③ which is equivalent to conventional hopping transport. A similar conclusion has been reached by *Chen*(2.41).

Cox and *Knight* (2.42-43) have interpreted their experimental results on the carrier drift mobility parallel to the c^{-1} axis in β -H₂Pc in terms of the band model. In contrast to these results *Mathur* and *Ramesh* (2.44) propose an argument based on the magnitude of the calculated transfer integrals for β -H₂Pc.

Mathur and *Singh* (2.45) assumed that the band theory was applicable in γ -PtPc crystals on the basis of the higher calculated transfer integrals of one order of magnitude for γ -PtPc than for β -H₂Pc. However, the results of mobility experiments on γ -PtPc show that the carrier mobility (holes and electrons) have a dominant mobility parallel to the crystal b -axis (2.45).

From the work of *Mathur et al* (2.44,2.46) and others (2.41,2.47-49), it can be concluded that the calculated bandwidths for H₂Pc (β -form) in the three directions a^{-1} , b^{-1} and c^{-1} are found to be anisotropic, varying from a few meV for directions parallel to a^{-1} and c^{-1} axes to 30-100 meV along the b^{-1} axis

(2.5). In order for the band model to be meaningful the following equation (2.5,2.13) must be obeyed ,

$$\tau = \frac{\hbar}{W} \dots\dots\dots 2.1$$

where τ is the mean free time for the charge carrier and is of the order of $\geq 10^{-13}$ sec. (2.47), \hbar is $h/2\pi$, and W is the band width. The calculated mobility in the b^{-1} direction is of the order of $0.4 - 1.0 \text{ cm}^2 \text{ V}^{-1} \text{ s}^{-1}$. Consequently electron and hole transports in the b^{-1} direction should be described by a simple band model, whereas a localised state model is presumably preferable in the a^{-1} and c^{-1} axes.

By comparison with inorganic materials the mobility of the charge carriers in metal phthalocyanines is very low,

Compound	Mobility (2.50) $\text{cm}^2 \text{ V}^{-1} \text{ s}^{-1}$
Si	1350
In	4500
GaAs	8000
CdS	340

The mobilities of charge carriers in metallophthalocyanines rarely exceed $1 \text{ cm}^2 \text{ V}^{-1} \text{ s}^{-1}$. The highest value of effective mobility claimed for thin films of phthalocyanines at room temperature was $1.3 \text{ cm}^2 \text{ V}^{-1} \text{ s}^{-1}$ for LuPc_2 (2.51), and for single crystal was $75-100 \text{ cm}^2 \text{ V}^{-1} \text{ s}^{-1}$ (2.5).

2.8) Band Structure of Phthalocyanines:

The energy band structure of metal free^(2.41) and metal phthalocyanines^(2.45-46) have been calculated using the *extended Hückel*(E.H) method. The formation of bands arises from the π -orbital interaction of adjacent macrocyclic rings in the stack of the phthalocyanine molecules^(2.52). This interaction of molecular pairs determines the band structure^(2.47,2.53). Earlier studies using the *extended Hückel* method were also carried out to deduce the interaction of different kinds of central metal atoms with the phthalocyanine rings^(2.45).

The band formed from the highest occupied molecular orbitals (HOMO) is called the valence band, while the lowest unoccupied molecular orbitals (LUMO) form the conduction band.

Experimental studies for the determining the electrical properties in single crystals of metal free^(2.54) and metal phthalocyanes^(2.55) show that both materials exhibit an intrinsic energy gap of 2.0 eV. This value, which was found by many workers^(2.5,2.42-43,2.56-58) for different sorts of phthalocyanines, gives evidence that it may be the intrinsic band gap for such compounds.

The intrinsic band gap of phthalocyanines may be estimated from the redox potentials in solution. A method which was used by *Turek et al*^(2.51), for the calculation of the band gap in LiPc and LuPc₂, employed the *Lyons equation*^(2.59). Here, the difference in dielectric constant between the

solution and solid states needs to be known. The free energy of solvation of a single ion changes with the change in the *dielectric constant*, ϵ , by the ratio $(1-1/\epsilon_2)/(1-1/\epsilon_1)$. On this basis *Lyon* obtained the following equation,

$$\Delta E = (E_{1/2}^{ox} - E_{1/2}^{red}) + S^+ + S^- \left(1 - \frac{1-1/\epsilon_2}{1-1/\epsilon_1}\right) \dots\dots\dots 2.2$$

where ΔE is equal to the thermal activation energy ($E/2$, as two charge carriers are created) for intrinsic conduction in the equation,

$$\sigma = \sigma_0 e^{\frac{-\Delta E}{2kT}} \dots\dots\dots 2.3$$

S^+ and S^- are the free energies of solvation of the ions, ϵ_1 is the *dielectric constant* of the solution in which the redox potential has been measured, ϵ_2 the dielectric constant of the thin film or the crystal, and $E_{1/2}^{ox}$ and $E_{1/2}^{red}$ are the oxidation and reduction potentials which are estimated from the redox potentials in solution(2.59),

$$A + e^- = A^- \quad E_{1/2}^{red} \quad \dots\dots\dots 2.4$$

$$A = A^+ + e^- \quad \Delta E_{1/2}^{ox} \quad \dots\dots\dots 2.5$$

where A is the constituting molecular unit.

Applying equation 2.2 to LuPc₂, LiPc and other compounds, *Turek et al* (2.51) have concluded that the agreement between the experimental activation energies and those calculated from equation 2.2 is very good.

Studies on the electrical properties in α and β forms of CuPc pointed to a similar band gap for both forms which indicate the unimportance of crystal structure(2.60-61).

Studies on the electrical properties (2.5,2.9,2.13) show that oxygen and other impurities play a significant role in lowering the value of the band gap .

The effect of conjugation on the band gap was studied and the best illustration was provided by the two dimensional polymer where band gap values of 0.26 eV have been reported(2.62). The broadening of the optical absorption of the material and its shift into the near infra-red prove that this value is of an intrinsic band gap, since there is a strong similarity between band gap and the first electronic absorption band (2.61).

The influence of the central metal atom and the role of the bridging ligand on the band structure have been studied(2.52,2.63). It was found that for the non-transition central metal atoms the band structure was determined only by the phthalocyanine inter-ring spacing. For larger inter-ring spacing the valence and the conduction bands become narrower while for short inter-ring spacing the bands become broader as shown in figure 2.5.

The phthalocyanine π -orbitals are made up of only the carbon atom p-orbitals which cannot mix with the s and p orbitals of the central metal atoms for reasons of symmetry. Therefore the inter-ring separation will determine the band width. In addition the inter-ring rotation leads to stack slipping which causes narrowing of the bands due to the overall decrease of inter-ring overlap (2.64). For example, the electrical conductivity of NiPcI_{1.0}

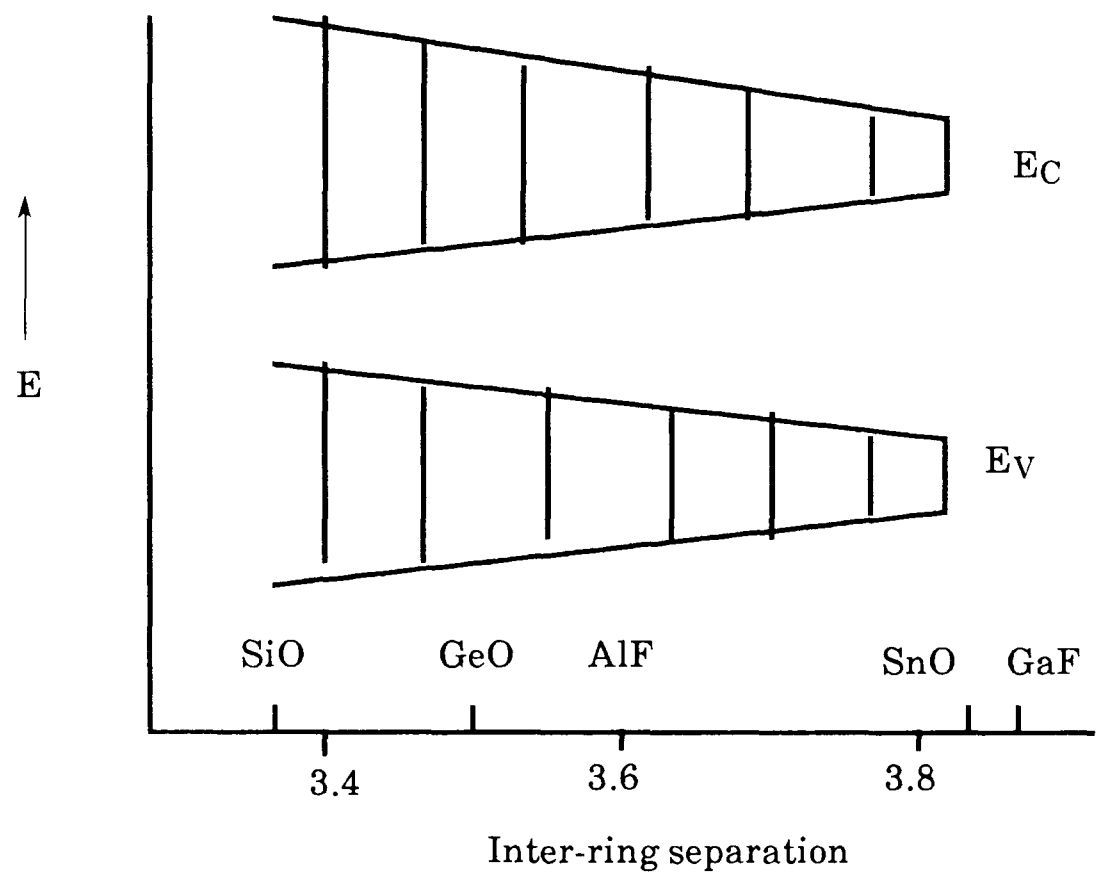


Figure 2.5 : The widths of the bands of phthalocyanines as a function of the inter-ring separation with non-transition elements.

is found to be only slightly greater than that of GaPcFI_{0.93} despite the fact that the inter-ring separation of NiPcI is shorter than that of GaPcFI (3.244 Å and 3.871 Å for NiPcI and GaPcI respectively) which suggests that the inter-ring rotation reduces the inter-ring overlap and thus reduce its electrical conduction (2.63).

For phthalocyanines with transition central metal atoms the band structures are determined by the overlap between metal dxz and dyz orbitals with the π-orbitals of the bridging ligand.

2.9) Mobility of Charge Carriers in Phthalocyanines:

A large number of measurements of the mobility of charge carriers in phthalocyanines have been carried out (2.5). Hall and transient photocurrent measurements have been used to determine the Hall and drift mobilities of electron and holes. In Hall mobility measurements, a sample carrying a current (I) in the x-direction is placed in a perpendicular into a magnetic field (H). The resulting deflection of carriers builds up an electric field in the direction perpendicular to I and H. This effect is called the *Hall effect*. The most important factor to be measured is the *Hall coefficient* (R_H) (2.65) which for n-type materials has the value,

$$R_H = \frac{-1}{n e} \dots\dots\dots 2.6$$

and for p-type materials,

$$R_H = \frac{+1}{p e} \dots\dots\dots 2.7$$

where n and p are the concentration of the electrons and holes respectively. From the formulae, the carrier type (electron and hole) and concentration can be estimated from the sign and magnitude of the *Hall coefficient*. If the conductivity is also known, the carrier mobilities defined by the equation, $\sigma = ne\mu_n$ or $\sigma = pe\mu_h$ can be calculated. The *Hall effect* in intrinsic semiconductors can be accurately measured only if the electron and hole mobilities are significantly different from one another.

The drift mobility (μ_d) is determined by different method. The surface of the material is irradiated to generate electron/ hole pairs, with application of an electric field (E) across the material. The transit time (τ) necessary for the mobile charge carriers to drift under the influence of this field is measured. The drift mobility can then be calculated using the relationship

$$\mu_d = \frac{d}{\tau E} \dots\dots\dots 2.8$$

where d is the thickness of the sample. This relation only applies in the absence of space charge and trapping effects (2.5).

There are many factors which can affect carrier transport in phthalocyanines;

a) Intermolecular overlap:

Because the intermolecular interaction in phthalocyanines is of *van der Waals* type and the separation is $\approx 3.4 \text{ \AA}$, the band is narrow and the mobility low. The strong intermolecular overlap of the π -orbital of the

metal(Cu) with the nitrogen atoms of the parallel arrangements makes the carrier mobility in CuPc higher than that for metal free (2.12,2.66-69).

The effect of the intermolecular interaction can be illustrated by two experimental observations (2.61);

- ① The enhancement of the conductivity, which must be due to enhancement of mobility, by the effect of high pressure (2.70-71).
- ② Spectroscopic studies of cofacially linked phthalocyanines show that the bandwidth decreases with intermolecular separation (2.72-73).

b) Disorder:

The density of imperfections such as, vacancies, dislocations, etc., in typical molecular crystals such as phthalocyanines tends to be high, which leads to a high trap density (2.74-75). This density is higher in polycrystalline materials such as evaporated films and polymeric materials (2.13). Consequently carrier mobility is low due to multiple trapping.

Crystallinity has a large effect on the transport properties of phthalocyanines. Table 2.1 shows the hole and drift mobilities of some phthalocyanines at different crystalline state. It shows that thin film or microcrystalline materials have a lower mobility than that of single crystal. The difference in the drift and Hall mobilities for CuPc (SC) may be due to traps of the order of $10^{13} - 10^{14} \text{ cm}^{-3}$ (2.65).

Reduction of the intermolecular distance and thus enhancement of the intermolecular overlap can be achieved by different approaches;

- ① Synthesis of a two dimensional conjugated polymer in which adjacent phthalocyanines share a benzene ring (2.62). Hall measurements indicate

Compound	crystalline state	Hall mobility cm ² V ⁻¹ s ⁻¹	Ref.	Drift mobility cm ² V ⁻¹ s ⁻¹	Ref.
H ₂ Pc	SC	0.1	39	$\mu_e = 1.2, \mu_h = 1.1$	43
H ₂ Pc	Mc	---	---	10 ⁻² -10 ⁻³ (positive holes are the majority carriers)	58
CuPc	Sc	75	39	7	57
CuPc	TF	---	---	10 ⁻³ -10 ⁻⁴	57

Table 2.1: The hall and the Drift mobilities of some phthalocyanines at different crystalline states. Measured along C' axis. (SC = single crystal, MC = Microcrystalline, TF = thin film)

an enhanced mobility ($40 \text{ cm}^2 \text{ V}^{-1} \text{ s}^{-1}$) which is presumably due to reduction in the intermolecular barriers.

- ② Edge-linking by polymerising phthalocyanines in a plasma discharge (2.76,2.3).
- ③ Cofacial linking using central metals of group III such as Si and Ge within the oxygen bridge (2.77) or transition metals with a bidentate ligand, such as a pyrazine bridge.
- ④ Open shell materials. This effect was first predicted by *Eley* (2.78). It has been studied by *Turek et al* (2.51) using LuPc_2 and LiPc which have free radical character, observed by ESR, indicating strong coupling between molecular units (2.51). X-ray measurements on single crystals of LiPc show an interplanar distance of 3.24 \AA which is smaller than the *van der Waals* value (3.4 \AA) (2.79). This low intermolecular distance gives rise to a high intermolecular interaction via incompletely occupied HOMO band. This effect can be illustrated by a high room temperature conductivity ($2 \times 10^{-3} \Omega^{-1} \text{ cm}^{-1}$) with a low activation energy of 0.2 eV .

c) Effect of Temperature:

The temperature dependence of the mobility (μ_0) is given by,

$$\mu_0 = \alpha T^{-n} \dots\dots\dots 2.9$$

This effect has been found in phthalocyanines with $1.3 \leq n \leq 1.5$ for holes and $1.5 \leq n \leq 1.9$ for electrons in β -form metal free phthalocyanine crystals (2.80). Similar values of n were found by other workers (2.42) along the c -1 axis. These values suggest that the charge transport is controlled by lattice phonon scattering over the studied temperature range (300-600 K) and at high vacuum (10^{-7} torr). The carrier motion depends on the interaction with

the periodic lattice and the scattering by phonons. Hence as the phonon density increases, as a result of the increase in temperature, the mobility will be reduced.

d) Effect of Traps:

Under the influence of shallow electron or hole traps the drift mobility (μ_d) increases with increasing temperature^(2.13) according to the equation,

$$\mu_d \approx \mu_0 e^{\frac{-E_t}{kT}} \dots\dots\dots 2.10$$

where E_t is the depth of the trap, and μ_0 is the trap free mobility^(2.9). The density of traps and their distribution in energy can be determined by measurements of SCLC ^(2.81).

2.10) Electrical Properties of Phthalocyanines:

The semiconducting properties of phthalocyanines were first observed in the late forties by *Eley*^(2.82) and *Vartanian*^(2.83). *Eley*^(2.84,2.78) proposed that the conductivity in phthalocyanines is due to thermal or optical excitation of the π -electrons from the (HOMO) to the (LUMO) molecular orbitals. The electrical conduction will then be either by the migration of these excited electrons or by the resulting holes. It is also known that under illumination by light, excitons (non-conducting) are created which can diffuse a considerable distance through the crystal before dissociation into a pair of charge carriers^(2.5).

Phthalocyanines have smaller mobilities than inorganic semiconductors by about three orders of magnitude^(2.6). Though the applicability of the band model for phthalocyanines has been challenged as shown in the previous section, it is still very convenient for the discussion of phthalocyanines. Furthermore, the mobility in the b^{-1} direction of the reciprocal lattice is in the limit as suggested by *Meier* ^(2.13) for narrow band conduction.

The intrinsic electrical properties of phthalocyanines are very rarely observed due to the effect of ambient gases and impurities. The conditions for intrinsic conduction are normally high temperature, high vacuum and high purity. (High purity can be achieved by successive sublimation). The energy gap in the intrinsic domain is 2.0 eV^(2.55).

The crystallinity has a large influence on the electrical properties of phthalocyanines. Monocrystalline materials contain a relatively small number of shallow traps within the band gap, and show higher carrier drift mobilities compared to the polycrystalline disordered materials^(2.5). On the other hand monocrystals are less permeable to gases compared to amorphous materials such as thin films and consequently they are more chemically pure.

The stacked metallophthalocyanines are ideal for electrical transport since the molecules in this structure are close enough to allow π -orbital overlap which provides a pathway for carrier delocalisation and migration. These materials can also be oxidised by doping to give partially filled bands.

The conduction pathway in phthalocyanines can be through the conduction band formed by inter-ring π -orbital overlap. It was found that for $(MPcF)_n$, where $M = Ga$ and Al (2.26) and a series of $(MPcO)_n$ where $M = Si, Ge, Sn$ (2.15) the conductivity increases as the central metal atom size decreases which provides evidence that the conductivity pathway can be through the conduction band formed by inter-ring π -orbital overlap. Furthermore, ESR studies suggest that partial oxidation of the phthalocyanine rings is induced by halogen doping, and results in greatly enhanced conductivity. Therefore, it would appear that the band (HOMO) formed by overlap of the phthalocyanine rings is the factor which is responsible for the electrical conduction in halogen-doped materials (2.48).

For phthalocyanines with a central transition metal atom, charge transport proceeds along the one dimensional chain of metal atoms through the dz^2 band(2.85). The evidence for this comes from the studies which show that the central metal atom is a centre of oxidation by iodine in $CoPc$. In addition the room temperature conductivity of $CoPcI$ is comparable with that of the doped $PtPc$ conductors despite the fact that the $Co-Co$ distance (3.12 \AA) is much greater than the $Pt-Pt$ distance (2.95 \AA)(2.86). Furthermore, the temperature dependence of the conductivity of $CoPcI$ is non-metallic compared to the isostructural $NiPcI$, which is metallic(2.87). Another example for such an electrical pathway can be illustrated by using an organic bridging group containing π -electrons, such as $(CoPcCN)_n$ and $(FePcCN)_n$ which allows delocalisation along the chain, resulting in room temperature d.c conductivities around $10^{-2} \Omega^{-1} \text{ cm}^{-1}$ despite the fact that big bridging groups increase the ring-ring separation. This conductivity is in the same range of conductivity as in the iodine doped phthalocyanines (2.85).

The effect of ambient gases on the properties of metallophthalocyanines has been studied by ESR which suggests the existence of free electrons. This signal is reduced by purification or heating under high vacuum, which suggests that adsorbed gases, mainly oxygen, or impurities due to contamination during preparations are responsible for this signal^(2.88-89).

When oxygen is incorporated into phthalocyanines the main equilibrium which must be considered^(2.5) is ;



The other possibility is that the complex MPc,O_2 may act as an electron acceptor



The effect of oxygen on a single crystal of CuPc has been studied by *Heilmeyer and Harrison*^(2.55). They show that in the presence of oxygen the crystal had an activation energy of 1.62 eV corresponding to the energy needed to liberate free charge carriers from the $(MPc)^+ , O_2^{\cdot -}$ complex, while in the absence of oxygen an intrinsic value of about 2.0 eV was found which is assigned to the intrinsic generation of the charge carriers.

Other studies show that oxygen can enter single crystals of phthalocyanines by thermal diffusion, and it was found that the rate of diffusion of oxygen inside a single crystal of PbPc at 242 °C is $7.2 \times 10^{-9} \text{ cm}^2 \text{ s}^{-1}$, i.e., over 50 μm in about one hour ^(2.,90). To achieve the intrinsic energy gap in phthalocyanines requires a careful purification and then annealing

at high temperature(normally above 100 °C) under high vacuum (10^{-6} Torr) for CuPc (2.60,2.55).

The doping of phthalocyanines by halogens such as iodine and bromine causes the formation of the known compound, $[(MPcX)I_y]_n$, which exhibits a decrease in the overall resistivity by many orders of magnitude (table 2.2) and the thermal activation energies by approximately fifty fold. This phenomenon has been recognized for a long time and can be followed by ESR(2.91). Raman spectroscopic studies have shown that the doped iodine is in the form of I⁻³ and I⁻⁵ (2.54).

Other agents may be used as dopant for phthalocyanines such as quinones and their derivatives(2.92), AsF₅(2.92), XeF₂(2.93) and others (2.94-95), which tend to oxidize or reduce phthalocyanines.. Auto-doping by using a mixture of two different metallophthalocyanines has also been investigated (2.96).

The effect of peripheral substitution of phthalocyanines has been studied and was found to give electrical conductivities which are similar to those of the peripherally unsubstituted polymers. On doping, they reach limiting values of 10^{-3} - 10^{-4} Ω^{-1} cm⁻¹ for M=Si and Ge respectively and show no significant variation with doping procedure. This may suggest that the measured conductivities are dominated by macroscopic properties such as grain boundaries(2.97).

Experimental results show that there is a correlation between electronic conductivity in phthalocyanines and their catalytic activity. It was found that:

Compound	σ ($\Omega^{-1} \text{ cm}^{-1}$)	Ref.
$[\text{AlPcF}]_n$	$< 10^{-7}$	16,26
$[\text{AlPcFI}_{3.4}]_n$	0.59	
$[\text{GaPcF}]_n$	$< 10^{-9}$	16,26
$[\text{GaPcFI}_{2.1}]_n$	0.15	
$[\text{SiPcO}]_n$	3×10^{-8}	5,99,100
$[\text{SiPcOI}_{1.55}]_n$	1.4	

Table 2.2: Effect of doping on a polycrystalline phthalocyanines

- ① The selectivity of the catalysis by phthalocyanine depends on the type of conduction. For example, decomposition of formic acid (HCOOH) is catalysed more strongly by n-type polymeric CuPc than by p-type monomeric CuPc (2.13)
- ② The catalytic activity ($\log K_a$) is a linear function of the thermal activation energy (E_a) (2.98),

$$\log K_a \approx \frac{1}{E_a} \dots\dots\dots 2.13$$

e.g., the oxidation of the acetaldehyde ethylene acetal to ethylene glycol monoacetate by Fe-M-polyphthalocyanine (M = Cr, V, Co, Ni, Zn).

- ③ The polymeric organic compounds which are characterised by a relatively high conductivity generally display a higher catalytic activity than the monomeric compounds (2.13).

2.11) Applications of Phthalocyanines in Technology:

Phthalocyanines have attracted a great deal of interest for many years for their interesting physical and chemical properties which promise many possibilities in various applications. However, the difficulties in producing a suitable form (film, crystals or fibres) for technological applications has been the main barrier, but this is under intense study.

Oxygen and nitrogen bridged phthalocyanines are insoluble and unsublimable, so previous work has only been carried out on polycrystalline powders. However, the synthesis of soluble polymers can be carried out by substitution of the peripheral hydrogens of the macrocyclic rings. These

may find applications in the deposition of films or in the growth of the crystals from solution.

The effects of gases such as NO₂, O₂, BF₃ and halogens on the electrical conductivity of phthalocyanines which are stable and easily prepared in thin film form, provide the bases of sensitive gas detector devices (gas sensors) (2.5, 2.99-101). Lead phthalocyanine is already used for the detection of low concentrations of NO₂, Cl₂, F₂ and O₃ (2.101).

The μ -fluoro bridged phthalocyanines show the most promising future with great potential for device application due to the possibility of sublimation and ability to form pure and high quality thin films. These materials are stable to heat, light, moisture and air although they tend to be oxygen doped. Doping with halogens enhances the conductivity by many orders of magnitude such that metallic behaviour is approached. Thermogravimetric analysis on doped materials shows a loss peak of the halogen with heating (2.93) and conversion back to undoped materials. Therefore, the finding of good reproducibility and long term stability of the doped phthalocyanine would be a great achievement in this field.

2.12) Objectives of this Research:

The objectives of this work can be summarized as follows:

- I) To explore the possibility of synthesising copolymers of cofacially stacked phthalocyanine polymers from AlPcF and GaPcF. The similarity in structure and properties of these materials make them suitable candidates for copolymerisation.
- II) To evaluate copolymerisation as a means of controlling the electrical

properties and introducing dopants.

- III) To study the frequency dependence of a.c conductivity as a measure of the presence of localised state near the *Fermi level*.
- IV) To compare the behaviour of different samples from evaporated films and compactions to give indications of the importance of crystallinity and disorder.
- V) To evaluate the materials for use in devices in collaboration with other workers.

CHAPTER THREE

EXPERIMENTAL TECHNIQUES

3.1) Electrical Conductivity:

The d.c. and a.c. electrical conductivity measurements were carried out on three forms of sample:

a) Compactions:

5 mm diameter pressed pellets from finely ground polycrystalline powder were prepared by using a *Carver die*. Thicknesses of 2-3 mm (measured by using a *travelling microscope*) were obtained by a 10 MPa operating pressure.

Electrodes were painted onto each face of the pellet using *silver loaded electrodag*. To ensure equality of electrode areas, the whole face was covered and great care was taken to prevent paint coating the sides of the pellet. Electrodag has good adhesive properties and it was possible to attach *Kynar* covered thin copper wire (0.5 mm diameter) to each face using the paint. The two wires were then supported by two small *Teflon clamps* (figure 3.1a) which were used to prevent thermal and mechanical strain on the wires. The pellets were then left to dry before mounting in the cryostat.

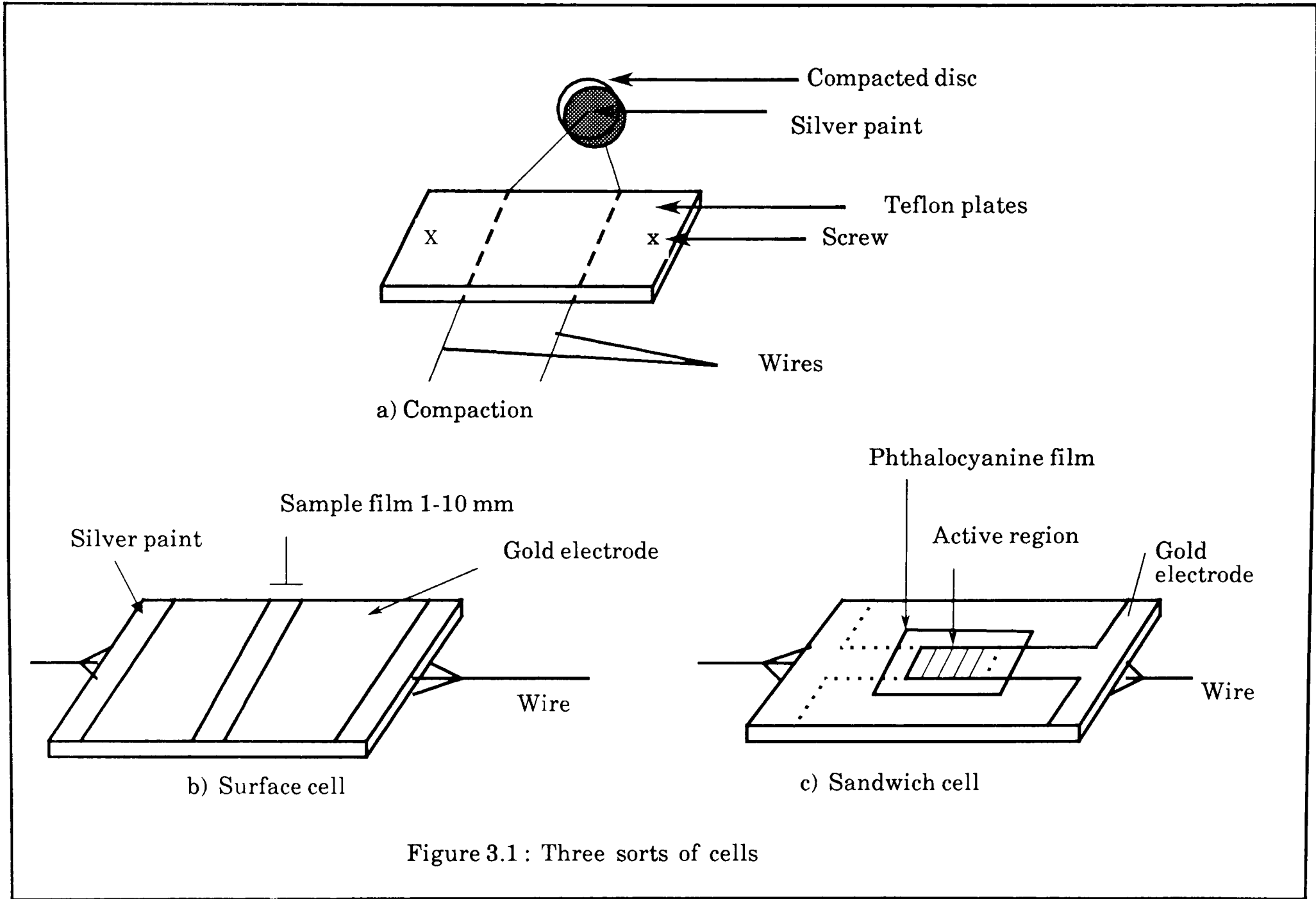


Figure 3.1 : Three sorts of cells

b) Surface Thin Films:

These films were prepared on glass or ceramic substrates ($1 \times 2 \text{ cm}^2$), which had been cleaned by immersing in chromic acid overnight and rinsing with distilled water many times, then drying in warm air. Due to their high resistance, these materials are suitable as substrates for conductivity measurements.

Gold electrodes were evaporated onto the film in the evaporation unit (Figure 3.2). By the use of appropriate masking, the ends of the films were coated with two electrodes of 400 \AA thickness with separation of 1-10 mm. *Kynar* covered thin wires were attached to the back of the substrate using *Araldite adhesive*. The exposed wires were then connected to the gold electrodes by silver paint. The use of the *Araldite adhesive* prevented the electrodes from peeling off due to thermal or mechanical strain; see figure 3.1b.

Thin surface films of AlPcF, GaPcF and the copolymer were prepared for iodine doping purposes in a similar way.

c) Sandwich Films:

These films were prepared on glass ($2 \times 2 \text{ cm}^2$), first cleaned by water with brushing to remove any tiny glass or dirt particles and left in chromic acid overnight, then rinsed with distilled water, dried in warm air and finally blown with a strong flow of nitrogen.

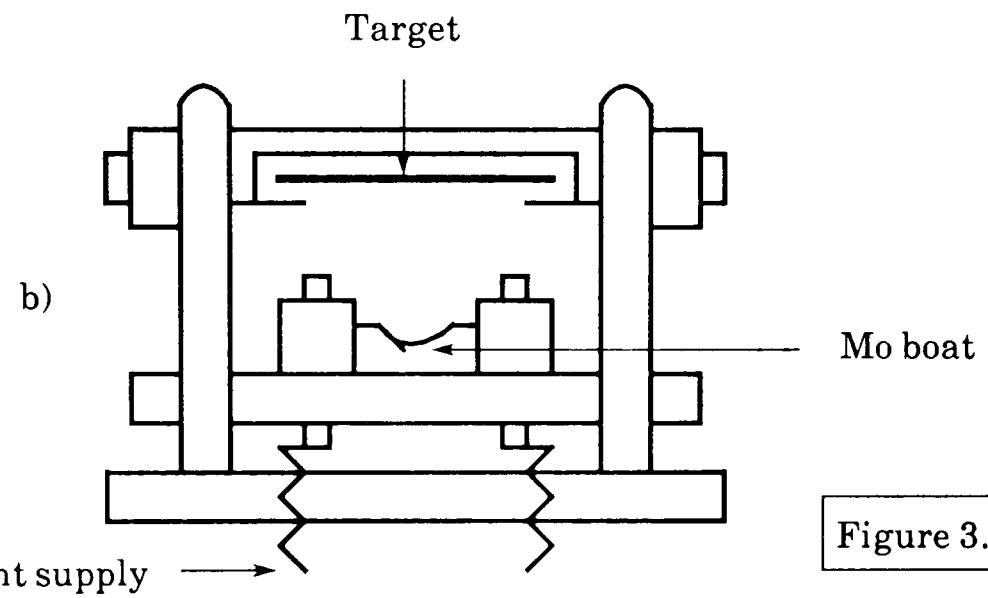
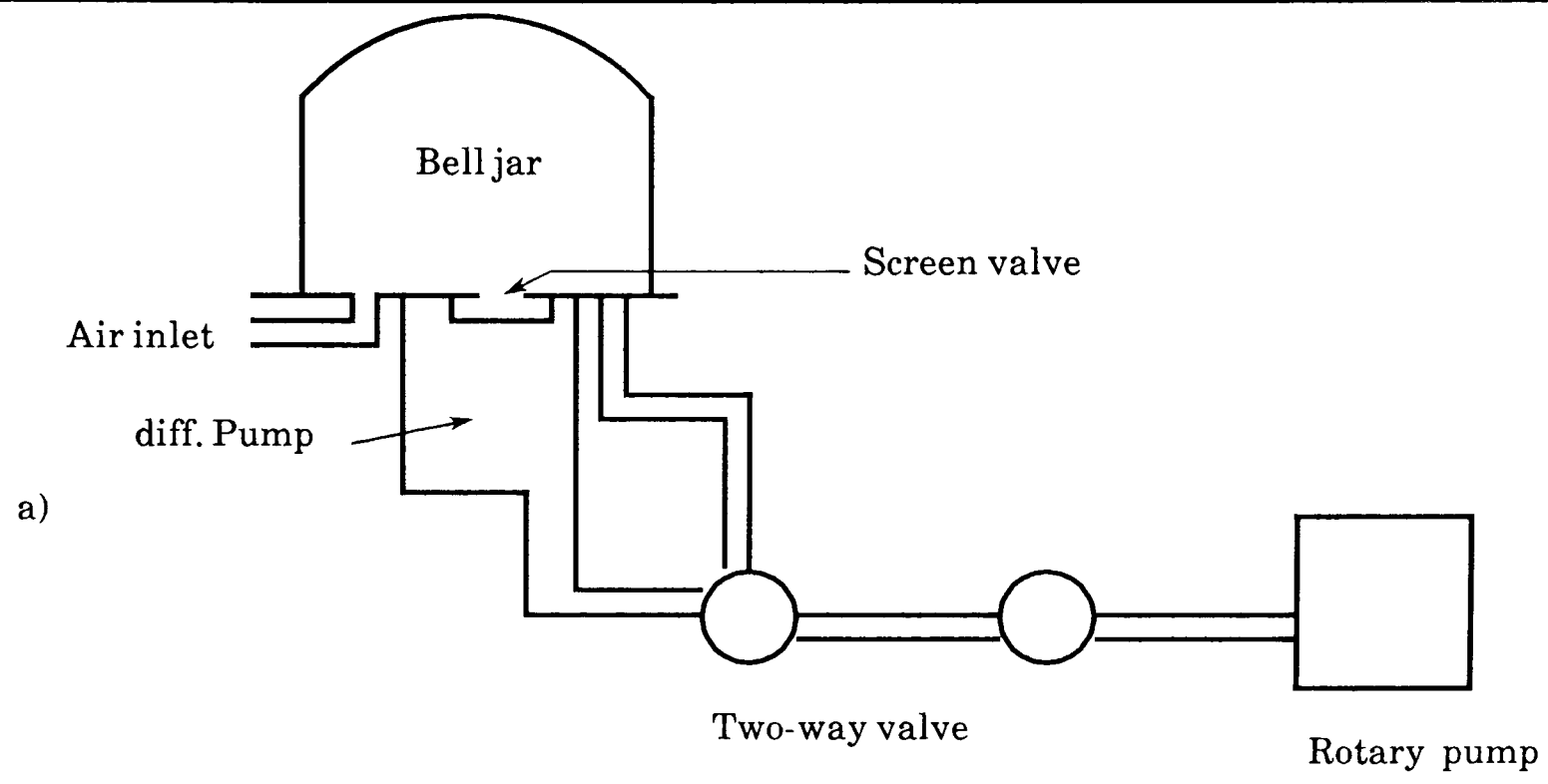


Figure 3.2: The Evaporator

The first gold electrode, of 400 Å thickness, was evaporated onto the glass surface using a T-shaped mask with stem width 0.5 cm (figure 3.1c).

The sample film, of thickness 1-2 μm, was then evaporated over the first gold electrode using another suitable mask (circular or square). The second gold film electrode (thickness of 400 Å) was evaporated over the sample film using the first mask in the opposite direction. The two electrodes overlapped at the stem region, so that the electrode active region was $0.5 \times 0.5 \text{ cm}^2$.

Because the conductance of the sandwich cell of AlPcF is higher than $10^{-4} \Omega^{-1}$, which is the highest conductance that can be measured by the 1621 precision capacitance measurement system, the electrode dimensions were changed to give a lower cell constant and hence a lower conductance. The cell was prepared using a mask of 1 mm width made of razor blades for evaporating the gold electrodes (400 Å thick). The AlPcF film (1 μm) was evaporated over the first gold electrode using a square or circular mask. The upper gold electrode was evaporated over the sample film by placing a mask perpendicular to the first gold electrode (figure 3.3a). This gives a higher resistance cell, suitable for measurement with the capacitance bridge. Care was taken to ensure the continuity of the upper gold electrode.

Discontinuities tend to arise due to the thickness of the first gold electrode plus the sample film, compared to the upper gold electrode as shown in figure 3.3b. A discontinuity causes a reduction of the capacitance from about 1000 pF, which is expected for a sandwich cell, to about 1.0 pF which is a capacitance of the surface cell. This may lead to the conclusion that the capacitance may only be between positions 1 and 2. The continuity

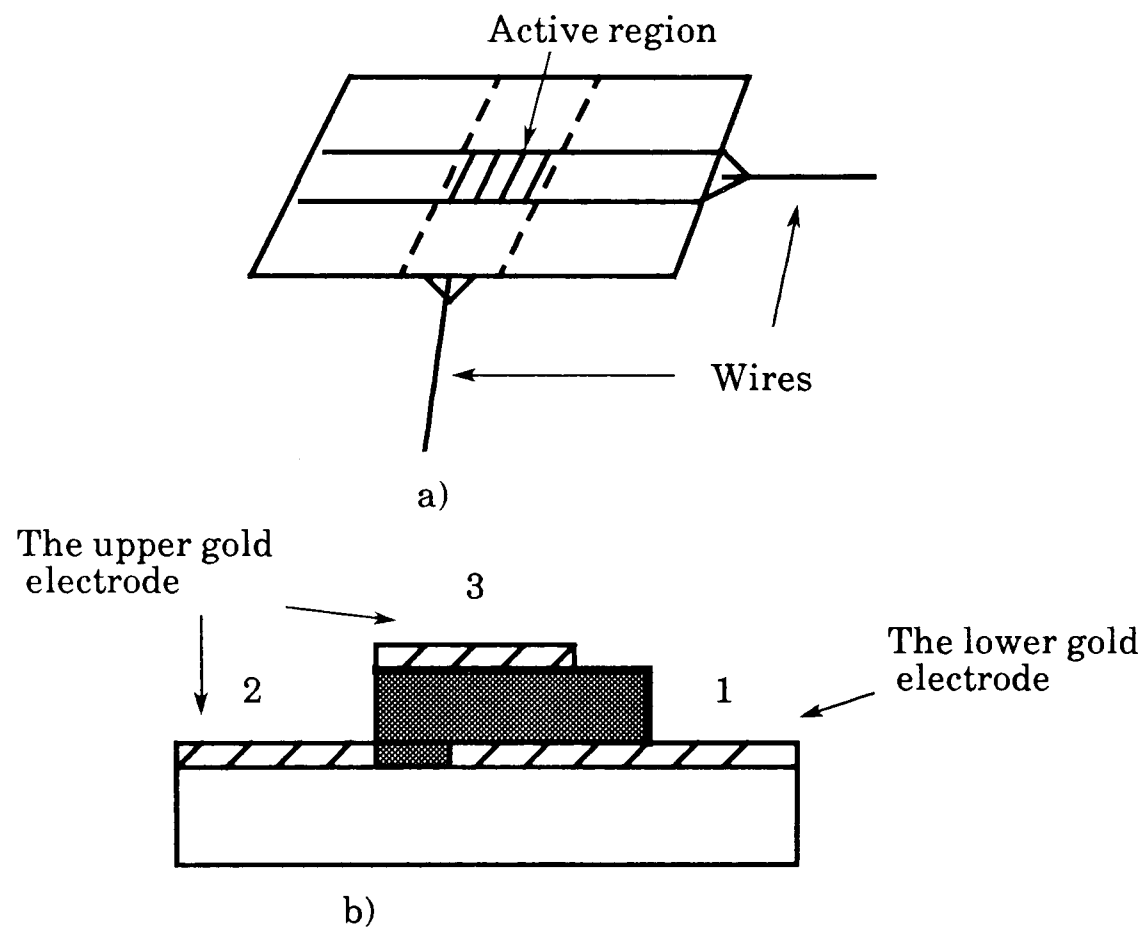


Figure 3.3: a) Crossed sandwich cell b) The discontinuity in the sandwich cell

of the electrode can also be examined by the measurement of the resistance between point 2 and 3.

Some difficulty was encountered in achieving good electrical continuity between the part of upper electrode deposited on the substrate(position 1) and that part deposited on the sample (position 3). Good sandwich cells were easily identifiable on measurement of their capacitance. These problems were greatly reduced by;

- ① Careful location of the evaporating source to avoid any shadowing by the edge of the sample film.
- ② The use of a mask which had bevelled edges on the underside in order to give a more gradual decrease in thickness at the edge of the phthalocyanine film.

A *Kynar* covered thin copper wire(as in the case of the surface cell) was attached to the back of the substrate using *Araldite glue* and the exposed wires then connected to the gold electrode by silver paint.

3.1.1) Purification of Phthalocyanines:

The materials studied, fluoro and chloro phthalocyanines, in addition to the copolymer, were insoluble in known phthalocyanine solvents. They contained considerable amounts of impurities which were difficult to remove by conventional methods.

Kenney et al (3.1) and other workers (3.2-4) have purified phthalocyanines by vacuum sublimation and gradient sublimation. *Entrainment sublimation* has also been used for phthalocyanine purification (3.5).

In this work phthalocyanines were purified by *entrainment sublimation* as a simple and effective technique. An *entrainment sublimer*, based on the design of *Wagner et al* (3.5), was set up by *Dr. C. Davies*, of this laboratory and is shown in figure 3.4. It consists of a solid copper tube, 50 cm long, with an internal bore of 3 cm. It is heated at one end by a pair of band heaters connected to two variacs and cooled by water at the other end. The apparatus is fitted in an asbestos housing and is thermally insulated by *Kieselguhr*. A series of 5 small holes along the length of the copper tube allow a *chromel-alumel* thermocouple to be inserted to measure the temperature gradient. A pyrex glass tube is placed inside the copper block and the material to be purified (1-2 g) is put at the end of a glass tube inside the pyrex tube. The phthalocyanine is positioned so that it is between the two heater bands. A nitrogen flow is drawn through the sublimer by a rotary pump fitted with a flow meter, and a needle valve is used to control the flow rate. The pressure of the system is measured by a *Pirani gauge* next to the flow meter. A liquid nitrogen trap is used to prevent the more volatile impurities from contaminating the pump.

In a typical experiment a nitrogen flow rate of $20 \text{ cm}^3\text{s}^{-1}$ was used after evacuating the system to about 2 Torr. The temperature was increased gradually by incrementing the variacs until the hot end reached the required temperature; this was maintained for 2 to 3 hours to get complete sublimation. The heaters were then turned off and the system allowed to cool with the nitrogen flowing. Then the glass tube was removed and the section containing the phthalocyanine cut out. The sublimed material was then scraped off the glass using a spatula.

A typical entrainment sublimation result is shown in figure 3.4b. The ALPcF which had been purified by chemical methods was a very fluffy, deep

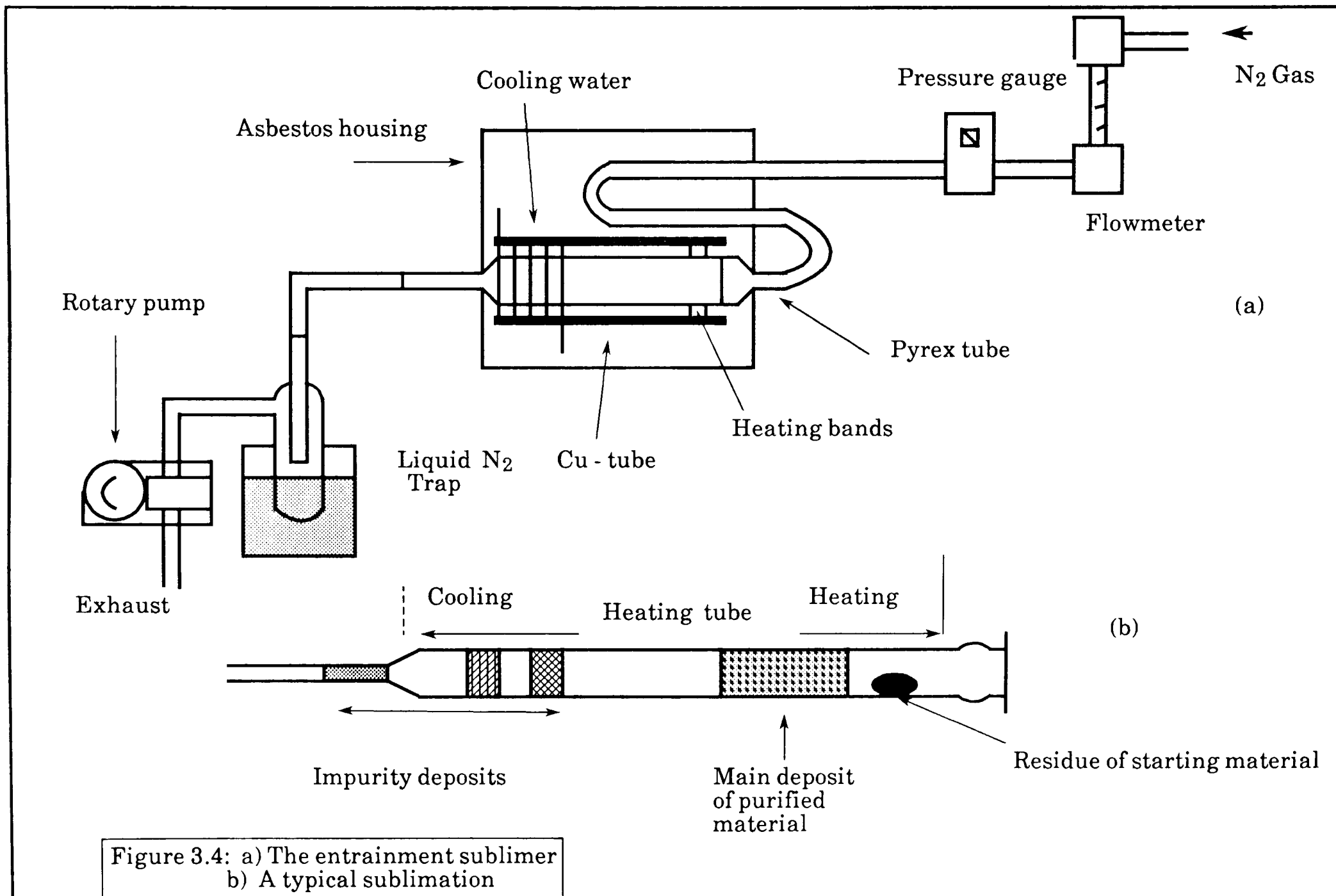


Figure 3.4: a) The entrainment sublimer
 b) A typical sublimation

blue crystalline sublimate, whereas the purified GaPcF sublimate gave much bigger crystals with a deep purple colour. After passing through the entrainment sublimer the GaPcCl sublimate was highly crystalline in comparison to AlPcF, (both sublimates were deep purple). The sublimation yield was 25-75%, depending on the purity of the starting material. The elemental analysis results of the sublimed materials are shown in table 4.1.

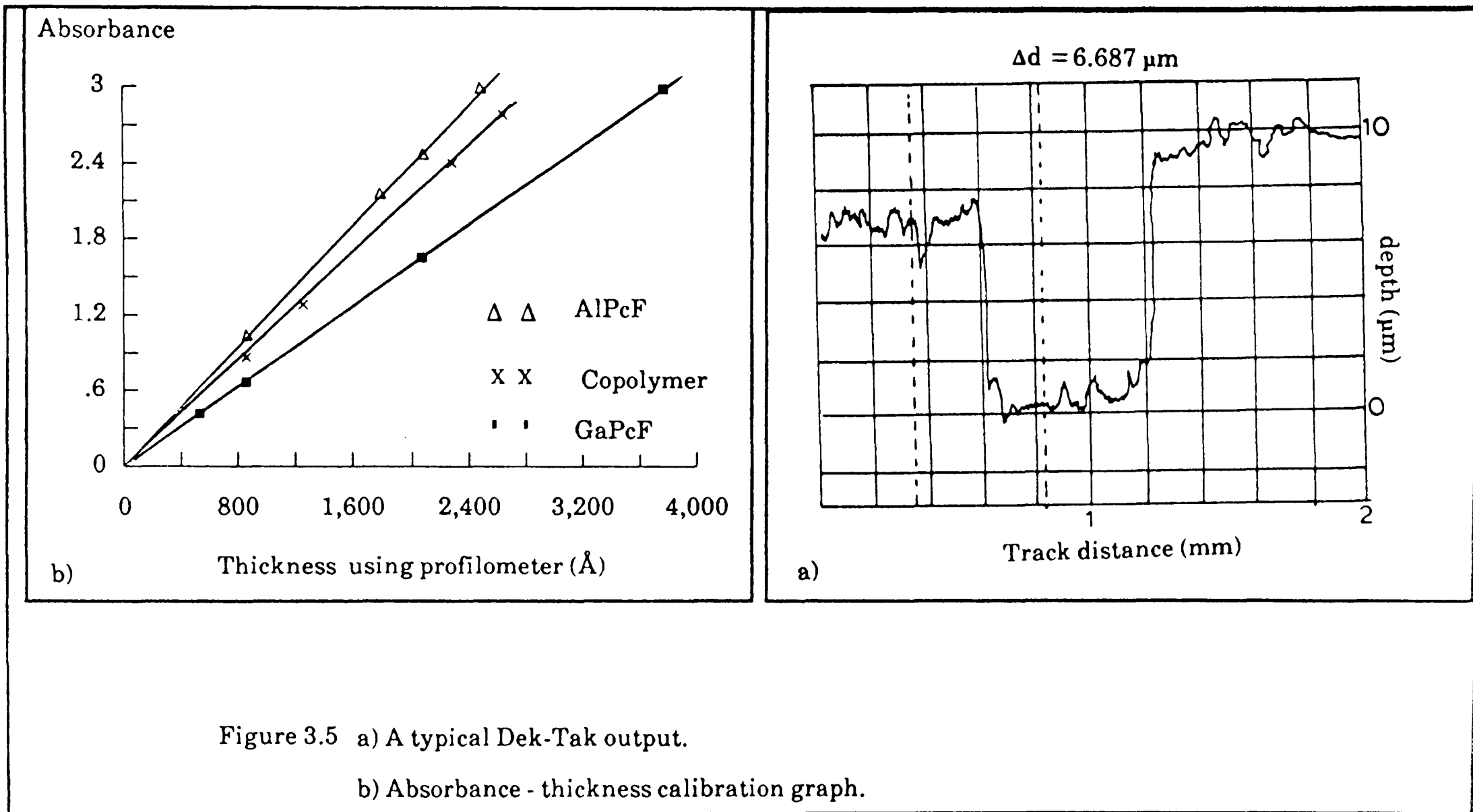
3.1.2) Film Preparation and Thickness Measurements:

All phthalocyanines used in this work were sublimed in a *Metrovac coating unit*. A vacuum of about 10^{-5} torr was achieved using a *silicone oil* diffusion pump backed up by a rotary pump^(3.6).

The films were obtained by the evaporation of the sample from an evaporating system (figure 3.2) using a molybdenum boat for the gold evaporation, or pyrex glass cone fitted with a spiral *Alichrome filament* for the phthalocyanines.

The film thickness was measured by a *Dek-Tak surface profilometer* which consists of a very fine stylus which can be drawn across a surface. Any change in the position of the surface causes a vertical motion of the stylus which is monitored. A typical output is shown in figure 3.5a. A typical graph of thickness against absorbance is shown in figure 3.5b, which permits the measurement of the thickness of thin films spectrometrically.

The film thickness was also measured by an *Edwards film thickness monitor* (3.7), which is based on a measurement of the change in resonant frequency of a quartz crystal as material is deposited onto it. This requires a knowledge of the density and acoustic impedance of the material being



sublimed as well as a correction factor which takes into account the relative position of the monitor head and sample with respect to the sublimation source. For most metals these values are well characterised, but unfortunately the same is not true for phthalocyanines, so the film thickness monitor was calibrated against a *Dek-Tak surface profilometer*. A typical graph for AlPcF is shown in figure 3.6.

3.1.3) D.C. Conductivity Measurement:

The sample holder is made of *Teflon* so that chemical inertness is maintained (figure 3.7). Film samples were first mounted onto square glass slides with glue and then inserted into the slot {1}. One wire from each was plugged into the appropriate socket {a} and the other wires were soldered to the common lead {M}. A *copper-constantan thermocouple* {T} was positioned close to the samples (at the middle of the holder). The holder was attached to a glass tube through which all the leads pass up to the electrical feed through. A metal to glass seal connects the feedthrough to the glass tube. The whole assembly was then placed inside the cryostat using a B34 glass joint. A glass ball joint on the end of a side arm allows the sample holder to be connected to a vacuum frame. Variable temperature conductivity measurement (80-373 K) were possible using a cryostat (figure 3.8). The samples sit inside an inner tube which was wrapped with *Nichrome* wire. A platinum resistance was held close to the outer wall of the glass with tape. The electrical connections pass up the side of the tube and through a glass side arm are sealed with *Araldite* glue. The cryostat was then placed inside a glass Dewar vessel. A soft *Teflon* gasket coated with grease enabled close contact between the head and *Dewar* vessel, and was held with metal spring clips. Polystyrene foam was placed around the *Dewar* vessel to provide further temperature isolation.

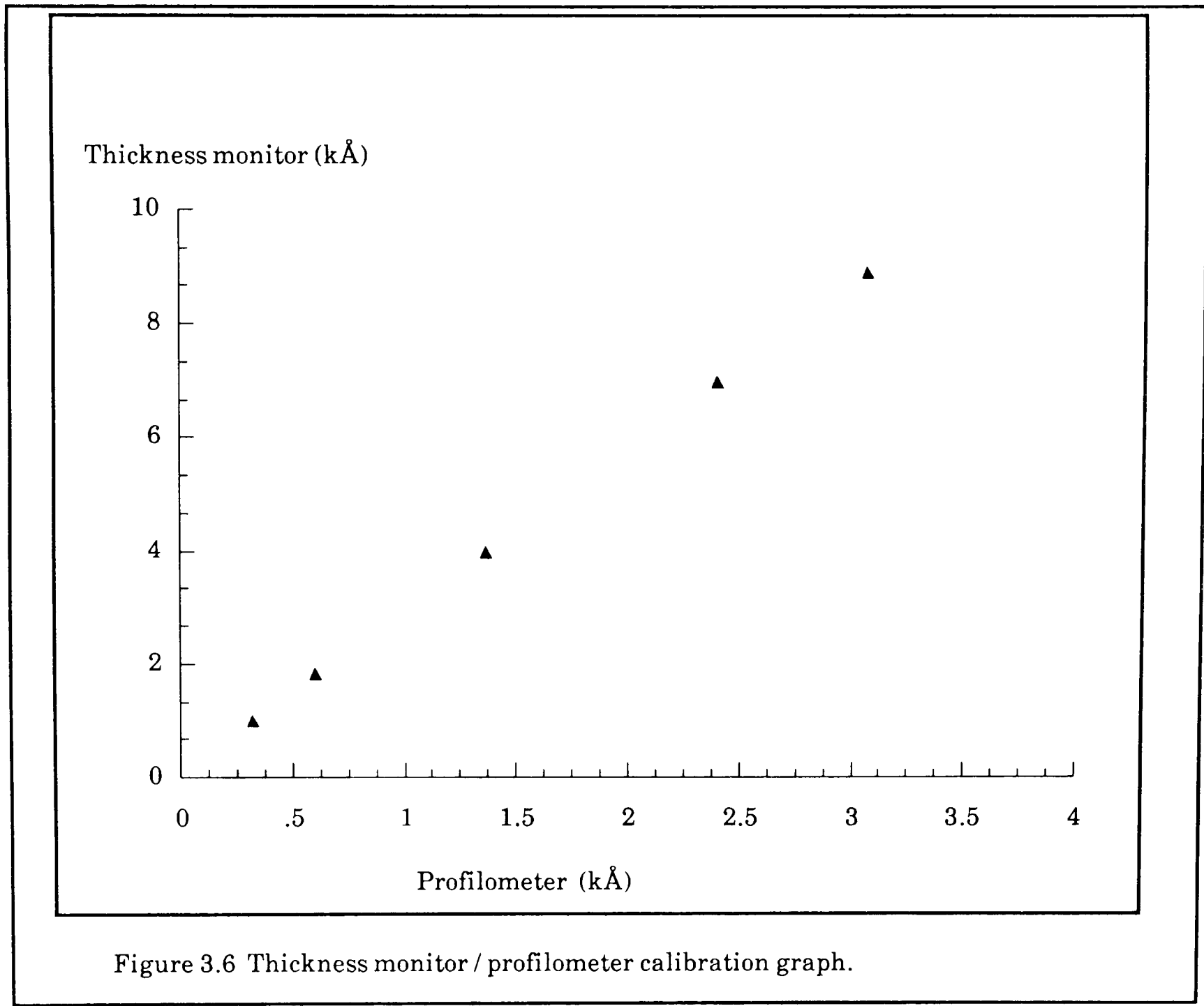


Figure 3.6 Thickness monitor / profilometer calibration graph.

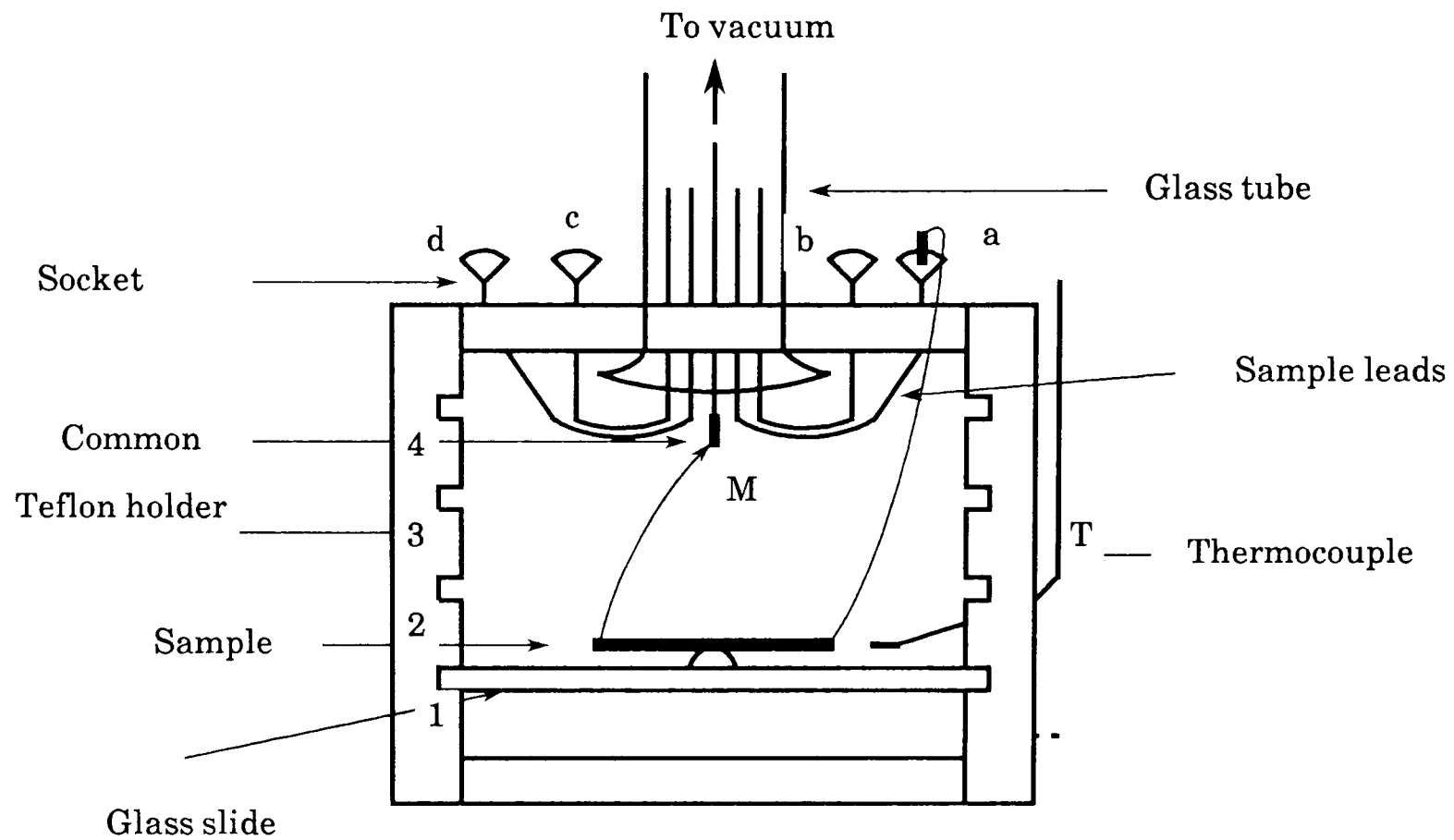


Figure 3.7: The sample holder

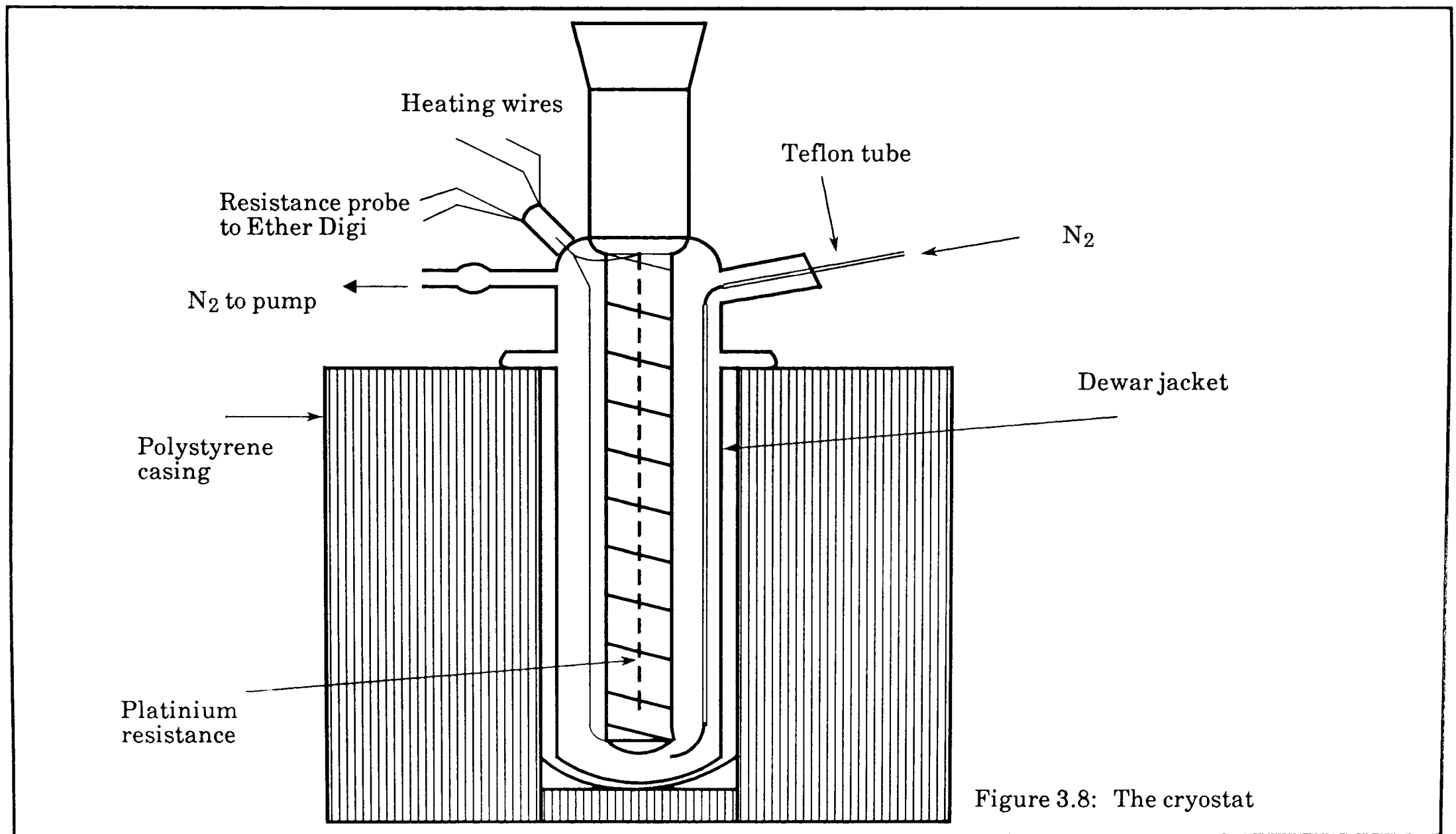
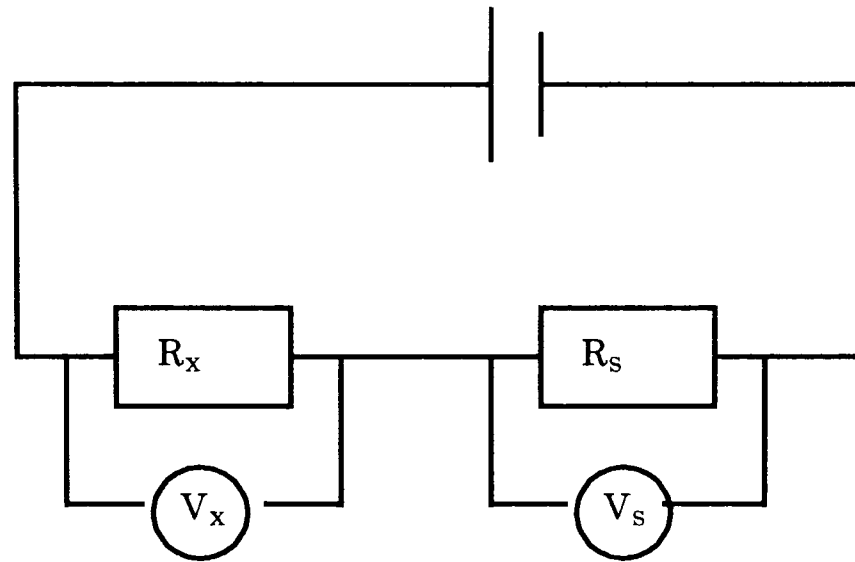


Figure 3.8: The cryostat

The resistance thermometer was connected to an '*Ether digi*' temperature controller. This instrument could switch between supplying current to a variac supply connected to a *Nichrome* wire or to a *solenoid valve* which enabled a flow of liquid nitrogen to be drawn by a rotary pump through the cryostat. Thus by dialling a temperature on the front panel of the '*digi*' the cryostat could be heated or cooled until the setting was reached and then maintained at this value to an accuracy of ± 0.5 °C . The actual temperature of the samples inside the inner tube was constantly monitored by the thermocouple.

3.1.3a) Measurement of Low Resistance Samples:

The method of electrical resistance measurement for low resistance samples of less than $10^7 \Omega$ is illustrated in the circuit diagram, figure 3.9. The voltages across the sample and across the standard resistor, as well as the value of the standard resistor enabled the sample resistance to be calculated. All the leads from the cryostat head were connected to a specially designed switching unit which was interfaced to a *Commodore 3032 PET* computer via a *Keithely 192 DVM* (digital voltmeter)(figure3.10). It was possible to switch between up to eight samples and ten standard resistors. With this unit a program was written which could perform the switching and display the resistance of each sample at any temperature (see appendix 1). Readings were not taken unless the temperature of the cell was constant to within ± 0.5 °C over a period of one minute. The conductivity was measured at different temperatures over the range 183-373 K. The conductivity of each sample was evaluated by inputting the cell constant at the end of the run.



Resistance of unknown

$$R_x = \frac{R_s \times V_x}{V_s}, \quad \sigma = \frac{1}{R_x} \frac{L}{A}$$

Figure 3.9: Circuit diagram for electrical resistance measurements
 R_s and R_x are the resistance of the standard resistor
and the sample respectively, V_s and V_x are the voltage
across the standard resistors and the sample, L and A
are the length and area of the sample.

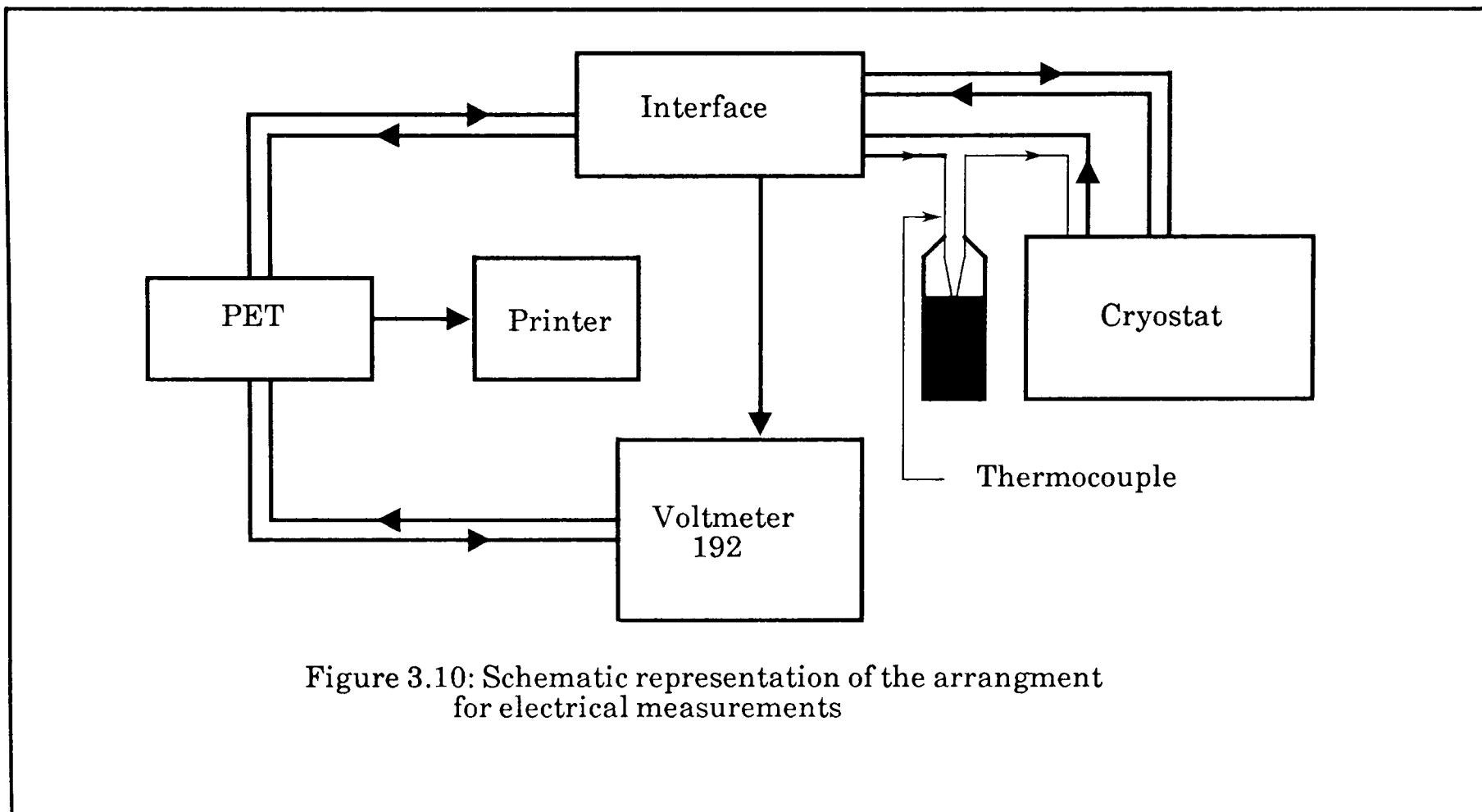


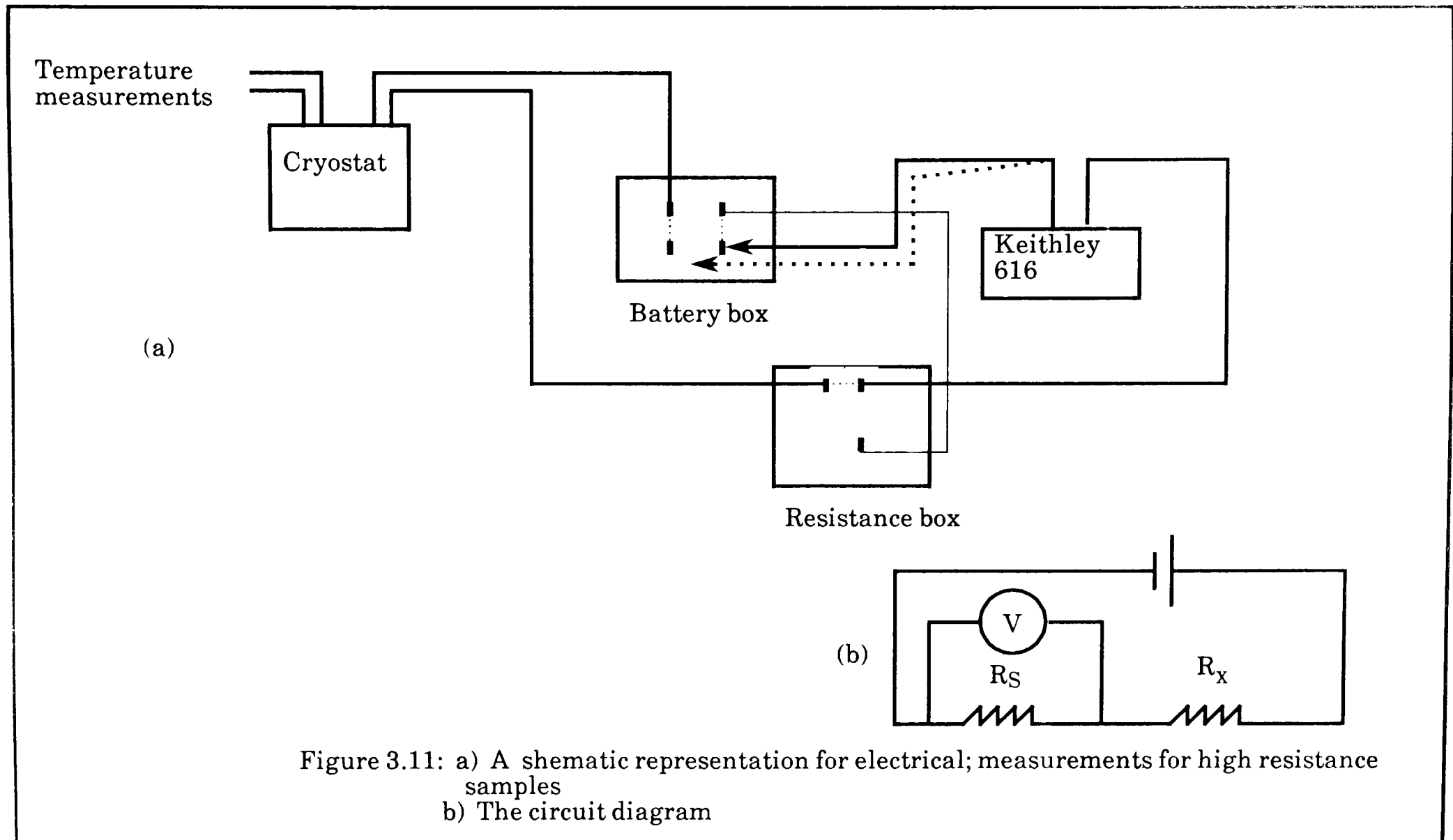
Figure 3.10: Schematic representation of the arrangement for electrical measurements

All the generated data was stored on a floppy disc. Graphs of conductivity against reciprocal temperature were then plotted using a specially written program (appendix 2)..

For the conductivity measurements of the compactions and sandwich cells one of the electrode wires was soldered to the common lead and the other was plugged into the socket{a} (figure 3.8). The glass substrate of the sandwich cell or the Teflon pieces of the compaction were inserted into one of the slots.

3.1.3b) The Conductivity Measurements of High Resistance Samples:

The above instrumentation was limited to samples of resistance less than $10^7 \Omega$ since the input impedance of the *DVM* was only $10^7 \Omega$. Some samples, such as surface films were too resistive, at all temperatures, others become too resistive on cooling . In this case a *Keithley* 616 electrometer (input impedance $2 \times 10^{14} \Omega$ (3.9) was used. Figure 3.11, shows a schematic representation for electrical measurements for high resistance samples. The temperature measurements were made as in the previous method using a program written for this purpose (appendix 3). The resistance of the sample (R_x) and the standard resistor(R_s) were measured and the conductivity was calculated for the temperature range 180-373 K at intervals of about 5-10 °C. The measured resistance never exceeded the resistance of empty cell ($10^{13} \Omega$), or the input impedance of the *Keithley* 616.



3.1.4) A.C. Conductivity

3.1.4a) Sample Preparation for A.C. Conductivity Measurements:

The a.c. conductivity measurements were carried out for the three kinds of sample (compaction, surface and sandwich films). Sample preparations were performed using the method already described, and the conductivity measurements were carried out using the same cryostat and temperature control system.

3.1.4b) Sample Holder and the A.C. Measurement System:

The holder was designed and set up in this laboratory in a similar way to the sample holder of the d.c. conductivity measurements. The glass tube sample holder was designed in such a way that electrical feedthrough consists of shielded cables to minimize the noise created by the induction effects. The whole assembly was enclosed in an earthed and mechanically fixed *Faraday cage* to prevent any external a.c. interference. Samples were measured individually to eliminate any possibility of the induction effect by many samples on each other.

A pair of shielded coaxial leads (1.5 m long) connected to a *General Radio* type A 1621 precision capacitance measurement system (3.10) which is supplied with 1616 precision capacitance bridge, a 1316 oscillator and a 1238 detector. Figure 3.12, shows a simplified diagram for the 1621 precision capacitance measurement system. This system was designed for the precise measurement of capacitors. Its high resolution for capacitance

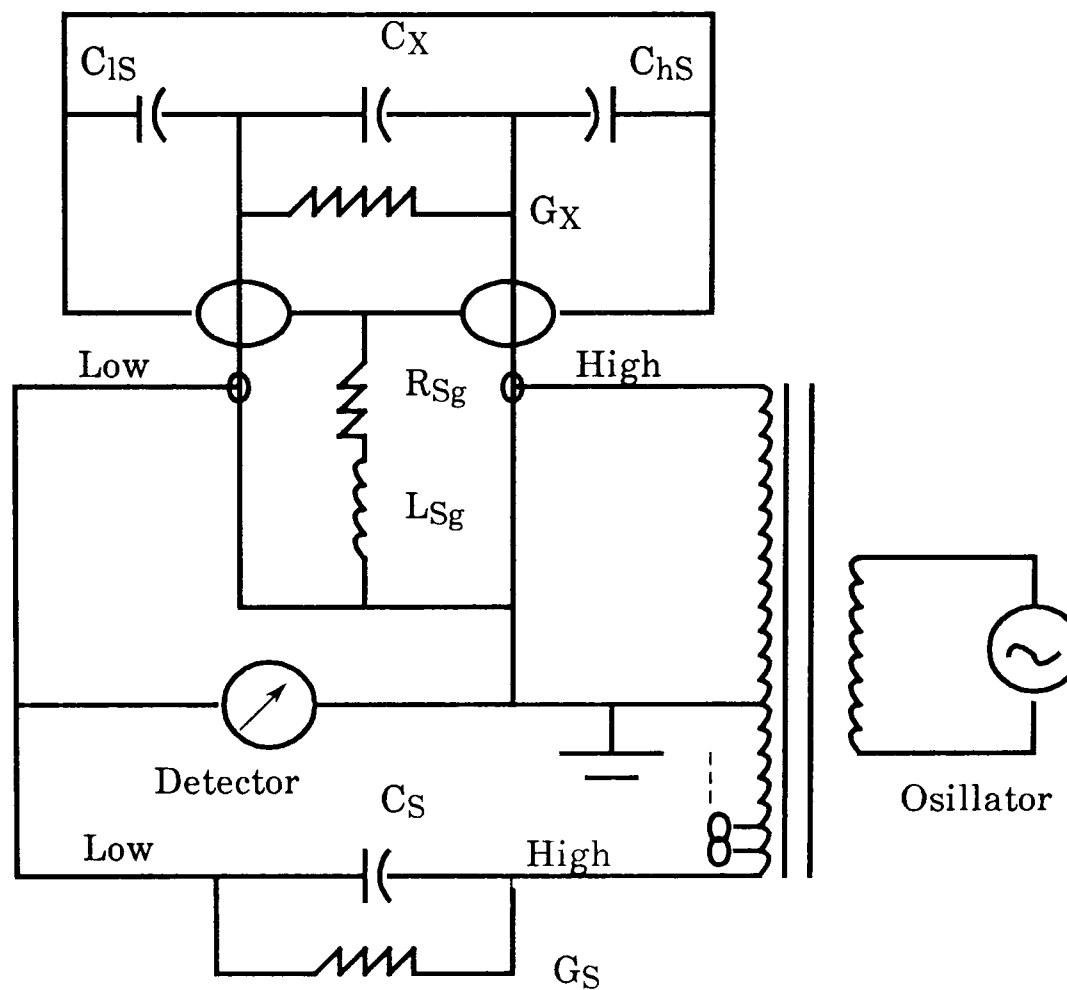


Figure 3.12: Simplified bridge diagram (3-terminal).

and conductance makes it well suited for standard capacitance measurements. It measures either 3-terminal or 2-terminal capacitors.

With the type 1616 precision capacitance bridge, the following ranges of capacitance and conductance can be measured as shown in table 3.1.

The 1316 oscillator in conjunction with the 1621 system, allowed the frequency dials to operate anywhere between 10 Hz and 100 KHz (3.11). The 1238 detector, complements the oscillator and bridge, by setting the frequency to match those of the oscillator (3.12).

In this work the 3-terminal method for capacitance measurements was used over frequency range 0.5 to 100 KHz , *Audio frequency range*. The 3-terminal measurement evaluates the direct capacitance and conductance. Shielded cables were used to connect the terminals to the capacitor (sample).

3.1.4c) Basic Bridge Circuitry:

For higher accuracy, resolution and stability in capacitance measurements at audio frequencies, a bridge with *transformer ratio arms* working in a similar way to the basic bridge (figure 3.13a) was used(3.10,3.13). The advantages of the *ratio arms* in a bridge are that higher accuracies can be obtained and that these ratios are virtually unaffected by time, temperature or voltage.

Figure 3.13b, shows a simple capacitance bridge with *transformer core* and a primary winding (N_p) connected to the generator. The ratio of the open-circuit voltages induced in the two secondary windings (N_s and N_x) is

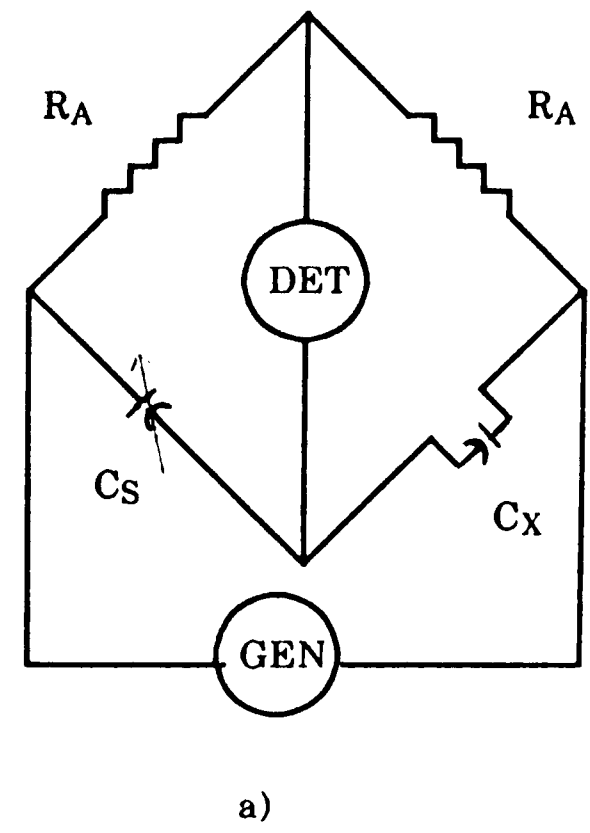
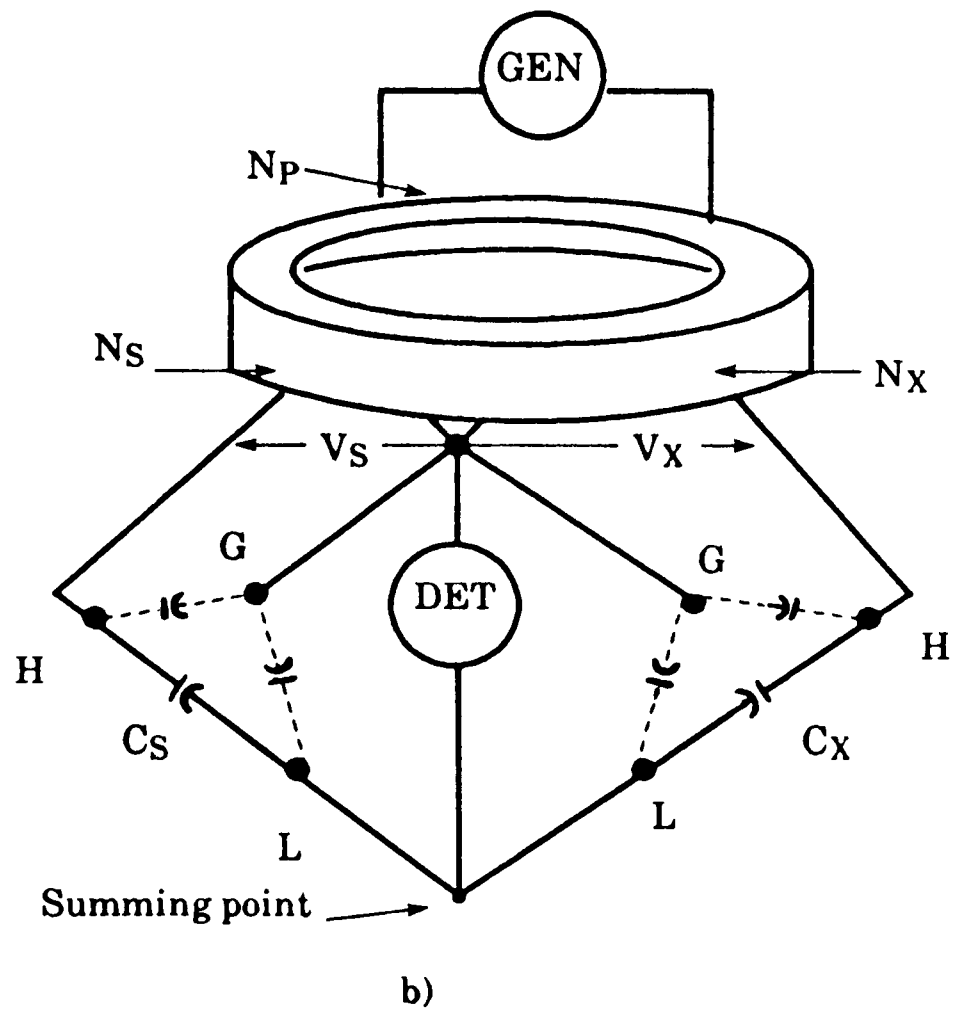


Figure 3.13: a) An elementary capacitance bridge with transformer ratio arms.
 b) An elementary capacitance measuring bridge.

equal to the ratio of the number of the turns. The two transformer secondary windings are used as the arms of the capacitance bridge with standard capacitor, C_S , and the unknown, C_X , as the other two arms in a conventional four-arm bridge network. The condition for balance or zero detector current, is shown to be:

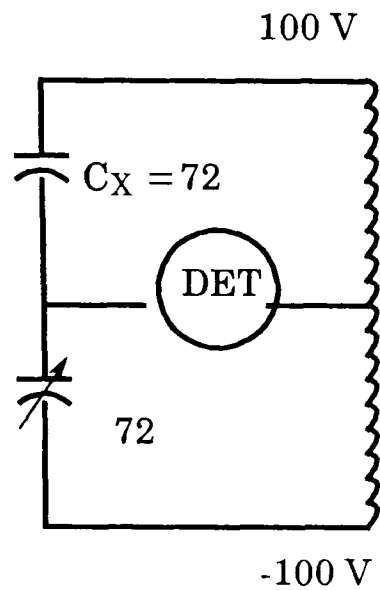
$$V_S C_S = V_X C_X \quad \text{therefore} \quad \frac{C_X}{C_S} = \frac{N_S}{N_X} \quad \dots\dots\dots 3.1$$

This balance condition is not affected by the capacitances shown from the H and L terminals of C_S and C_X to the terminal G connected to the junction of the ratio arms, where G is the guard point in the bridge.

In three terminal capacitance measurement, the bridge measures only the direct capacitance, C_X , of the unknown in terms of the direct capacitance, C_S , of a standard, where all capacitances to G from H or L are excluded.

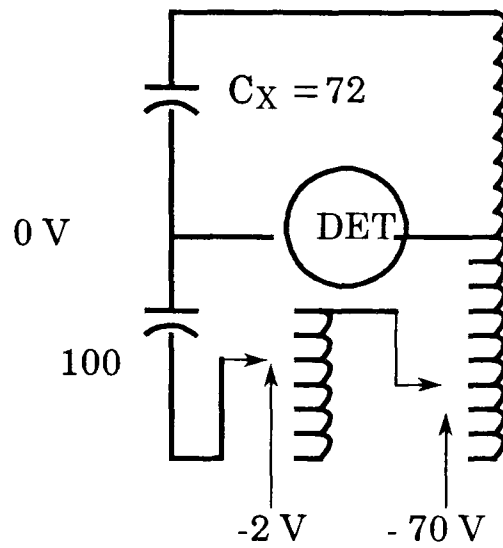
Figure 3.14 shows the way of balancing a simple *transformer-ratio capacitance bridge* on which the 1616 bridge is based (3.10). For simplicity the generator and primary winding are not shown. The two secondaries have 100 turns each, with one volt applied per turn. The capacitance in the unknown arm is assumed to be 72 pF.

Figures 3.14a and 14b show two ways of balancing the bridge. In figure 3.14a the two arms are equal and the bridge is balanced in the conventional way. In figure 3.14b, the standard capacitor is fixed at 100 pF and balanced against the 72 pF "unknown" by connection of the standard to 72 V obtained from suitable taps on the transformer windings.



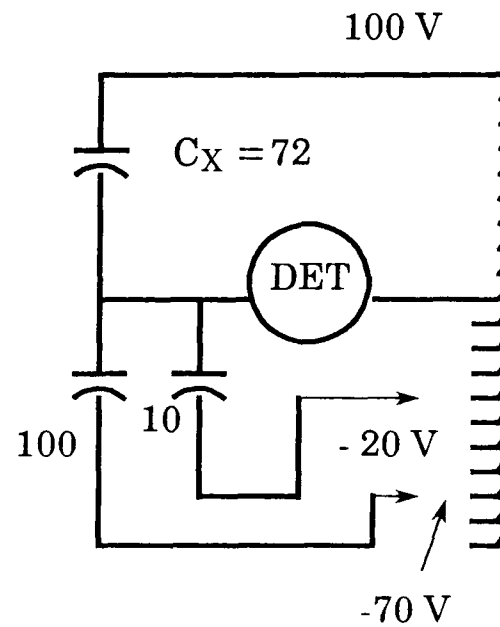
a)

Fixed ratio
variable capacitor



b)

Multiple dividers
single fixed capacitor



c)

Single Divider
multiple fixed capacitors

Figure 3.14: Circuitry for three methods of balancing a transformer ratio capacitance bridge

	Terminal	Range
Capacitance	2-terminal	0.1 aF \rightarrow 10 μ F (10 ⁻¹⁹ \rightarrow 10 ⁻⁵ F)
	3-terminal	0.1 aF \rightarrow 1.0 μ F (10 ⁻¹⁹ \rightarrow 10 ⁻⁶ F)
Conductance	2-terminal	100 a Ω^{-1} \rightarrow 1000 μ Ω^{-1} (10 ⁻¹⁶ \rightarrow 10 ⁻³ Ω^{-1})
	3-terminal	100 a Ω^{-1} \rightarrow 100 μ Ω^{-1} (10 ⁻¹⁶ \rightarrow 10 ⁻⁴ Ω^{-1})

Table 3.1: Conductance and capacitance ranges

In figure 3.14c, on which the 1616 capacitance bridge is based, a 100 pF capacitor is connected to the 70 V tap and a 10 pF capacitor to the 20V tap. The resulting current balances that of the 72 pF "unknown".

In the 1616 bridge, there are 12 capacitance standards, one for each multiple of 10, from 100 nF down to an effective value of 1 aF and there are 5 conductance standards, one for each multiple of 10 from 10 $\mu\Omega$ down to 1 f Ω .

3.1.4d) Procedure for A.C. Conductivity Measurements:

The front panel controls were set as follows.

- I). Frequency (oscillator). Measurements were made at each of the following frequencies: 500 Hz, 1, 3, 5, 7.5, 10, 30, 50, 75, and 100 KHz. This set of frequencies was repeated for each sample temperature.
- II). Frequency (Detector), was adjusted for each oscillator frequency. A maximum response was achieved by matching the frequencies of the detector and oscillator.
- III). Output voltage range set at 15.0 V.
- IV). Time constant set at 0.1 sec. (for immediate response).
- V). Phase shift set at 180. Gain was adjusted to obtain the most sensitive response for each measurement.

To enable the capacitance and conductance introduced by the insulator and the leads the following measurements were made over the full range of frequencies and temperatures used :

- ① Using a surface cell without a sample. This gave the shunt resistance of the cell insulation and substrate, as well as the capacitance between the leads.

② As above, with a 1 mm break in the circuit at the cell. This gave the inter-lead capacitance and the shunt resistance of the lead-throughs.

These measurements showed that measurements of resistance up to $10^9 \Omega$ could be made without significant error, and lead capacitances were normally negligible.

3.2) Thermal Analysis:

A *Stanton redcroft TG-750 thermobalance* system was used. Figure 3.15 shows the block diagram for this system. It consists of:

- I). Electronic microbalance, *CI Mark 2C balance*.
- II). Microfurnace
- III). Temperature programmer.
- IV). Recorder CR 600 with two channels.

(Channel 1 to record temperatures which appear on the chart paper as millivolts, and Channel 2 to record the signal from the balance, which is proportional to the weight).

- V). DTG unit. It is connected to the balance control unit and the recorder.

The derivative channel of the recorder set on one of the sensitive ranges available, 1 mV, set on channel 1 of the recorder. The DTG was set at position 1. The response time of the DTG unit decreases from position 3 to position 1 (3.14).

In this work the weight recorded on channel 2 at 10 mV d.c sensitivity range and the derivative on channel 1 on 1 mV d.c sensitivity range.

The system was set as follows:

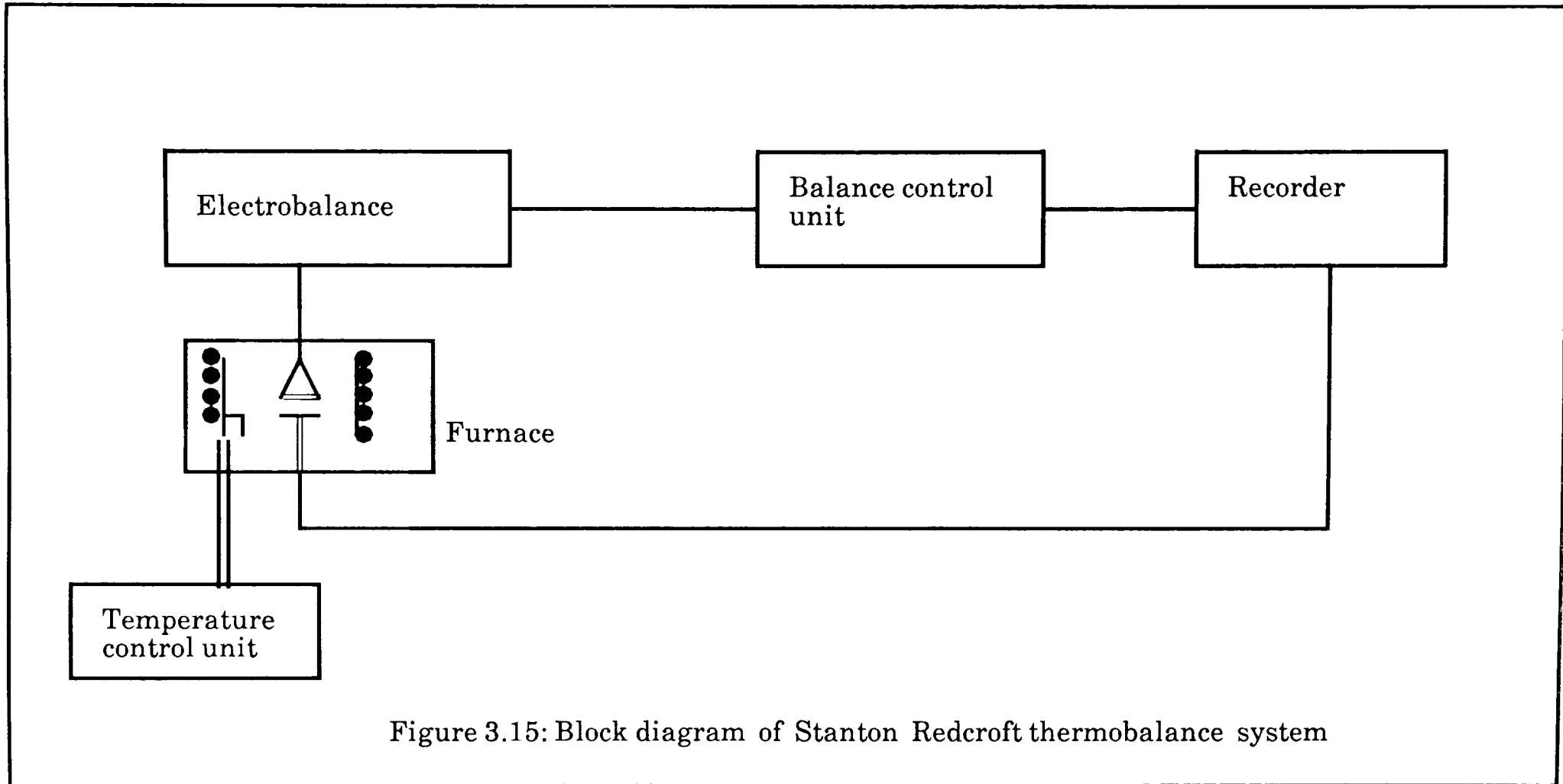


Figure 3.15: Block diagram of Stanton Redcroft thermobalance system

- ①. Heating rate = $20\text{ }^{\circ}\text{C}/\text{min}$. A *chromel-alumel* thermocouple was positioned in contact with the furnace wall and was used as a sensor for the temperature controller. The sample temperature was measured by a specially designed plate-type platinum vs. a 13% rhodium-platinum thermocouple. The plate was positioned at a distance of approximately 0.5 mm from the sample pan.
- ②. Chart speed = $5\text{ cm}/\text{min}$
- ③. Sample weight = 1 mg using platinum sample pan of 6 mm diameter.
- ④. Atmosphere = Nitrogen gas flow at rate $5\text{ cm}^3/\text{min}$.
- ⑤. Balance range = 1.0
- ⑥. Temperature hold = $600\text{ }^{\circ}\text{C}$

3.3) X-Ray Diffraction:

3.3.1) X-Ray Generation:

X-rays which are used in diffraction experiments are produced by different processes. In this work a beam of electrons accelerated through 30 kV, is allowed to strike a metal target (copper). The incident electrons have sufficient energy to ionize some of the copper 1s (K shell) electrons. An electron in an outer orbital (2p or 3p) immediately drops down to occupy the vacant 1s level and the energy released in the transition appears as X-rays radiation. For copper, 2p to 1s transitions (K_{α}) have a wavelength of 1.5418 \AA and 3p to 1s transitions (K_{β}), have a wavelength of 1.3922 \AA . The K_{α} transition occurs much more frequently than the K_{β} transition, i.e., K_{α} radiation is much more intense, so it is widely used in diffraction experiments. The type of generator used in this work was *Philips PW 1130* with a Cu K_{α} target, and usually Ni to filter out K_{β} radiation.

3.3.2) Other Instrumental Specifications:

In this work the *Debye-Scherrer method* was used, and the X-ray diffraction patterns of all compounds studied were recorded with a *Philips Debye-Scherrer PW 1024 camera* with a diameter of 111.5 mm. The sample tube was a *Lindemann tube* of 0.2 mm internal diameter and 0.01 mm thickness. It was rotated at a revolution per minute, and the exposure time was 2 hours.

3.4) Electron Microscope:

An electron microscope type *JEOL JSM - 35C*, was used. Generally an electron microscope consists of three major sections, as is shown in figure 3.16.

- I. Electron optical column {1-7}.
- II. Vacuum system { 14}.
- III. Electronics and display system {8-13}.

3.4.1) Detectors:

Generally, there are two kinds of detectors;

- ① Electron detectors, which detect the electrons passing through the sample, or reflected by it.
- ②- Dispersive X-ray detectors, which detect the x-ray emitted by the sample as a result of the bombardment by a beam of electrons.

There are two types of dispersive detectors:

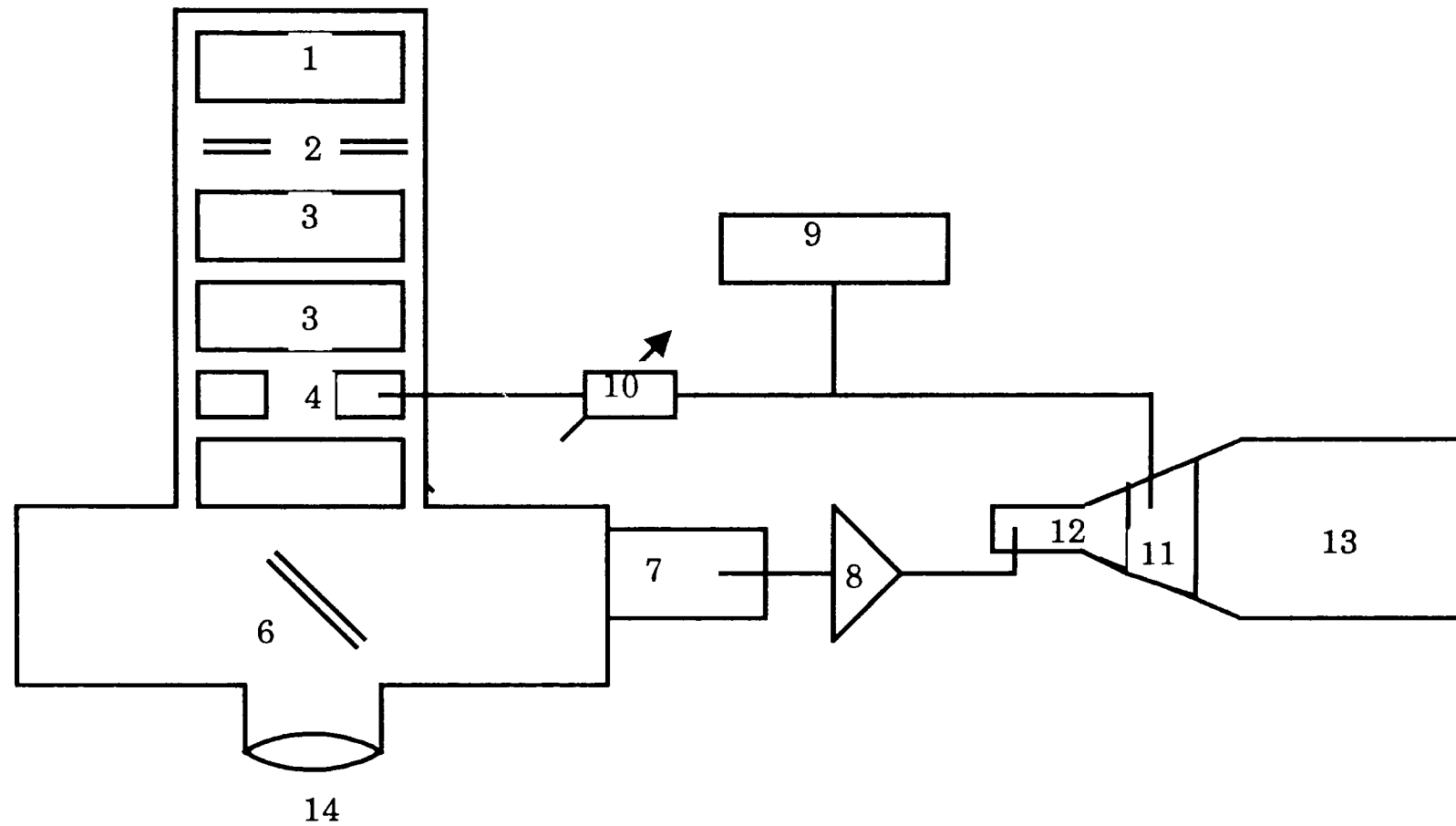


Figure 3.16: Layout of scanning electron microscope

Electron optical column

1. Electron gun 2. Anode disc 3. Condenser lens 4. Scan coil 5. Objective lens 6. Specimen 7. Detector

Display/electronic

8. Signal amplifier 9. Waveform generator 10. Magnification control 11. Scan coils 12. CRT brightness control 13. CRT display screen 14. Vacuum connection

1. Wave Length Dispersive System (WDS):

This is the earliest type of SEM (*scanning electron microscopy*) microanalysis. It determines the elemental composition of the specimen, by analysing the wavelength of the X-rays emitted from it. The X-rays generated by the specimen pass through a collimeter and are then allowed to strike a crystal of known lattice spacing.

Two types of crystals were used in this work to detect Al and Ga. For Al detection a TAP (*thallium hydrogen phthalate*) crystal with lattice spacing $2d = 25.757 \text{ \AA}$ was used, whilst LiF crystal with $2d$ -spacing = 4.027 \AA (3.15) was used for Ga detection. The *Bragg law* dictates that only X-rays with a wavelength λ will emerge from the crystal, where $n\lambda = 2d \sin \theta$ (see chapter 4). All other wavelengths will either be absorbed by the crystal or pass through it and be lost. The emerged X-rays are usually detected by a gas proportional detector.

2. Energy Dispersive X-Ray Detector (EDX):

This is an alternative approach to WDS. It depends on the use of a solid-state detector in which the semiconducting crystal is the key component.

In this work a silicon crystal doped with lithium was used (p-type silicon). This sort of detector is often called a Si(Li) or lithium drift detector. If X-rays strike the front face of the crystal, its energy is transferred by collision. A single photon colliding with the crystal will be absorbed by a silicon atom, releasing an electron. This energetic free electron is scattered inelastically through the silicon, producing free electrons and holes. With an applied field (ξ) the electron/ hole pairs are separated, each

migrating in an opposite direction and a current pulse is formed. The energy required to create an electron/hole pair in silicon is 3.8 eV(E). The number of electron/ hole pairs (n) can easily be calculated:

$$n = \frac{\xi}{E} \dots\dots\dots 3.2$$

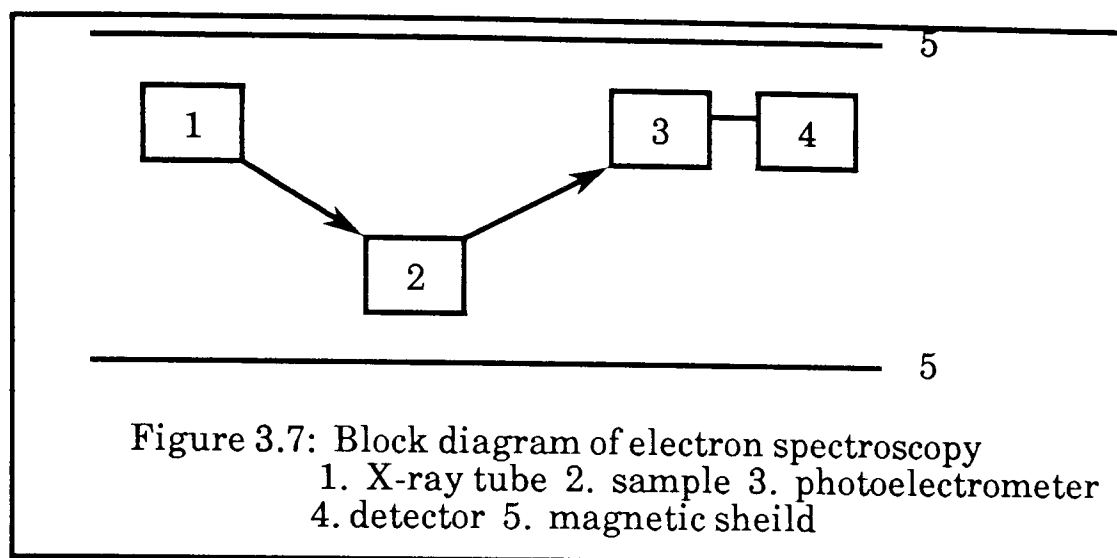
It is clear that the charge pulse from the detector is directly proportional to the energy of the incident X-rays(ξ) .

In this work both detectors, EDX and WDX, were used for the qualitative and quantitative analysis of Ga and Al in AlPcF, GaPcF and the copolymer films deposited on glass and carbon substrates.

3.5) X-Ray Photoelectron Spectroscopy (XPS):

XPS and depth profiling were carried out on samples 1 μ thick for AlPcF, GaPcF and the copolymer using a *VG ESCALAB MAR 11* spectrometer with a Mg anode as a source for K_{α} line X-rays (1253.6 eV) with a *multi channel electron multiplier* used as a detector. The energy range studied was 0-1000 eV and the vacuum level was 10^{-9} Torr (The experiments were performed by *Dr. M. R. Fahy, Institute for Molecular Science, Japan*).

The skeleton diagram of an experimental *XPS* unit is shown in figure 3.17



3.6) Photoconductivity:

The photoconductivity measurement system and the circuit diagram are shown in figure 3.18.

A light of certain intensity from a quartz-iodine source was passed through a monochromator using a system of condensing lenses. The monochromated light was then focused onto a rotating light chopper which interrupted the light at a constant frequency. The chopped light was then directed onto the sample to be studied. The sample (sandwich cell) was mounted in an *Oxford instrument F100* cryostat and connected in series with a battery and standard resistor. The change in voltage across the standard resistor was fed into the *lock-in amplifier* which responded to the alternating component of the signal at the chopping frequency. The meter reading on the *lock-in amplifier* was presented in digital form by connecting a *DVM* to the amplifier output. The relative light intensity was measured by an *ORIEL* model 7102 thermopile fitted with a silica window and placed in the sample position.

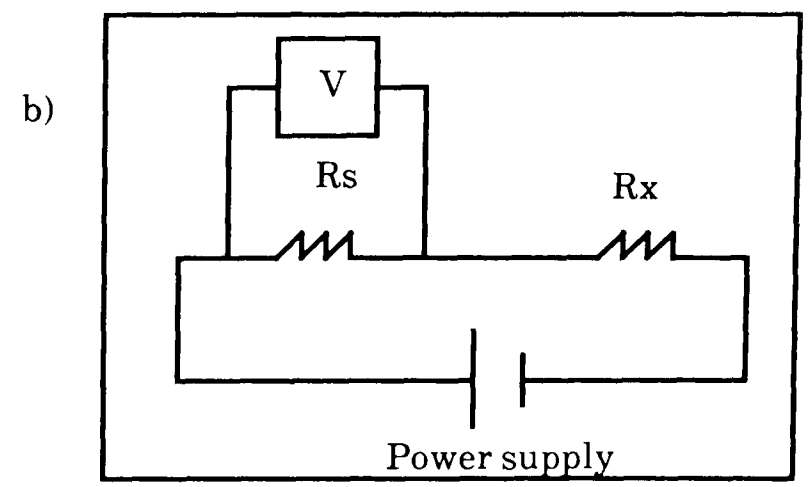
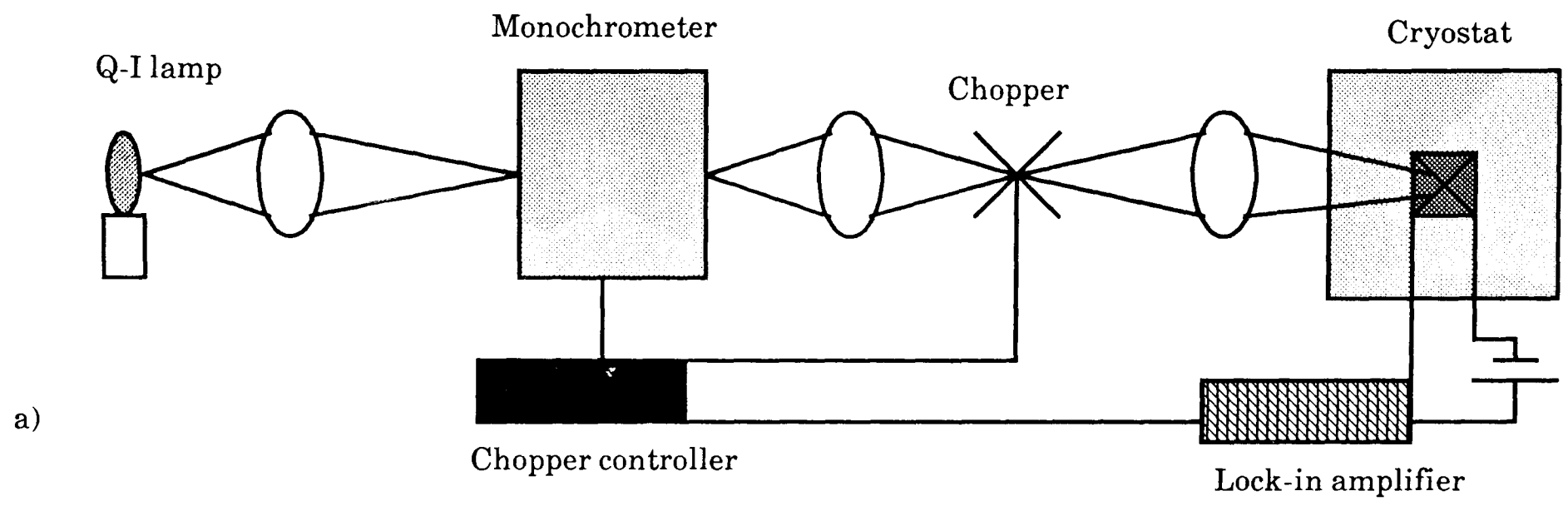


Figure 3.18 : a) The photoconductivity measurement system.
 b) The circuit diagram .

3.7) Spectroscopy:

3.7.1) U.V-Visible:

The measurements were carried out using a *Perkin-Elmer 552 spectrometer*. Spectra of were measured on thin films of thickness about 200 Å evaporated on to silica substrates. A base line was drawn first using two blank silica cells. The U.V and visible solution spectra were measured in chlorobenzene or chloronaphthalene. The solution spectra in the u.v region could not be performed because of strong absorption by the solvent.

3.7.2) I.R:

The measurement was carried out using a *Nicolet DX Fourier-transform IR spectrometer*. Measurements were made on both nujol mulls and sublimed films of 0.5-1 µm thickness samples.

3.7.3) Mass Spectroscopy:

A *VG-7070E mass spectrometer* was used. The FAB (*fast atom bombardment*) technique was applied. Xenon was employed as the fast atom beam and a matrix consisting of concentration 1 part/2 parts H₂SO₄/H₃PO₄ respectively was used.

CHAPTER FOUR

SYNTHESIS AND CHARACTERISATION OF THE MATERIALS

4.1) Synthesis of the Materials:

4.1.1) Phthalocyaninato aluminium fluoride, AlPcF:

This compound was prepared by the route in figure 4.1a, which involved the formation of AlPcCl from phthalonitrile, followed by hydrolysis to the hydroxide followed by treatment with aqueous hydrofluoric acid(40%), which yielded the polymeric fluoride(4.1).

(a) Phthalocyaninato aluminium chloride, AlPcCl:

A mixture of phthalonitrile(20g), aluminium trichloride(2.5g) and quinoline(twice distilled and then deoxygenated with nitrogen, 50 cm³) was refluxed for 30 minutes. The reaction mixture was cooled to approximately 0 °C and filtered. The isolated solid was washed with benzene, carbon tetrachloride and acetone and dried at 110 °C. Yield was 10.1(25%). The product (10g) was sublimed using the entrainment sublimer(see chapter3) under a nitrogen atmosphere to give a purple polycrystalline sublimate(4.5g,40%).

(b) Phthalocyaninato aluminium fluoride, AlPcF:

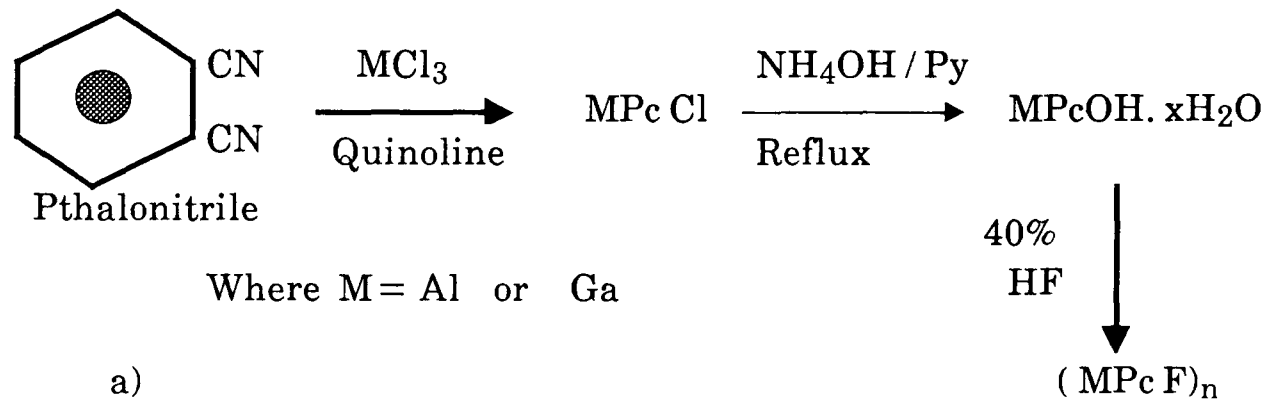
A mixture of AlPcCl(4.5g), concentrated ammonium hydroxide(100 cm³) and pyridine(50 cm³) was refluxed for 7 hours. The resulting solid was filtered, washed with conc. ammonium hydroxide and hot water and dried at 110 °C. Yield was 3.0g, assumed to be AlPcOH.xH₂O. A portion of this product(1g) was evaporated to dryness on a steam bath with three separate portions of 40% hydro fluoric acid(20 cm³ each time). The resulting solid was washed with water, methanol, pyridine and acetone and dried at 110 °C. Yield was 0.8g(54%), of a purple microcrystalline powder. The product was sublimed at 480 C under a nitrogen atmosphere to give a blue fluffy sublimate (0.6g,75%).

4.1.2) Phthalocyaninato gallium fluoride, GaPcF:

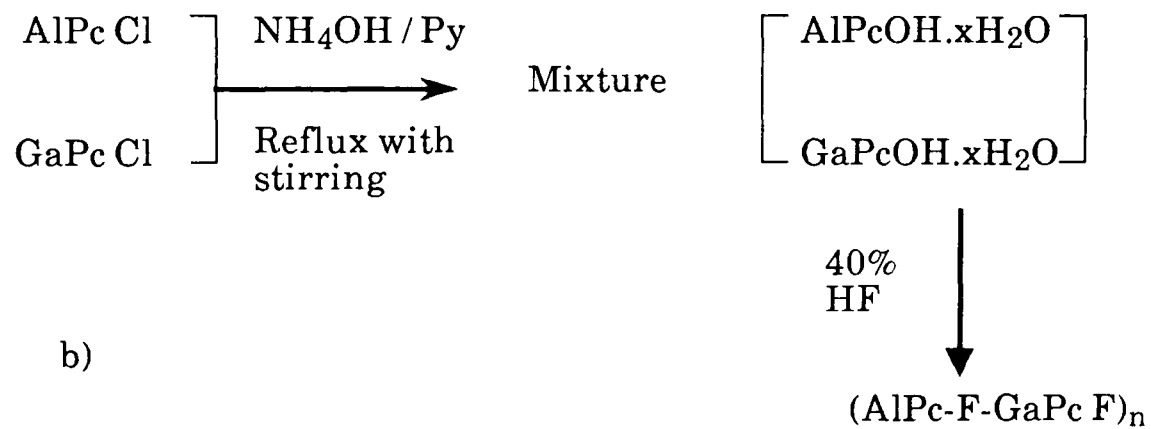
This compound was prepared by the same route of AlPcF as shown in figure 4.1.

(a) Phthalocyaninato gallium chloride, GaPcCl:

A mixture of phthalonitrile(18.18g), Gallium(III)chloride(5g) and quinoline (distilled three times and deoxygenated with nitrogen, 100 cm³) was refluxed for 1 hour (particular attention was paid to exclude water during the reaction) The reaction mixture was cooled to about 0 C and then filtered and washed with toluene and methanol and dried at 110 °C. Yield (20g,22%). On sublimation under a nitrogen atmosphere, a purple sublimate (10.5g,53%) was obtained in which crystals of larger size than AlPcF were present.



a)



b)

Figure 4.1: Preparation routes for AlPcF, GaPcF and their copolymer.

(b) Phthalocyaninato gallium fluoride, GaPcF:

A mixture of GaPcCl (3g), conc. ammonium hydroxide (70 mls) and pyridine (70 cm³) was refluxed for 20 hours. The reaction product was filtered and the solid was washed with water, methanol and acetone and dried at 110 °C. The yield was 2.0g assumed to be GaPcOH. xH₂O. A portion of this product (1.0g) was evaporated to dryness on a steam bath with three separate portions of 40% hydrofluoric acid (20 cm³ each time). The resulting solid was washed with water, methanol, pyridine and acetone and dried at 110 °C. Yield was 0.85g(65%). Sublimation at 430 °C, under a nitrogen atmosphere gave a purple thin film sublimate (0.6g, 70%).

4.1.3) The copolymer (AlPcF - GaPcF)_n, 1:1 mole ratio:

This compound was prepared by a method developed from the procedure of *Kenney et al* (1) as outlined in figure 4.1b. A mixture of the sublimed chlorides (AlPcCl and GaPcCl) was first hydrolysed and then treated with hydrofluoric acid.

Synthesis of the Copolymer

A mixture of sublimed AlPcCl (0.5745g, 1 mmole) and GaPcCl (0.6172g, 1 mmole), conc. ammonium hydroxide (30 cm³) and pyridine (30 cm³) was refluxed with magnetic stirring for 20 hours. The reaction mixture was cooled and filtered. The solid was isolated and washed with pyridine, conc. ammonium hydroxide, hot water, methanol and acetone and dried at 110 °C. The product was a fine blue powder which was assumed to be an intimate mixture of AlPcOH.xH₂O and GaPcOH.xH₂O (yield 0.9g). A portion of this product (0.45g) was evaporated to dryness on a steam bath

with three separate portions of 40% hydrofluoric acid (15 mls each time). The resulting solid was washed with pyridine, water, methanol, acetone and dried at 110 °C (Yield 0.41g,70%). On sublimation at 560 °C and under a nitrogen atmosphere gave 0.25g(61%) of a purple polycrystalline powder.

4.1.4) Other Materials:

Metal-free and copper phthalocyanines(H_2Pc and $CuPc$ respectively) were supplied by Aldrich Chemical Company Ltd, while chromium phthalocyanine was supplied by Eastman Kodak Company.

4.2) Characterisation of the Materials:

4.2.1) Elemental Analysis:

Table 4.1 shows the elemental analysis values for the prepared compounds. The analyses of $AlPcF$, $GaPcF$ and their copolymer show a good agreement with the calculated values. The elemental analysis of the copolymer sublimed at 420 °C, is similar to $GaPcF$ analysis which may suggest the fractionation of the copolymer. However, the elemental analysis of the copolymer sublimed at 560 °C has good agreement with the calculated values.

Compound	Element	MPcCl sublimed		MPcF		
		%Calculated	%Found	Before sublimation		Sublimed
				%Calculated	%Found	%Found
AlPcX	C	66.85	67.16	68.66	66.81	66.82
	H	2.78	2.98	2.89	2.98	2.87
	N	20.07	19.28	20.07	19.18	20.01
GaPcX	C	62.22	62.11	63.93	61.18	63.24
	H	2.61	2.48	2.68	2.61	2.58
	N	18.15	17.73	18.63	17.36	18.18

	Elements	% Calculated	Before sublimation	Sublimation at 420 °C	Sublimation at 560 °C
Copolymer 1:1	C	66.37	65.78	63.91	66.47
	H	2.76	2.90	2.85	2.75
	N	19.36	19.06	18.22	19.14

Table 4.1: The elemental analysis.

4.2.2) U.V and Visible Spectroscopy:

1) Solution:

It was difficult to find a suitable solvent for AlPcF. It is insoluble in most of the known phthalocyanine solvents, such as, chlorobenzene, 1-chloronaphthalene. It is sparingly soluble in quinoline and the spectrum shows a broad band which may be due to formation of a charge transfer complex (figure 4.2).

The other compound, GaPcF, is sparingly soluble in 1-chloronaphthalene and chlorobenzene which give a spectrum, shown in figure 4.3. It is a characteristic phthalocyanine spectrum (4.2-3), with two intense peaks at 690 nm (*Q-band*) and at 340 nm (*B or Soret band*). The difference between the spectra of GaPcF and H₂Pc is the splitting of the peak around 700 nm into a doublet in the case of H₂Pc, and this reflecting the fact that H₂Pc has lower symmetry (D_{2h} point group), while the symmetry of the GaPcF is D_{4h}.(4.2,4-6).

The copolymer gave a spectrum which is characteristic of the highly symmetrical phthalocyanines as it shown in figure 4.4, which is also similar to the GaPcF spectrum.

The chlorophthalocyanines (AlPcCl and GaPcCl) give spectra characteristic of symmetrical phthalocyanines.

2) Solid-films:

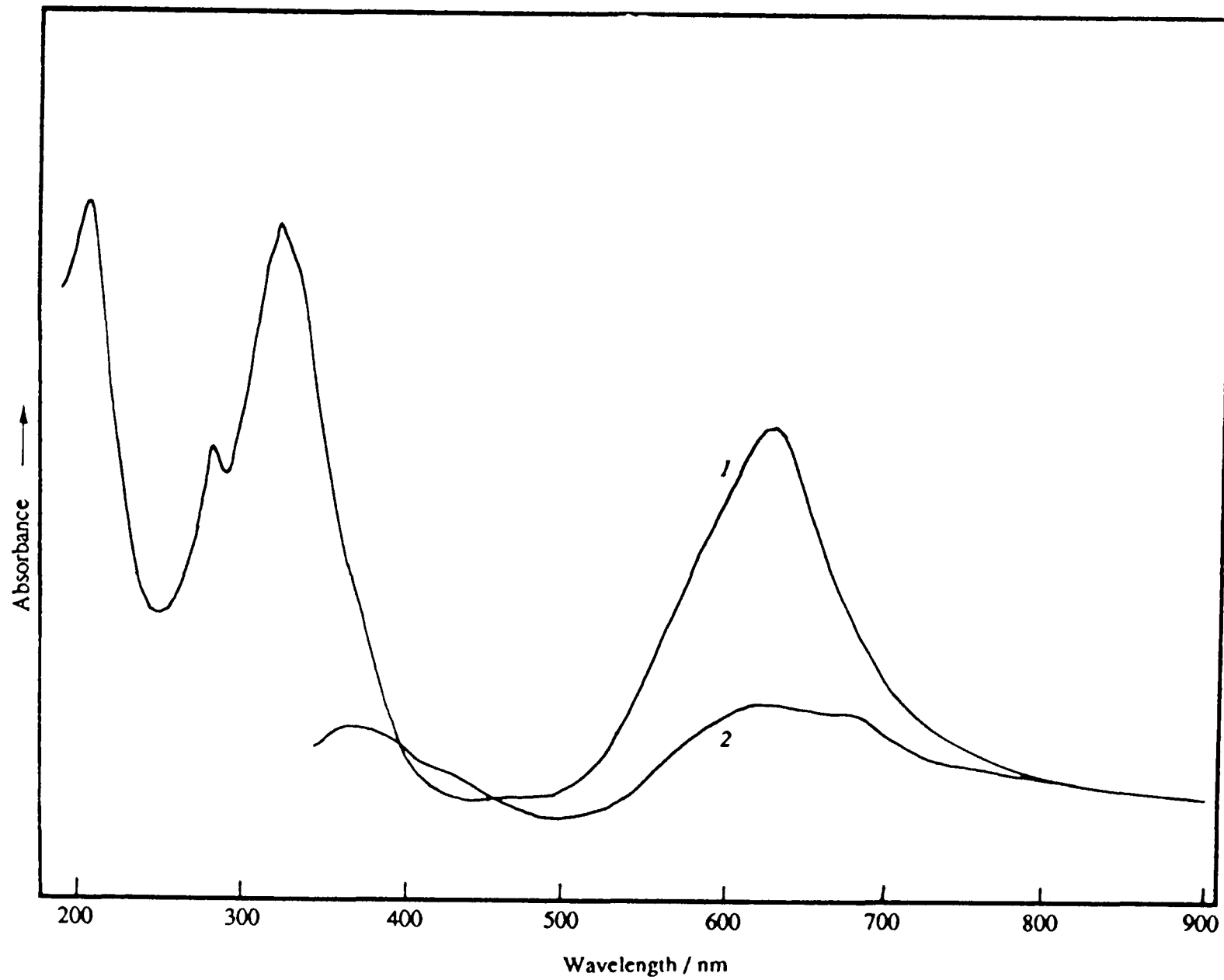


Figure 4.2: U.V spectra for AlPcF
1) solid film
2) solution (quinoline)

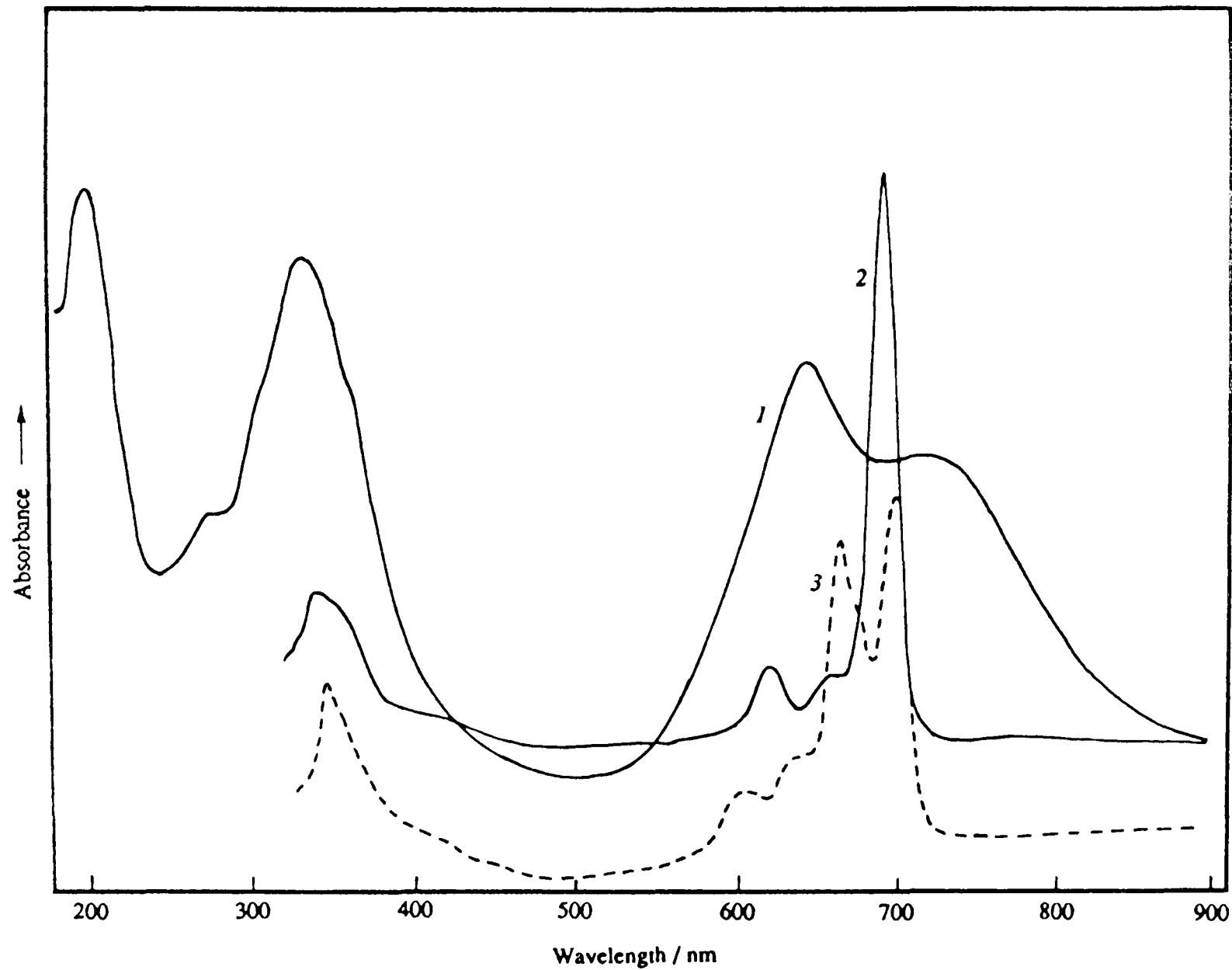


Figure 4.3: U.V spectra for GaPcF⁻ 1) Solid film.
 2) Solution (1-chloronaphthalene).
 3) H₂Pc (solution, 1-chloronaphthalene).

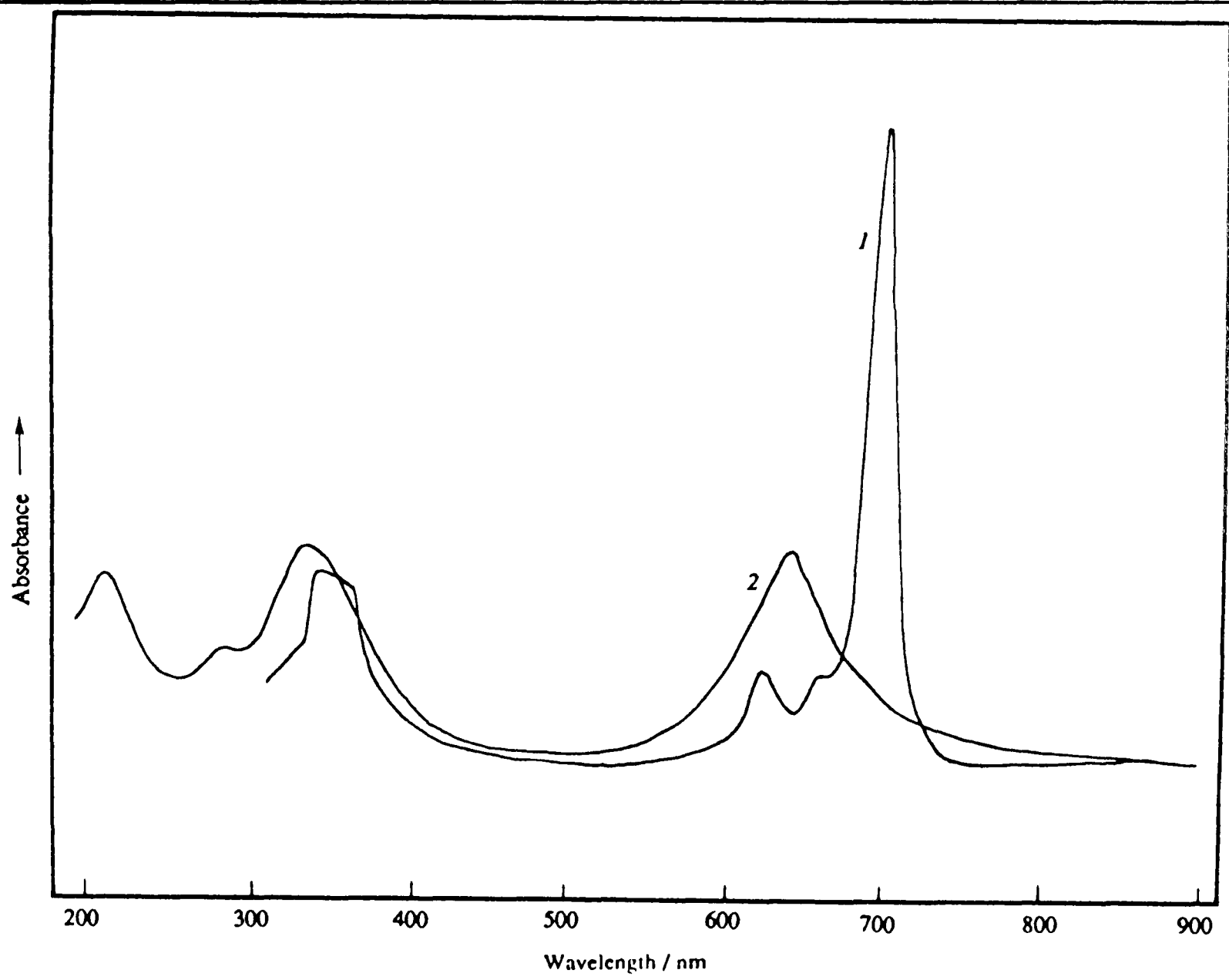


Figure 4.4: U.V spectra for the copolymer
1) solution (1-chloronaphthalene)
2) solid film)

The relatively narrow *Q*-bands in solution transformed into a broad peak in the solid which can be explained as due to unresolved *Davydov splitting*. The amount of splitting is a measure of the interaction energy between molecules having different site symmetries. It is observed both for *Q* and *Soret bands* (4.2,4.7), the two main bands of MPc s which are both described as $\pi - \pi^*$ transition(4.8-10).

A thin film of AlPcF shows a spectrum which contains two main peaks at 770 nm and at 340 nm (figure 4.2), while a thin film of GaPcF shows a spectrum consisting of bands at 635 nm with a shoulder at 710 nm in addition to the peak at 330 nm(Figure 4.3). The copolymer shows a band at 645 nm with a very small shoulder at 700-710 nm(figure 4.4).

A thin film of two equal layers (AlPcF over GaPcF) gave a spectrum similar to the spectrum of the copolymer, but different in the ratio of the intensities of absorption at 645 nm and at 700 nm (R.A), as shown in the following table,

Compound	R.A
GaPcF	1.22
Mixture	2.19
Copolymer	3.46

4.2.3) I. R Spectroscopy:

Thick films of AlPcF, GaPcF and the copolymer show similar spectra to those obtained from nujol mulls on KBr discs. They contain characteristic phthalocyanine bands(4.3.,4.11-12). The peaks at 600-400 cm^{-1} are associated

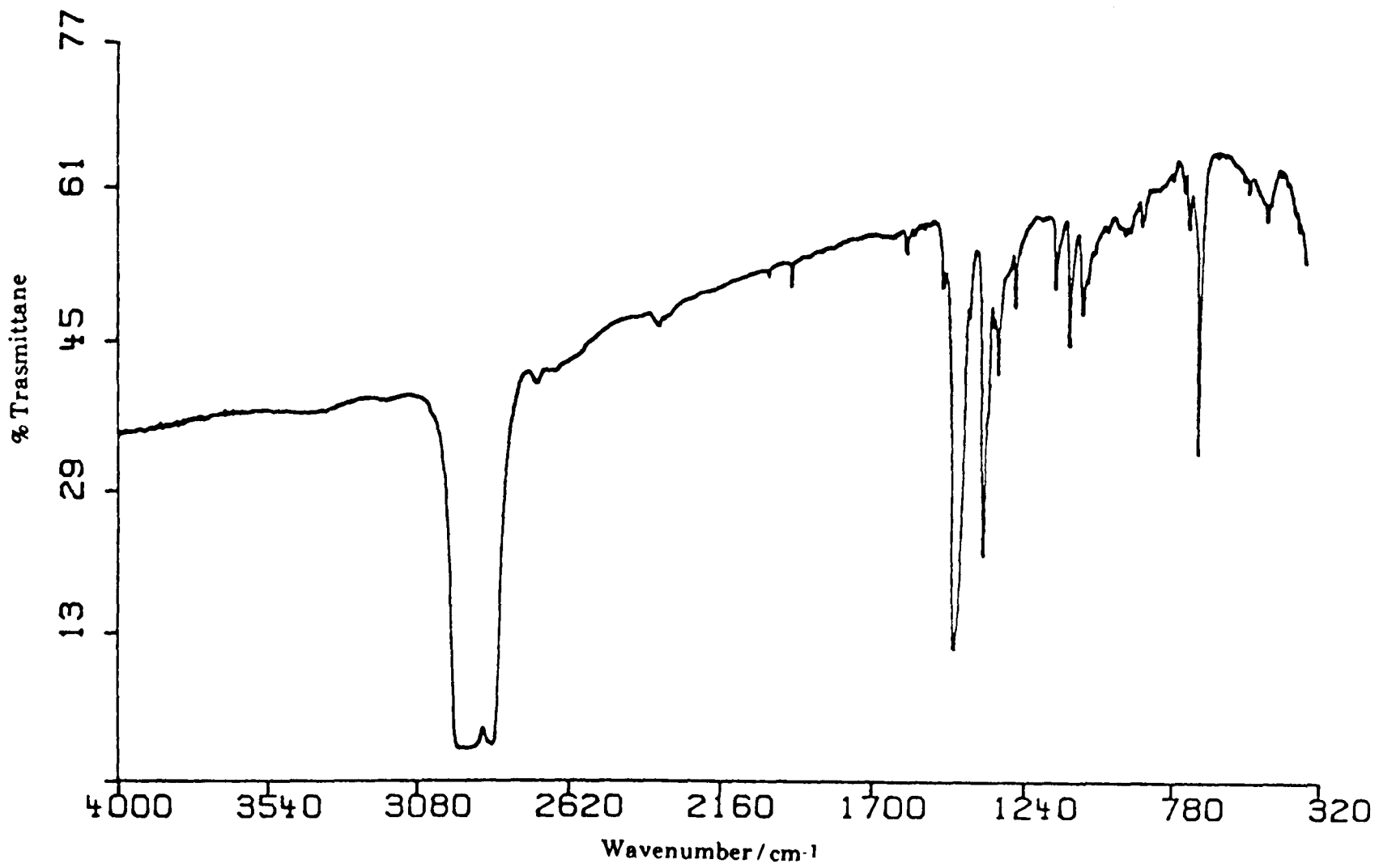
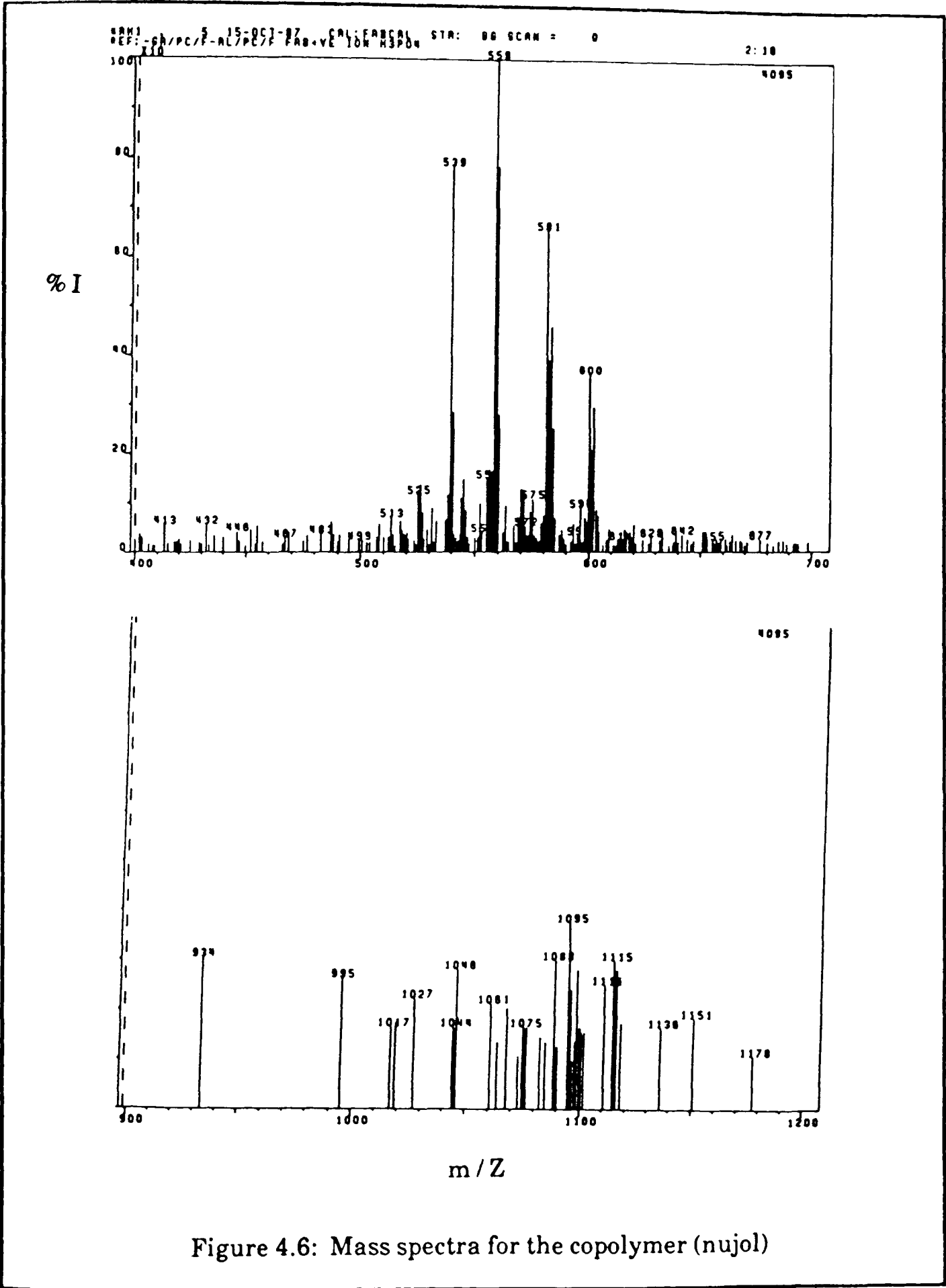


Figure 4.5: I.R spectra for the copolymer (nujol)



with the metal-halogen stretching vibrations. The broadness of the bands (500-550 nm) assigned to the Al-F and Ga-F has been attributed to the polymeric nature of the materials^(4.1) (see figure 4.5).

4.2.4) Mass Spectra:

Because of the intractable nature of the phthalocyanines which is due to their insolubility, involatility and stability, special techniques have been used to obtain the mass spectra of the phthalocyanines^(4.13).

The fast atom bombardment (FAB) technique ^(4.14) has been used for the determination of the structure of phthalocyanine^(4.15), organometallic compounds ^(4.16), and other complex compounds ^(4.17).

In this work *FAB* has been used for the identification of AlPcF, GaPcF and their copolymer. Xenon was used as the fast atom beam and a mixture of H₂SO₄/H₃PO₄ as the liquid matrix.

Molecular ions (AlPcF and GaPcF) were detected in the spectra of AlPcF and GaPcF respectively. These molecular ions were also detected in the spectrum of the copolymer but with different intensities, in addition to the molecular ions of the dimers, and clusters of dimers with other ions (see figure 4.6).

4.3) Thermal Analysis:

The term *thermal analysis* describes several techniques in which some physical parameters of the system are determined as a function of temperature. The principal techniques of thermal analysis are dynamic

thermogravimetry (TG) and differential thermal analysis(DTA). In thermogravimetry the change in mass with temperature is measured , while in differential thermal analysis the change in the temperature of the sample with the temperature is recorded. Quantitative measurements of the mass change are possible by determination of the distance between the two points of interest on the the mass axis of the (weight/T) curve. In derivative thermogravimetry, the derivative of the mass change with respect to time, dm/dt , is recorded as a function of temperature, T, or time, t:

$$\frac{dm}{dt} = f(T \text{ or } t) \quad \dots\dots\dots 4.1$$

The curve obtained is the first derivative of the mass change curve. A series of peaks are obtained instead of the stepwise curve in which the area under the peaks are proportional to the total mass change of the sample. Differential thermogravimetry, DTG, is a complementary technique to DTA, spectroscopy and X-ray analysis. In the DTG the ratio of change of mass with temperature(dm/dT)is recorded. The measurement of the change in current or conductivity with temperature is a thermoanalysis technique.

In this work TG and DTG are both used to determine sublimation temperatures.

4.3.1) Factors Effecting Thermogravimetric Analysis:

There are a large number of factors which effect the nature, precision and accuracy of the experimental results. The most important factors can be divided into two categories (Instrumental factors and Sample characteristics):

1) Instrumental Factors:

I) Heating Rate:

For any given temperature interval, the extent of decomposition or sublimation is greater at a slow rate than at a faster rate. Where successive changes are involved, the appropriate rate of heating is necessary to determine these changes. A heating rate of $20\text{ }^{\circ}\text{C min}^{-1}$ proved suitable for phthalocyanine samples.

II) Chart Speed:

The chart speed has an effect upon the mass-loss curve. As the chart speed is increased a definite flattening of the curves occurs. High chart speed shows more separation of the changing steps. It is recommended that a chart speed of $15\text{-}20\text{ cm.hr}^{-1}$ is used for heating rate $1\text{-}6\text{ }^{\circ}\text{C min}^{-1}$ (4.12). A chart rate of 30 cm hr^{-1} (0.5 cm min^{-1}) proved suitable for this work.

III) Effect of Buoyancy:

Buoyancy is due to displacement of air or gas by the sample holder, which reduces the actual weight. This effect increases with the density of the gas and the size of the sample container. It should be kept in mind that the density of the gas phase decreases with temperature, and as a certain amount of the sample is required, it is not possible to reduce the size of the crucible. In this work no buoyancy effect was observed under the constant nitrogen flow.

IV) Effect of Convection Current:

As a result of heating, and due to the heat transfer by convection, the heated gas along the furnace wall displaces the sample boat down the centre of the furnace which causes an increase in sample weight. *Simkin*

(4.18) has noticed a constant effect under atmospheric conditions which was sufficiently small to be neglected.

V) Effect of Furnace Atmosphere:

In this work, as heating started, an immediate decrease in the weight was noticed, which may be due to the convection currents in the nitrogen gas causing a flowing stream of gas displacing the sample boat upwards.

Nitrogen gas flow has many effects on the decomposition rate and temperature. It removes the gases due to decomposition or sublimation processes which may occur in the phthalocyanines during heating, so the reaction rate will increase.

In general, furnace atmosphere has a big influence on the mass change curve which depends on the type of the reaction and the nature of the decomposition .

VI) The Sample Holder:

The material from which the sample holder is made, and its shape, have important influences on the TG curve. The material used for construction of the sample holder should have no effect on the TG curve if it does not react with the sample. Sample holders range from flat plates to deep crucibles of various capacities. The loss of the material by sublimation or decomposition occurs more readily from the shallow dish than from the crucible. In this work the crucible used gave satisfactory results.

VII) Sensitivity of the Recording Instrumentation:

Mass sensitivity is a critical parameter in thermogravimetry. Greater sensitivity of the thermobalance permits the use of smaller samples. A sensitivity of 25 μg can be attained using the *Stanton Redcroft TG-750*

thermobalance. In selecting TGA sensitivities, the initial factor is the rate of weight loss. For a small rate of weight loss the DTG sensitivity can be improved by either using a larger sample or a higher heating rate or a combination of both. The optimum conditions for recording sensitivity in this work were obtained with an input range of 10 mV dc sensitivity for TG, and 1 mV for DTG measurements (4.19).

viii) Effect of Temperature Measurements:

A temperature gradient is formed between the sample and the furnace wall which causes an error into measurement of the sample temperature. This problem was studied by *Newkirk*(4.20). He measured the temperature difference between thermocouples placed inside the crucible and near the furnace wall. He found that the error in temperature measurement will be small at low heating rates. In this work the heating rate was $20\text{ }^{\circ}\text{C min}^{-1}$ which was proved satisfactory for DTG measurements. The thermocouple was kept as near as possible to the sample.

2) Sample Characteristics:

①) Sample Mass and Size:

Sample size can effect the TG curve in different ways,

(a) The rate of diffusion of the product gas through the space around the solid particles.

(b) The existence of large thermal gradients through the sample, particularly if it has a low thermal conductivity. In this work a sample of less than 1 mg was used.

The smaller the particle size, the greater the extent to which equilibrium is reached, and at any given temperature, the greater the extent of the decomposition or sublimation (4.21).

In this work the phthalocyanine samples were finely ground. For the mixture, it was found that there is no difference if the components were ground before or after mixing.

② Sublimation and Condensation:

Condensation of volatile products on the cooler parts of the weighing system may result in the TG curves being unreproducible. In this work some of the samples materials, such as AlPcF, deposited on the hanging wire of the boat which increases the experimental weight. The deposited materials may touch the walls of the glass tube through which the suspension wire is passing, which will cause an error in the sample weight measurement. Care was taken to overcome this problem. The hanging wire was cleaned very well before each run and a higher rate of nitrogen gas flow was used to carry the sublimed materials further down the furnace.

③ Other Factors:

Any heat of the reaction will effect the temperature difference between the furnace and the sample, causing the sample temperature to lead or to lag behind the furnace temperature depending whether the reaction is exothermic or endothermic. In this work the process is certainly endothermic and no effect was noticed. The effect of solubility of gases in solids is difficult to ascertain (4.22), but the nitrogen flow removes the released gases and vapours as a result of heating down the furnace.

4.3.2) Thermogravimetry, Results and Discussion:

Thermogravimetric analysis studies on doped aluminium and gallium phthalocyanines have been carried out by many workers (4.23-28) to determine the composition of the doped materials. It was found, that pure and unoxidized phthalocyanines ($M = Al, Ga$) do not show weight loss below 400 °C (4.29-30).

In this work sublimed AlPcF, GaPcF, their copolymer and their mixture (1:1 mole ratio) were studied thermogravimetrically. In figures 4.7 and 4.8, the TG and DTG graphs are shown. Table 4.2 shows the percentage weight loss, maximum weight loss temperature, the T_i (initial weight change temperature) and T_f (the final weight change temperature) and the weight change interval ($T_f - T_i$) for the four compounds.

There are two possibilities to explain the weight change in this type of compound. It is either decomposition or sublimation. The sublimation process can be established from the deposited sublimate on the boat holder and the upper cooler part of the furnace, as is clear from the case of the AlPcF, and the existence of some decomposition can be deduced from the white residue in the sample boat. The sublimation process for these polymers may be understandable in terms of a depolymerisation process (4.1).

Actually, decomposition is known in AlPcF and GaPcF (4.29-31) and other phthalocyanines. Figure 4.9, shows the decomposition of CrPcF under different conditions.

Table 4.2, shows a similar maximum weight loss temperature range for the copolymer and the mixture which can be understandable in terms of interaction of both GaPcF and AlPcF (4.6) and then copolymerisation at high

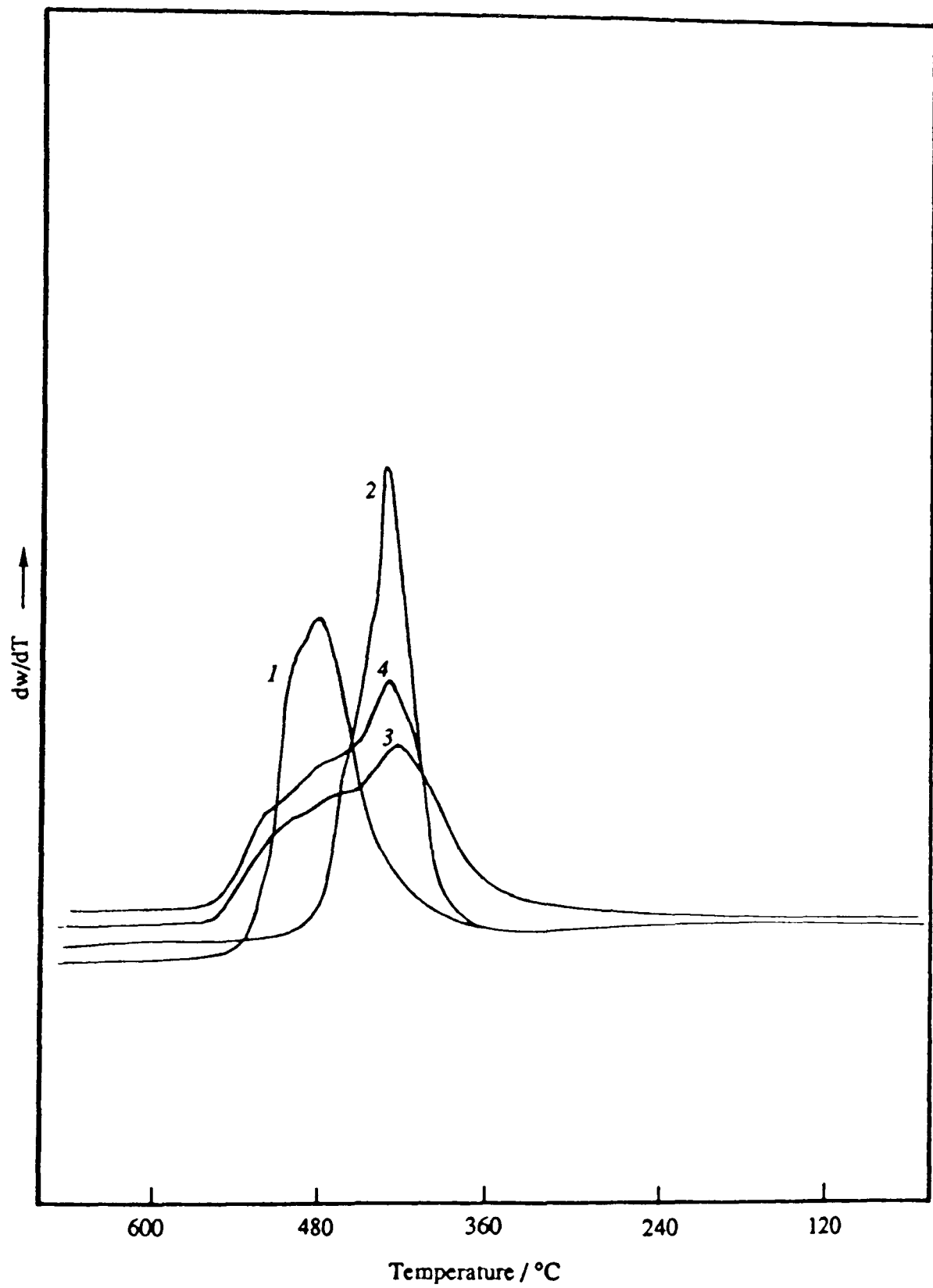


Figure 4.7: The DTG graphs for 1. AlPcF, 2. GaPcF,
3. The copolymer, 4. The mixture.

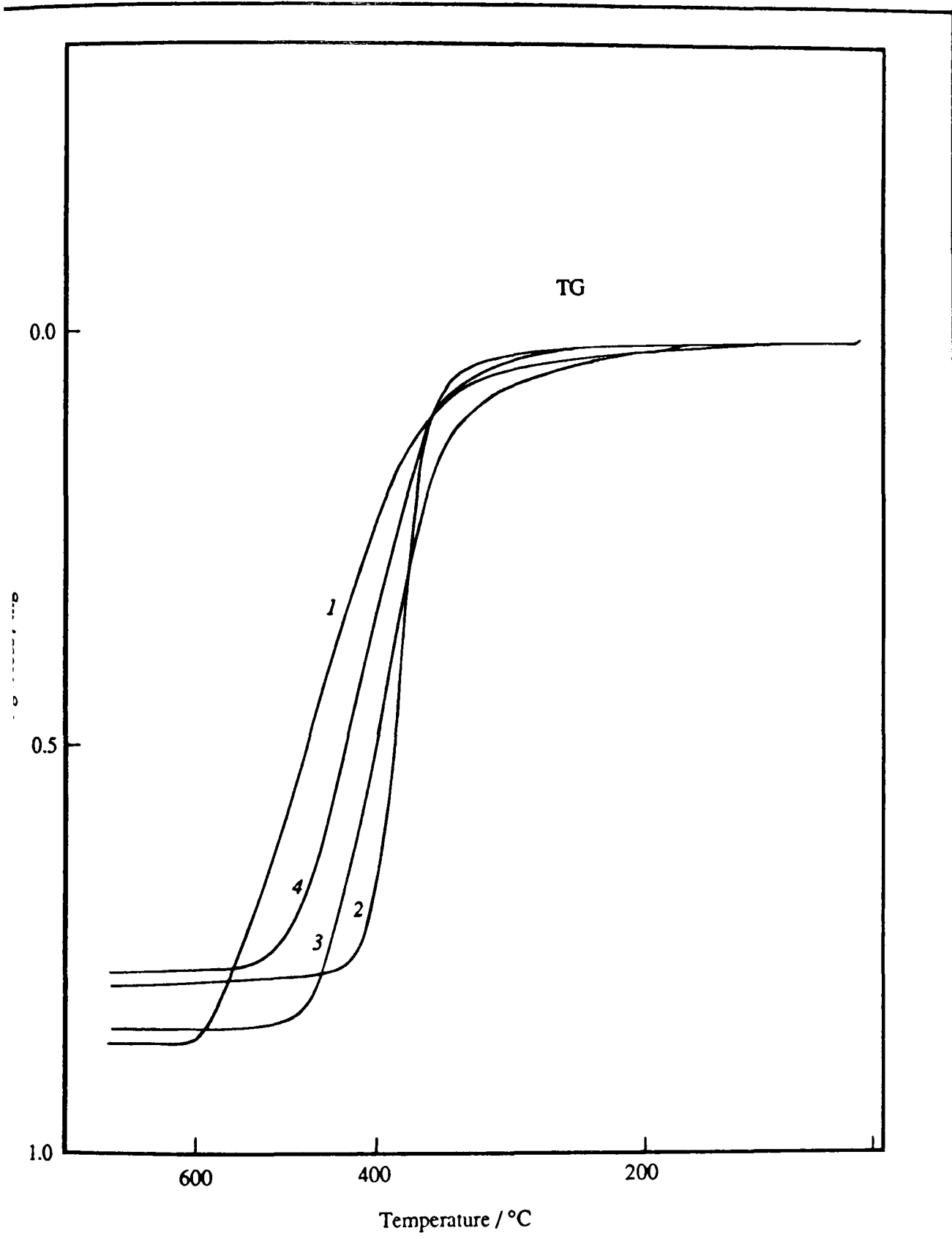


Figure 4.8: The TG graphs for 1. AlPcF, 2. GaPcF, 3. The copolymer, 4. The mixture.

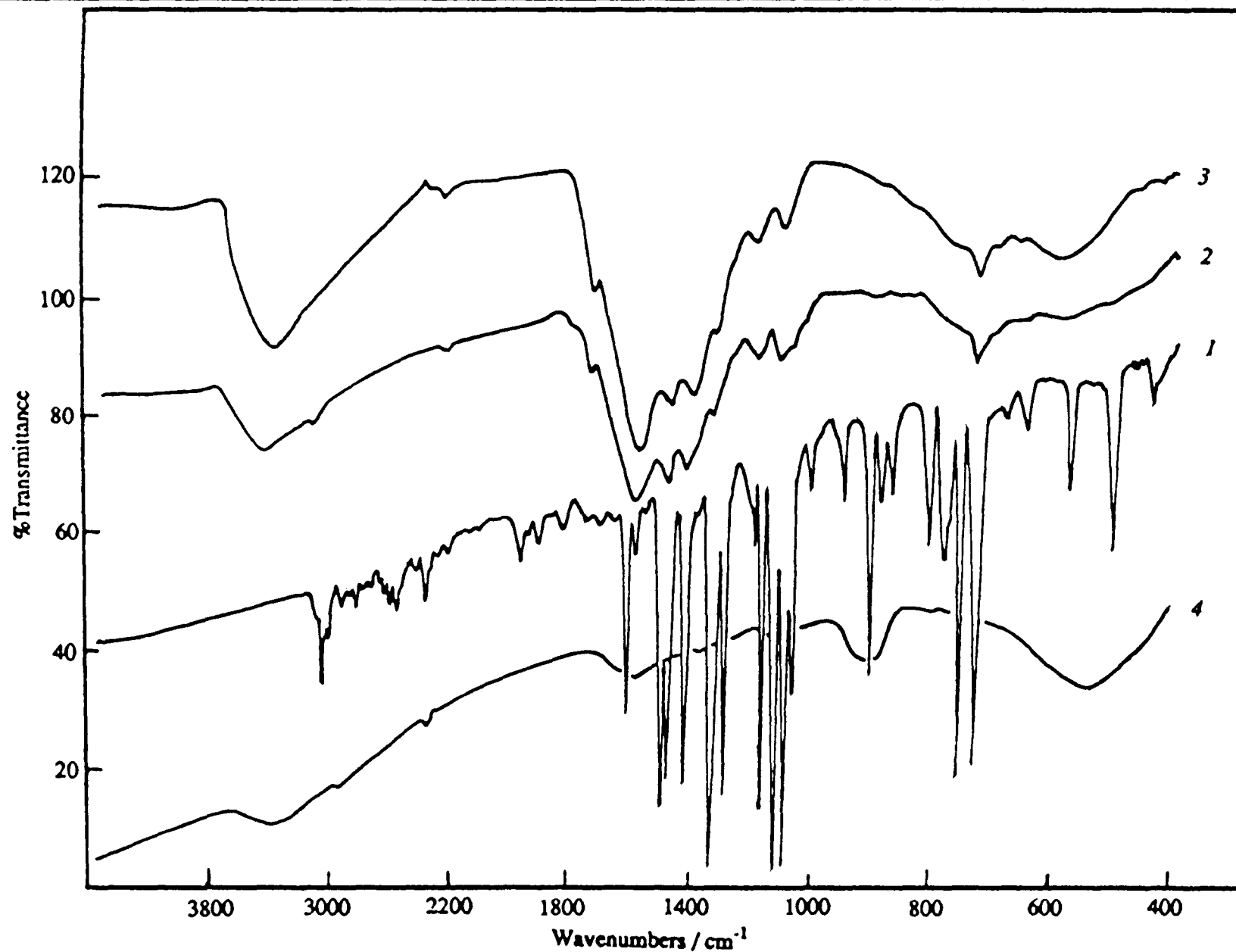


Figure 4.9: I.R spectra ,effect of annealing

- 1) At room temperature
- 2) One hour heating(250 0C)at normal pressure
- 3) Heating overnight under vacuum (10⁻² torr)
- 4)Heating overnight (250 0C) under normal pressure.

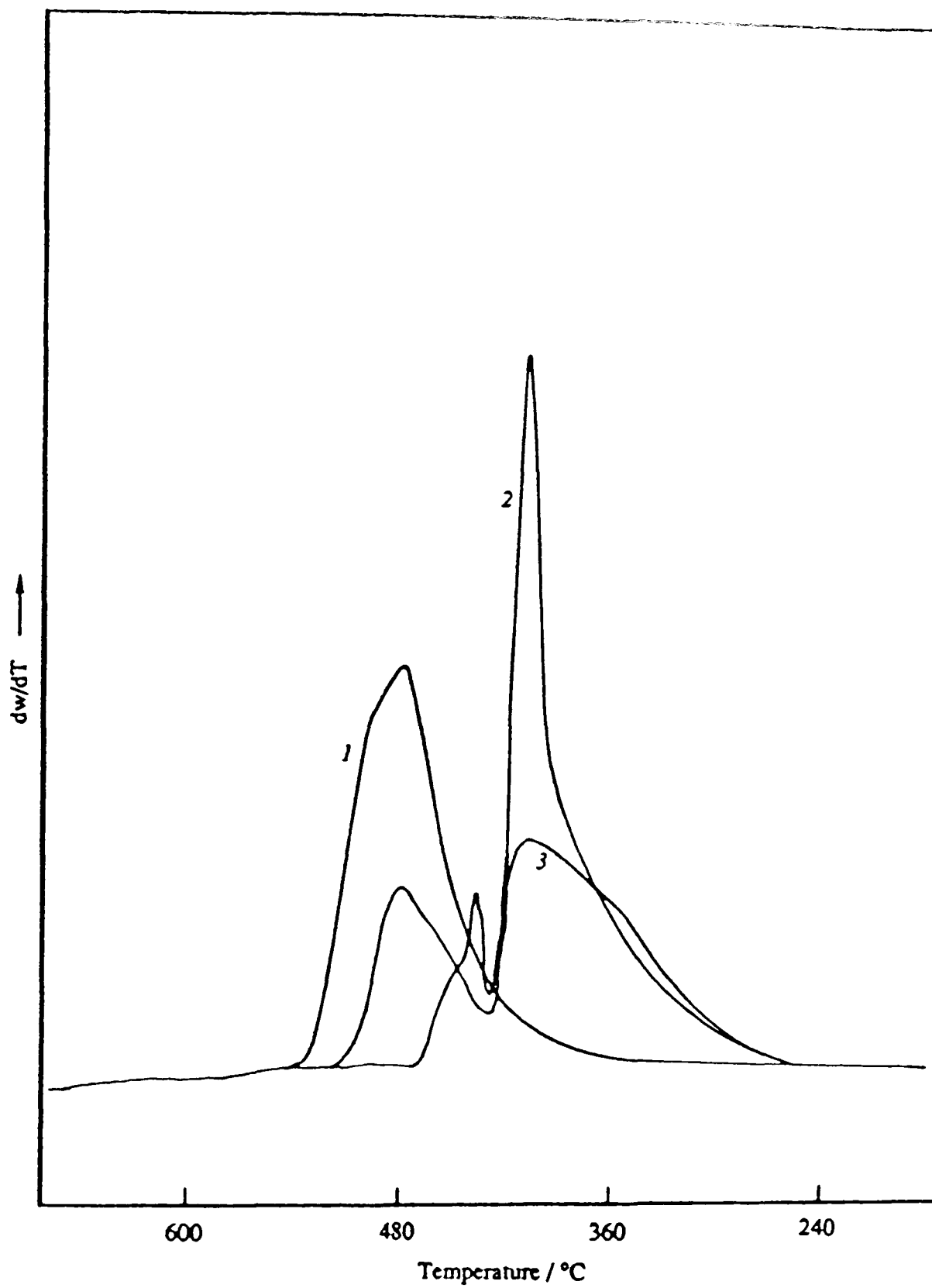


Figure 4.10: The DTG graphs for 1. AlPcF 2. H₂Pc (2), 3. The mixture .

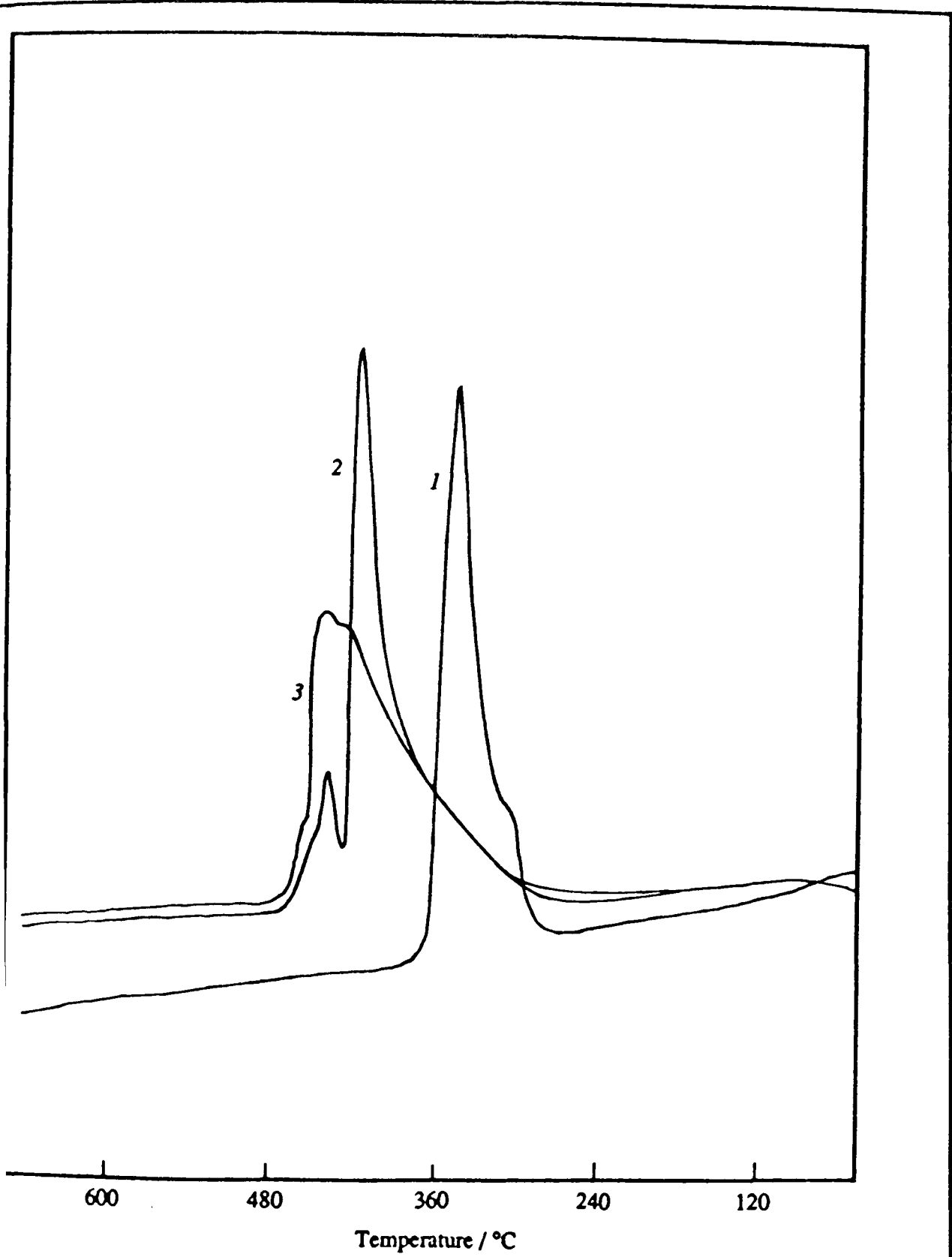


Fig. 4.11: The DTG graphs for 1. CuPc , 2. H₂Pc , 3. Their mixture .

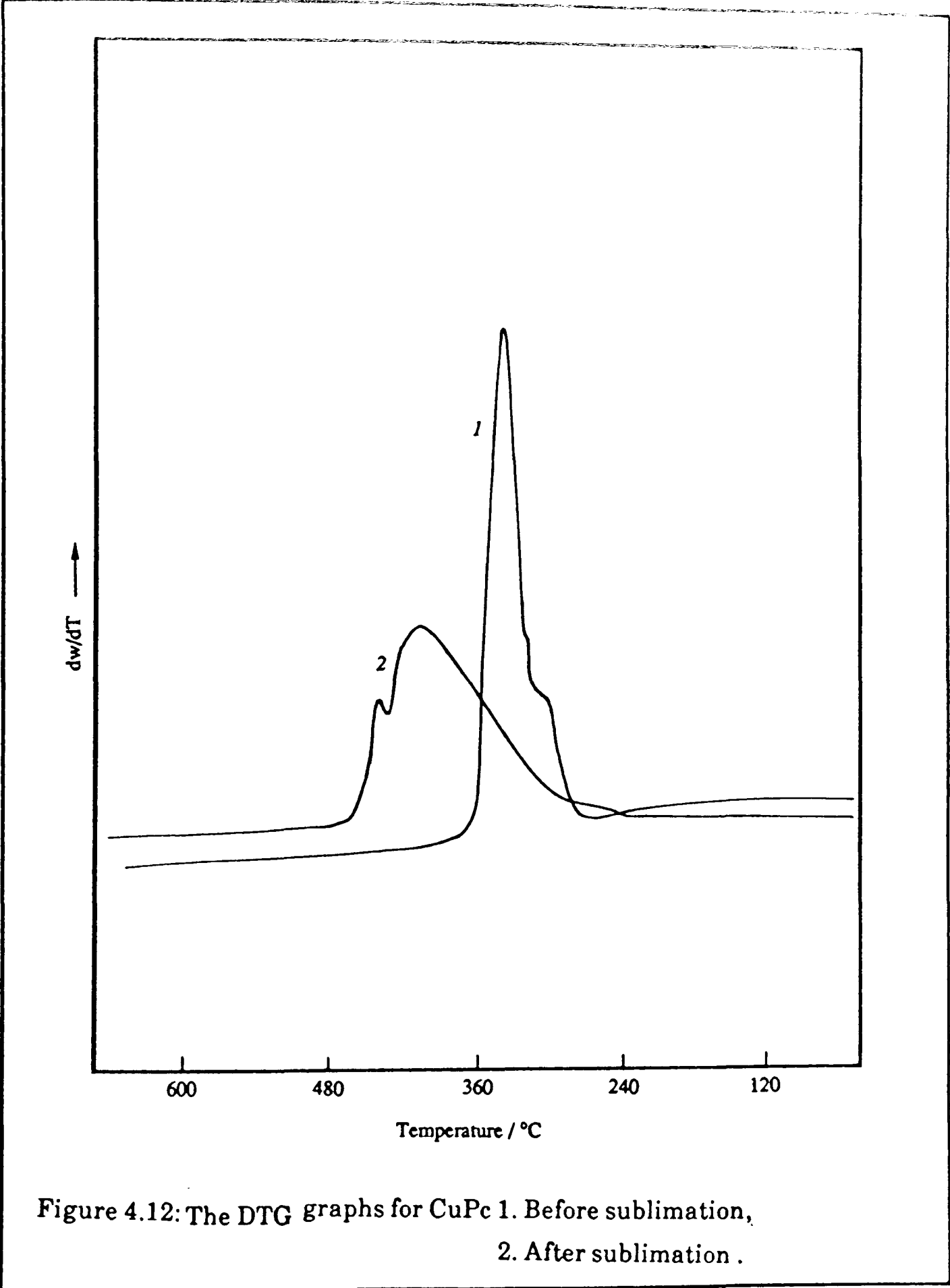


Figure 4.12: The DTG graphs for CuPc 1. Before sublimation,
2. After sublimation .

temperatures (more than 400 °C) which is equivalent to the formation of a solid solution, especially as, GaPcF and AlPcF are isomorphous and both Ga and Al are trivalent atoms.

Figure 4.10 shows that TGA of sublimed AlPcF and H₂Pc together with their mixture (1:1 mole ratio). Because there is no specific interaction between the two components, the mixture was sublimed at the characteristic sublimation temperatures of AlPcF and H₂Pc.

Many other attempts were made to see the nature of the interaction between different phthalocyanine mixtures. Figure 4.11 shows, the TGA of sublimed CuPc, H₂Pc and their mixture. The maximum weight loss has shifted towards the higher temperature.

The CuPc before sublimation has higher weight loss temperature than sublimed CuPc and this is may be due to the interaction of CuPc with its impurities which may be mainly H₂Pc (see figure 4.12).

4.4) Structural Analysis by X-Ray Diffraction:

The X-rays of interest to diffraction workers occur in the range 0.2-2.5 Å. However, The X-ray region of the spectrum covers the range 0.02 Å to slightly over 100 Å, figure 4.13.

4.4.1) Diffraction:

By analogy with the diffraction of light by an optical grating, crystals act as three dimensional gratings for diffraction of X-rays, because interatomic spacings in the crystal are approximately equal to the X-ray

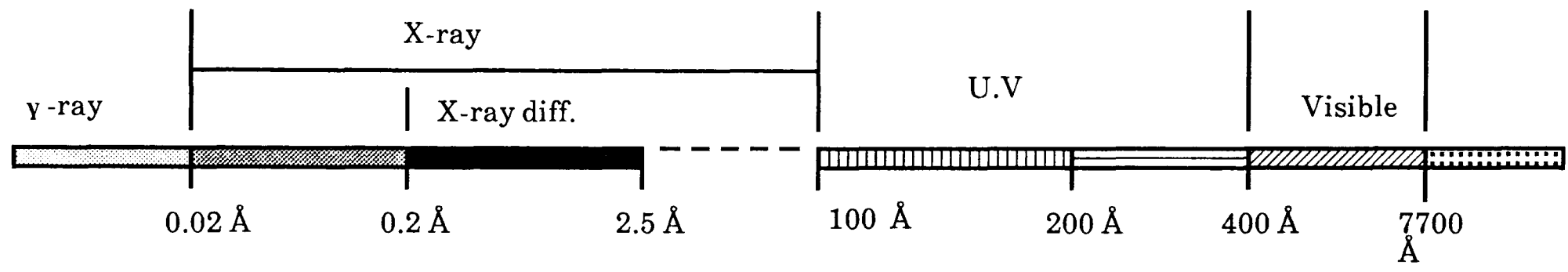


Figure 4.13: The X-ray of interest to diffraction.

Compound	% weight loss	% Residue	Maximum weight loss temperature (°C)	T _i (°C)	T _f (°C)	(T _f - T _i) °C
AlPcF	90.3	9.7	480	300	560	260
GaPcF	82.0	17.9	430	300	500	200
Copolymer	83.5	16.5	430 - 480	160	560	400
Mixture	81.7	22.4	430 - 480	280	560	280

Table 4.2: Thermogravimetric analysis results.

wavelength. So, X-ray diffraction is an extremely important tool for the measurements of the interplanar spacing, determination of crystal symmetry, and actual atomic positions. The information is useful for identification purposes and following solid state reactions.

X-ray diffraction was first discovered by *von Laue* in 1912. He systematised the experimental results quantitatively by the following three conditions which must be met simultaneously for diffraction to occur in three dimensions, which are called *Laue equations*:

$$a (\cos \alpha - \cos \alpha_0) = h \lambda \quad \dots\dots\dots 4.2$$

$$b (\cos \beta - \cos \beta_0) = k \lambda \quad \dots\dots\dots 4.3$$

$$c (\cos \gamma - \cos \gamma_0) = l \lambda \quad \dots\dots\dots 4.4$$

where a,b and c are spacing in three directions; α_0 , β_0 and γ_0 are the angles between the incident beam and the rows of the atoms in three directions; α , β and γ the angles between the diffracted beam and the three rows, h, k and l integers and λ is the wavelength of the X-rays. Crystals are infinite arrays of atoms or molecules. They can act as a multiple slit system and hence can diffract X-rays when the three above conditions are satisfied. Rows and columns of atoms or molecules form sets of layers with regular spacing. The integers h, k and l can be regarded as three numbers of the planes along the three dimensions. Maximum reinforcement occurs if the

difference in the distance travelled by any two rays is an integral number of λ (h,k,l).

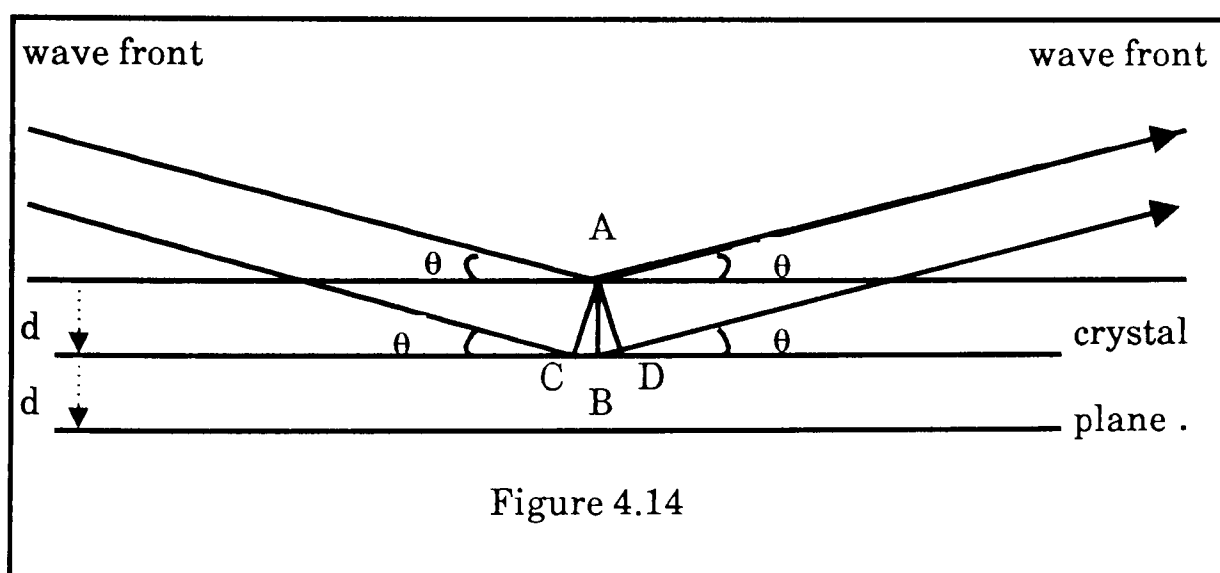
4.4.2) The Bragg Law:

Soon after *Laue's* work, *Bragg W. L.* showed that *Laue's conditions* were equivalent to reflection from a lattice plane and that the effect could be described by the simple equation:

$$n\lambda = 2d \sin \theta \quad \dots\dots\dots 4.5$$

This equation called the *Bragg law*, in which n is an integer, λ the wavelength of the X-ray, d the interplaner spacing and θ the angle of incidence of the X-ray beam on the plane.

The *Bragg law* of diffraction is to regard crystals as built up in layers or planes, such that each acts as a semi-transparent mirror, figure 4.14.



If an X-ray wave strikes a crystal at point A with an angle of incidence θ , it is reflected at the same angle. The wave which penetrates to the next plane just beneath the surface with an interplaner distance AB or d behaves

similarly when it strikes the second plane at point B. It must therefore travel further by distance $CB + BD$ (where $CB = BD$). By simple geometry and trigonometry, it can be shown that CB and BD are each equal to $d \sin \theta$, so that, $CB + BD = 2d \sin \theta$. Since the condition for reinforcement is that waves be in phase, an X-ray reflection will be observed only when the additional path difference, $CB + BD$ or $2d \sin \theta$, is an integral number of wave lengths. Using n to represent the integral order and λ the wavelength of the X-ray, we therefore write $n \lambda = 2d \sin \theta$.

In a crystalline powder, the tiny crystals are oriented at random. If such powder is struck by an X-ray beam, many planes will be so oriented that *Bragg's law* is satisfied and an X-ray diffraction pattern is obtained. To be certain that all possible planes are exposed to the X-ray beam, a cylindrical specimen is usually employed and rotated on its own axis during exposure.

4.4.3) Unit Cell:

In crystals the atoms are arranged periodically in three dimensions. This arrangement can be represented by a repeat unit called the unit cell, which is defined as the smallest repeating unit which shows the full symmetry of the crystal structure.

The seven crystal systems listed in table 4.3, are the seven independent unit cell shapes that are possible in three dimensional crystal structures. The symmetry of the crystal is linked with the symmetry of the unit cell and the arrangement of the crystal faces depends on the shape of the unit cell.

The sides of the unit cell are called the axes and are designated a, b and c. The angles between the axes are α (between b and c), β (between a and c) and γ (between a and b). The network formed by lines in three directions joining equivalent atoms is called a space lattice or simply lattice.

The *Miller indices* are used to enable discussion of planes and to have a mathematical basis for calculations of interplaner spacing of structures. To assign a *Miller index* one must first choose an origin for the three dimensional unit cell, which can be done arbitrarily, but the usual way is to choose the lower left corner of the unit cell. Any particular set of planes is described by the numbers of parts into which it divides the a, b and c axis. Three numbers are required and represented by h, k and l which are called *Miller indices*.

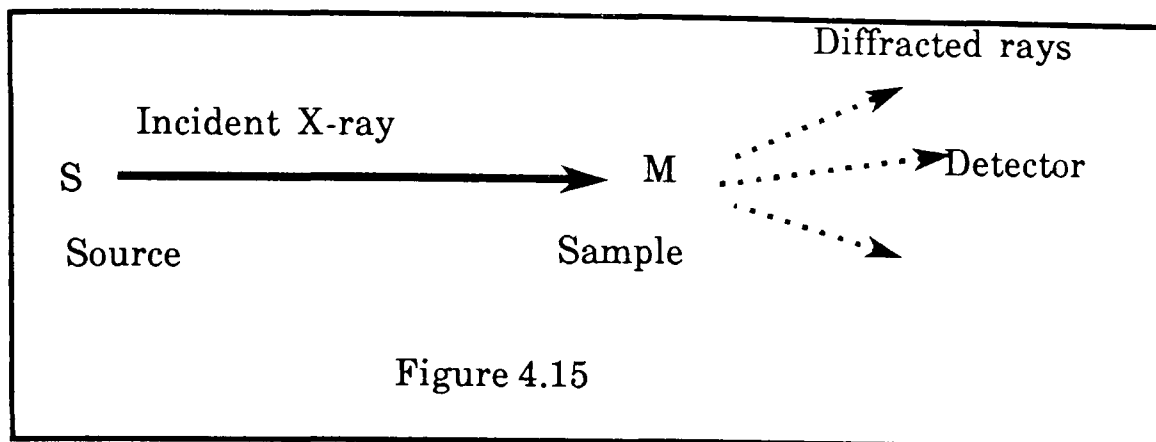
4.4.4) The X-Ray Diffraction Techniques:

The X-ray diffraction experiment requires:

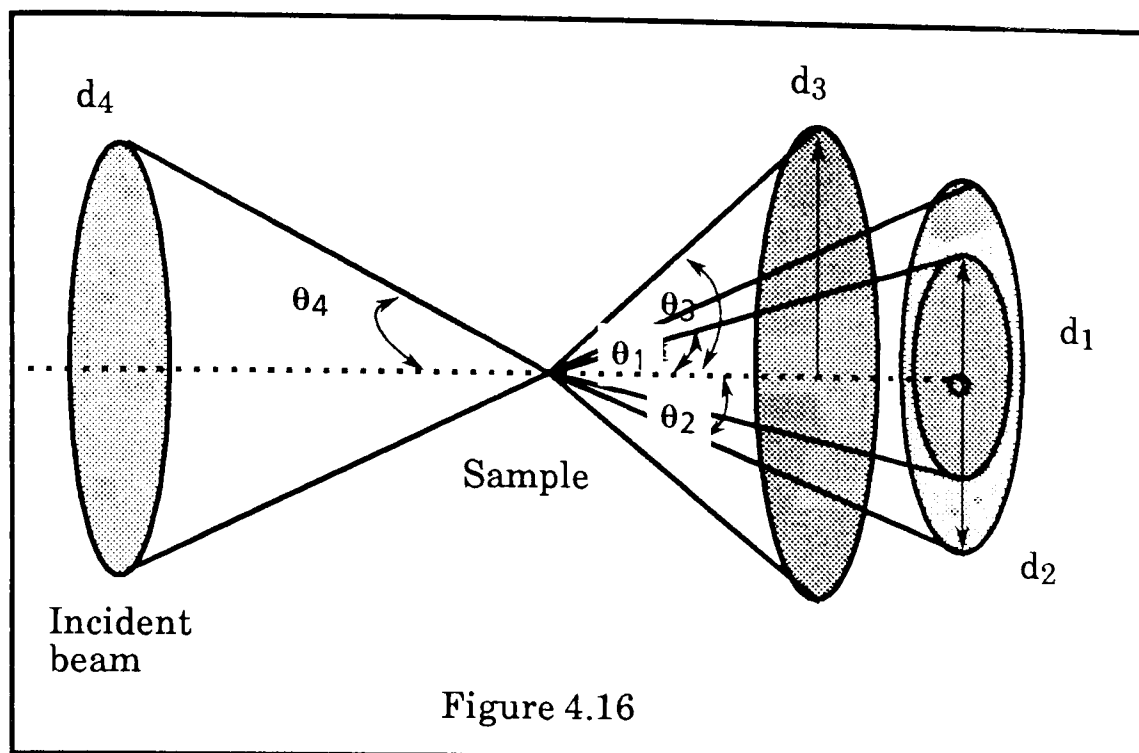
- ① X-ray radiation source - variable wavelength or monochromatic.
- ② Sample - single crystal, powder or solid specimen.
- ③ Detector - photographic film (*Debye-Scherrer* and *Guinier* focusing methods) or radiation counter (diffractometers), (figure 4.15).

(1) The powder methods:

A monochromatic beam of X-ray strikes a finely powdered sample which has crystals randomly arranged in every possible direction. In such a sample, the various lattice planes are present in every possible orientation.



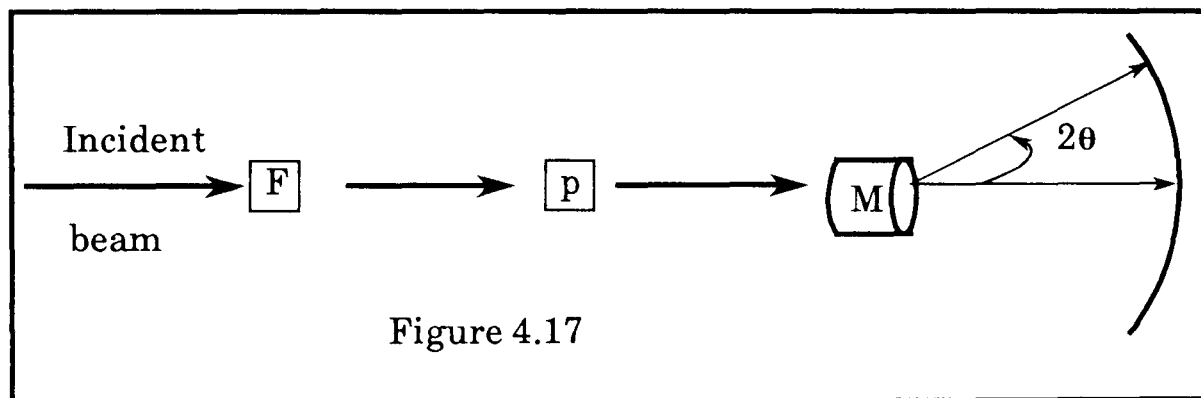
For each set of planes, at least some crystals must be oriented at a Bragg angle, θ , to the incident beam. Thus diffraction occurs for these crystals. All the diffracted rays from sets of planes of spacing d_1 , will generate a cone of angle $2\theta_1$. Planes of spacing d_2 will generate a cone of angle $2\theta_2$, and so on (figure 4.16). If for any reason the total number of orientations of irradiated crystallites is too small the diffraction rings will be discontinuous rather than continuous and of uniform intensity. This can be overcome to some extent by rotating the sample in such a way as to cause each crystallite to assume a variety of orientations with respect to the X - ray beam. However, the rotation process will increase the proportion of contributing crystallites by less than 35% (4.32). The fineness of the subdivisions of the sample is of critical importance for the quality and reliability of the reflections obtained.



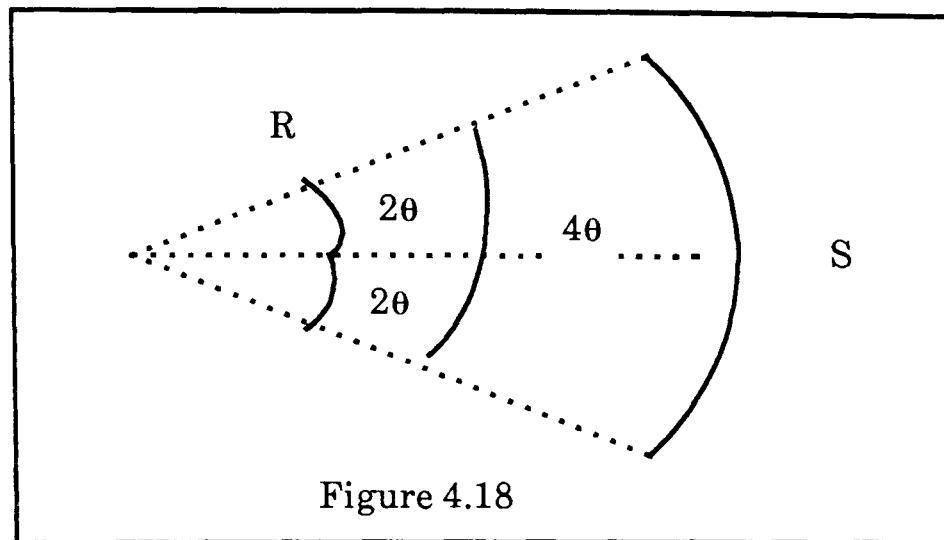
Each crystalline substance has its own characteristic powder diffraction pattern which may be used for its identification. Standard patterns are given in the powder diffraction file (known as *JCPDS* or *ASTM file*)^(4.33). Mixtures of substances may be identified, provided that the patterns of the components are available for comparison. Powder X-ray diffraction analysis is the perfect technique for line mixture analysis, since each component produces its characteristic pattern independently of the others. In the same way the powder X-ray method may be used as a rough check on purity provided the impurities are present as a separate crystalline phase.

a) The Debye-Scherrer Method:

The incident beam is usually passed through a filter F to obtain the characteristic K_{β} radiation, while the K_{α} rays are collimated by the pinhole system (p) and then pass through the small cylindrical sample (M). Sections of various diffracted cones are intercepted by the cylindrical strip of photographic film. The powder specimen is rotated about its cylindrical axis in order to increase the number of particles contributing to each reflection (figure 4.17).



To obtain d-spacing from the *Debye-Scherrer film*, the separation, S, between pairs of corresponding arcs is measured. If the camera has radius, R (figure 4.18), then:



$$4\theta = \frac{S}{R} \quad \dots\dots\dots 4.6$$

$$\theta = \frac{S}{4R} \quad (\text{in radians}) \quad \dots\dots\dots 4.7$$

since there are $360/2\pi$ degrees per radian, then:

$$\theta = \frac{360}{2\pi} \times \frac{S}{4R} \quad \dots\dots\dots 4.8$$

$$\frac{4\theta}{360} = \frac{S}{2\pi R} \quad \dots\dots\dots 4.9$$

Therefore d may be obtained for each pair of arcs. The disadvantages of this method are:

- ① The exposure time is long (6-24 hours).
- ② The closely spaced arcs are not well resolved. This is because the X-ray beam is divergent and the spread increases in the diffracted beam, although the incident beam enters the camera through a pinhole slit and collimator tube. If more resolution is required, then a finer collimator is used, the resulting diffracted beam has less intensity, and longer exposure

times are needed. In addition to that, the amount of background radiation detected by the film increases with exposure time, so a weak line may be lost in the background.

b) Focusing Methods:

An intense incident beam is used with the result that excellent resolution of lines is obtained and exposure time is much reduced (10 min. to 1 hour). A convergent beam is obtained by placing a bent single crystal of quartz or graphite between the X-ray source and the sample. This bent crystal is orientated so that it diffracts the incident beam and converts it from a divergent into a convergent beam. Then the beam strikes the sample and the diffracted beams are arranged to focus at the surface of the film.

c) Diffractometry (Spectroscopic Powder Technique):

This gives a series of peaks on chart paper. A convergent beam is also used to give good resolution of peaks. Both peak positions and intensities (height) are obtained from the chart. A radiation counter detector is used.

(2) Single Crystal Methods :

This method is used to determine the nature of the unit cell and its dimensions which can be extended to determine the lattice type and the crystal structure.

Monochromatic X-rays and an optimum crystal size (about 0.2 mm) are used. The detector may be either a film or a counter.

There are three main film techniques : rotation (oscillation), *Weissenberg* and precession methods.

4.4.5) Factors Affecting Intensities:

These factors are needed to be considered quantitatively if one is interested in carrying out crystal structure determinations. But in unit cell determination in single crystal methods, or to fingerprint materials in powder methods, it is normal to use intensity data without applying any of these correction factors.

a) Polarization Factor:

The X-ray radiation from the X-ray tube is regarded as unpolarized, but after being diffracted is polarized. The degree of polarization depends upon the angle through which it scattered. According to the *Thomson equation*:

$$I_x \propto \frac{1}{2} (1 + \cos 2\theta) \quad \dots\dots\dots 4.10$$

where I_x is the scattered intensity at point x , and 2θ is the angle between the direction of the incident beam and the diffracted beam which passes through x , and the term $1/2(1 + \cos 2\theta)$ is called a *polarization factor*.

b) Velocity(Lorentz) Factor:

The planes which make an angle with the rotation axis are in reflecting position for a longer time than those parallel to the axis. The problem is geometrical one resulting from the angular velocity of these planes. Values of the polarization factor combined with a *Lorentz factor* have been tabulated(4.34).

c) Temperature Factor:

From the kinetic theory of matter, some thermal motion of the atoms or molecules will continue even in the crystal. The amplitude of these vibrations has an adverse effect on the diffraction intensity until at a sufficiently high temperature, the intensity becomes zero.

This factor has been calculated mathematically by *Debye* and *Waller*(4.35).

d) The Atomic Scattering Factor:

This may be defined as the ratio of the amplitude ray scattered by an atom at rest to that scattered by a single electron. This factor arises because atoms do not exist as points in space, but possess finite sizes which are of the same magnitude as the the X-ray wave lengths used in the diffraction studies. Each atom in the crystal scatters X-rays by an amount related to the scattering factor, f_0 , of that atom . It is proportional to atomic number and decreases with the *Bragg angle* θ .

e) The Structure Factor:

This depends on the position of the atom in the unit cell and its scattering power (the atomic scattering factor). The intensities are proportional to the square of the *structural factor* (F), which is expressed by:

$$I_{hkl} \propto \left| F_{hkl} \right|^2 = \left\{ \sum_i f_i \cos \left[2\pi (h x_i + k y_i + l z_i) \right] \right\}^2 + \left\{ \sum_i f_i \sin \left[2\pi (h x_i + k y_i + l z_i) \right] \right\}^2 \quad \dots \quad 4.11$$

where h, k and l are *Miller indices* of the reflections and x_i , y_i and z_i are the coordinates of atoms in the unit cell and f_i the scattering factors of all the atoms, and \sum_i indicates that the summation carried out over all the atoms in the unit cell.

f) Multiplicity Factor:

This is related to the number of reflections that contribute to an observed powder line. Taking the d-spacing formula for a cubic crystal (table 4.3).

$$\frac{1}{d^2} = \frac{h^2 + k^2 + l^2}{a^2} \quad \dots \quad 4.12$$

It can be shown that lattice planes, such as (013), (031), (103), etc., all have the same d-spacing. Therefore, reflections which have the same d-spacing

will be superimposed. The multiplicity of the powder line is the number of lines, one from each set of planes, that are superimposed to give the observed line.

g) The Absorption Factor:

When X-ray pass through a material their intensity is reduced by absorption . The difference in the energy between the incident and transmitted X-rays is due to scattering and conversion to thermal energy. For X-ray beam of intensity, I, the change in it's intensity will be:

$$\frac{dI}{I} = -\mu' dx \quad \dots\dots\dots 4.13$$

where dx is the thickness and μ' is the linear absorption coefficient of the materials and has the dimension of inverse distance. Ideally, for single crystal work, the crystal should be spherical so as to have the same absorption factor in all directions.

4.4.6) Result and Discussion :

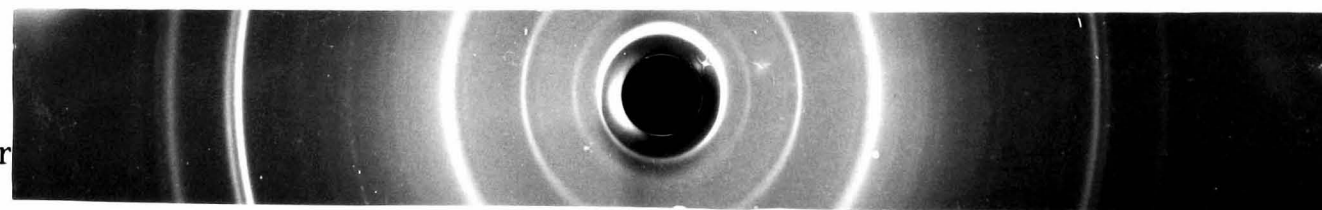
A powder photograph technique (*Debye-Scherrer*) was used to study sublimed AlPcF, GaPcF, their copolymer and their mixture (1:1 mole ratio). The interplanar spacing values are tabulated in table 4.4. A typical photograph is shown in figure 4.19

The d-spacing was calculated according to the *Bragg equation*. The linear equivalent on the film of the angle of deviation, 2θ , was measured (the film being in an asymmetric position). The d-spacing was calculated by

a) AlPcF



b) Copolymer



c) GaPcF



d) Mixture



Figure 4.19: Atypical powder diffraction photograph.

<i>Cubic</i>	--	$d = \frac{a}{\sqrt{h^2 + k^2 + l^2}}$ or $\frac{1}{d^2} = \frac{h^2 + k^2 + l^2}{a^2}$
<i>Tetragonal</i>	--	$\frac{1}{d^2} = \frac{h^2 + k^2}{a^2} + \frac{l^2}{c^2}$
<i>Orthorhombic</i>	--	$\frac{1}{d^2} = \frac{h^2}{a^2} + \frac{k^2}{b^2} + \frac{l^2}{c^2}$
<i>Hexagonal</i>	--	$\frac{1}{d^2} = \frac{4}{3} \frac{h^2 + hk + k^2}{a^2} + \frac{l^2}{c^2}$
<i>Monoclinic</i>	--	$\frac{1}{d^2} = \frac{h^2}{a^2 \sin^2 \beta} + \frac{k^2}{b^2} + \frac{l^2}{c^2 \sin^2 \beta} - \frac{2hl \cos \beta}{ac \sin^2 \beta}$
<i>Triclinic</i>	--	$\frac{1}{d^2} = \left[(abc)^2 (1 - \cos^2 \alpha - \cos^2 \beta - \cos^2 \gamma + 2 \cos \alpha \cos \beta \cos \gamma) \right]^{-1}$ $\left[(bc \sin \alpha h)^2 + (ac \sin \beta k)^2 + (ab \sin \gamma l)^2 + \right.$ $2abc^2 (\cos \alpha \cos \beta - \cos \gamma) hk +$ $\left. 2a^2 bc (\cos \beta \cos \gamma) kl + 2ab^2 c (\cos \gamma \cos \alpha - \cos \beta) hl \right]$
<i>Rhombohedral</i>	--	$\frac{1}{d^2} = \frac{(h^2 + k^2 + l^2) \sin^2 \alpha + 2(hk + kl + hl)(\cos^2 \alpha - \cos \alpha)}{a^2 (1 - 3 \cos^2 \alpha + 2 \cos^3 \alpha)}$

Table 4.3: Formulas relating interplanar spacings (d) with lattice parameters and Miller indices(hkl).

Compound	This work		Literature (ref.34)	
	% I	d-values	% I	Literature (ref.34)
AlPcF	100	12.617	100	12.00
	90	3.5927	100	3.66
	50	5.7119	10	5.67
	20	9.0729	10	9.08
GaPcF	100	12.617		
	90	3.6686		
	90	3.8241		
	70	5.6253		
	50	8.8376		
Mixture	100	12.617		
	90	5.6253		
	70	3.8241		
	60	3.6686		
	60	3.5927		
	50	8.8376		
Copolymer	100	12.617		
	50	3.7047		
	30	5.7119		
	20	8.8376		

Table 4.4: X-ray diffraction pattern data. (I) is the intensity.

making use of a valuable table of interplanar spacings as a function of θ or 2θ (4.36). The intensities were estimated visually. The intensity of the lines were matched with the darkest line of all the four films (100% I). A background diffraction for the empty cell was taken, and its pattern subtracted from the samples patterns.

There are several factors which contribute to scattering and diffraction at angles other than those of the *Bragg reflections* produced by the radiation employed:

- ①) Lattice imperfections of various kinds
- ②) X-ray scattered by the air in the camera
- ③) Secondary fluorescence from the specimen
- ④) Compton (incoherent) scattering (due to elastic collision between an electron and the phonon).

From table 4.4, GaPcF and AlPcF show a similar diffraction pattern which is because the compounds are isomorphous (4.25). There are differences in the d-values and also the differences in the intensities of the lines.

Kenney et al (4.1) have studied the powder diffraction for both sublimed AlPcF and GaPcF. They suggested that the ring-ring separation is 3.66 Å in AlPcF and 3.86 Å in GaPcF which can be identified from table 4.4. Single crystal studies on GaPcF(4.37-38) show that interplanar spacing is 3.879 Å.

Because the two compounds are isomorphous one may expect that some of the lines of their mixture pattern will be superimposed. In table 4.4, and figure 4.19 all the lines appear in the mixture of both compounds. The line 5.62 (d-value) which has higher intensity in the mixture pattern may be as

a result of superimposition. Annealing of the mixture at 400 °C (30 °C below the sublimation temperature. of GaPcF) under nitrogen gas flow does not change the X-ray pattern which suggests that there is no change in the crystal structure under these conditions.

The copolymer pattern is slightly different than that of the mixture. The d-value of 3.7 Å, suggests that ring-ring separation is intermediate between the two compounds, AlPcF and GaPcF.

It is worth mentioning that GaPcF, GaPcCl and AlPcCl have a Triclinic structure^(4.37-39). The approximate *van der Waals* thickness of the ring is 3.4 Å^(4.1,4.39).

4. 5) The Electron Microscope:

The scanning electron microscope (SEM) and electron microprobe microanalyser (EPMA) are two powerful instruments which permit the observation and characterisation of organic and inorganic surfaces. The area to be examined is irradiated with a finely focused electron beam, which may be static or scanned across the surface of the specimen. The type of the signal obtained is from characteristic X-rays, back scattered electrons, secondary electrons, *Auger* electrons, and photons of different energies.

In SEM, the signal of greatest interest is from secondary and back scattered electrons, since they vary as a result of differences in surface topography as the electron beam is scanned across the specimen.

In EPMA, the primary radiation of interest are the characteristic X-rays, which are emitted as a result of the electron bombardment. By

analysis of the characteristic X-radiation qualitative and quantitative compositional information can be obtained. Its main limitations are that it cannot distinguish between ionic and non-ionic and isotopic species, and cannot at present detect the very low atomic number elements ($Z < 4$).

Both instruments are very similar, so many manufacturers have constructed instruments able to operate as SEM and EPMA, such as the instrument used in this work (*JEOL JSM-35C*).

This technique is widely used since its invention in the early 1960's. The instrumentation and the theory behind it is well known, so it is not intended to repeat it in this thesis. The main point is the interaction between the specimen and incident electron beam. Different kinds of interaction mechanisms can occur as a result of this interaction, as mentioned earlier (figure 4.20), and the signal produced can then be detected in different ways (see chapter.3). Of course, there are many operating conditions and limitations which must be considered.

The collected data consist of either a wavelength or energy and a count-rate. The count-rate is proportional to concentration. These data can be used as a quantitative or qualitative analysis of the specimen under study.

In this work electron microscopy is used for the determination of Al and Ga atoms in AlPcF and GaPcF and in their copolymer. Two kinds of detectors were used (WDS) and (EDX) (see chapter 3) .

4.5.1) Qualitative and Quantitative Determination of Al and Ga:

Two kinds of dispersive X-ray detectors were used (EDX and WDS) to detect Al and Ga in AlPcF, GaPcF and their copolymer films deposited on

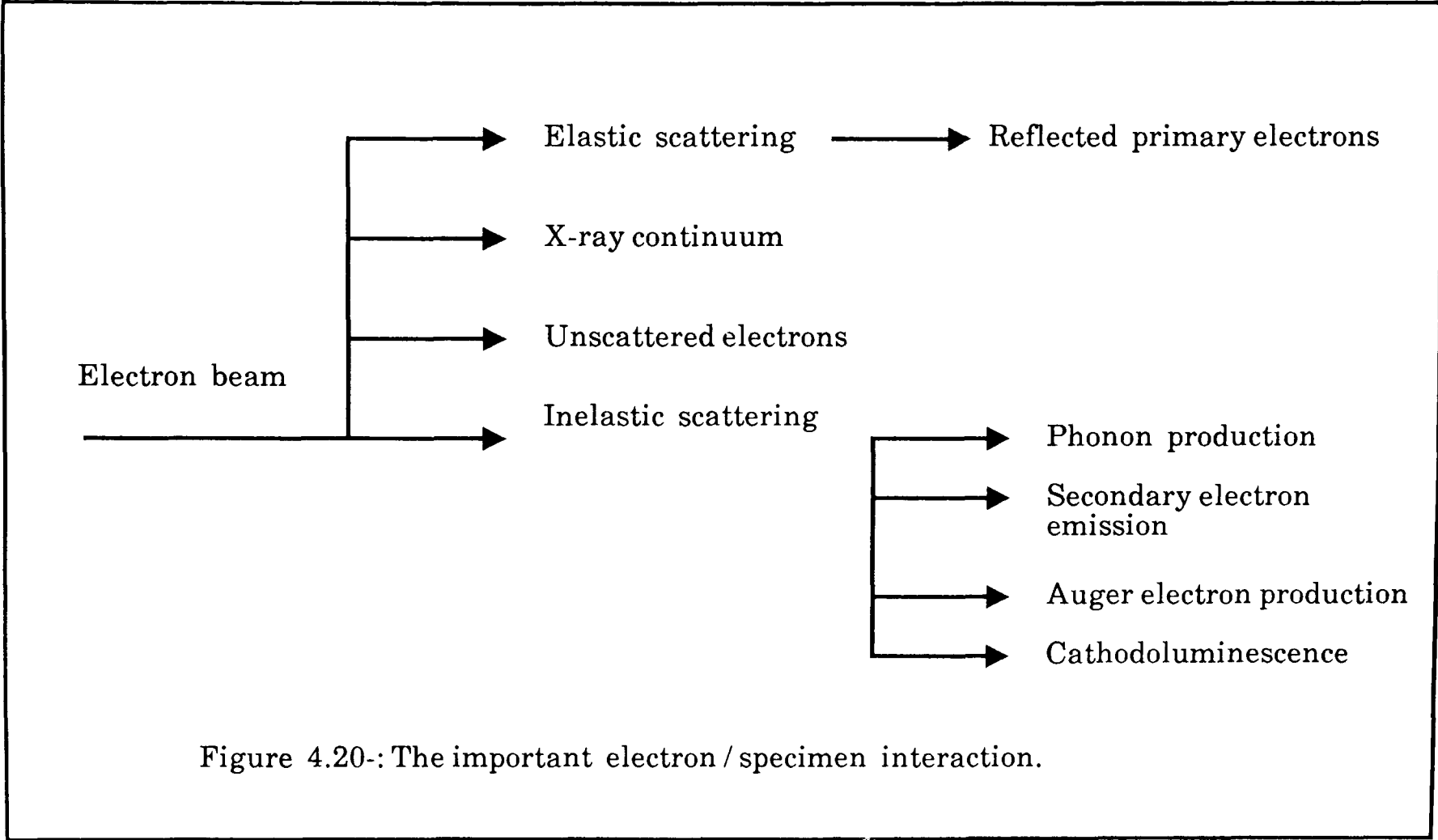


Figure 4.20-: The important electron / specimen interaction.

two kinds of surfaces, glass and carbon, both free of Al and Ga. The detected energy was K_{α} for both elements with accelerating voltage 20 keV, and the energy L_{α} for Ga and K_{α} for Al with accelerating voltage 10 keV.

a) The EDX Detector:

Thin film specimens of AlPcF, GaPcF and their copolymer of thickness of 1 μm were prepared by sublimation. An area of square centimeter of all the three samples was scanned over a complete energy spectrum. Al and Ga were detected. Figures 4.21-23, show the X-ray spectrum of count rate against energy (keV) for AlPcF, AlPcF and the copolymer to detect Al and Ga. Table 4.5, shows the percentage of Al and Ga in the three compounds after subtraction of the background counts calculated from figures 4.21-23.

From table 4.5, the percentage concentration of Al and Ga is lower than the expected (50% of each), and the Ga is slightly higher than Al.

The main sources of error in this technique are :

1) The background count due to the X-ray continuum and the overlap of the X-ray peak from the K_{α} of Si (1.74 keV) in the glass with the X-ray peak from K_{α} of Al. The background intensity is highest at the lower end of the spectrum (< 5 keV). The K_{α} line is 1.486 keV for Al (see table 4.6).

2) The detecting crystal is exposed directly to the source of X-ray (adjacent to the specimen), which creates problems due to the contamination of the detector by hydrocarbons from the vacuum system. From table 4.5, it seems that the background intensity has a big influence on the Al intensity value in both AlPcF and copolymer films by using the EDX system.

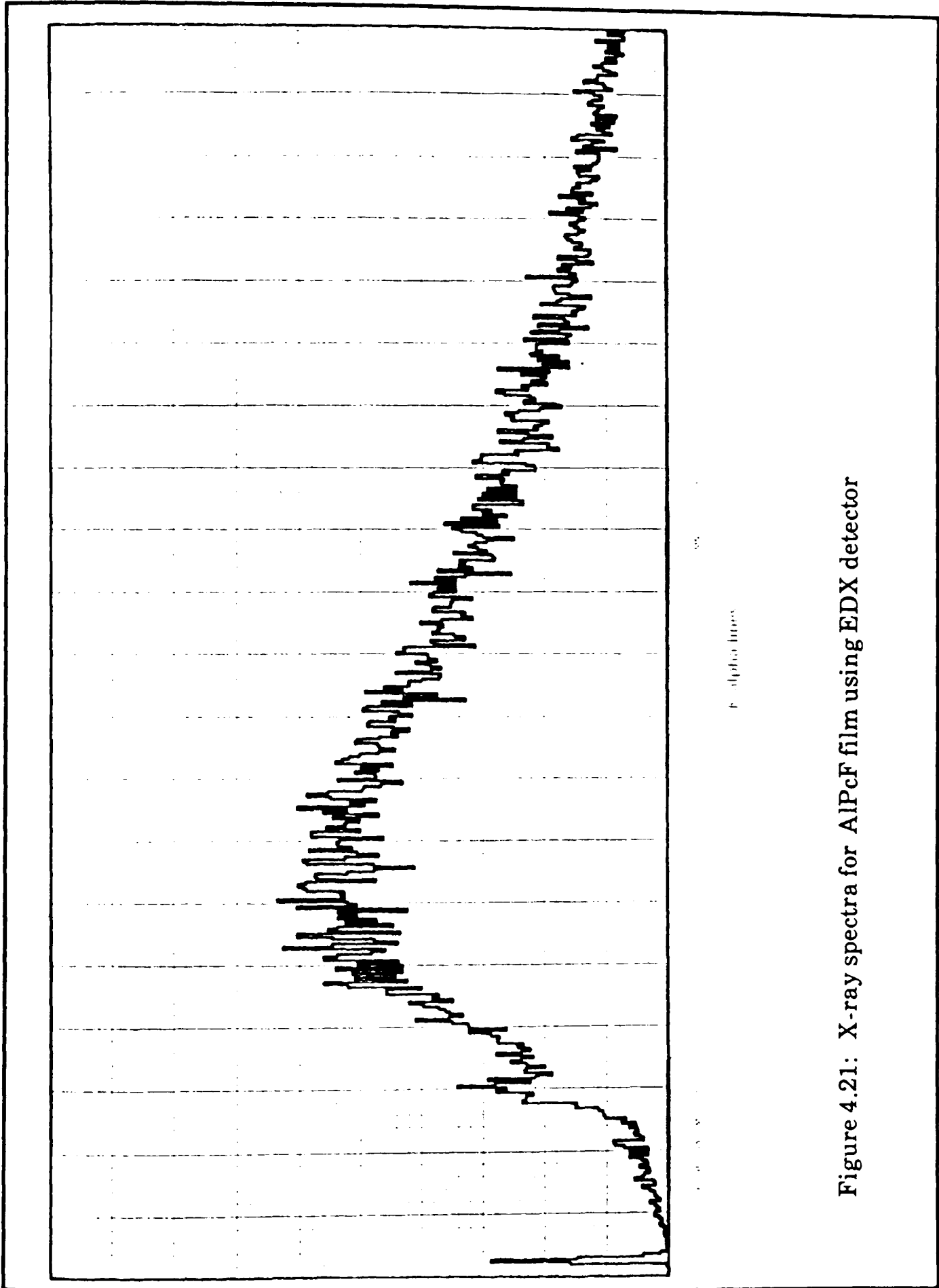


Figure 4.21: X-ray spectra for AlPcF film using EDX detector

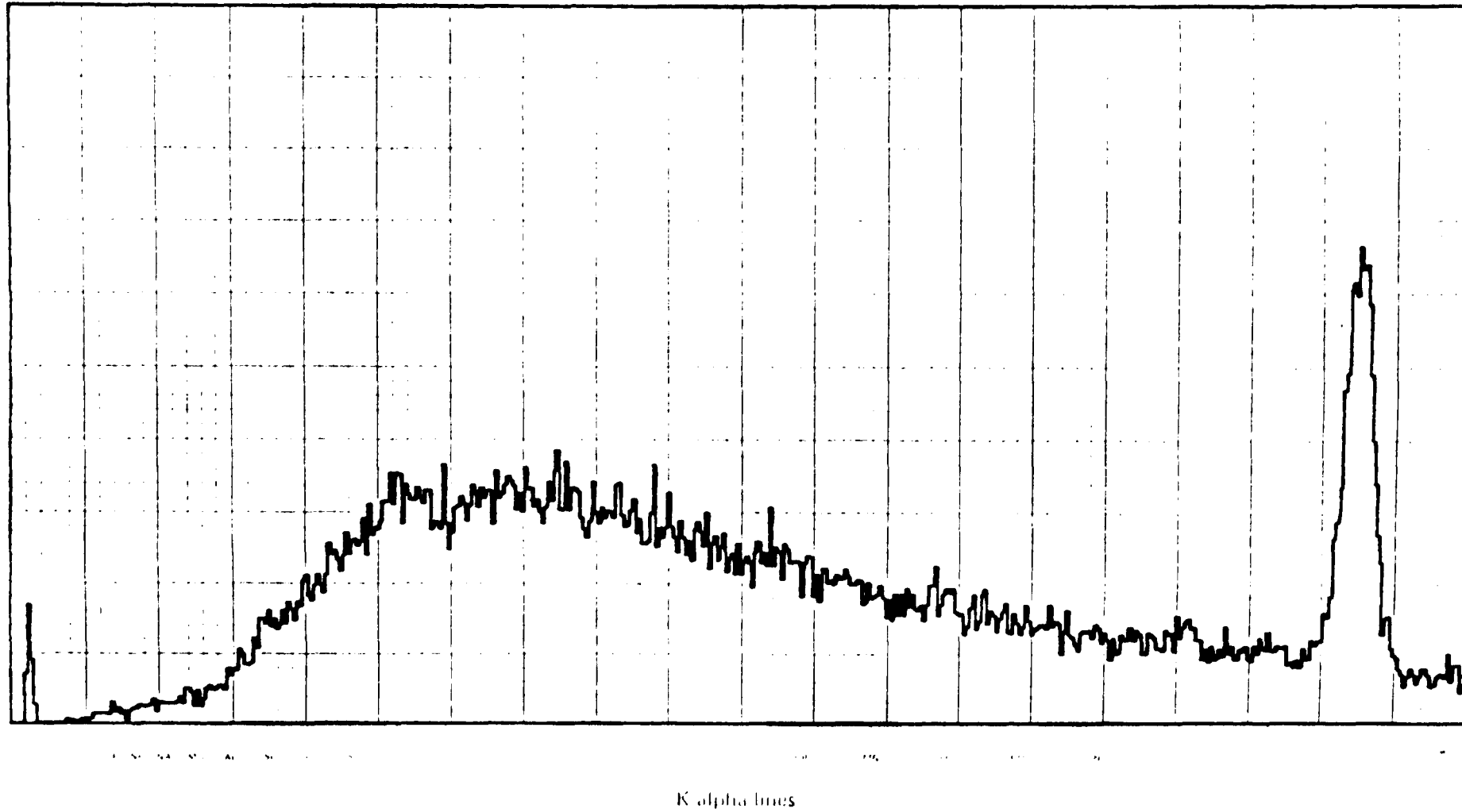


Figure 4.22: X-ray spectra for GaPcF film using EDX detector

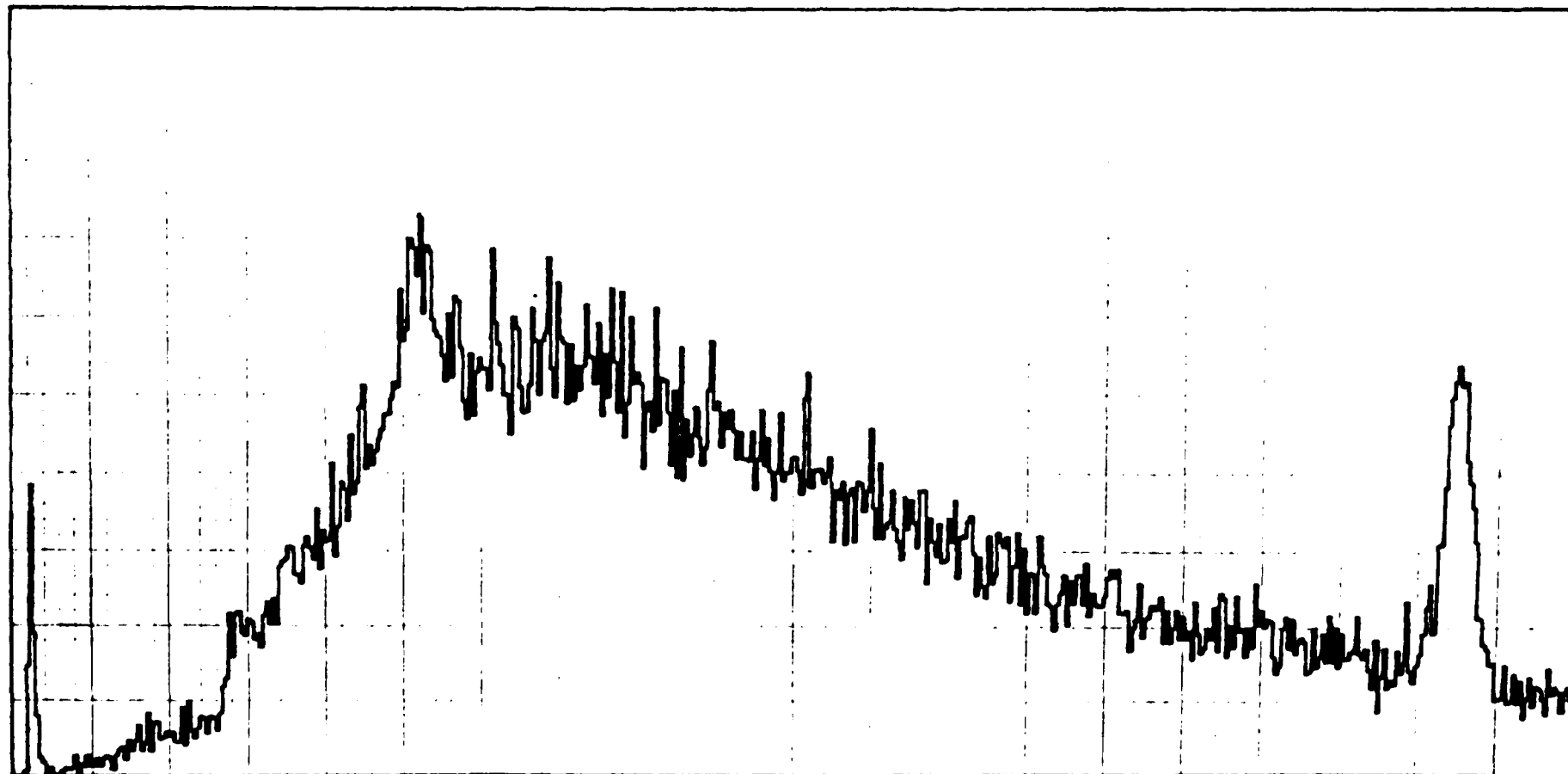


Figure 4.23: X-ray spectra for the copolymer film using EDX detector

Film	Number of counts (K_{α})						Average	
	Al			Ga			Al	Ga
AlPcF	193	163	151	---	---	---	169	---
GaPcF	---	---	---	2135	2320	2345	---	2267
Copolymer	63	62	43	780	741	789	56	770
% in the copolymer after thickness correction							30	44
% in the copolymer after normalization							40	60

Table 4.5: Percentage of Al and Ga in the copolymer using glass substrate, with accelerating voltage 20 eV.

Elements	Line	E (KeV)	λ (Å)	E_{exit} (KeV)
Al	K α	1.486	8.341	1.560
Ga	L α	1.098	11.292	1.117
Ga	K α	9.241	1.341	10.366

Table 4.6: The energy and excitation (edge) energy for Al and Ga.

b) The WDS Detector:

The same samples were analysed using the wavelength dispersive system to eliminate the above problems.

Films of AlPcF, GaPcF and their copolymer, 1 μm thick, were sublimed on carbon substrates (10 mm diameter). The accelerating voltage was 20 keV and the counting rate was 20 sec count⁻¹. The count at three different detector positions and at two different specimen position was taken. Table 4.7, shows the detection of K_{α} from Al and Ga.

To reduce the excitation of Al by the fluorescence (4.40-41) of Ga it was necessary to reduce the acceleration voltage from 20 keV to 10 keV. Table 4.8, shows the detection of K_{α} from Al and L_{α} from Ga.

Actually, it is difficult to use the X-ray count as a direct indication of concentration because the physics of X-ray emission is very complex. Details of the geometry of the system and the behaviour of the specimen are needed. Reducing the accelerating voltage may reduce the resolution of the instrument.

By reducing the effect of fluorescence and the elimination of the Si background effect using a carbon substrate the concentrations of Al and Ga are calculated to be 60% and 40% respectively. These measurements indicate that the surface concentration in a sublimed film is 60% AlPcF and 40% GaPcF instead of the equal concentration of the two species originally present. Whilst these measurements are subject to significant error for reasons already discussed, it is unlikely to be as great as 10%. Furthermore the XPS measurements give an almost identical result. It must therefore

Film	Position of the detector						Average		number of counts K _a
	Al			Ga			Al	Ga	
	99.7	90.7	81.7	97.1	93.1	89.1			
GaPcF	-----	-----	-----	1155	2734	1083	-----	1615	
AlPcF	1335	7111	1790		-----	-----	5548	-----	
Copolymer	1459	5028	1352	1004	1675	1100	3654	637	
	1202	4962	1350	1079	1711	1040			
% of Al and Ga in the copolymer							66	39	
% of Al and Ga after normalization							63	37	

Table 4.7: Percentage of Al and Ga in the copolymer using carbon substrate with accelerating voltage 20 KeV.

Film	Position of the detector						Average		number of counts
	Al (K_{α})			Ga (L_{α})			Al	Ga	
	99.7	90.7	81.7	132	123	114			
AlPcF	54	4779	108	-----	-----	-----	4655	-----	
	54	4685	90	-----	-----	-----		-----	
GaPcF	-----	-----	-----	14	1240	38	-----	1223	
	-----	-----	-----	42	1264	23	-----		
Copolymer	67	2642	92	12	478	33	2565	452	
	82	2815	86	22	479	28			
% of Al and Ga in the copolymer							56	36	
% of Al and Ga after normalization							61	39	

Table 4.8: Percentage of Al and Ga in the copolymer using carbon substrate with accelerating voltage 10 KeV.

be concluded that, whilst the copolymer can be sublimed to give good quality films which are very similar in composition to the starting material, the difference in volatility of the two monomer units has led to a slight enrichment in the AlPcF towards the free surface, and presumably a corresponding enrichment in GaPcF towards the substrate.

Figure 4.24, shows a typical morphology of the film surface on carbon substrates for AlPcF. The rough surface of the film may have influence on the quantitative analysis since it has a big influence on the scattered X-rays.

Complex mathematics and statistics must be applied to transform the raw data into fully quantitative results taking into account the different effects(4.41).

4.6) X-Ray Spectroscopy:

4.6.1) X-Ray Photoelectron Spectroscopy (XPS):

Electron spectroscopy techniques measure the kinetic energy of electrons that are emitted from matter as a consequence of bombarding it with ionising radiation, $h\nu$, or high-energy particles (4.42-43). The kinetic energy, E_k , of the ionized electron is equal to the difference between the energy, $h\nu$, of the incident radiation and the binding energy or ionisation potential E_b of the electron.

$$E_k = h\nu - E_b - \Phi_{sp} \quad \dots \quad 4.14$$

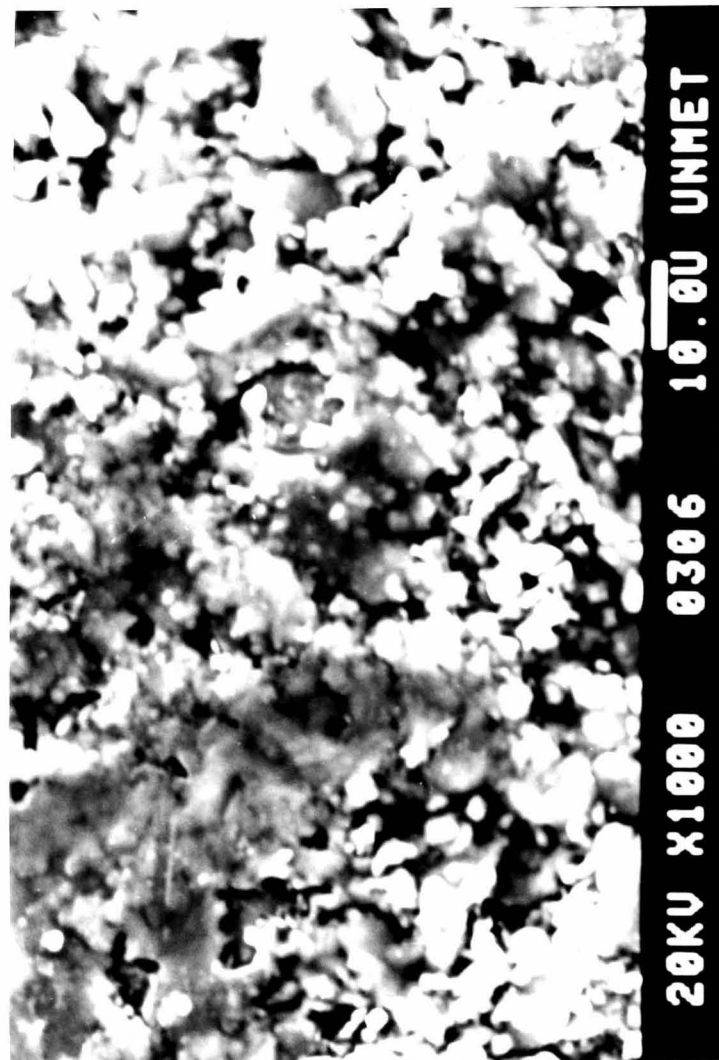


Figure 4.24: Typical morphology of film surfaces carbon substrates.

where Φ_{sp} is the work function of spectrometer materials and E_b is the binding energy. For a given atom, a range of E_b values is possible corresponding to the ionisation of electrons from different inner and outer valence shells, and these E_b values are characteristic of each element. Measurement of E_k and E_b provides a means of identification of atoms and forms the basis of the ESCA (electron spectroscopy for chemical analysis) technique. The ionizing radiation that is used in ESCA is usually either X-rays or ultraviolet light and the techniques are then known as XPS (X-ray photoelectron spectroscopy) and UPS (ultraviolet photoelectron spectroscopy) respectively. The main difference between the two techniques is that different electron shells are accessed and hence ionised by the different wavelength of radiation (4.44).

The electrons produced in ESCA are not very energetic (usually their energy is much less than 1 keV) and are rapidly absorbed by solid matter. Consequently they can not escape from solids unless they are ejected within 20-50 Å of the surface (4.44) so any changes in the bulk cannot be monitored.

XPS is a widely used technique for the elemental analysis of surfaces and the near surface region. In addition the technique also provides information about the chemical environment of the observed atoms (4.42-44).

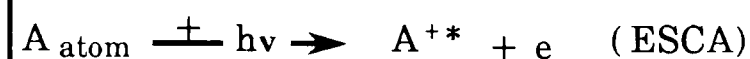
There are many factors affecting XPS analysis (4.45):

- ① Variation of the binding energies due to instrumental factors, history and preparation of the samples.
- ② Instrumental sensitivity
- ③ Effect of the surface uniformity on the electron take off angles.
- ④ X-ray excited *Auger transition*.

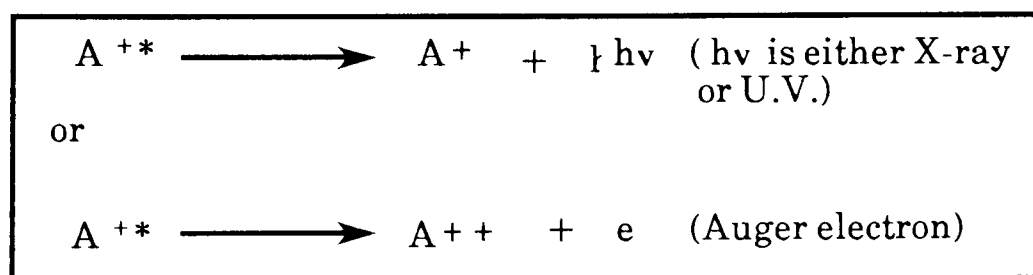
- ⓐ Sample damage by the X-ray radiation
- ⓑ Charge transfer and formation of satellite peaks.

4.6.2) Auger Electron Spectroscopy:

The *Auger process* (4.46) occurs after an atomic level has been ionised by incident photons or electrons. The hole in the inner shell is filled by one electron from a less tightly bound level and a second electron escapes into the vacuum with the remaining kinetic energy, this means that the ejected and detected electrons are not the primary ionised electrons as in the ESCA but are produced by secondary processes involving the decay of ionised atoms from excited state to the lower energy state(4.44).



where A^{+*} refers to an ionized atom which is in an excited state. This excited state arises if the electron is ejected from an inner shell, leaving a vacancy. The excited atom decays when electrons drop into the vacancies in lower energy levels.



In this work an *Auger electron* peaks appear as a result to the photoelectron process. The photoelectron process and the *Auger process* are shown in figure 4.25.

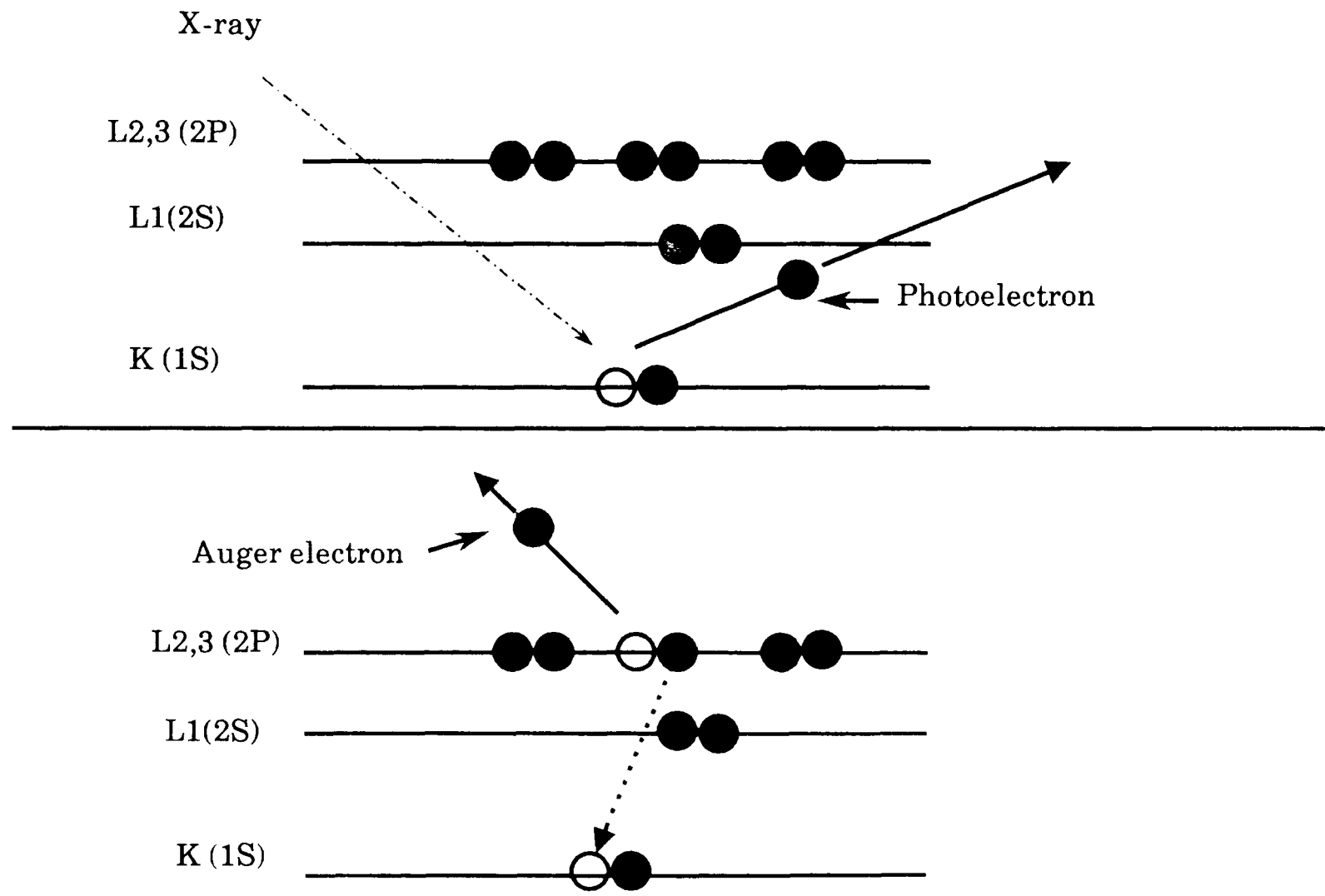


Figure 4.25 : Electron spectroscopy.

4.6.3) Results and Discussion:

In this work XPS and depth profiling were used to estimate the amount of both Al and Ga on the surface and in the bulk of the films of AlPcF, GaPcF and their 1:1 mole ratio copolymer. These techniques were used previously by Drs. *Dann* and *Fahy* of *Nottingham University* (4.47-48) to assess the damage in the surface of the iodine implanted phthalocyanines.

Figure 4.26 shows a full range X-ray photoelectron scan for GaPcF. C, F, Ga and N appear to be present in approximately the right proportions. The peak at 25 eV may be oxygen adsorbed on the film which is probably taken from the residual gases in the vacuum system. For peaks positions see ref.49.

Figure 4.27 shows a full range X-ray photoelectron scan for AlPcF. C, F and N appear in about the right proportions. The Al line at 74 eV is very weak, but if the sensitivity factor is taken into account, then it approaches the expected intensity. The spectrum is very noisy due to sensitivity. There appears to be impurity contamination in the film as well.

Figure 4.28 shows a full range X-ray photoelectron scan for the copolymer. The first obvious change is the reduction in the peak height of fluorine. The C/N ratio remaining almost constant, which indicate that there is no change in the spectrum of the organic ring system during copolymerisation. There is also a new peak at 540 eV which may be oxygen.

Figures 4.29-4.31 show the expected fluorine peak. The peaks for AlPcF (Figure 4.29) and GaPcF (Figure 4.30) had a good signal to noise ratio and

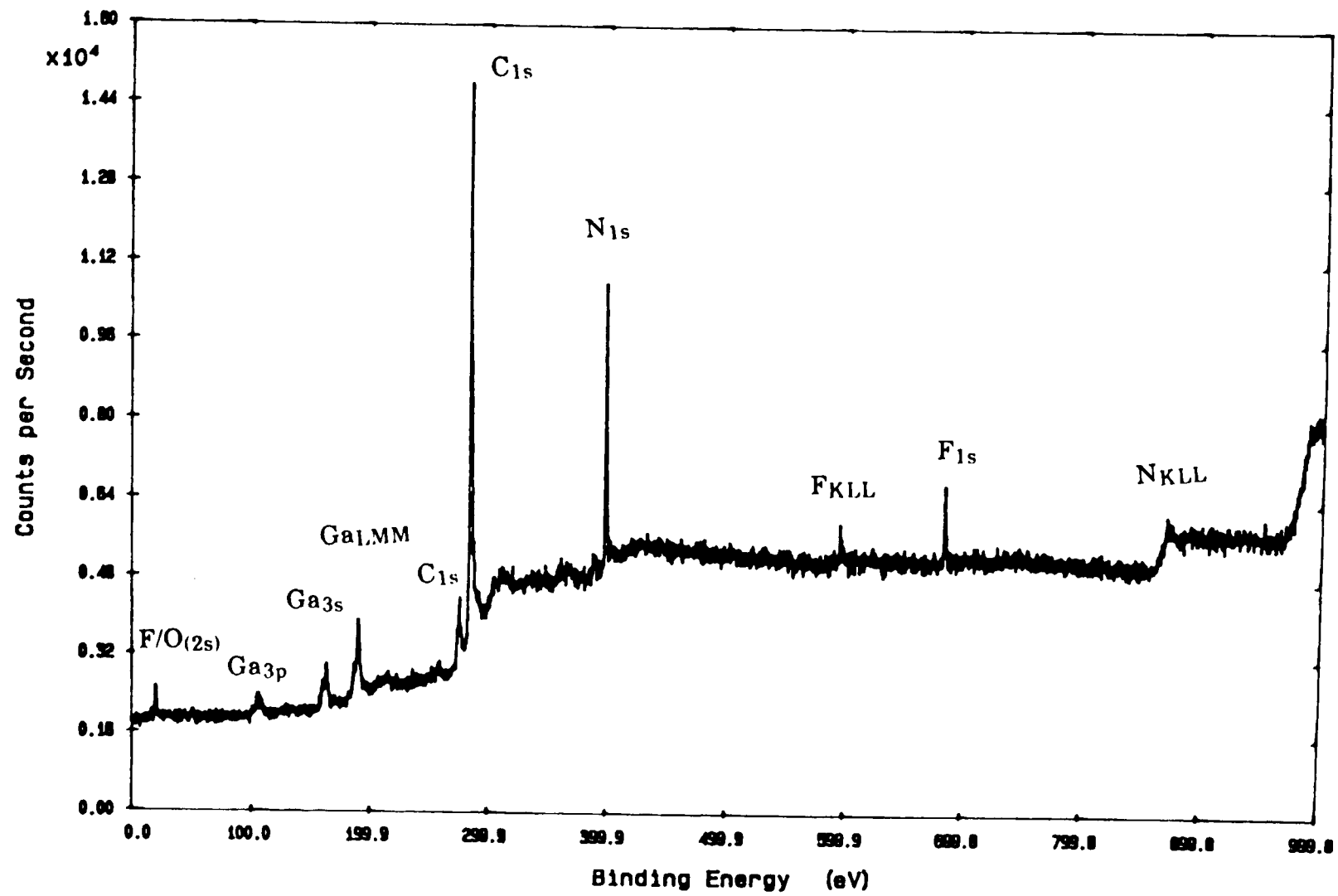


Figure 4.26: A full range X-ray photoelectron scan for GaPcF.

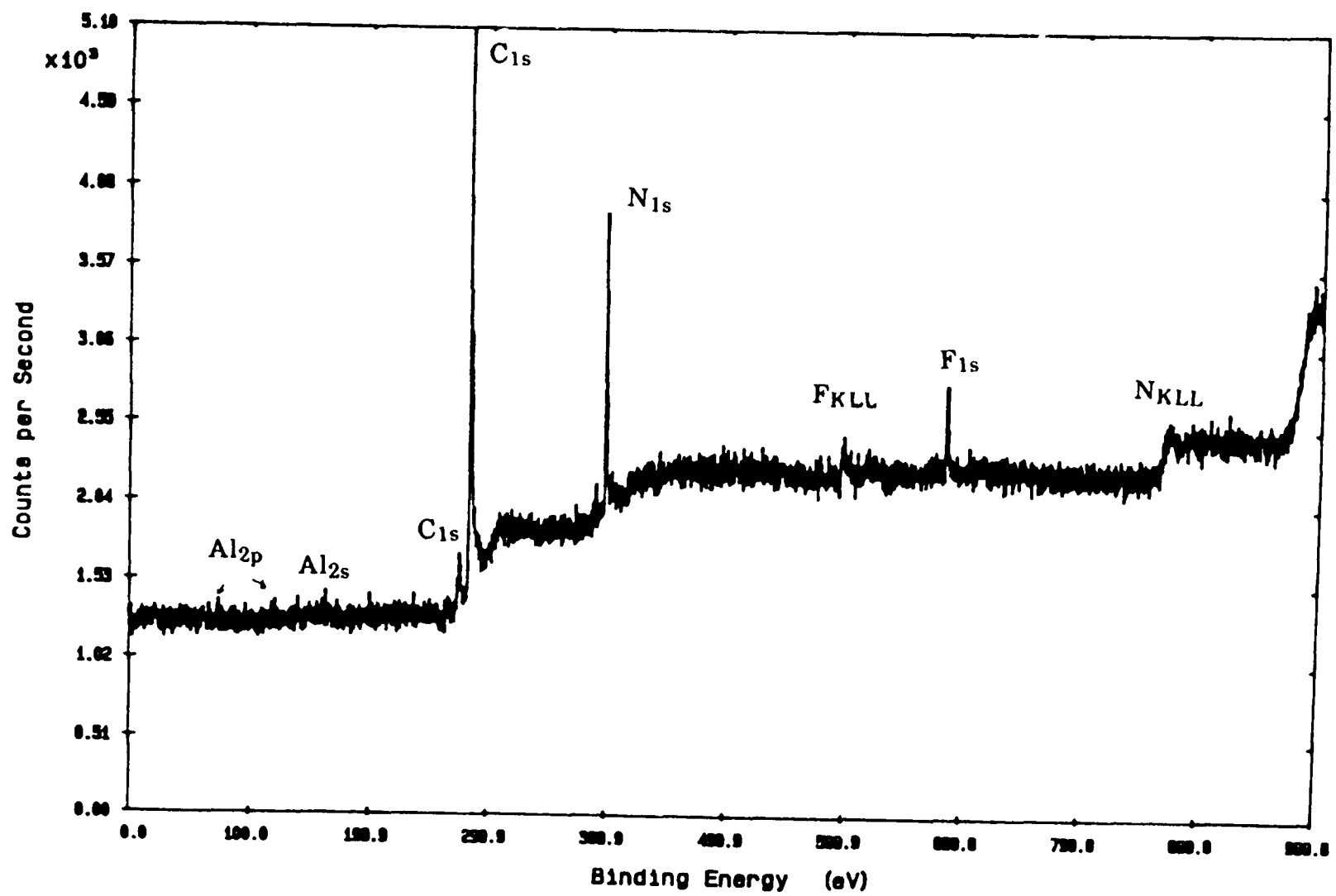


Figure 4.27: A full range X-ray photoelectron scan for AlPcF.

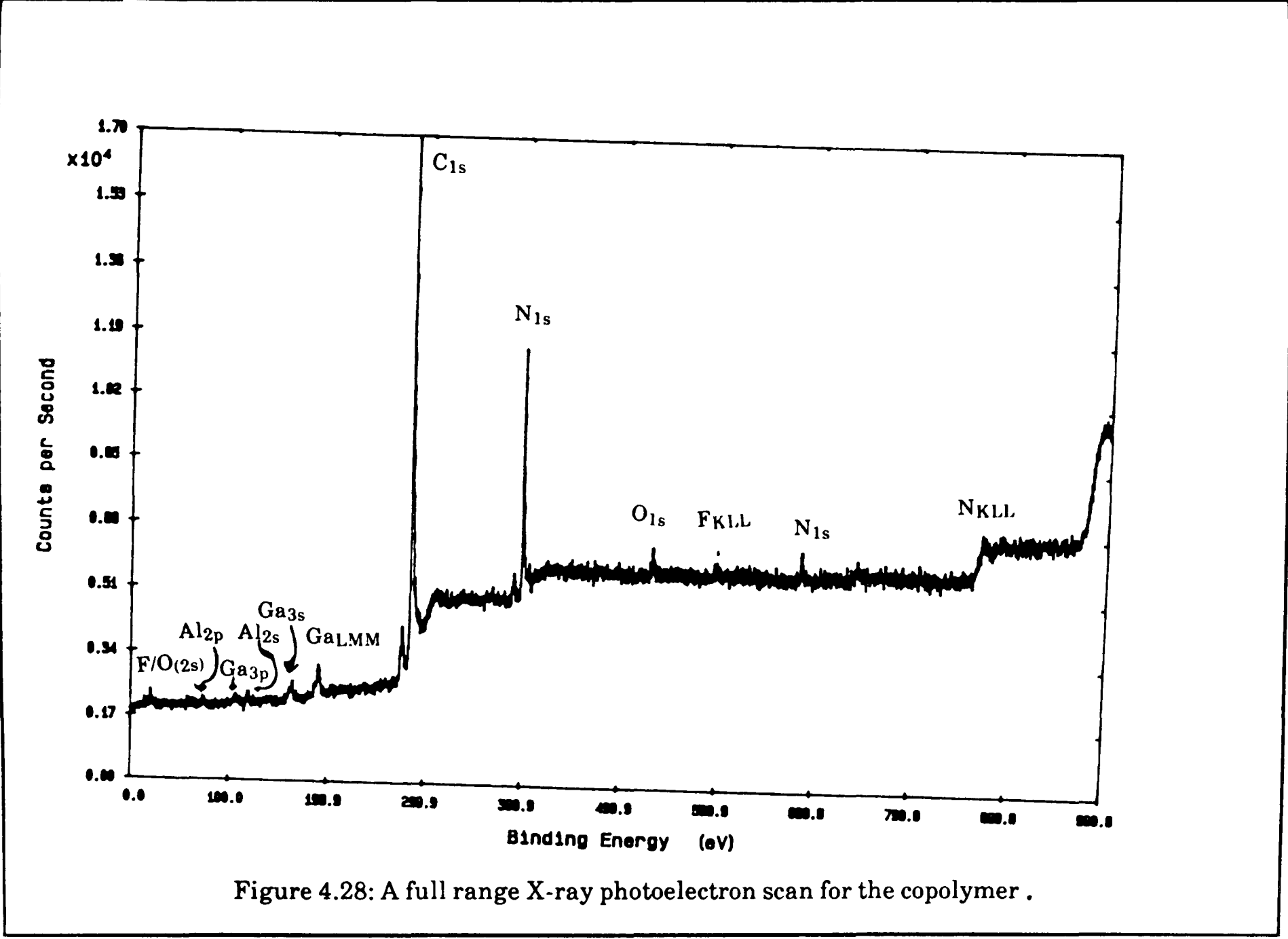


Figure 4.28: A full range X-ray photoelectron scan for the copolymer .

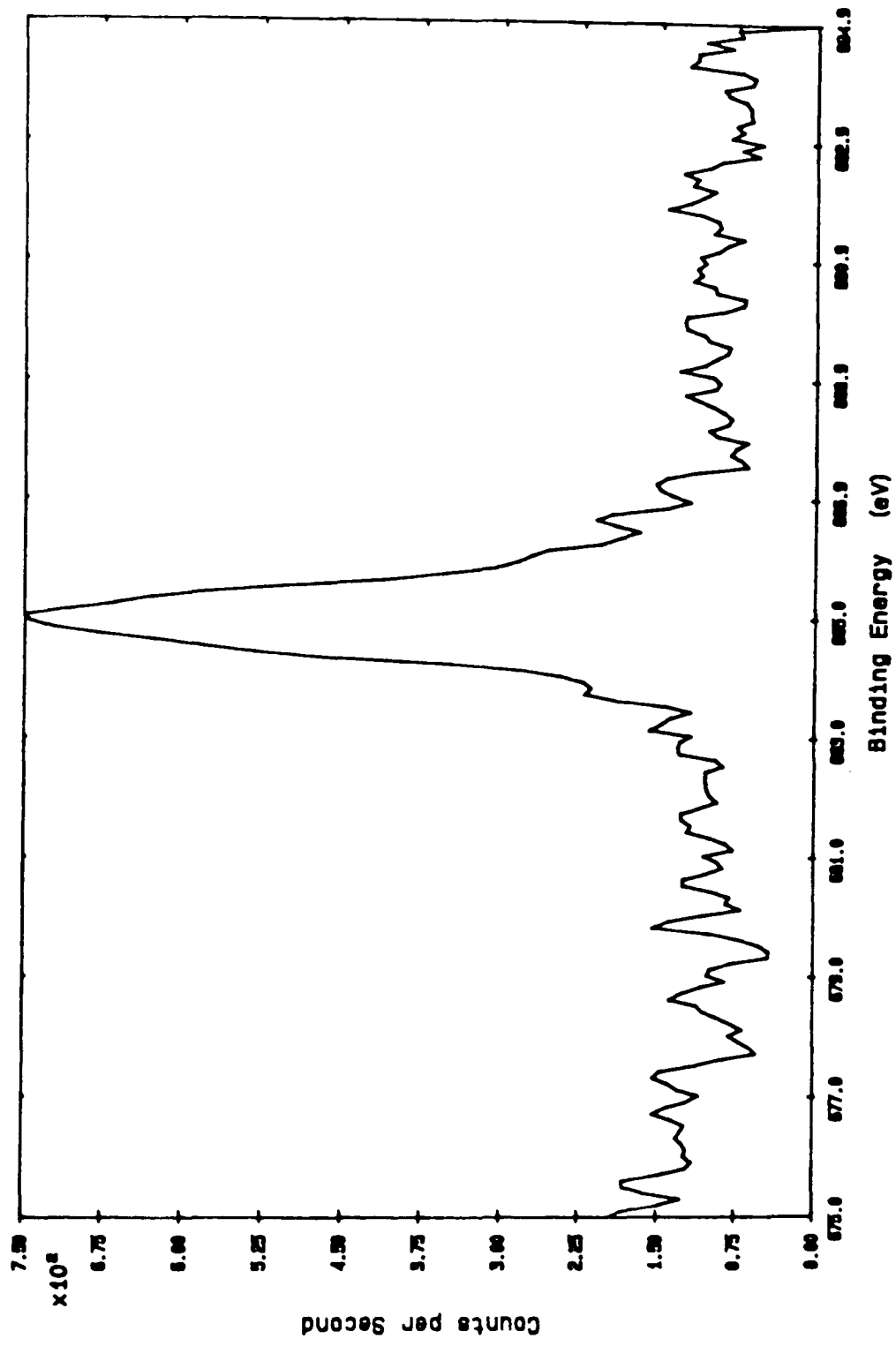


Figure 4.29: The fluorine peak for AlPcF.

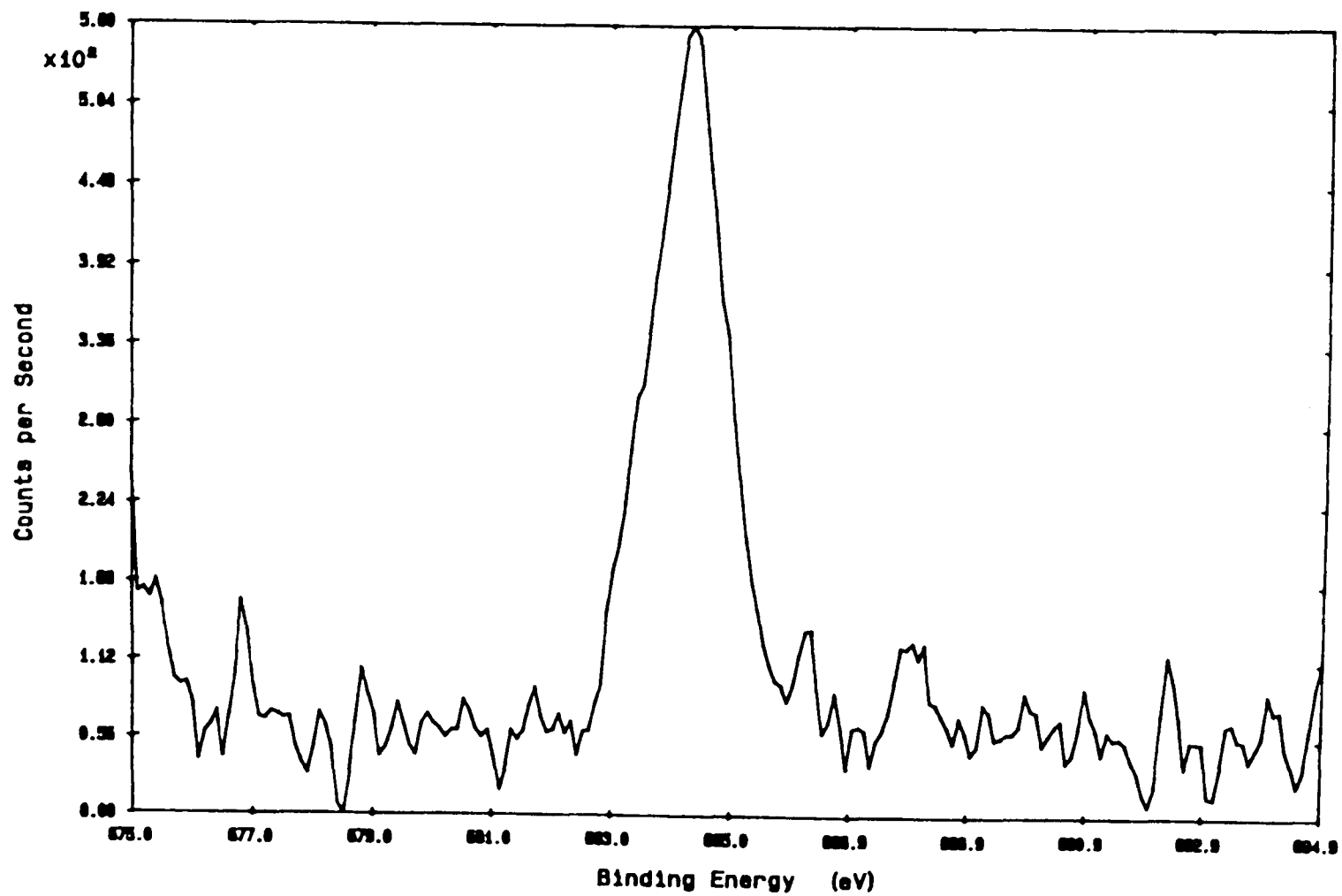


Figure 4.30: The fluorine peak for GaPcF

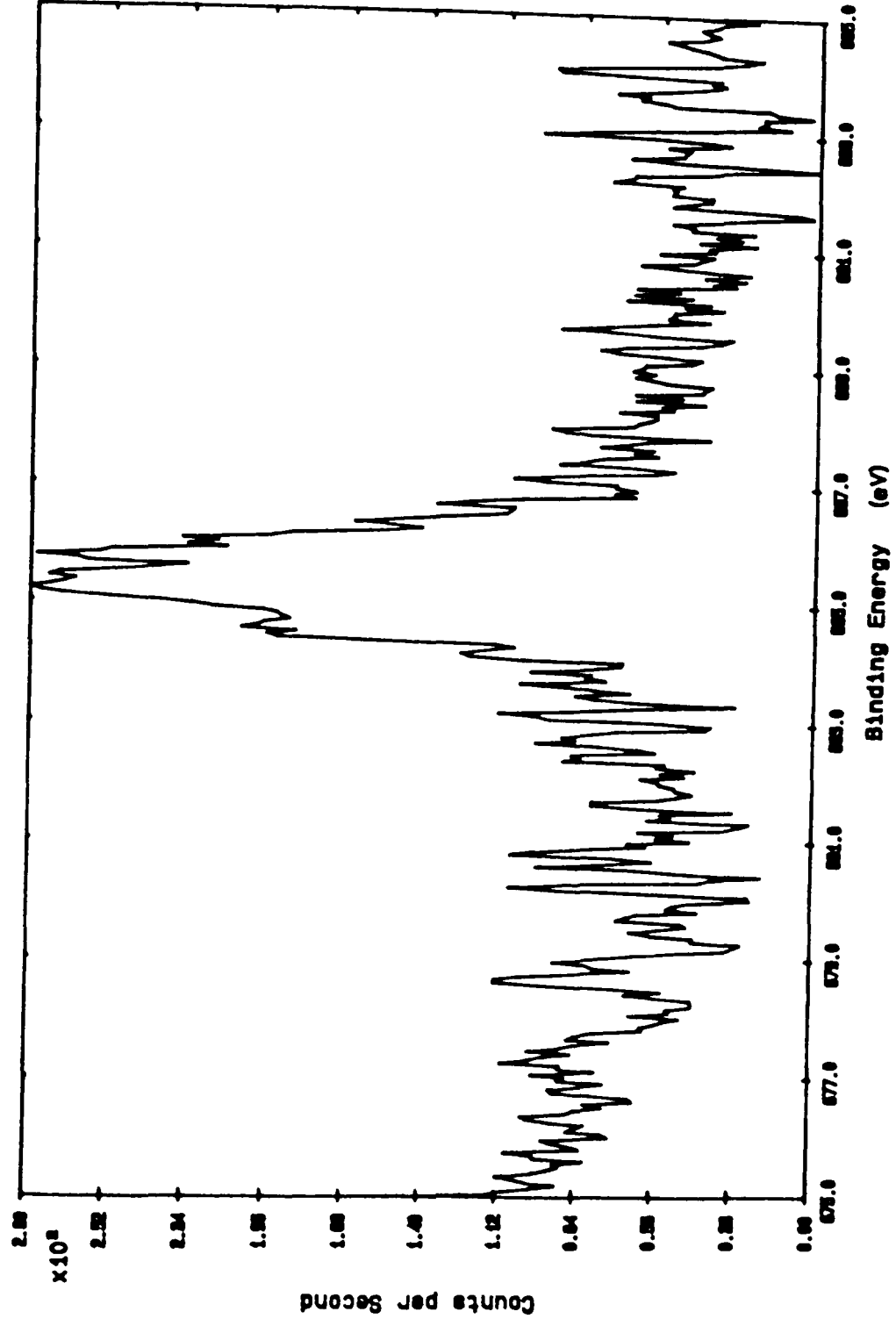


Figure 4.31: The fluorine peak for the copolymer

are quite sharp (from long, high resolution scan). There is a shift of about 0.8 eV between the peaks. However, the spectrum for the copolymer (Figure 4.31)(with the same test conditions) is much more noisy, which may be due to some charging which has occurred, given that the peak has shifted to higher energy. The noise levels are such that it is not possible to separate out the Al-F-Al and Ga-F-Ga let alone the Al-F-Ga. However, the copolymer fluorine peak is somewhat broadened accounting for the lower peak height and reflecting the three possible environments for fluorine. Using thinner samples (to lower charge up) it may be possible to separate the peaks using very long scan times.

The XPS results show that the ratio of Aluminium to Gallium is 60:40 rather than the expected 50:50, based on the proportions of starting materials in the preparation. Since the XPS techniques only samples the top 50 Å (4.44) of the film there are two possible explanations for the observation.

- ① Since the volatility of the two metal phthalocyanines, as shown by TGA, are different it is possible that there has been some fractionation during the sublimation processes during which the copolymer is temporarily depolymerised . If this is the case, there is expected that a concentration gradient would exist in the film.
- ② In common with many other phthalocyanines, some degradations occurs during sublimation of both materials (4.50). Since the extent of degradation depends both upon the central metal atom and the sublimation conditions, it is expected that the gallium has suffered more degradation than the aluminium phthalocyanine, particularly during the film deposition step where the temperature can be less precisely controlled.

To explain the problem further some depth profiling studies were carried out using argon ion bombardment to remove the surface layers and permit analysis of the subsurface layers. The measurements were carried out using an accelerating voltage of 7 keV and a beam current of 10 μ A. The results are shown in figure 4.32 covering an etch time of 200 minutes. Such high energies do, of course, cause degradation which is reflected in the rapid loss of nitrogen as volatile fragments. The important observation is that the Al:Ga ratio remains constant at 60:40 with experimental error as the surface layers are eroded. It is not at present possible to relate etch time to the thickness of film eroded.

On the basis of this evidence which is in good agreement with results from electron microscopy (which sample the bulk), it can be concluded that the film is homogeneous in composition and that there has been some change in composition during sublimation. This conclusion does not conflict with the results of microanalysis for C,H and N, which are not very sensitive to small changes in composition, and in any case were carried out on samples after entrainer sublimation but before film deposition.

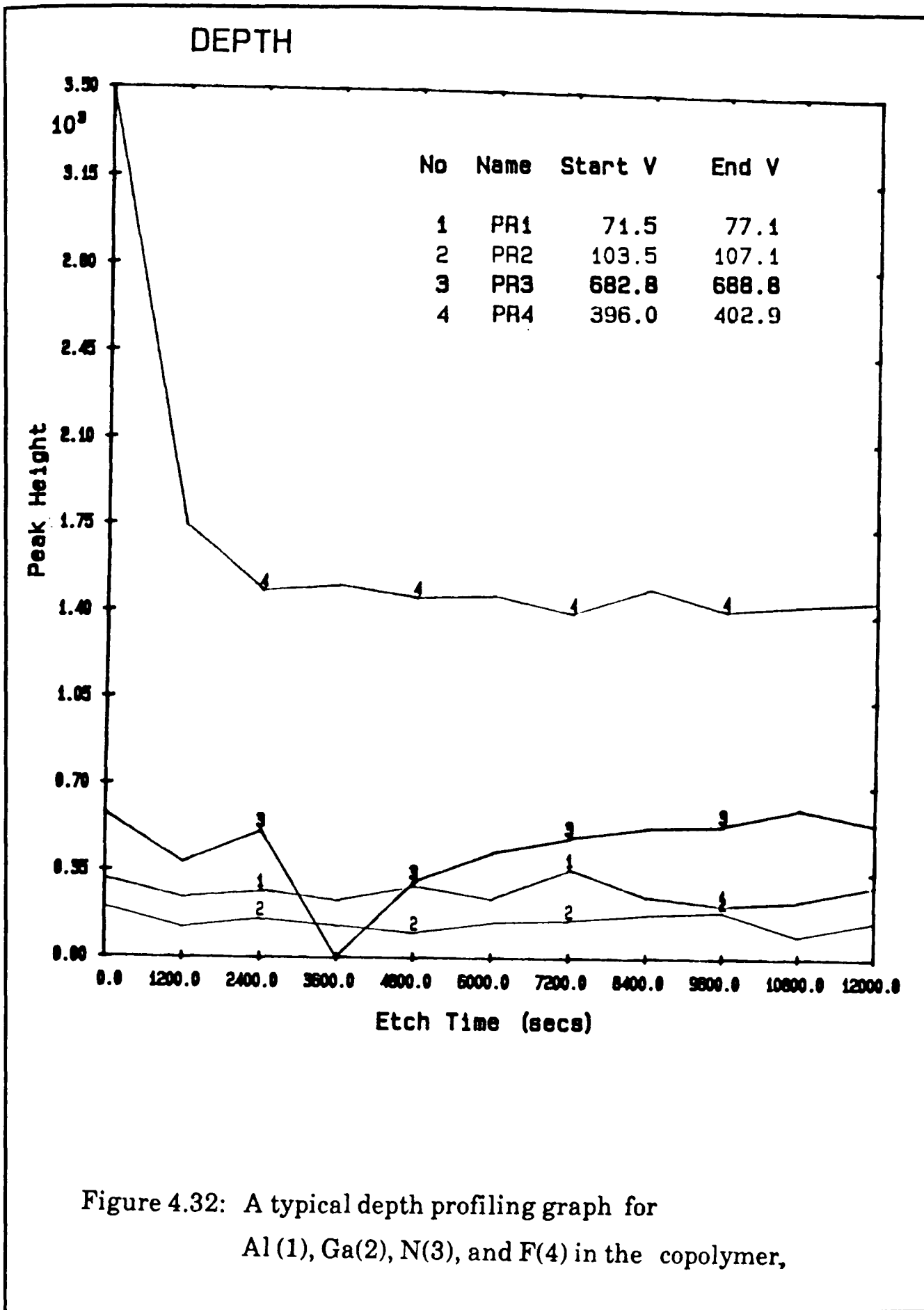


Figure 4.32: A typical depth profiling graph for Al (1), Ga(2), N(3), and F(4) in the copolymer,

CHAPTER FIVE

D.C. CONDUCTIVITY

The semiconducting properties of phthalocyanines were recognized in the late forties by *Eley* (5.1) and *Vartanian* (5.2). Many studies were carried out later to investigate their electrical properties. In most cases the *Arrhenius* relationship is obeyed:

$$\sigma = \sigma_0 e^{\frac{-E_a}{kT}} \dots\dots\dots 5.1$$

where σ is the conductivity at temperature, T, σ_0 is the *pre-exponential* conductivity, E_a is the activation energy for conduction and k is *Boltzmann constant*. When the conduction is intrinsic, then the behaviour may be described by the band theory equation:

$$\sigma = \sigma_0 e^{\frac{-\Delta E}{2kT}} \dots\dots\dots 5.2$$

where ΔE is the intrinsic *band gap*.

Even with careful purification the conduction in phthalocyanines tends to be extrinsic, but intrinsic conductivities have been observed in single crystals above 140 °C(5.3) and the energy gap in the intrinsic domain is 2.0 eV (5.3-6).

The electrical conductivity results for this work will be summarized in the following sections.

5.1) The D.C. Conductivity Results:

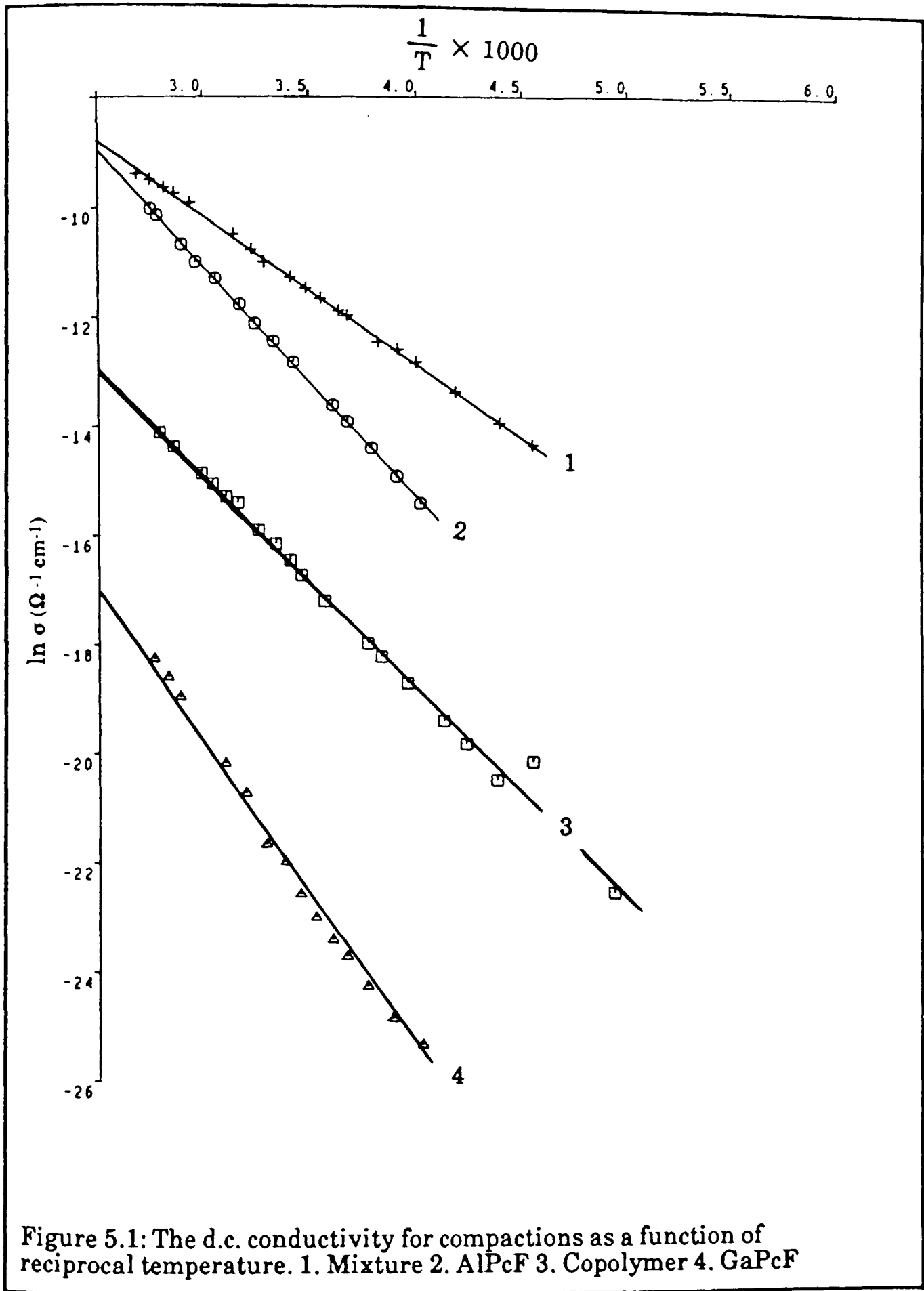
The d.c. conductivity of the three compounds, AlPcF, GaPcF and the copolymer (1:1 mole ratio) were studied using a *two probe method*. The compacted discs, surface and sandwich films were prepared as described in chapter 3. The conductivity measurements were carried out at a range of temperatures, 180-360 K.

a) Compacted Discs:

The d.c. conductivities of pressed pellets of AlPcF and GaPcF polycrystalline powders, at room temperature and about 10^{-5} Torr, were found to be $3.5 \times 10^{-6} \Omega^{-1} \text{cm}^{-1}$ and $2.8 \times 10^{-10} \Omega^{-1} \text{cm}^{-1}$ respectively, which is consistent with the previously published work (5.7-10). The d.c. conductivity of the copolymer was $6.5 \times 10^{-8} \Omega^{-1} \text{cm}^{-1}$, and of a mixture of 1:1 mole ratio of AlPcF and GaPcF was found to be $1.3 \times 10^{-5} \Omega^{-1} \text{cm}^{-1}$. Heating and cooling runs showed similar or identical behaviour, with no evidence of hysteresis.

The graphs of the d.c. conductivity of AlPcF, GaPcF, copolymer and the mixture as a function of reciprocal temperature are shown in figure 5.1. The room temperature conductivity values and the activation energies, evaluated on the basis of the least square analysis, are shown in table 5.1.

The conductivity of samples with resistances more than $10^7 \Omega$ were measured by the system shown in figure 3.11, while the lower resistance samples were measured by the system shown in figure 3.10.



Compound	Compacted disc			Surface cell			Sandwich cell		
	σ ($\Omega^{-1} \text{ cm}^{-1}$)	ΔE (e.V)	σ_0 ($\Omega^{-1} \text{ cm}^{-1}$)	σ ($\Omega^{-1} \text{ cm}^{-1}$)	ΔE (e.V)	σ_0 ($\Omega^{-1} \text{ cm}^{-1}$)	σ ($\Omega^{-1} \text{ cm}^{-1}$)	ΔE (e.V)	σ_0 ($\Omega^{-1} \text{ cm}^{-1}$)
AlPcF	3.5×10^{-6}	0.69	1.1×10^{-4}	1.0×10^{-6}	0.78	7.5×10^{-5}	2.4×10^{-8}	0.86	1.0×10^{-6}
GaPcF	2.8×10^{-10}	0.94	3.7×10^{-4}	$< 10^{-10}$ *	-----	-----	3.5×10^{-12}	1.10	6.2×10^{-10}
Copolymer	6.5×10^{-8}	0.84	2.8×10^{-6}	6.8×10^{-8}	0.86	2.8×10^{-6}	2.3×10^{-10}	0.988	2.5×10^{-8}
Mixture	1.3×10^{-5}	0.49	1.5×10^{-4}	-----	-----	-----	-----	-----	-----

Table 5.1 The d.c. conductivities and the apparent band gap for the compounds studied.
 (*) estimated from the conductivity of the compacted disc.

b) Surface Films:

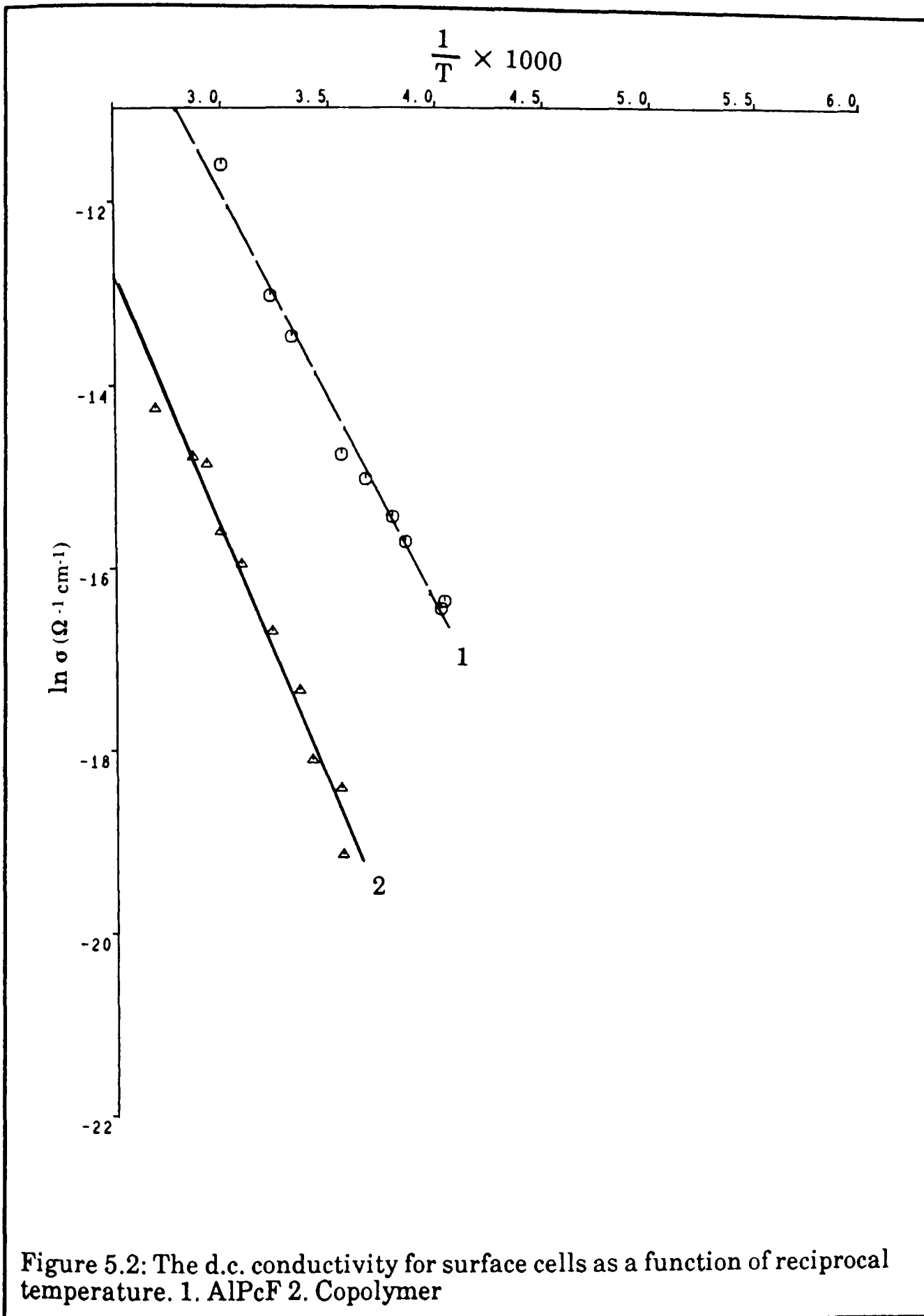
Figure 5.2 shows the conductivity measurements as a function of reciprocal temperature for surface films of AlPcF and the copolymer. Due to the high resistances of both AlPcF and the copolymer films at low temperature ($5 \times 10^9 \Omega$ and $5 \times 10^{11} \Omega$ respectively) the conductivity measurements were carried out over the temperature range 363-248 K. It was not possible to measure the conductivities of GaPcF surface films due to the high resistance ($> 2 \times 10^{13} \Omega$ at room temperature) which is approaching the input impedance of the *Keithley* 616 electrometer ($10^{14} \Omega$) (5.11-12). In addition, the resistance of the system without samples is about $10^{13} \Omega$.

The activation energies, from table 5.1, show that the samples were extrinsic with acceptor levels lying above the valence band. No or very little hysteresis was found for these films.

c) Sandwich Film:

Sandwich films of phthalocyanines have been studied by many workers (6.13-17). However no work has been reported in the literature concerning the dark d.c conductivity of sandwich cells of either AlPcF or GaPcF.

Figure 5.3 shows the graphs of the conductivity of the sandwich films for the three compounds, AlPcF, GaPcF and the copolymer, while figures 5.4-6 show the graphs of the conductivity of the sandwich films for AlPcF, the copolymer and GaPcF respectively as compared to surface films and compacted discs for the three materials as a function of reciprocal



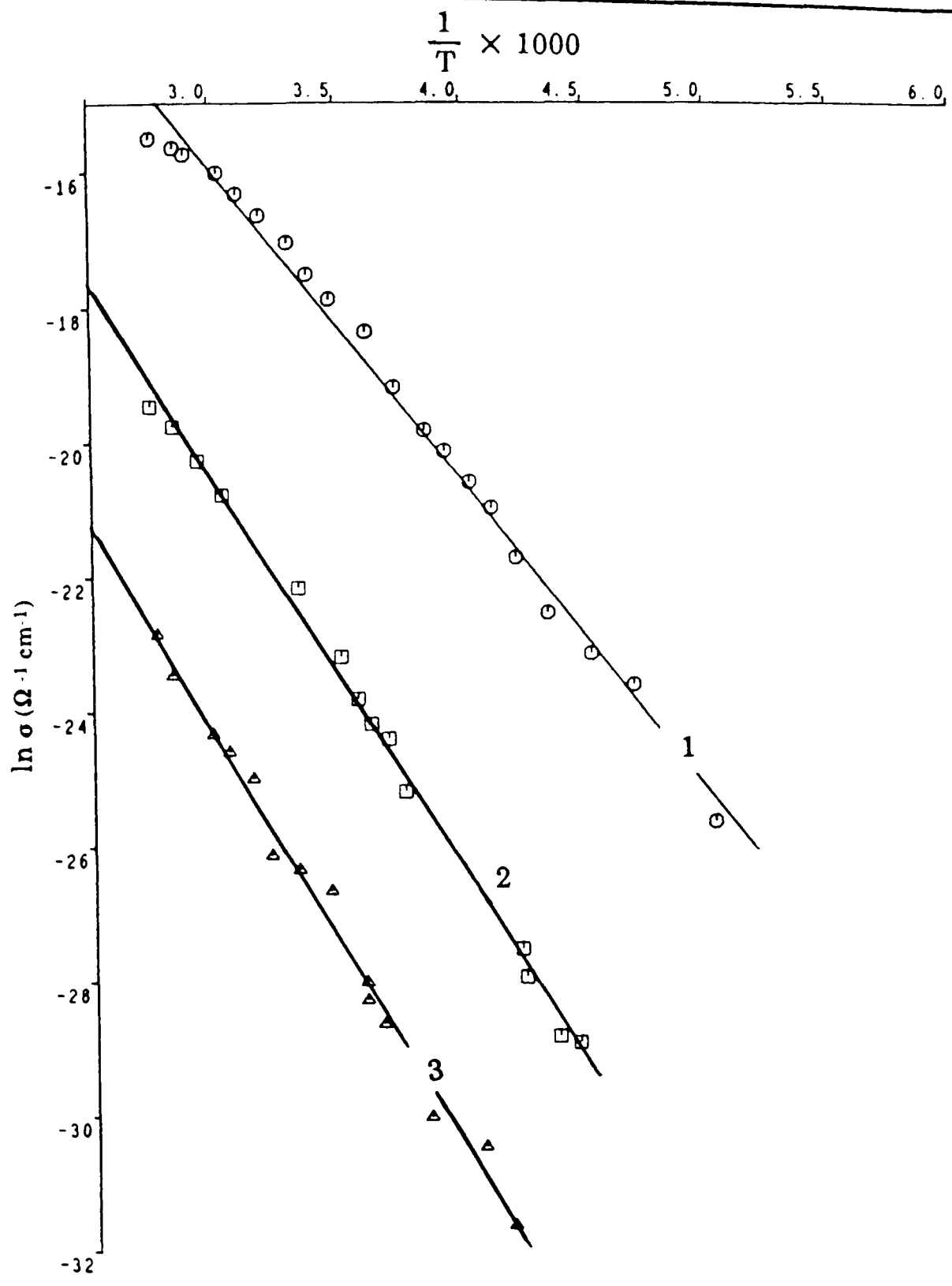
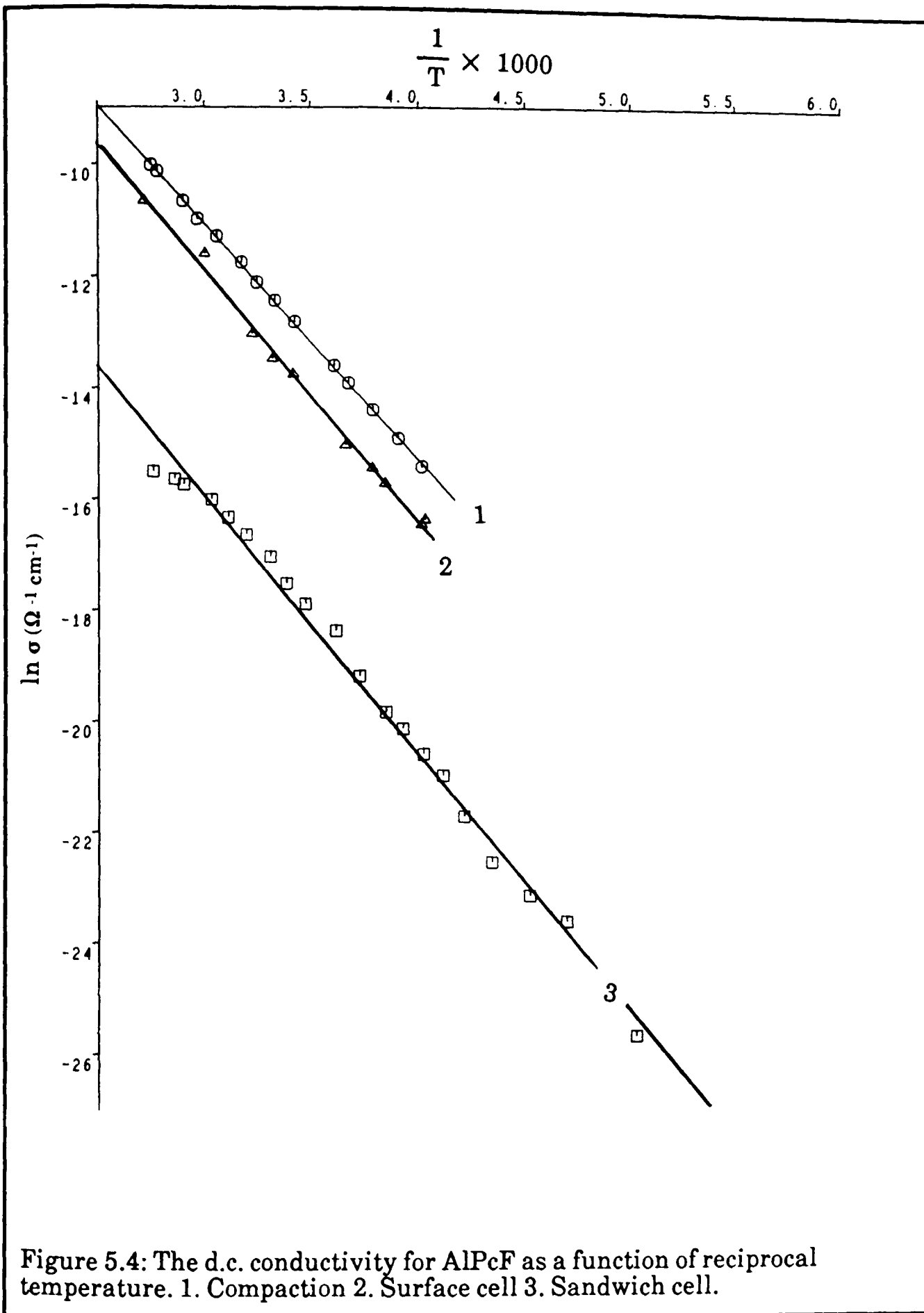


Figure 5.3: The d.c. conductivity for sandwich cells as a function of reciprocal temperature. 1. AlPcF 2. Copolymer 3. GaPcF



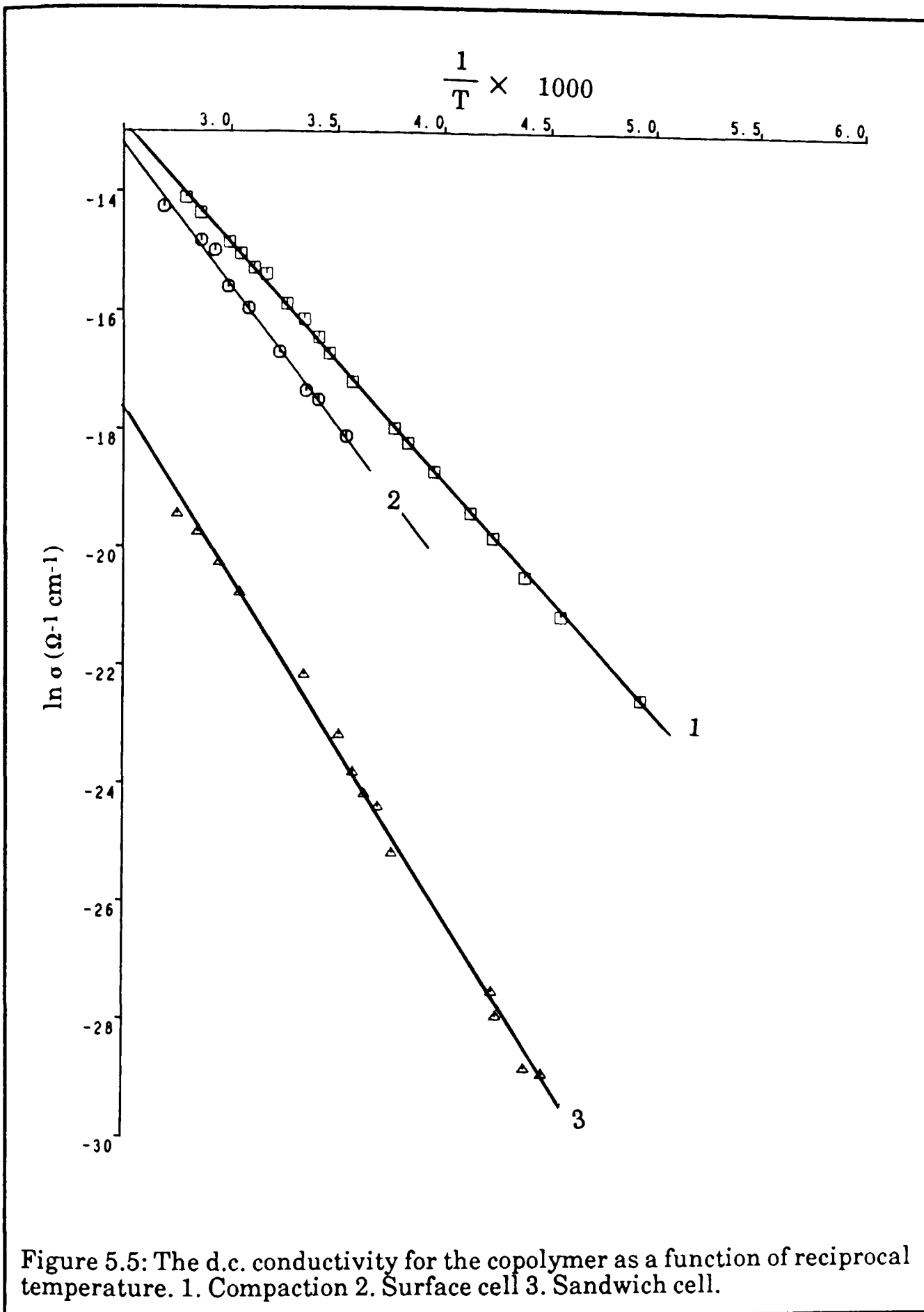


Figure 5.5: The d.c. conductivity for the copolymer as a function of reciprocal temperature. 1. Compaction 2. Surface cell 3. Sandwich cell.

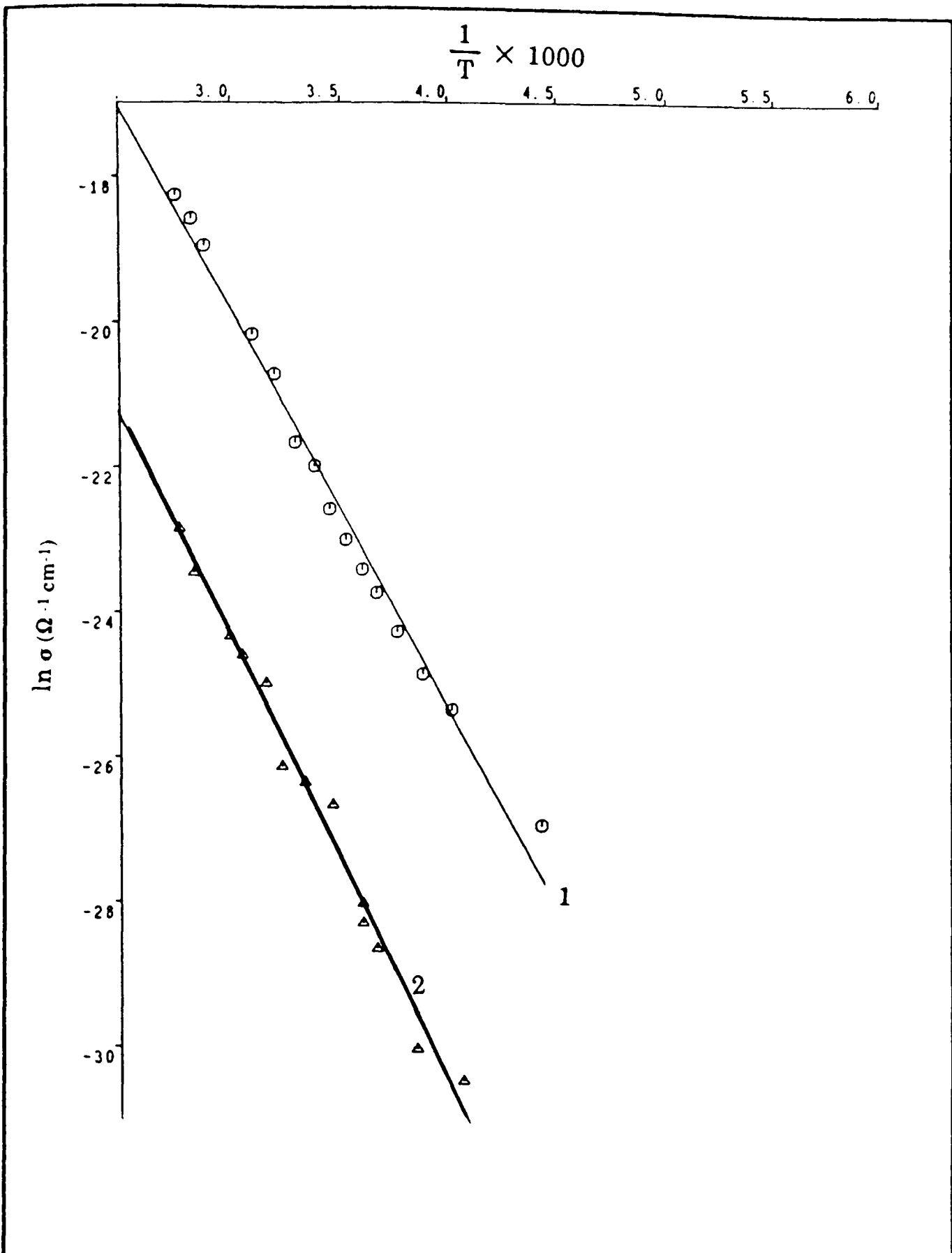


Figure 5.6: The d.c. conductivity for GaPcF as a function of reciprocal temperature. 1. Compaction 2. Sandwich cell.

temperature. They show that sandwich films for the three compounds have much lower conductivity than the surface films and compacted discs,

$$\sigma (\text{compaction}) > \sigma (\text{surface}) > \sigma (\text{sandwich})$$

The conductivity values are shown in table 5.1. The conductivity sequence for the three cells is consistent with the sequence for the conductivity measurements carried out by *Waclawek* and *Zabkowska* on PbPc(5.13). No or very little hysteresis was found.

5.2) Discussion of the D.C Conductivity:

Figure 5.1 shows that the d.c conductivity of compacted discs of the copolymer is intermediate between that of AlPcF and GaPcF.

$$\sigma (\text{AlPcF}) > \sigma (\text{copolymer}) > \sigma (\text{GaPcF})$$

This sequence is consistent with the interplaner spacing of these compounds as found by *Kenney et al* (5.8,5.18), from X-ray diffraction studies (see chapter 4, table 4.4), and the band widths defined from I.R reflectance of doped materials (5.10). The unsublimed materials gave higher conductivities ($1.5 \times 10^{-4} \Omega^{-1} \text{cm}^{-1}$ and $< 10^{-6} \Omega^{-1} \text{cm}^{-1}$ for AlPcF and GaPcF respectively) (5.7), reflecting the lower purity.

The d.c conductivity of compacted disc of 1:1 mole ratio mixture of AlPcF and GaPcF is higher than that for either AlPcF or GaPcF.

Some insight into the reasons for the difference between the conductivities of AlPcF, GaPcF and the copolymer is provided by band theory. If it is assumed that the materials are p-type extrinsic

semiconductors as a result of oxygen complexation, then the conductivity(5.19) is given by :

$$\sigma = \mu_h e \sqrt{2 n_A} \left[\frac{2\pi m_h k T}{h^2} \right]^{\frac{3}{4}} e^{-\frac{(E_A - E_V)}{2kT}} \dots\dots\dots 5.3$$

where μ_h is the hole mobility, n_A is the acceptor concentration, m_h is the hole effective mass and E_A and E_V are the energies of the acceptor level and top level of the valence band respectively.

Firstly the value of $\Delta E = E_A - E_V$ is higher for the gallium compound than for the aluminium (table 5.1) suggesting that oxygen acts as a stronger acceptor in AlPcF than in GaPcF.

Secondly, by considering the *pre-exponential factor* the influence of the energetic term is avoided

$$\sigma_0 = \mu_h e \sqrt{2 n_A} \left[\frac{2\pi m_h k T}{h^2} \right]^{\frac{3}{4}} \dots\dots\dots 5.4$$

The experimental values, shown in table 5.1 show that

$$\sigma_0(\text{AlPcF}) > \sigma_0(\text{GaPcF})$$

and that the copolymer has an intermediate value. These differences must reflect differences in μ_h , m_h and n_A . Consider each of these variables in turn,

a) Mobility of holes (μ_h):

Although no precise measurements of mobility have been made in these materials, values of the band width (which is related to mobility) have been obtained from spectroscopic measurements (5.10). They show that the band width for AlPcF > GaPcF, reflecting the shorter intermolecular spacing for AlPcF (figure 5.7).

b) Effective mass (m_h):

The above spectroscopic studies (5.10) also yield effective mass (which is inversely related to band width). Here the effective mass for GaPcF is greater than for AlPcF.

c) The acceptor concentration (n_A):

The weaker interaction between O₂ and GaPcF suggests that the concentration under vacuum is lower. This is supported by studies on iodine doping which suggest that iodine is more readily removed from GaPcF than AlPcF(5.8).

From the above consideration it is clear that the observed values of σ_0 are in agreement with expectation, and reflect both the higher mobility and higher oxygen concentration in AlPcF. The effect of effective mass is clearly not dominant. The copolymer σ_0 has a value intermediate between those of its components reflecting the fact that if it is a block copolymer then the carriers must travel through regions of both AlPcF and GaPcF and with their different mobilities and acceptor concentrations.

A mixture of two phthalocyanines has been studied by other workers (5.20). They found that a mixture of two different metalphthalocyanines (CuPc/VoPc) leads to a decrease in the activation energy with a big increase

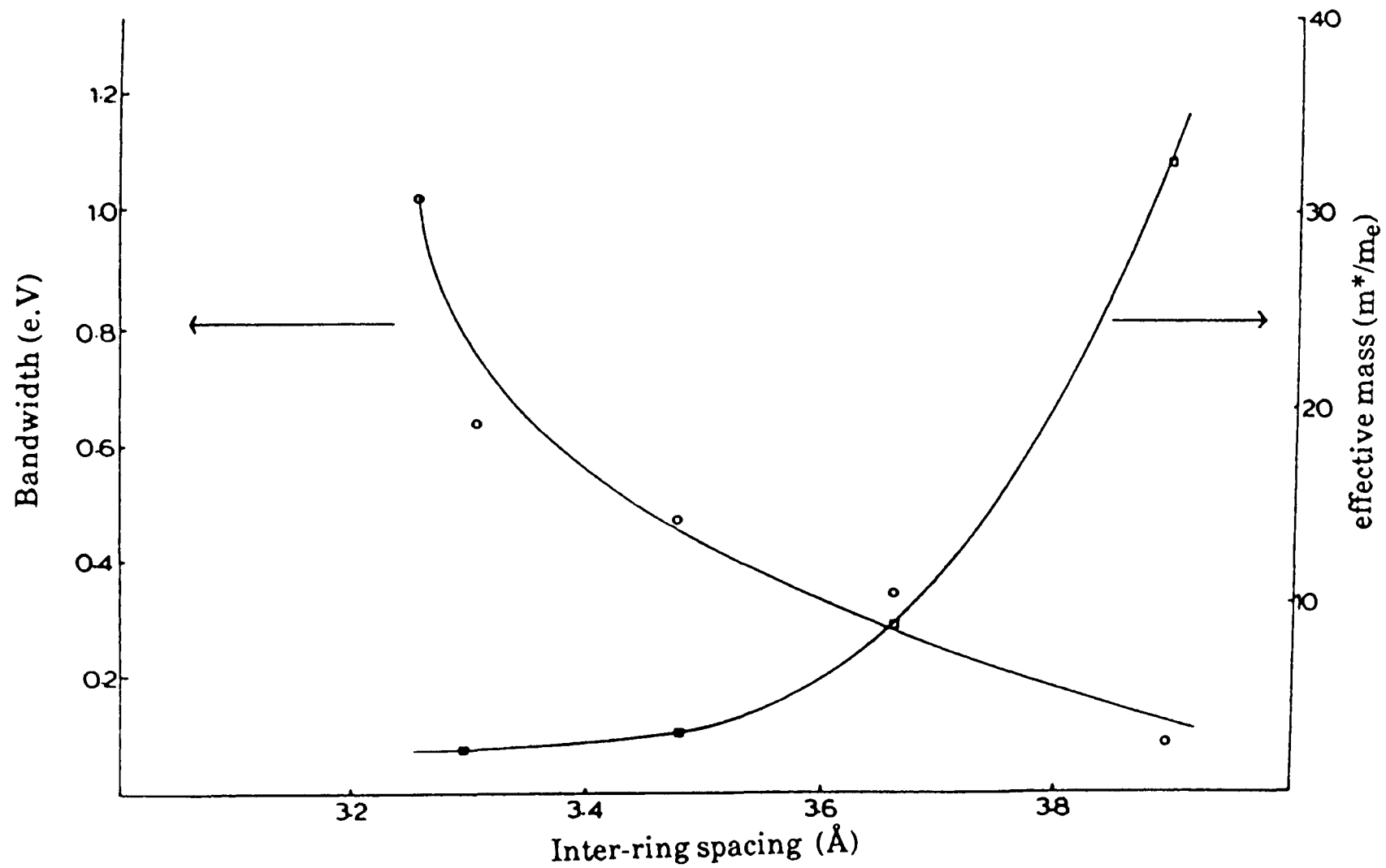


Figure 5.7: The Variation of band width and electron mass with inter-ring spacing for various phthalocyanines.

in the conductivity as compared to the separate components. The low activation energy of the mixture was assigned to the difference between the donor level and the conduction band edge. Therefore one of the components acts as a dopant towards the other and leads to a strong increase in the conductivity by increasing the number of charge carriers (6.21).

The difference between the conductivities of the mixture and the copolymer is interesting and important in this investigation. The conduction model can be explained as follows:

a) AlPcF:

Figure 5.8a shows the proposed band structure for AlPcF. The band width is that derived spectroscopically (6.10) and the intrinsic band gap is assumed to be 2.0 e.V, which is in line with other phthalocyanines. The position of the oxygen acceptor level is located on the basis of the observed apparent band gap.

b) GaPcF:

Figure 5.8b shows the proposed band structure for GaPcF. The slightly narrower bands are based on values obtained spectroscopically resulting in a slightly greater band gap. The apparent band gap locates the acceptor level slightly higher than in AlPcF, reflecting both the lower value band edge and the weaker binding of the oxygen.

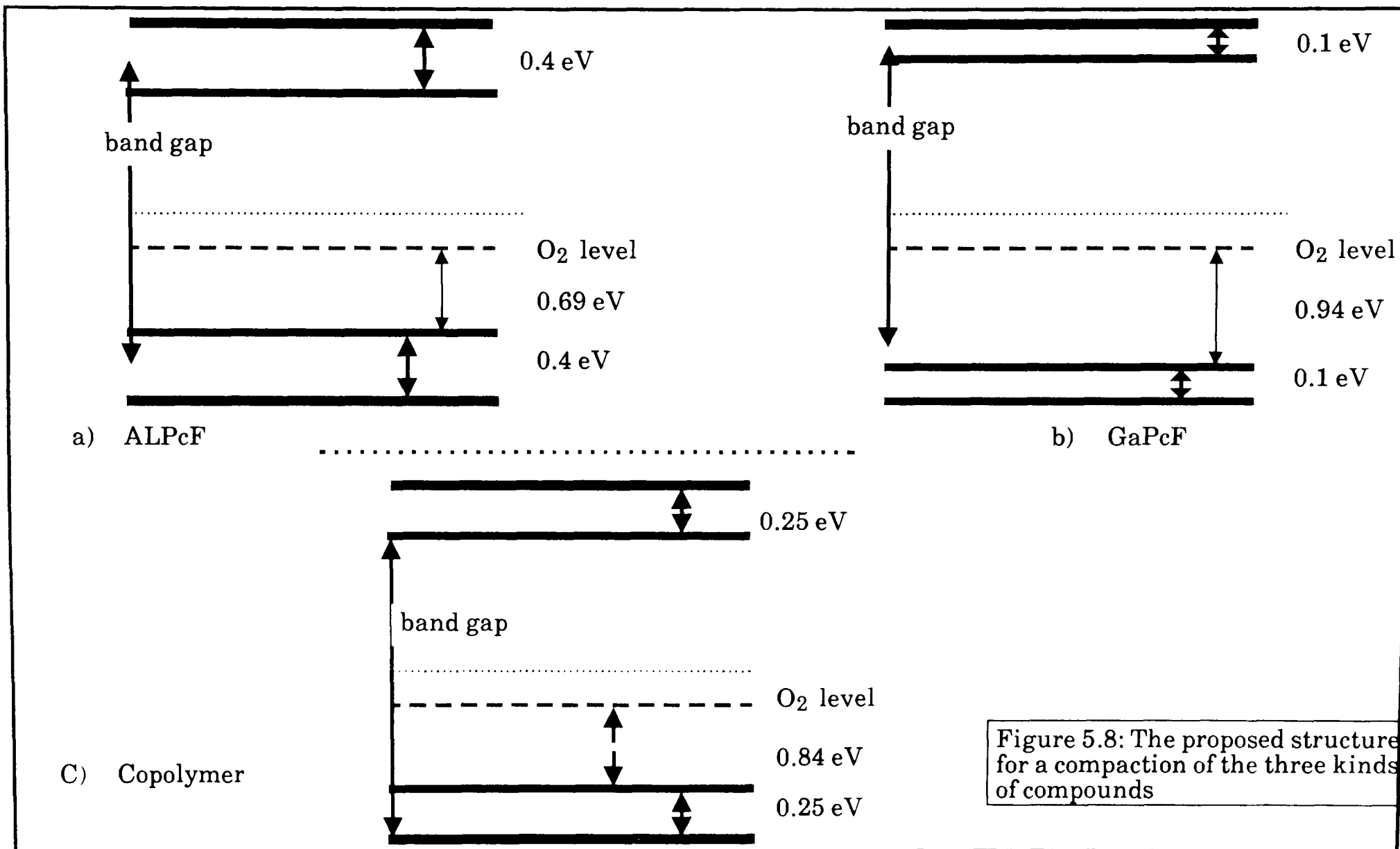


Figure 5.8: The proposed structure for a compaction of the three kinds of compounds

c) The Copolymer:

The experimental results show clearly that the properties of the copolymer lie between those of its components, suggesting an intermediate band structure (figure 5.8c). The basis of this band structure is most readily apparent if it is assumed that whilst Ga-F-Ga, Al-F-Al, and Al-F-Ga are all present, the latter dominates. Clearly the band width and band gap will have intermediate values. Furthermore, if the oxygen sits between molecular planes, the position of its band gap located between GaPcF and AlPcF in the copolymer is likely to be intermediate between those of the pure homopolymers. Accordingly, the proposition, that control of conductivity of linear polymers can be achieved by copolymerisation is supported by experimental observation.

d) The Mixture:

The remarkable observation that a compaction of a mixture of GaPcF and AlPcF has a significantly higher conductivity than a similar compaction of the copolymer suggests that structural factors play a major role. The mixture is presumably composed of crystalline particles of the two components and interaction is limited to their interface. The enhanced conduction is therefore to be limited to the interface region.

It is proposed that the intimate contact between two related semiconductors enhances the surface conductivity in a way which has been discussed for inorganic materials particularly in relation to the adsorption of gases (5.22) as shown in figure 5.9:

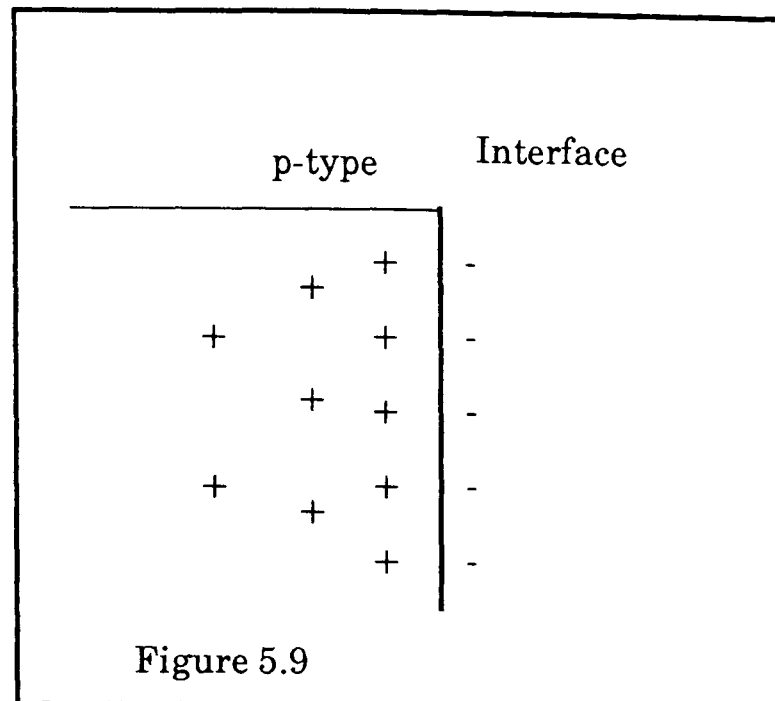


Figure 5.9 shows a p-type semiconductor where electron acceptor states (in this case the other, more electron accepting, component of the mixture), are present on the surface. The result is an increase in charge carriers at the interface, and a consequential increase in conductivity in the surface region. The enhanced conductivity, $\Delta\sigma$ is given by:

$$\Delta\sigma = \Delta n e \mu_e + \Delta p e \mu_h \dots\dots\dots 5.5$$

where Δn and Δp are the changes in electron and hole concentrations respectively.

It is therefore proposed that the observed conductivity reflects an enhanced conductivity at the surface of either one or both of the components.

Table 5.1 shows the apparent band gap values for the temperature range studied. The low values suggest that the conductivities are extrinsic.

The higher activation energy for GaPcF relative to AlPcF compactions may be due to the weaker oxygen-GaPcF interaction compared to oxygen-AlPcF interaction. This will reduce the activation energy for AlPcF compared to GaPcF.

Due to the presence of AlPcF and GaPcF in an equal amounts in the copolymer, this will make its apparent band gap intermediate between that for GaPcF and AlPcF, while the higher conductivity for the mixture will reduce the apparent band gap, as explained earlier.

The amorphous nature of the film makes the apparent band gap for the surface film a little higher than that of the compacted disc. The higher apparent band gap for the sandwich film compared with that of the compacted disc and surface films may be due to the perpendicular stacking of the phthalocyanines to the electrical pathways and its effect upon electrical transport, which is explained later.

The d.c. measurements were taken after the samples had been heated at 363 K and 2.0×10^{-5} Torr for a week to anneal them and to expel as far as possible the adsorbed gases (see figure 5.10). The low values of the activation energies can be attributed to many factors including impurities, adsorbed oxygen, imperfections and trapping centres. The samples were purified once by entrainer sublimation and sublimed again during film formation but this was not sufficient to remove all the impurities (5.4,23-25). At normal temperatures the conduction is influenced by an electron trap level located above the valence edge (5.3,5.5). These electrons will be released from the acceptor traps with the increase of temperature.

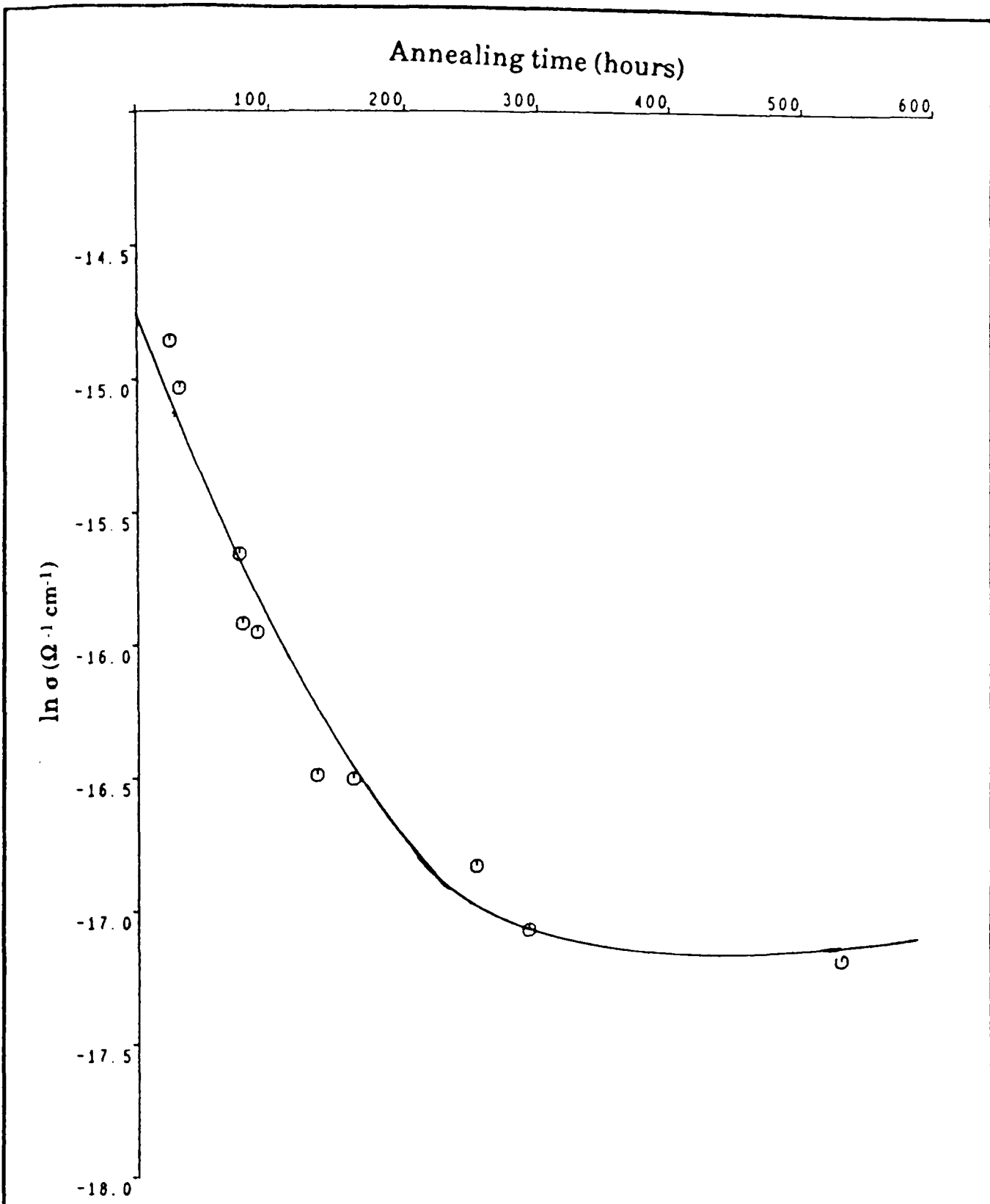


Figure 5.10: Atypical graph for d.c. conductivity as a function of annealing time for sandwich cell of AlPcF (annealing at 90°C and 2.0×10^{-5} torr)

Oxygen is an almost unavoidable dopant of molecular semiconductors (5.21,5.26-27). It was found that oxygen molecules are trapped on the surface and in the bulk of the crystal and cause the *Fermi level* to move closer to the valence band i.e., it acts as a dopant. An increase in its concentration induces a high density of free charge carriers^(5.28). Figure 5.11 shows that annealing of the sample under vacuum has a large effect on the conductivity measurements which may be due to removal of the adsorbed oxygen, as well as changes in crystallinity. Even with a long period of annealing a totally time independent value of conductivity could not be achieved. Actually, only a minute amount of impurity is enough to greatly perturb the electrical properties of molecular semiconductor (5.21,5.29). Therefore, it seems that the experimental annealing may not remove all the adsorbed oxygen from the samples (5.28-30). Even a vacuum of 10^{-12} torr still contains about 3×10^4 particles per cm^3 (5.25), so measurements would have to be made on samples maintained permanently under ultra-high vacuum.

Figure 5.2 and table 5.1, show that the conductivity of a surface cell of the copolymer, is intermediate between that for AlPcF and GaPcF. Figure 5.3 shows the same conductivity sequence for the sandwich films of the three compounds,

$$\sigma_{AlPcF} > \sigma_{copolymer} > \sigma_{GaPcF} \quad (\text{for surface and sandwich cells})$$

which are consistent with the interplanar spacing mentioned as above.

Figures 5.4-6 and table 5.1 show that the d.c. conductivities of compacted discs are a little higher than those of surface cells. This is may be because the compacted discs were prepared under a compaction a pressure of 10 MPa, at which the inter-particle resistance is expected to be eliminated (5.31). The

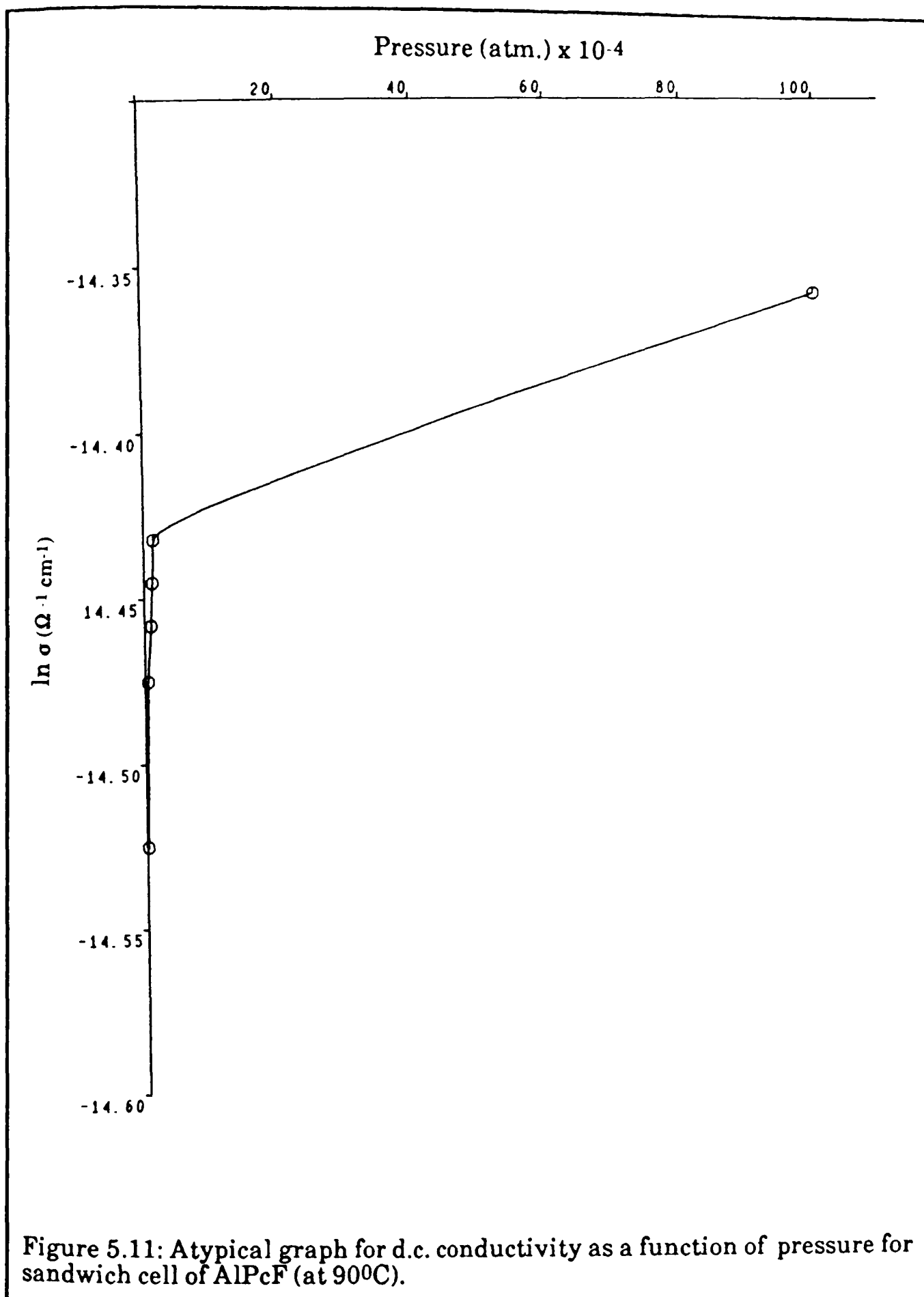


Figure 5.11: Atypical graph for d.c. conductivity as a function of pressure for sandwich cell of AlPcF (at 90°C).

activation energy suggests the existence of shallow traps or acceptor levels due to adsorbed oxygen which increase the charge carrier density. The expected trapped oxygen, present either due to diffusion or introduced during preparation of the samples is of higher concentration in the disc than in the film due to its surface to bulk ratio. Oxygen can diffuse even into a single crystal (5.32). It was found that the conductivity of a compacted disc of β -carotene increases more compared to single crystals, if exposed to methanol vapour (5.33). In addition to that, the adsorbed oxygen may be eliminated more easily by the experimental vacuum (2×10^{-5} torr) from the surface film than from the compacted discs. The higher conductivity of the compacted discs compared to the surface films can also be interpreted by percolation effect in the compaction. The compacted disc is composed of a large number of crystallites compacted near to each other, so the conductivity will be averaged over different orientations while the film is an amorphous system consisting of crystallites separated from each other, where the conductivity will be reduced by the less conductive amorphous region. Annealing of the film decreases the conductivity which is assumed to be due to removal of impurities and possibly increases the crystallinity of the film (5.10). Slow and regular sublimation rates lead to an ordered molecular arrangement of the sublimed films which gives partially crystalline layers (5.34-36). In this work annealing of the samples at 363 °K and $\approx 10^{-5}$ torr was carried out routinely in order to obtain pure samples with constancy in their properties. All these factors play an important role in deciding the final value of the measured conductivity for both films and compacted discs.

Figures 5.4-6 and table 5.1 show that the conductivity of the sandwich cells is much lower than the surface cells (about two orders of magnitude) which may be attributed to:

1) The stacking arrangement of the crystallites of the sublimed films are parallel to the substrate or electrode film planes, while the conduction direction is perpendicular to the usual conduction pathway (i.e., down the stack) (5.10,5.37-38). The fact that the conductivity occurs through the conduction band formed by the overlap of the phthalocyanine ring (5.39) will make the conductivity anisotropic.

2) Under the influence of a high applied field it is expected that some polarisation of the sample occurs^(5.25), with excess electrons trapped near the positive electrode and excess holes near the negative electrode. This has the effect of reducing the observed conductivity. The field used was not, however, sufficient for the current to be space charge limited, which has been observed in phthalocyanines by other workers^(5.40-45) as the current/voltage relationship was strictly *Ohmic*.

5.3) Iodine Doping:

Most of the work reported in this thesis was carried out on materials which had been purified by entrainment sublimation, and in many cases by one further sublimation during the deposition of the film. As a pointer to further work, it is worth reporting some preliminary experiments on iodine doping using copolymer of approximately mole ratio, 2:1, 1:1 and 1:2, which had been sublimed but not submitted to the full vapour phase sublimation purification process. However, since the iodine doping process causes such a dramatic enhancement of conductivity, by removal of electron from the valence band, the presence of less electrically active impurities is likely to have a minor or negligible influence.

Surface cells of thickness 0.5 μm were prepared with an electrode gap of 2 mm and width of 10 mm. The conductivity as a function of time was observed when in the presence of iodine vapour (doping). Firstly significant differences between the rates of doping were observed, with the materials reaching equilibrium in the following times:

AlPcF:GaPcF	1:0	2:1	1:1	1:2	0:1
Equilibrium times (min.)	30	27	20	10	15

The equilibrium conductivities of the doped samples are shown in figure 5.12

The rate of uptake of iodine appears to be dependent on the intermolecular spacing which is larger in GaPcF than in AlPcF and intermediate in the copolymers (chapter 4).

It is clear that the conductivities of the copolymers, where fully doped, are somewhat less than those of the separate materials which has also been observed for doped phthalocyanine mixtures (5.46). This suggests that disorder does have some adverse effect on electron transport in the semi-metallic phase. The observed behaviour shows a remarkable similarity with that exhibited by classical alloys, when a metal forms an alloy an increase in resistivity is observed. For the case where one metal contains a low concentration of another, then the resistivity (ρ) is given by,

$$\rho = \rho_0 + \rho(T) \quad \dots\dots\dots 5.6$$

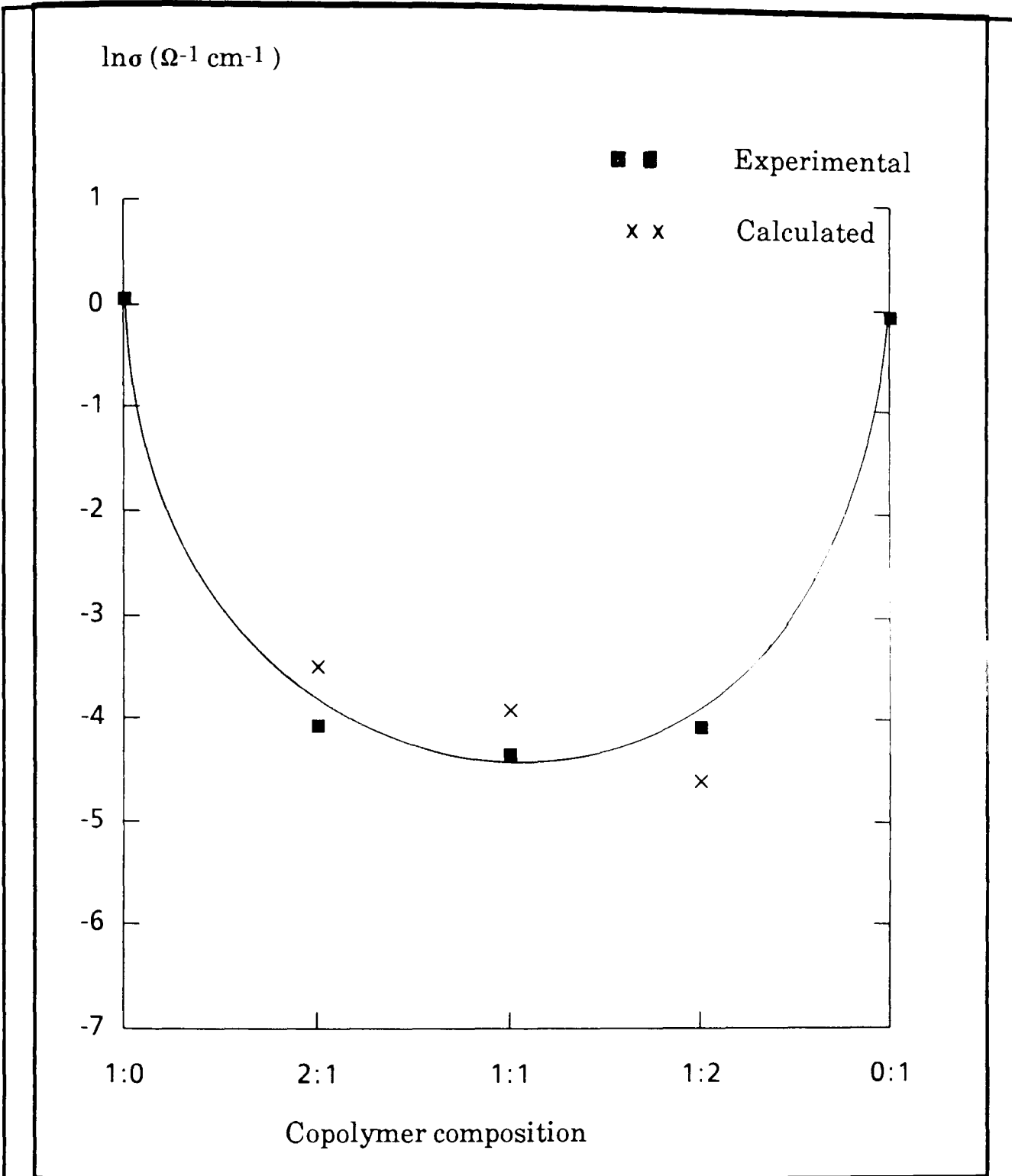


Table 5.12: The experimental and calculated conductivity for the iodine doped copolymers.

where $\rho(T)$ is the temperature dependent component of the resistivity due to the thermal motion of the lattice, and ρ_0 is the temperature independent contribution of the resistivity due to scattering by the impurity. This relationship, which is known as *Mathiessen's rule* (5.47), has been extended to describe the behaviour observed for the full concentration range. In this case, ρ_0 is given by

$$\rho_0 = \text{constant } x(1-x) \quad \dots\dots\dots 5.7$$

where x is the mole fraction of one component and $1-x$ that of the other.

Taking the constant as $300 \Omega \text{ cm}$, a reasonably good fit is obtained with the experimental data available..

Whilst further and more detailed investigation is required, particularly of the temperature dependence in the low temperature region, these results do suggest that these highly doped one-dimensional "alloys" do have some characteristic in common with classical alloys.

CHAPTER SIX

A.C . CONDUCTIVITY

6.1)-Introduction:

6.1.1) Dielectric Properties:

If a d.c. voltage V is applied across a parallel plate capacitor with vacuum, a dielectric charge Q will be stored on the electrodes, thus,

$$Q = C_0 V \quad \dots\dots\dots 6.1$$

where C_0 is the capacitance of the vacuum capacitor which is given by:

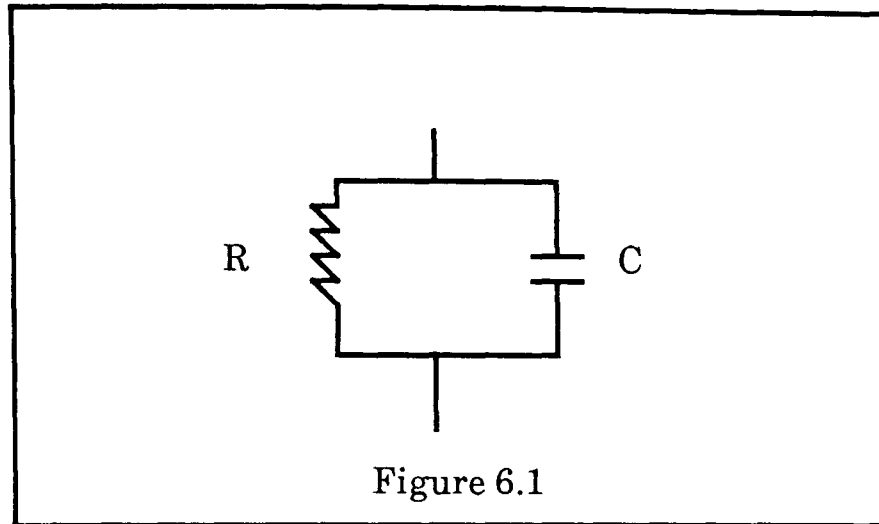
$$C_0 = \epsilon_0 \frac{A}{d} \quad \dots\dots\dots 6.2$$

where A and d are the electrode area and spacing respectively and ϵ_0 is the *permittivity* of free space ($8.854 \times 10^{-12} \text{ Fm}^{-1}$). When the capacitor is filled with a substance its capacitance (C) will be:

$$C = C_0 \epsilon' = \epsilon_0 \epsilon' \frac{A}{d} \quad \dots\dots\dots 6.3$$

where ϵ' is the *relative permittivity* (ie, relative to the space), and sometimes called the dielectric constant. The $\epsilon_0 \epsilon'$ is the *absolute permittivity* of the substance. A real dielectric will possess a finite conductivity when d.c

voltage is applied and can be considered as a parallel combination of ideal resistance R and a perfect capacitor C (6.1) as in figure 6.1



This device will obey *Ohm's law* under dc fields. The d.c. conductance, G , of the dielectric is given by:

$$G = \frac{1}{R} = \sigma \frac{A}{d} \quad \dots\dots\dots 6.4$$

where σ is the conductivity.

If a sinusoidal voltage at frequency, ω , is applied then,

$$V = V_0 \sin \omega t \quad \dots\dots\dots 6.5$$

where the angular frequency $\omega = 2\pi f$, and f is the operating frequency (Hz). Then the charge Q on the capacitor plate can be written as:

$$Q = CV = C V_0 \sin \omega t \quad \dots\dots\dots 6.6$$

The charging current (I_C) is the rate of change of charge with time:

$$I_C = \frac{dQ}{dt} = \omega C V_0 \cos \omega t \quad \dots\dots\dots 6.7$$

$$I_C = \omega C V_0 \sin \left(\omega t + \frac{\pi}{2} \right) \quad \dots\dots\dots 6.8$$

The peaks of the current wave form are displaced in time by $\pi/2$ (quarter of a period) from those of the voltage waveform(6.2).

Using a complex notation, where $j = \sqrt{-1}$, the impedance(Z) of the real dielectric is given by:

$$\frac{1}{Z} = \frac{1}{R} + j\omega C \quad \dots\dots\dots 6.9$$

In simplest cases of a *perfect dielectric*, $R = \infty$ (ie, $G = 0$).

$$Z = \frac{1}{j\omega C} \quad \dots\dots\dots 6.10$$

The device will impede the flow of current by an amount which varies with frequency(Hz)(6.1).

In the case of a real dielectric, in addition to the charging current(I_C) a simultaneous loss current(I_l) may appear in phase with the voltage,

$$I_l = G V \quad \dots\dots\dots 6.11$$

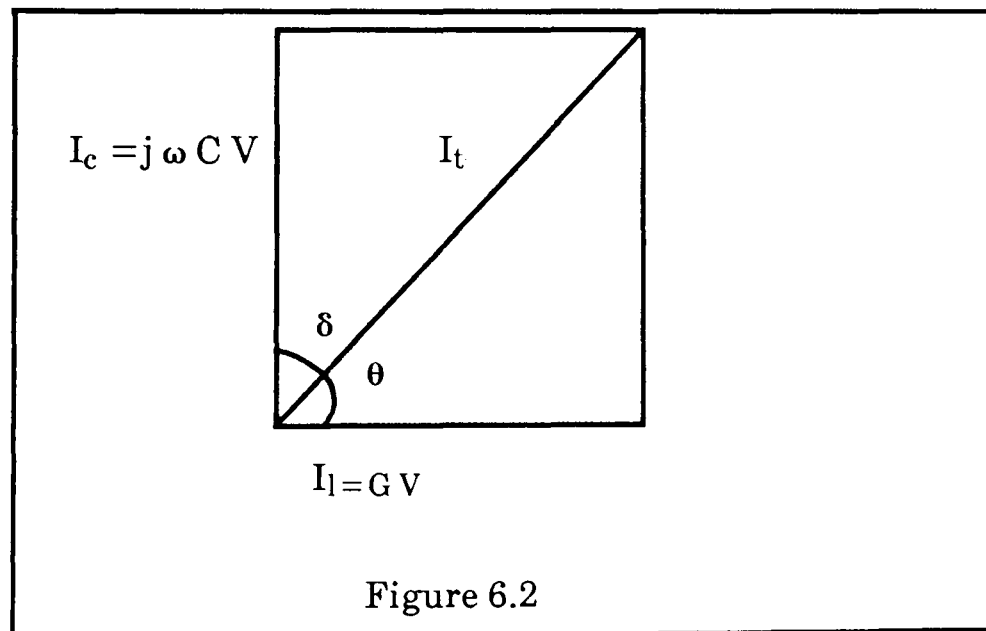
G represents the conductance of the dielectric. Then the total current flowing across the capacitor given by,

$$I_t = I_C + I_l \quad \dots\dots\dots 6.12$$

$$= j \omega C V + G V \quad \dots\dots\dots 6.13$$

$$= (j \omega C + G) V \quad \dots\dots\dots 6.14$$

I_t is inclined at a phase angle θ to the applied voltage, V , and a loss angle δ to the imaginary axis as shown in figure 6.2 below,



It has become conventional to express the existence of a loss current in addition to the charging current by the introduction of a complex permittivity(6.3),

$$\epsilon^* = \epsilon' - j \epsilon'' \quad \dots\dots\dots 6.15$$

where ϵ' is the relative permittivity as used before and $j \epsilon''$ is associated with the resistive vector.

By analogy with an ideal capacitor, one can express the complex capacitor, C^* , of a real dielectric as,

$$C^* = \epsilon^* C_0 \quad \dots\dots\dots 6.16$$

where $C_0 = \epsilon_0 A/d$ (equation 6.2) for a parallel plate capacitor. The impedance, Z , is given by,

$$Z = \frac{1}{j \omega C^*} = \frac{1}{j \omega C_0 (\epsilon' - j \epsilon'')} \quad \dots\dots\dots 6.17$$

From equation 6.9

$$Z = \frac{R}{(1 + j \omega C R)} \quad \dots\dots\dots 6.18$$

Combination of equations 6.17 and 6.18, and using equation 6.3, and then equating real and imaginary parts,

$$\epsilon'' = \frac{1}{\omega R C_0} \dots\dots\dots 6.19$$

From equation 6.2, then,

$$\epsilon'' = \frac{d}{\omega R \epsilon_0 A} = \frac{\sigma}{\omega \epsilon_0} \dots\dots\dots 6.20$$

where σ is the dielectric conductivity $= \omega \epsilon'' \epsilon_0$. This dielectric conductivity is the sum over dissipative effects.

It is important to note that,

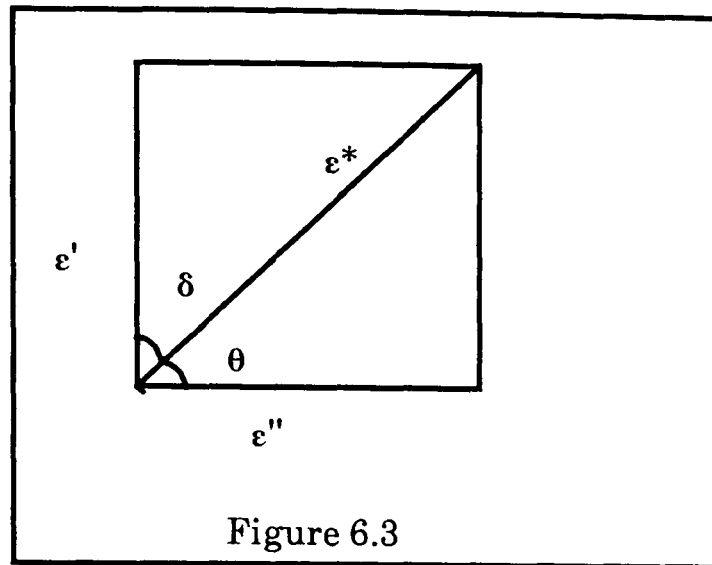
$$\frac{\epsilon''}{\epsilon'} = \frac{1}{\omega R C} \dots\dots\dots 6.21$$

where ϵ''/ϵ' defined as being equal to the quantity $\tan \delta$ (for any material of any geometry)^(6.1). This definition is consistent with $\delta = 90 - \theta$ from figure 6.2.

Thus,

$$\tan \delta = \frac{\epsilon''}{\epsilon'} = \frac{1}{\omega R C} \dots\dots\dots 6.22$$

which is called the loss tangent, dielectric loss, or dissipative factor, figure 6.3,



From consideration of figure 6.2, $\sin \delta$ is a measure of the resistive impedance and hence the heat dissipated.

The relative *permittivity* (dielectric constant), ϵ' , is intrinsic to the material and normally varies only slowly with temperature and pressure, while ϵ'' and σ vary sharply with temperature, pressure and other variables such as impurities and structure^(6.1).

Substituting equations 6.3 and 6.19 in equation 6.14,

$$I_t = (j \omega \epsilon' + \omega \epsilon'') C_0 V_t \quad \dots\dots\dots 6.23$$

The current density $J = I_t/A$, traversing a capacitor under the applied field strength, $E_t = V_t/d$, becomes after substitution equation 6.3 in equation 6.23,

$$J = (j \omega \epsilon' + \omega \epsilon'') \epsilon_0 E_t \quad \dots \quad 6.24$$

6.1.2) The Dielectric Relaxation:

The relative permittivity, or *dielectric constant*, ϵ' , of a medium is related to the *polarizability*, α , and *dipole moment*, μ , of its molecules^(6.3-4), each of which has a characteristic relaxation time τ ^(6.5). At very low frequencies, approaching d.c, permanent dipoles align themselves along the field acting upon them and thus contribute fully to the total polarization of the dielectric, and the *permittivity* is equal to the *static permittivity*, ϵ_s . At high frequencies where the angular frequency, ω , exceeds $1/\tau$ in the infrared and beyond, the variation in the field is too rapid for the dipoles to follow, so that, their contribution to the *polarisation*, and hence to the *permittivity*, is negligible^(6.6), and the sample behaves very similarly to a non polar polymer. If ω is of the order of $1/\tau$, then the *polarisation* lags in phase because of internal retarding or *friction forces*, giving rise to a loss characterised by ϵ'' . At such a frequency the *loss factor*, ϵ'' , exhibits a peak with a maximum value at $\omega \tau = 1$.

The fall in the total *polarization* is referred to as *dielectric relaxation* or dispersion. The frequency at which the fall in polarization occurs can vary from low frequencies of the order of 10^{-1} Hz and below for larger macromolecules to frequencies up to 10^{12} Hz for small molecules ^(6.7).

6.1.3) Debye Equations:

Debye treated the case of a single freely rotating dipole (6.5,6.8) and derived the equation

$$\epsilon^* = \epsilon_\infty + \frac{\epsilon_S - \epsilon_\infty}{1 + j\omega\tau} \quad \dots\dots\dots 6.25$$

where ϵ_S and ϵ_∞ are the *permittivity* at approaching zero and infinite frequency respectively.

Separating the real and imaginary parts(6.6), we find,

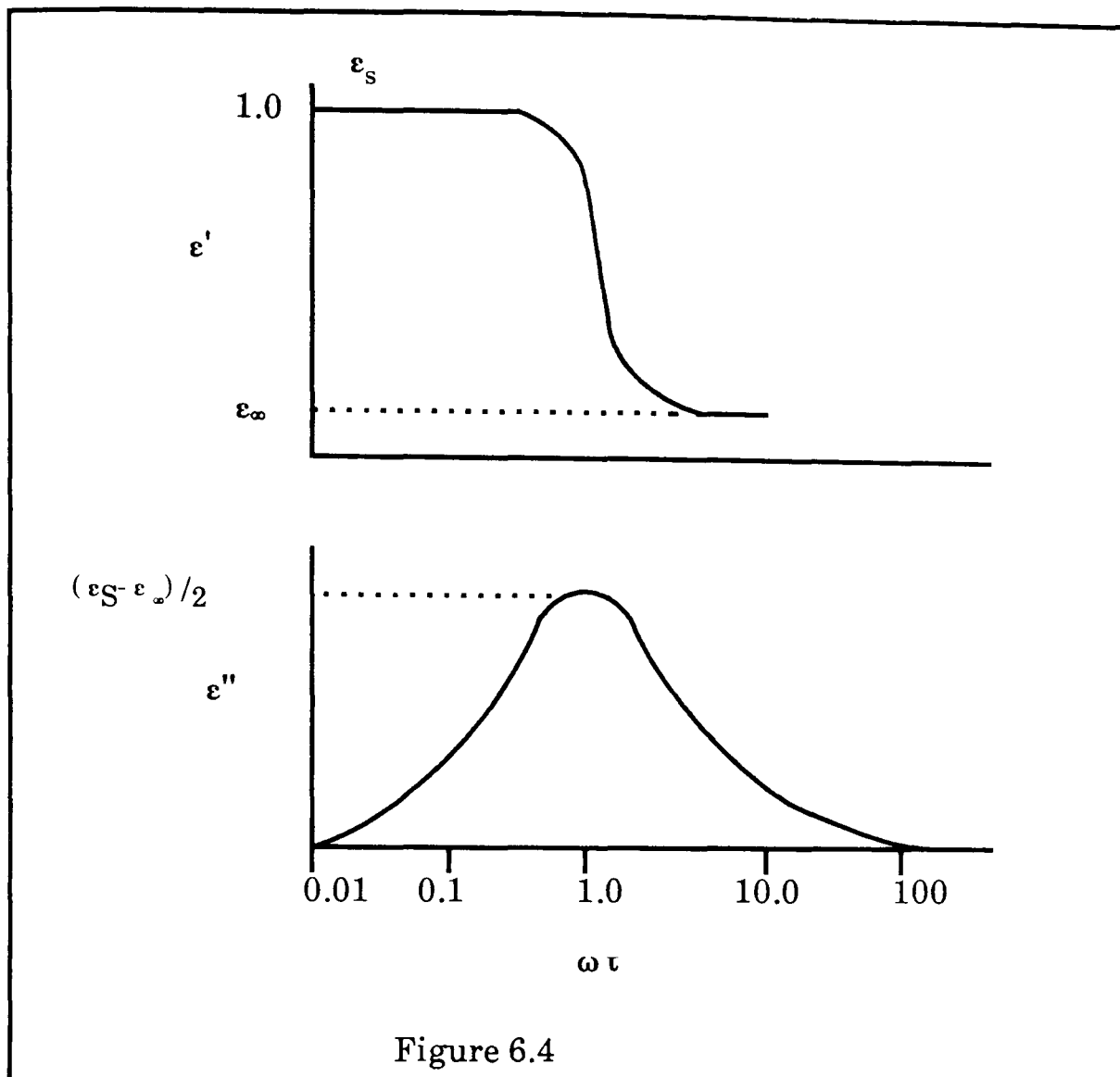
$$\epsilon' = \epsilon_\infty + \frac{\epsilon_S - \epsilon_\infty}{1 + \omega^2\tau^2} \quad \dots\dots\dots 6.26$$

$$\epsilon'' = \frac{(\epsilon_S - \epsilon_\infty)\omega\tau}{1 + \omega^2\tau^2} \quad \dots\dots\dots 6.27$$

$$\tan \delta = \frac{\epsilon''}{\epsilon'} = \frac{(\epsilon_S - \epsilon_\infty)\omega\tau}{\epsilon_S + \epsilon_\infty\omega^2\tau^2} \quad \dots\dots\dots 6.28$$

Equations 6.26 and 6.27 known as the *Debye equations* (6.8-9), and give rise to a variation of ϵ' and ϵ'' with frequency as shown in figure 6.4 .

ϵ' decreases with frequency. This decrease is called the *dispersion* of the *dielectric constant*. The difference is known as the magnitude of the



relaxation and is a measure of the *orientation polarization*. In the relaxation region ϵ'' passes through a maximum at a frequency $\omega \tau$. The maximum value of ϵ'' occurs when $\omega \tau = 1$, and $\epsilon''_{\max} = \epsilon_s - \epsilon_{\infty}/2$, thus by determining the frequency at which ϵ'' is maximum, then the relaxation time τ can be found.

Combination of equations 6.26 and 6.27 yields the equation of a circle in the complex (ϵ', ϵ'') plane (6.3,6.11). Only the semicircle over which ϵ'' is positive with its centre on ϵ' axis has physical significance(6.9). Actually, a semicircular plot of ϵ'' vs ϵ' as in figure 6.5 is a characteristic of the *Debye loss process*.

From equation 6.27 the predicted loss peak is symmetric about the frequency $\omega = 1/\tau$ when plotted as ϵ'' vs $\log \omega$, with a maximum loss of $(\epsilon_S - \epsilon_\infty)/2$ with a width at half height of 1.144 decades(6.12).

Many materials, especially long chain molecules and polymers, show a broader *dispersion curve* and lower maximum loss than would be expected from the *Debye equations* (6.26-27). In such cases the $\epsilon'' - \epsilon'$ curve falls inside the *Debye semicircle* (6.9,6.11), as shown in figure 6.5 . The most important attempts which have been made to represent the behaviour of such systems by empirical equations(6.11) are:-

6.1.3a) Cole - Cole Equation,:

$$\epsilon^* = \epsilon_\infty + \frac{\epsilon_S - \epsilon_\infty}{1 + (j \omega \tau)^{1-\alpha}} \quad \dots\dots\dots 6.29$$

where τ is the mean *relaxation time*(6.8). The experimental results on a considerable number and variety of dielectrics generally expressed by the above formula involving a single new empirical parameter(6.8), α , which is may be interpreted as a spreading factor of the actual *relaxation time* about the mean value τ . The formula produces asymmetrical arc about a line through the centre within the *Debye semicircle* as shown in figure 6.5.

If a single relaxation time is assumed the plot is a complete semicircle with centre on the ϵ' axis.

6.1.3b) Cole - Davidson Equation:

$$\epsilon^* = \epsilon_\infty + \frac{\epsilon_S - \epsilon_\infty}{(1 + j \omega \tau)^\beta} \quad \dots\dots\dots 6.30$$

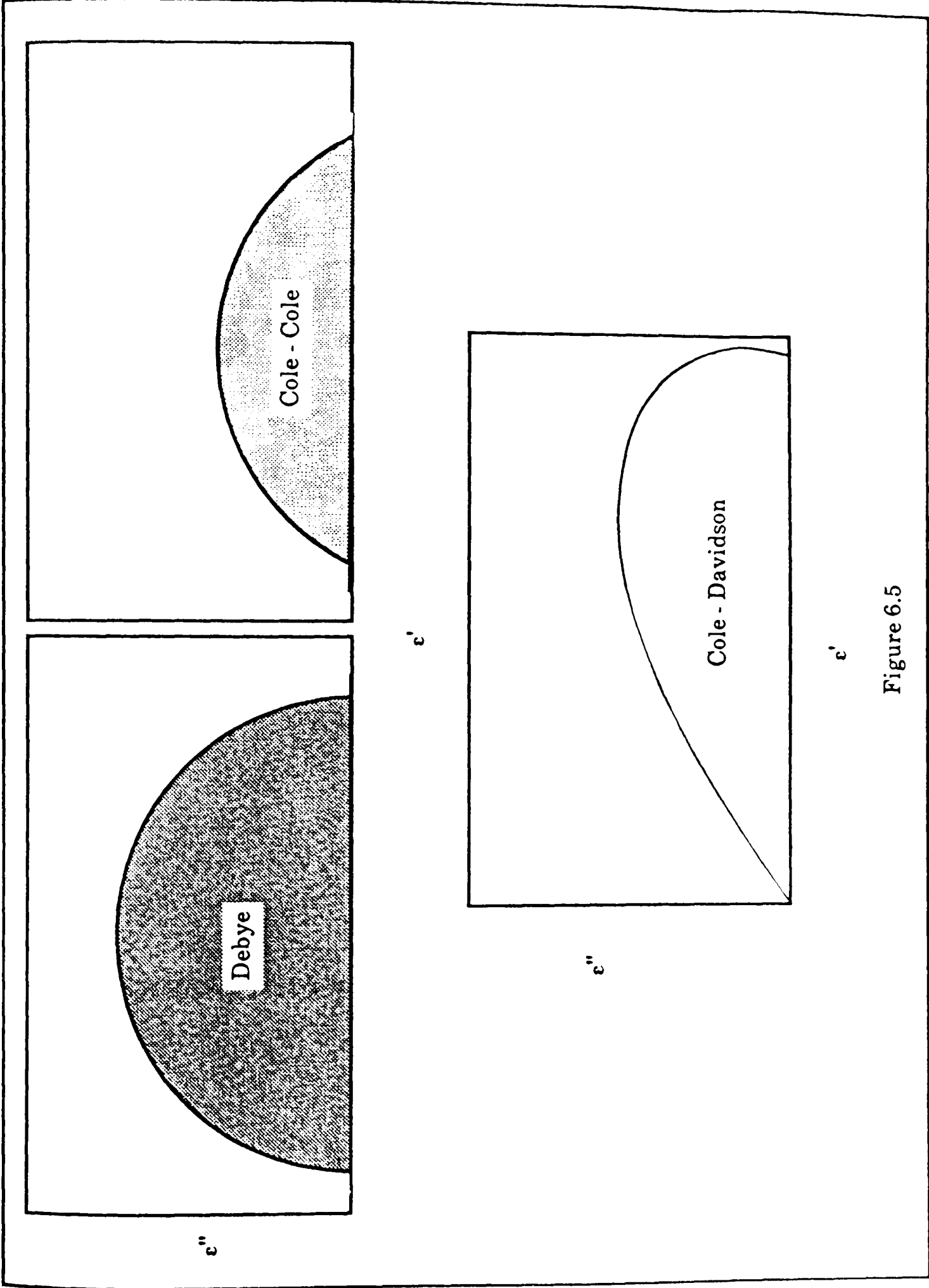


Figure 6.5

where β is constant to be derived from experimental results^(6.13). *Cole* and *Davidson* found that the experimental results for certain materials do not have symmetry. The $\epsilon'' - \epsilon'$ plot being a *skewed arc*^(6.11). This arc would be obtained from a series of *relaxation mechanisms* of decreasing importance extending to the high frequency side of the *main dispersion*. When $\alpha = 0$ or $\beta = 1$, the two models reduce to the *Debye model*, equation 6.25.

The *Cole - Cole* and *Cole - Davidson* types of behaviour can be understood as arising from existence of continuous spread of *relaxation times*, each of which alone would give rise to a *Debye type* of behaviour^(6.11).

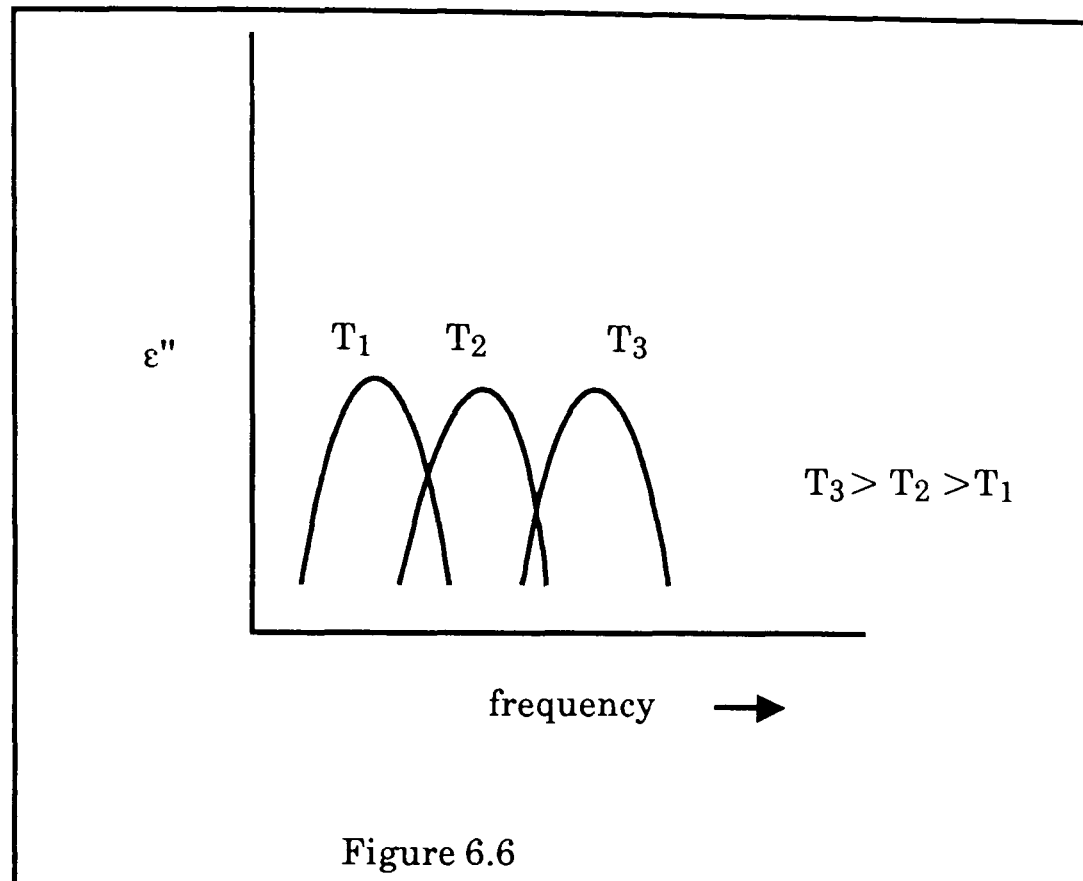
6.1.4) Dipolar Loss in Polymeric Solids:

The amorphous medium of many polymeric solids permits a considerable degree of molecular motion^(6.14). Where this motion involves the movement of a permanent dipole, then a *Debye loss* is observed. In the same polymers, several different dipolar losses are observed resulting from the rotation of polar side groups and other dipolar molecular motions.

Polymers commonly show a *loss peak* that extends over a wide range of frequency, i.e., a *flatter loss peak* which can be explained by the distribution of relaxation times due to presence of many mobile sections (dipoles) in different environments. The more mobile dipoles will follow the electric field at higher frequencies than the dipoles that are more restricted.

The effect of temperature on the *loss peak* for polar polymers is in qualitative agreement with the fact that the polymer chains become more

mobile as the temperature is raised. Thus the *loss peak* shifts to higher frequencies as the temperature is increased (6.15) as it is shown in the figure 6.7 .



6.1.5) A.C. Conductivity:

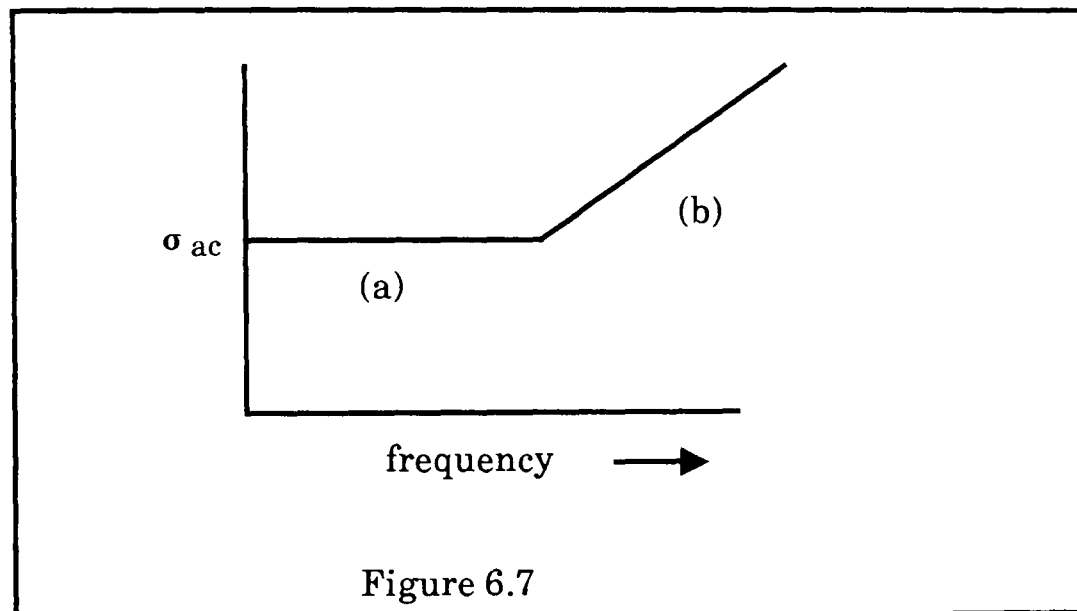
The materials described in this thesis, either do not possess a molecular dipole in the solid state, or those dipoles are not capable of rotating in response to an alternating field. Thus the measurements of the conductivity by an ac bridge might be expected to yield a constant value equal to that obtained by dc since,

$$\sigma = \epsilon_0 \epsilon'' \omega \quad \dots \dots \dots 6.31$$

where

$$\epsilon'' = \frac{1}{\omega R C_0} \quad \text{and} \quad C_0 = \epsilon_0 \frac{A}{d}$$

However, in certain temperature regions, many solids show a frequency dependent conductivity region (b) in addition to the expected frequency independent region (a), as illustrated in figure 6.7.



The behaviour can be described by the equation,

$$\sigma_T = \sigma_{dc} + A \omega^n \quad \dots\dots\dots 6.32$$

$$A \omega^n = \sigma_{ac} \quad \dots\dots\dots 6.33$$

then

$$\sigma_{ac} = \sigma_T - \sigma_{dc} \quad \dots\dots\dots 6.34$$

where σ_T is the conductivity measurement by a.c., σ_{dc} is a frequency independent component which may be identified with the d.c conductivity, which is temperature dependent. A and n are constant, with $0 < n < 1$, where n can be determined from a plot of $\ln(\sigma_T - \sigma_{dc})$ vs $\ln \omega$, which gives a straight line of slope n.

Much theoretical work has been carried out to explore models(6.17-19) interpretation of the $A \omega^n$ term. The work has been summarised by Long (6.16). Although the models differ somewhat, there is a strong body of evidence to suggest that the process responsible is the hopping of carriers between a distribution of hopping sites (6.20-21).

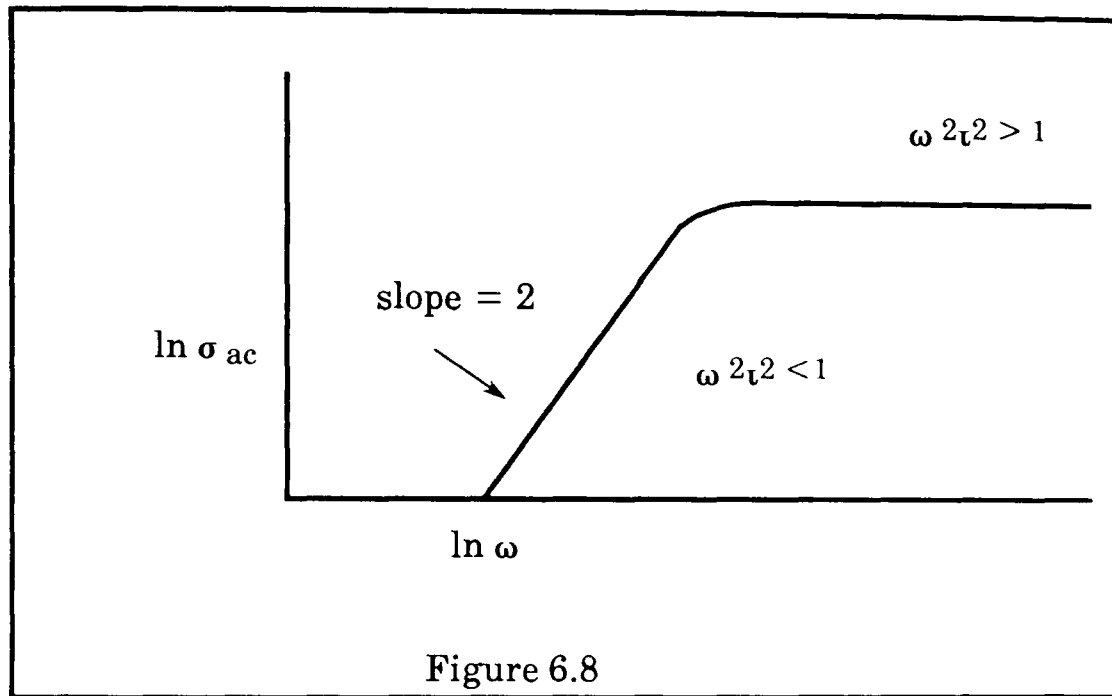
Consider first the hypothetical case of a solid in which electrons can hop between pairs of sites, all of which are identical, in response to the a.c. field. The movement of electrons is equivalent to the rotation of a dipole, and since all the electrons move in an identical way the process will be characterised by a *single relaxation time*. Hence,

$$\epsilon'' = \frac{(\epsilon_S - \epsilon_\infty) \omega \tau}{1 + \omega^2 \tau^2} \quad \dots\dots\dots 6.35$$

since $\sigma_{ac} = \epsilon_0 \epsilon'' \omega$, the contribution to the conductivity due to this process is,

$$\sigma_{ac} = \frac{\epsilon_0(\epsilon_S - \epsilon_\infty) \omega^2 \tau}{1 + \omega^2 \tau^2} \dots\dots\dots 6.36$$

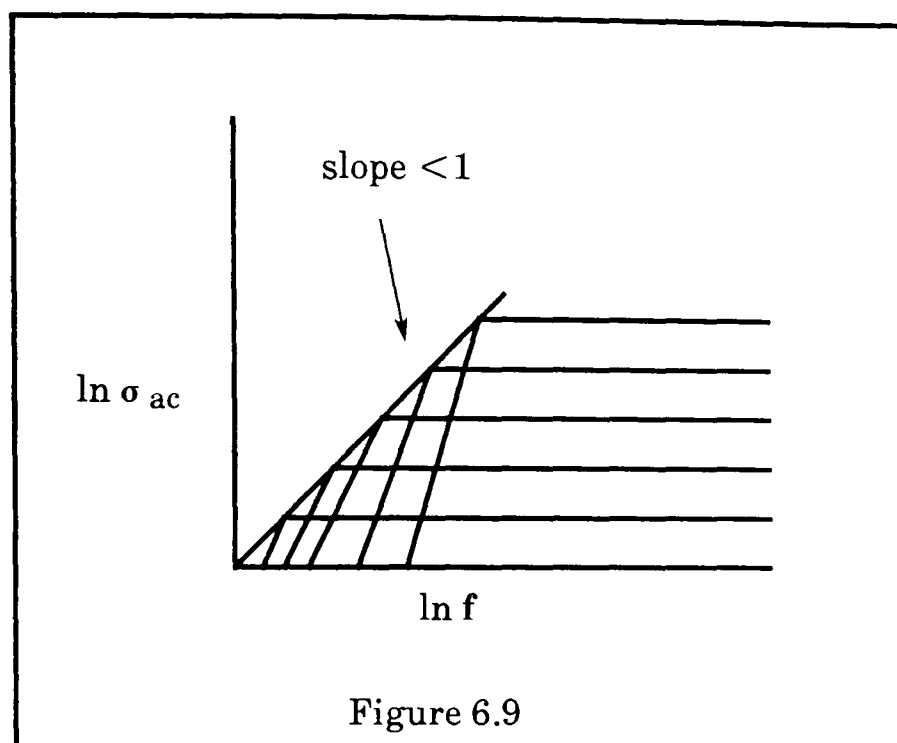
At low frequencies $\omega^2 \tau^2 < 1$, and σ is proportional to ω^2 . At high frequencies $\omega^2 \tau^2 > 1$ and σ is independent of frequency as shown in figure 6.8.



Clearly this does not agree with experiment. However, *Mott* (6.22) has postulated a broad distribution of sites, with a corresponding distribution of relaxation times, all of which contribute to the frequency dependent process. Thus equation 6.36 must be replaced by,

$$\int_0^\infty \sigma_{ac} = n(\tau) \alpha \omega^2 \tau (1 + \omega^2 \tau^2)^{-1} d\tau \dots\dots\dots 6.37$$

where $n(\tau)$ is the density of pairs characterised by a relaxation time, and α is a polarizability term (6.23). This summation is shown diagrammatically in figure 6.9



The resultant slope is no longer 2, but < 1 typically 0.8 (6.17). The theory thus provides a physical model to explain the observed $A \omega^n$ term.

As a consequence of the *Kramers-Kronig relation*, which relates the frequency dependence of the real and imaginary parts of a variable, it can be shown that,

$$C = C_{\infty} + A_1 \omega^{n-1} \dots\dots\dots 6.38$$

where C is the capacitance at a given temperature and frequency, C_{∞} is the capacitance at the highest frequency, which is virtually temperature independent (6.24). A plot of $\ln(C - C_{\infty})$ vs $\ln \omega$ gives a straight line of slope

(n-1). In practice hopping sites can be lattice defects(6.18,6.25-26), adsorped gases(6.27), or of impurity centres(6.17,6.28). In partially amorphous materials, such as studied in this work, the concentration of lattice defects is likely to be very high and to dominate the frequency dependent process. Furthermore, the hopping will make its biggest contribution where there is a high concentration of both occupied and vacant sites, i.e., at the *Fermi level*, where sites occupancy is one half. *Mott* (6.11,6.29-30) has deduced a relation between the density of states at the *Fermi level* and the frequency dependent conductivity

$$\sigma_{ac} = \frac{1}{3} \pi e^2 k T \left[N(E_f) \right]^2 \alpha_1^{-5} \left[\ln \left(\frac{v_{ph}}{\omega} \right) \right]^4 \omega \quad \dots \dots \dots 6.39$$

where α_1 is the fall off the *electric wave function* with distance from the defect centre, and v_{ph} is the phonon frequency. Putting α as the reciprocal of the interplanar spacing, and $v_{ph} = 1.0 \times 10^{12}$ Hz. The equation 6.39, reduces to $\sigma_{ac} \propto \omega^n$, with $n \approx 0.8$ for frequencies $\leq 10^5$ Hz(6.27). Knowing σ_{ac} , it is possible to estimate the density of states at the *Fermi level* [$N(E_f)$].

The importance of this equation is that in addition to giving an estimate of defect concentration, it permits a reliable comparison of the degree of imperfection of different samples of the same or related materials.

6.2) Results and Discussion:

6.2.1) AlPcF:

a) Conductivity measurements:

Figure 6.10 shows the frequency dependence of a.c. conductivity at a series of temperatures, for compactions of AlPcF. At 24 °C the conductivity is virtually independent of frequency. However, as the temperature is lowered the conductivity starts to increase with frequency, until below -60 °C the conductivity is frequency dependent over the entire range studied. This behaviour is characteristic of a material exhibiting both a measurable d.c. conductivity which is frequency independent, and a frequency dependent conductivity resulting from the hopping of carriers between randomly distributed sites(6.16,6.20,6.31) which varies as ω^n . The increase in a.c. loss at high frequencies can be attributed to the contribution of the closely spaced states to the loss(6.16). The results for the surface cell (figure 6.11) and the sandwich cell (figure 6.12) are qualitatively similar.

An alternative presentation of the data, in which the natural logarithm of the conductivity is plotted against reciprocal temperature is given in figures 6.13-15. The d.c. conductivity is also plotted in the same way. From these plots it is clear that the low frequency, frequency independent conductivity can be identified with the d.c. conductivity, which represents the transport of charge through the material by a process such as band conduction(6.32,6.33). It is also clear that the frequency dependent hopping

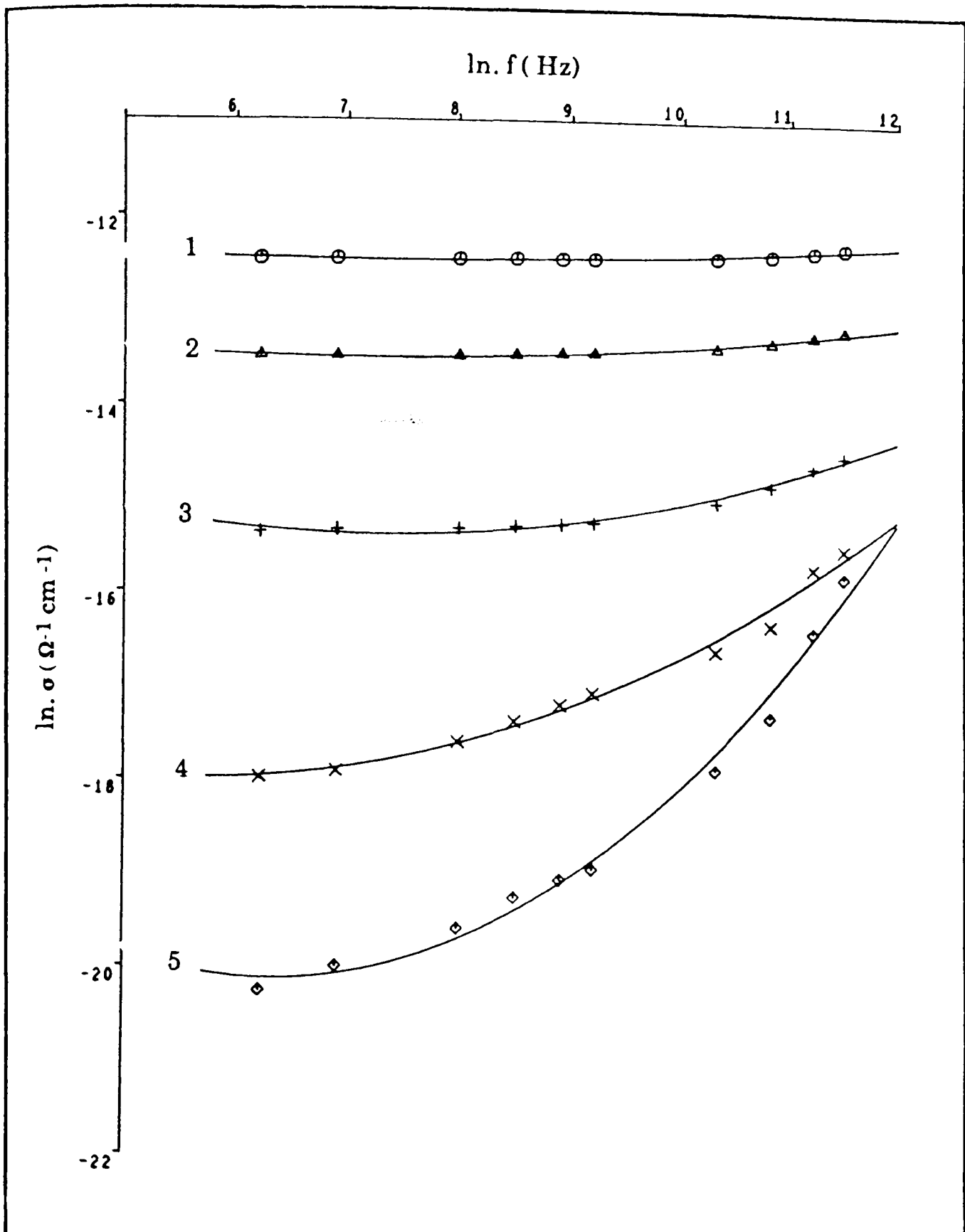


Figure 6.10: The frequency dependence of a.c. conductivity at a series of temperatures for compaction of AlPcF. 1(24), 2(0°C), 3(-30°C), 4(-60°C), 5(-90°C).

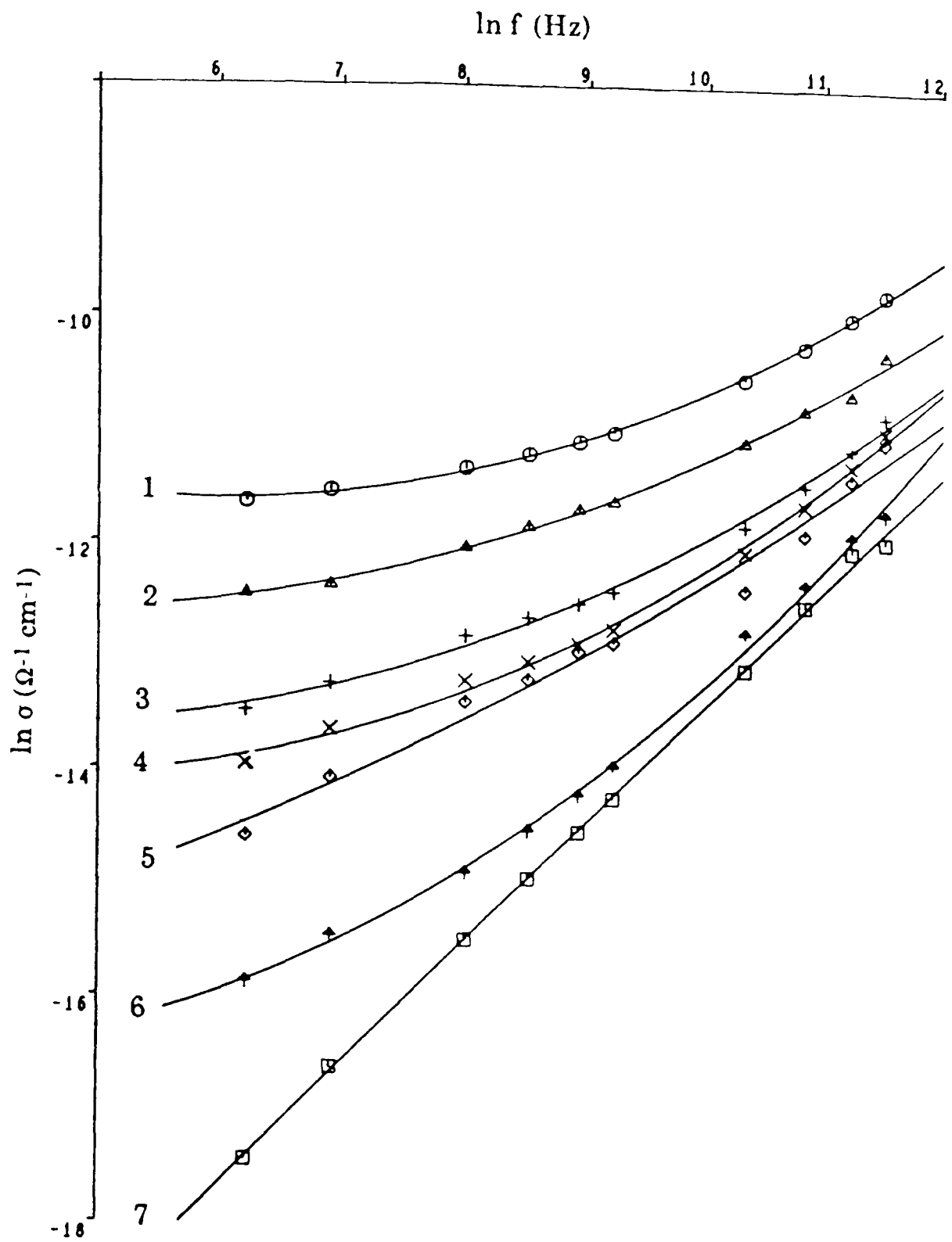


Figure 6.11: The frequency dependence of a.c. conductivity at a series of temperatures for compaction surface cell of AlPcF. 1(900°C), 2(600°C), 3(240°C), 4(0°C), 5(-25°C), 6(-60°C), 7(-100°C).

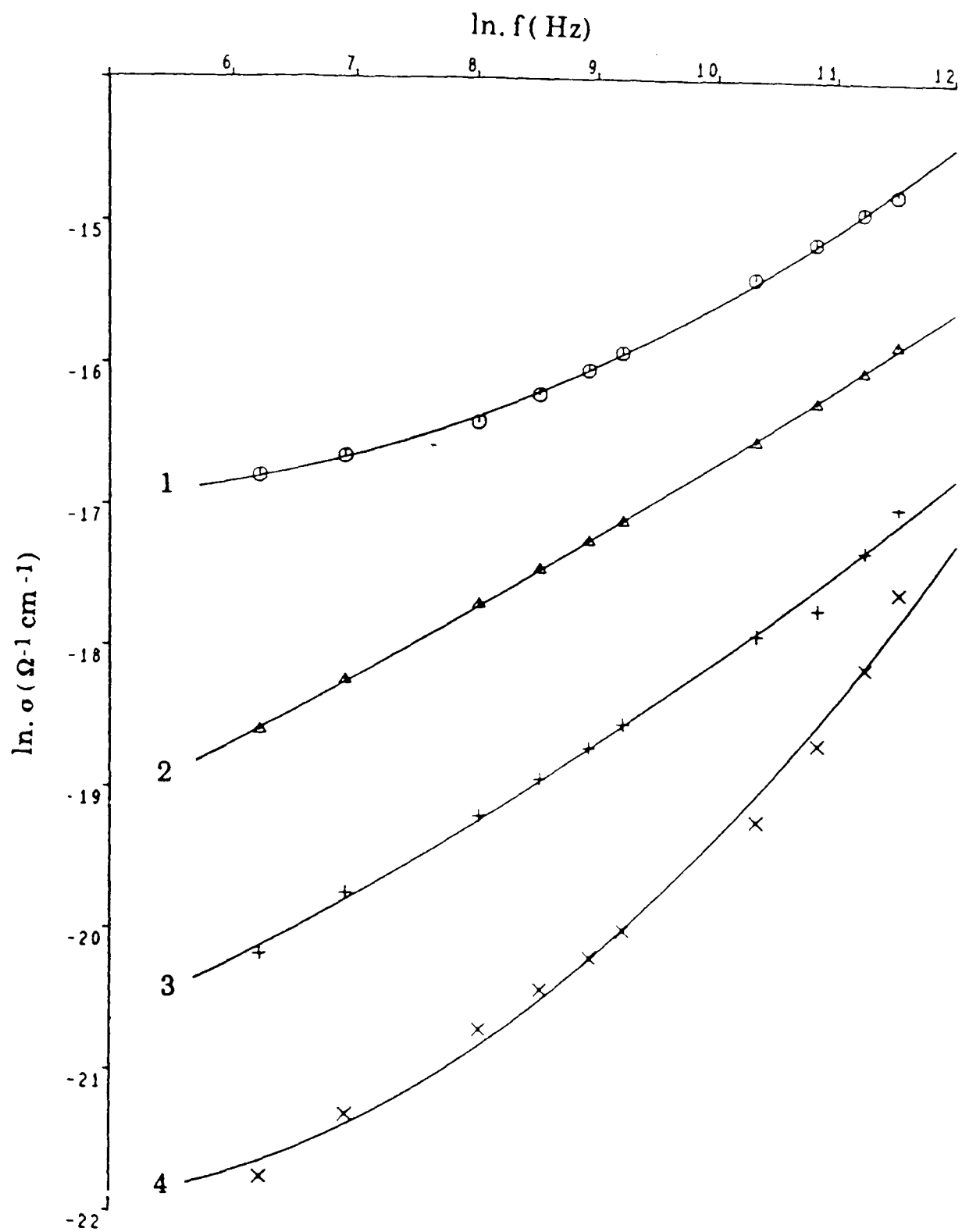


Figure 6.12: The frequency dependence of a.c. conductivity at a series of temperatures for sandwich cell of AlPcF. 1(0°C), 2(-30°C), 3(-60°C), 4(-90°C).

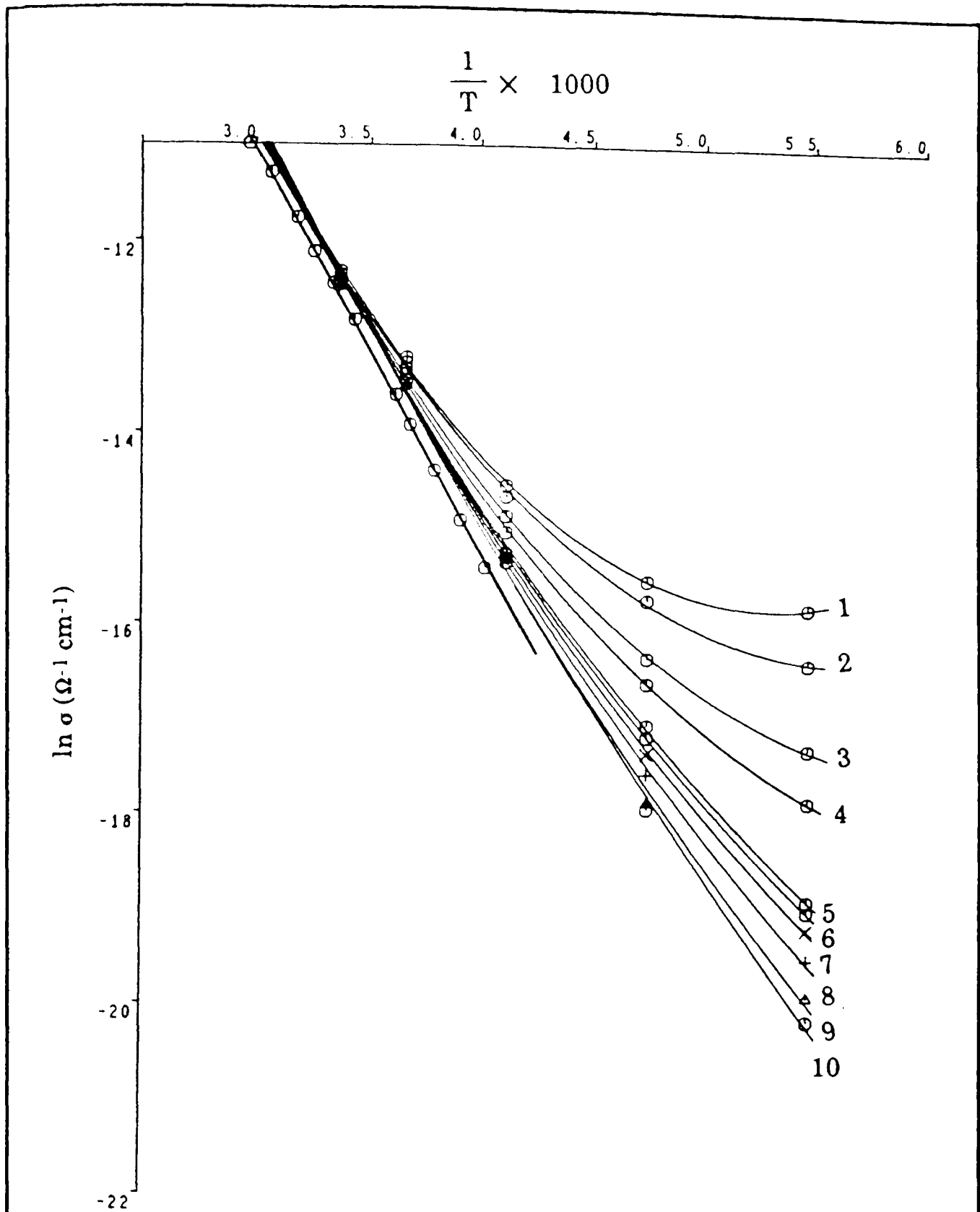


Figure 6.13: The d.c. conductivity and the frequency dependence of a.c. conductivity at a series of temperatures for compaction of AlPcF. 1(100Hz), 2(75Hz), 3(50Hz), 4(30Hz), 5(10Hz), 6(7.5Hz), 7(5Hz), 8(3Hz), 9(1Hz), 10(0.5Hz).

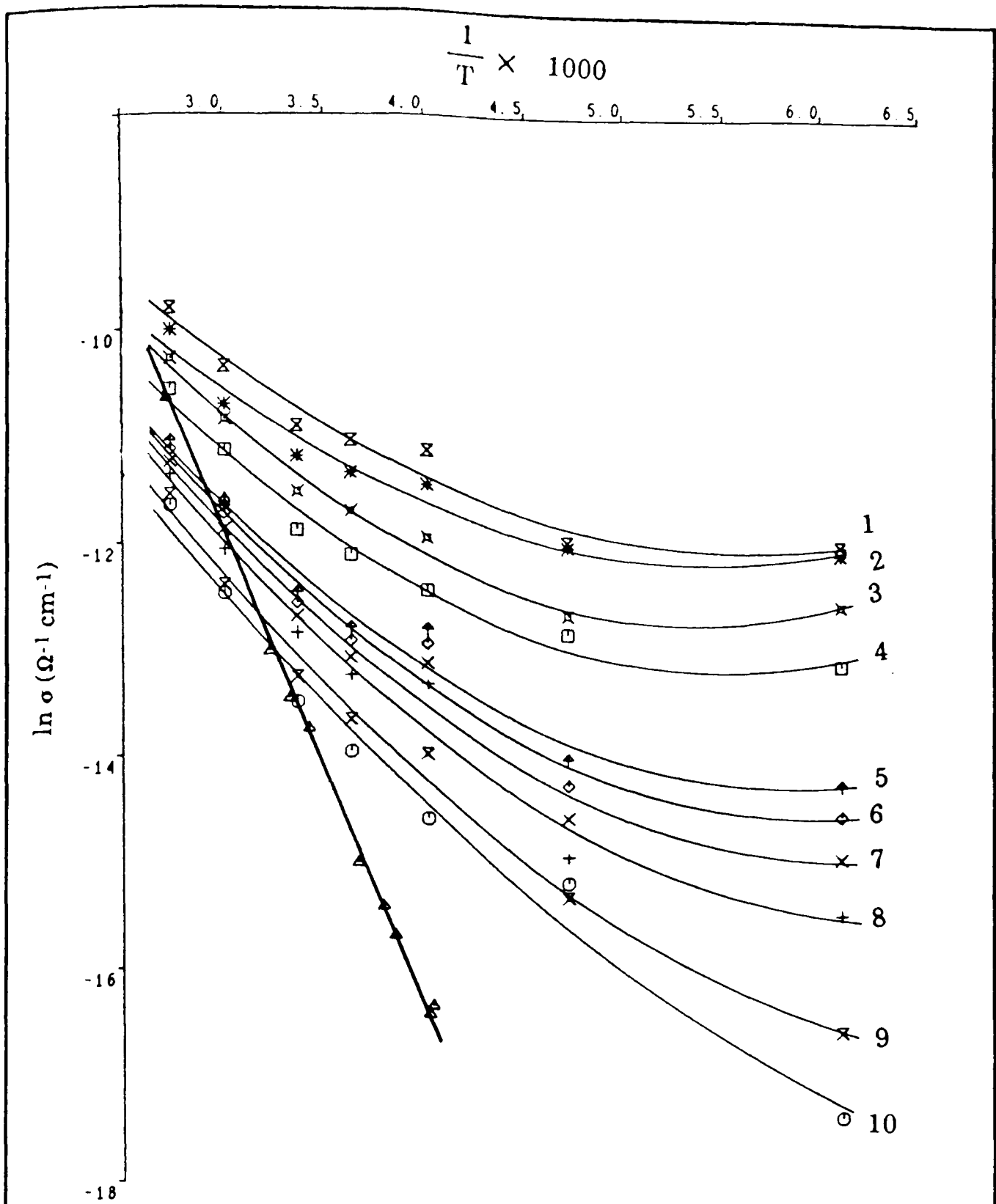


Figure 6.14: The d.c. conductivity and the temperature dependence of a.c. conductivity at a series of frequencies for surface cell of AlPcF. 1(100Hz), 2(75Hz), 3(50Hz), 4(30Hz), 5(10Hz), 6(7.5Hz), 7(5Hz), 8(3Hz), 9(1Hz), 10(0.5Hz).

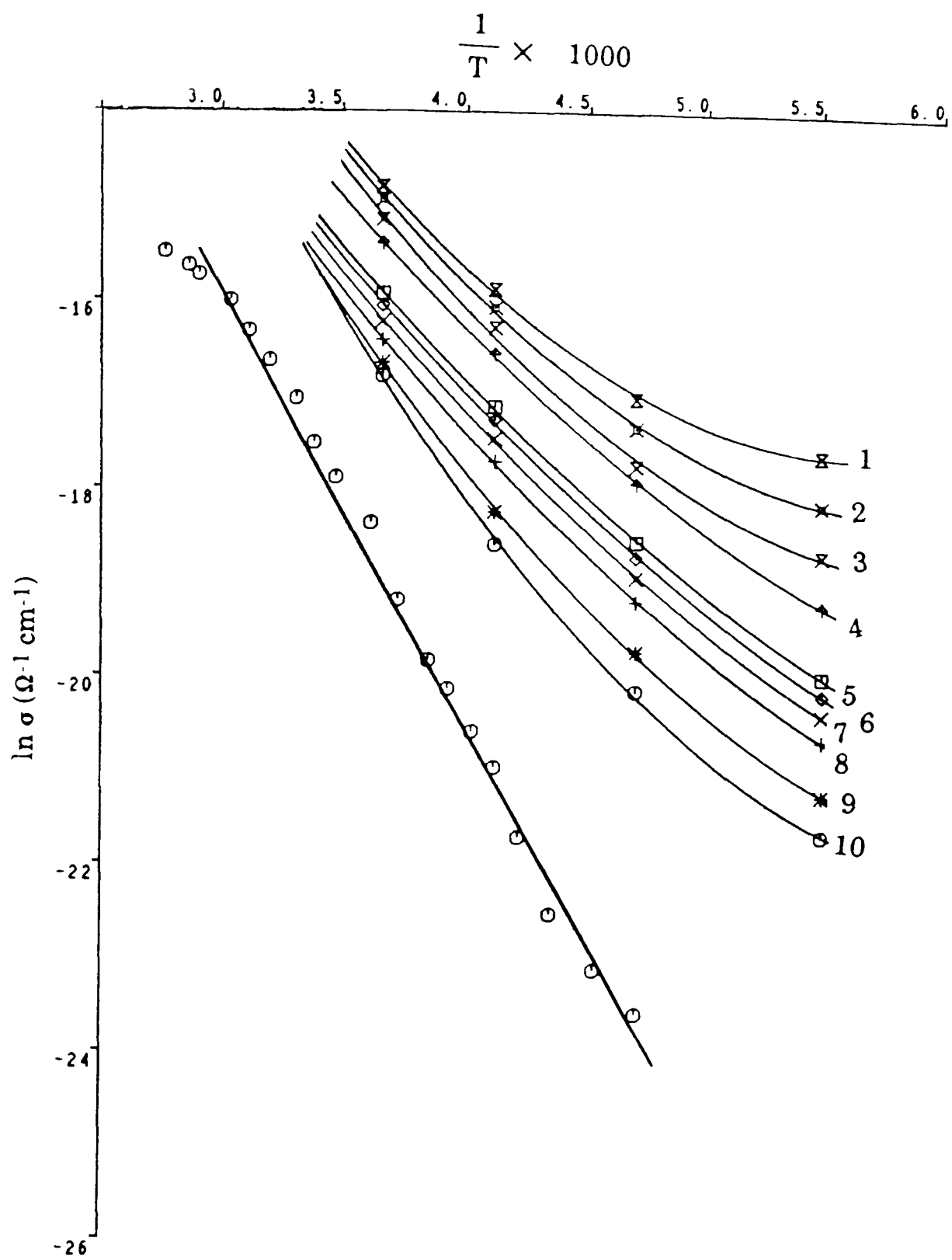


Figure 6.15: The d.c. conductivity and the temperature dependence of a.c. conductivity at a series of frequencies for sandwich of AlPcF. 1(100Hz), 2(75Hz), 3(50Hz), 4(30Hz), 5(10Hz), 6(7.5Hz), 7(5Hz), 8(3Hz), 9(1Hz), 10(0.5Hz).

conductivity has a much lower temperature dependence, reflecting the smaller energy barriers involved.

Thus we may describe the observed conductivity, σ_T , by the equation

$$\sigma_T = \sigma_{dc} + \sigma_{ac} \quad \dots\dots\dots 6.40$$

where

$$\sigma_{dc} = \sigma_0 e^{\frac{-E_a}{kT}} \quad \dots\dots\dots 6.41$$

$$\sigma_{ac} = A\omega^n = \sigma_{ac(0)} e^{\frac{-E'_a}{kT}} \quad \dots\dots\dots 6.42$$

where E_a is the thermal activation energy and E'_a is the activation energy for the hopping conduction, which may have some frequency dependence.

Subtraction of the extrapolated d.c. conductivity gives the pure a.c. conductivity (σ_{ac}) from which the hopping activation energy can be estimated (table 6.1). The results show that the activation energies for hopping are small and decrease with frequency, as was also observed by *Sakai et al* for CuPc(6.31).

Although the different types of cells (sandwich, surface and compaction) show qualitatively similar behaviour, there are significant quantitative differences which are summarised in figure 6.16. Firstly at low frequencies where the observed conductivity approaches the d.c. conductivity^(6.34), the same sequence of conductivities is observed as was found by d.c.

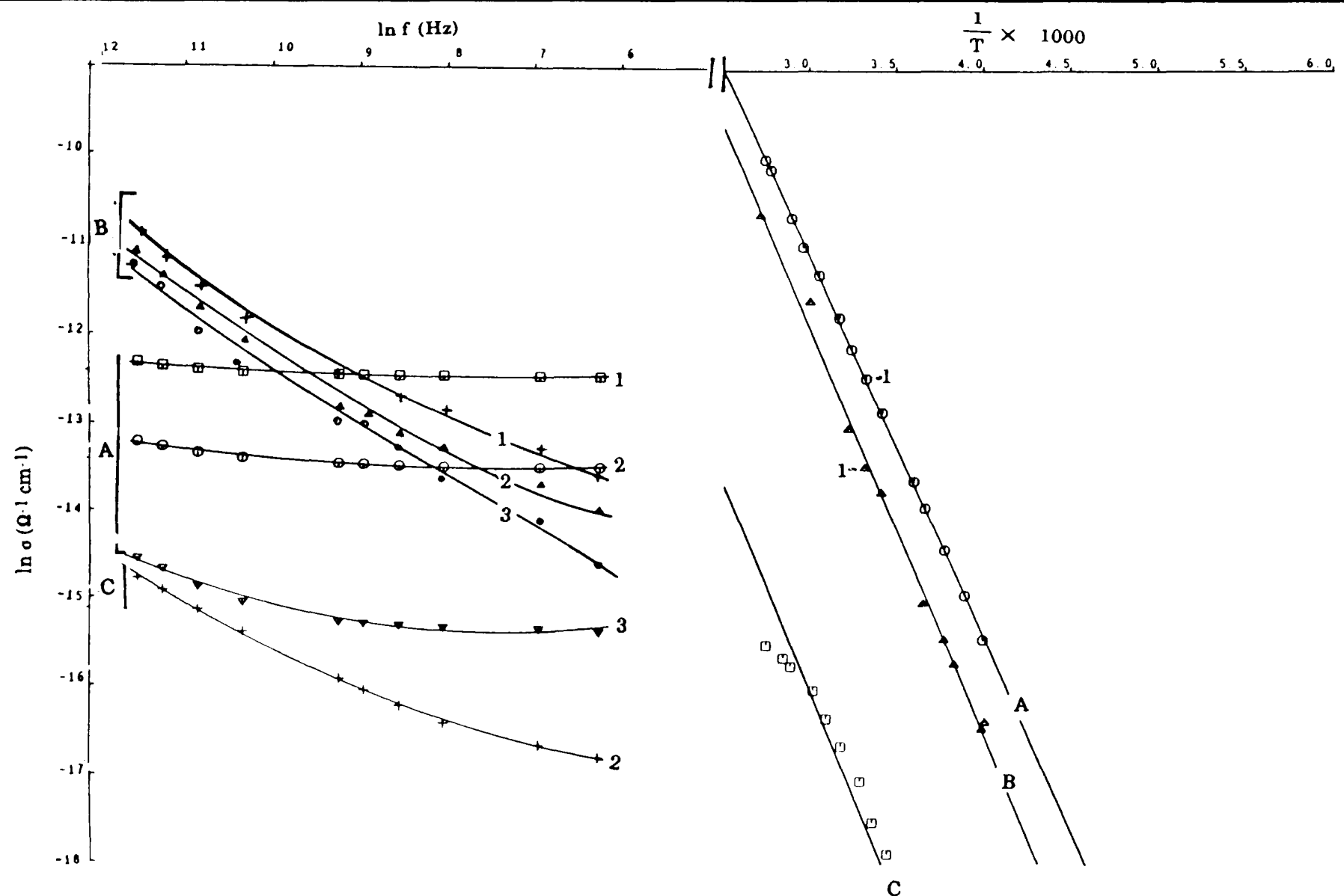


Figure 6.16: The a.c. and d.c. conductivities at different temperatures for AlPcF. (1 = 24 °C, 2 = 0 °C, 3 = -30 °C for compaction (A) and surface cell (B), and 4 = 0°C for sandwich cell (C)).

Compound	f KHz	Compaction		Surface cell		Sandwich cell	
		E'_a/eV	$\Delta E/eV$	E'_a/eV	$\Delta E/eV$	E'_a/eV	$\Delta E/eV$
AlPcF	0.5	0.15	0.69	0.10	0.78	0.08	0.86
	10	0.12		0.06		0.2	
	100	0.05		0.03		0.12	
GaPcF	0.5	0.12	0.94	0.10	1.10
	10	0.11				0.09	
	100	0.09				0.05	
Copoly.	0.5	0.13	0.84	0.10	0.86	0.12	0.98
	10	0.09		0.08		0.08	
	100	0.02		0.08		0.01	
Mixture	0.5	0.13	0.49	Table 6.1 The activation energy (E'_a) for hopping conduction at three different frequencies and the apparent band band gap (ΔE) for the band conduction for different compounds and cells.			
	10	0.11					
	100	0.06					

measurements,

$$\sigma_{compaction} > \sigma_{surface} > \sigma_{sandwich} \quad \dots\dots\dots 6.43$$

The agreement between results at low frequencies and those from d.c. suggests that the observed differences are not due to the build up of space charge, which tends to be a slower process.

As the frequency increases the sequence of conductivities changes to,

$$\sigma_{surface} > \sigma_{compaction} > \sigma_{sandwich} \quad \dots\dots\dots 6.44$$

which is clearly a consequence of a different contributions from the frequency dependent hopping conductivity^(6.18). Assuming the *Mott model*^(6.29), then this implies different densities of hopping states near the *Fermi level*. Using the *Mott and Davis formula* (equation 6.39) it is possible to estimate the density of hopping states near the *Fermi level* from values of the frequency dependent conductivity. Using data at 24 °C and 10⁵ Hz with α as the reciprocal of the interplanar spacing and V_{ph} equal to 10¹² Hz^(6.35,6.27), values of 8.9x 10¹⁹ eV⁻¹cm⁻³ and 1.8x10²⁰ eV⁻¹cm⁻³ are achieved for the compaction and surface cells respectively (table 6.2). This suggests a higher degree of disorder in the surface cell than in compaction.

The types of disorder measured by this experiment are those which give states in the band gap, particularly in the region of the *Fermi level*^(6.29).

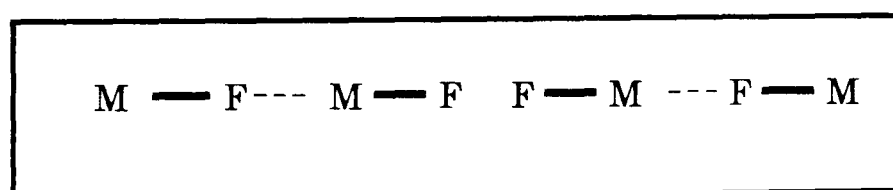
The compaction can be regarded as an array of randomly orientated crystallites compressed so as to give good electrical contact between them^(6.36,6.37). The crystallites are expected to be relatively highly ordered

Compound	Density of states ($N(E_f)$) eV ⁻¹ cm ⁻³		
	Surface cell	Compaction	Sandwich cell
AlPcF	1.81×10^{20}	8.89×10^{19}	1.8×10^{19}
Copolymer	1.37×10^{20}	4.34×10^{19}	4.65×10^{18}
GaPcF	-----	1.59×10^{19}	3.85×10^{18}
Mixture	-----	6.87×10^{19}	-----

Table 6.2: Density of states for three sorts of cells at 24 °C and 5.0 KHz

with a relatively low trap density. In contrast the evaporated films have been shown, by transmission electron microscopy (6.38), to be primarily amorphous, with small and widely separated crystalline regions. Thus the electrical properties are expected to be dominated by the amorphous region with a higher trap density.

There is a marked difference in the frequency dependent component of conductivity between that of the surface cell and that of the sandwich cell. Since the two films are deposited under similar conditions it must be assumed that the defect concentrations are similar. It therefore must be concluded that the distribution of hopping sites is more favourable for hopping when the field is along the surface (Surface cell) than when the field is normal to the surface (Sandwich cell). Since the polymer chains lie along the surface we must assume that the hopping sites are associated with minor defects within the chain, e.g., slight rotations of the ring about the Al-F-Al axis, or possibly fluorine atoms facing each other as is shown below,



b) Capacitance Measurements:

Figure 6.17 shows the variation of capacitance as a function of frequency for sandwich cells of AlPcF at different temperatures. It shows that capacitance is highly temperature dependent at low frequency but tends to a common value at high frequency.

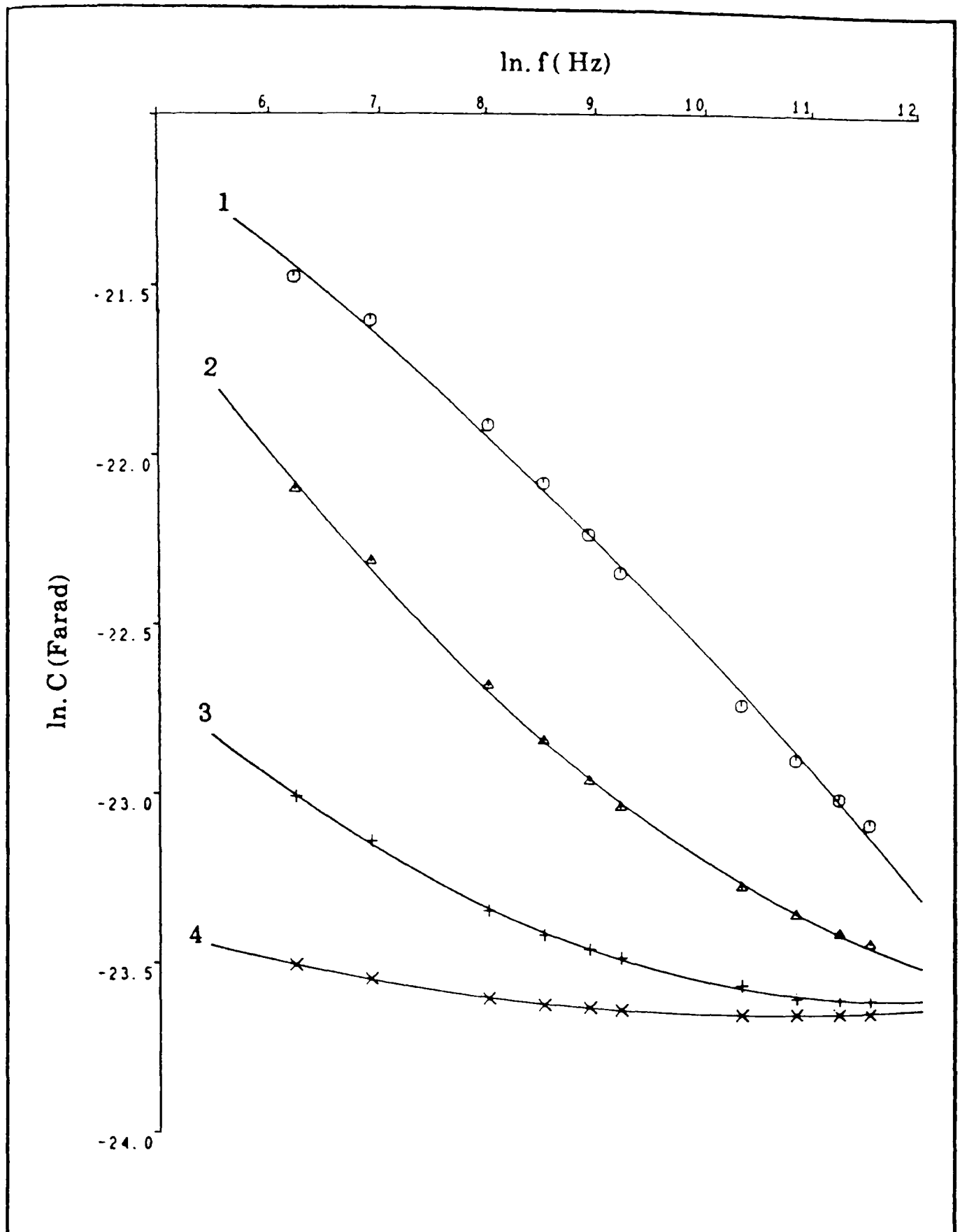


Figure 6.17: The variation of capacitance as a function of frequency at different temperatures for sandwich cell of AlPcF. 1(0°C), 2(-30°C), 3(-60°C), 4(-90°C).

Figure 6.18 shows the variation of the frequency dependent component of conductivity with frequency for the sandwich cell of AlPcF at different temperatures. According to equation 6.33 the slopes of the straight lines obtained give the value of n . Now if equation 6.33 is obeyed, the *Kramers-Kronig relation* may be used to obtain the frequency dependence of the capacitance^(6.16, 6.28) (equation 6.38). From figure 6.17 C_{∞} is taken at 10^5 Hz as 6.2×10^{-11} F. Allowing for the dimensions of the samples this corresponds to a *relative permittivity* of 7.0, which is in agreement with the *relative permittivity* of phthalocyanines, e.g. the relative permittivity of compacted disc of impure copper phthalocyanine is about 5.5 at 10^5 Hz (6.39), taking into account the error due to thickness measurements, which is about ± 2 .

From figure 6.19 it can be seen that equation 6.38 is closely obeyed. Furthermore, the values of n (table 6.3), obtained from the slopes of figures 6.18 and 6.19, are in good agreement, particularly for lower temperatures. Thus the materials show the expected consistency between conductivity and capacitance behaviour.

The capacitance of the compacted discs and surface cells were very small and nearly equal to the capacitance of the empty cell. So no conclusion could be drawn.

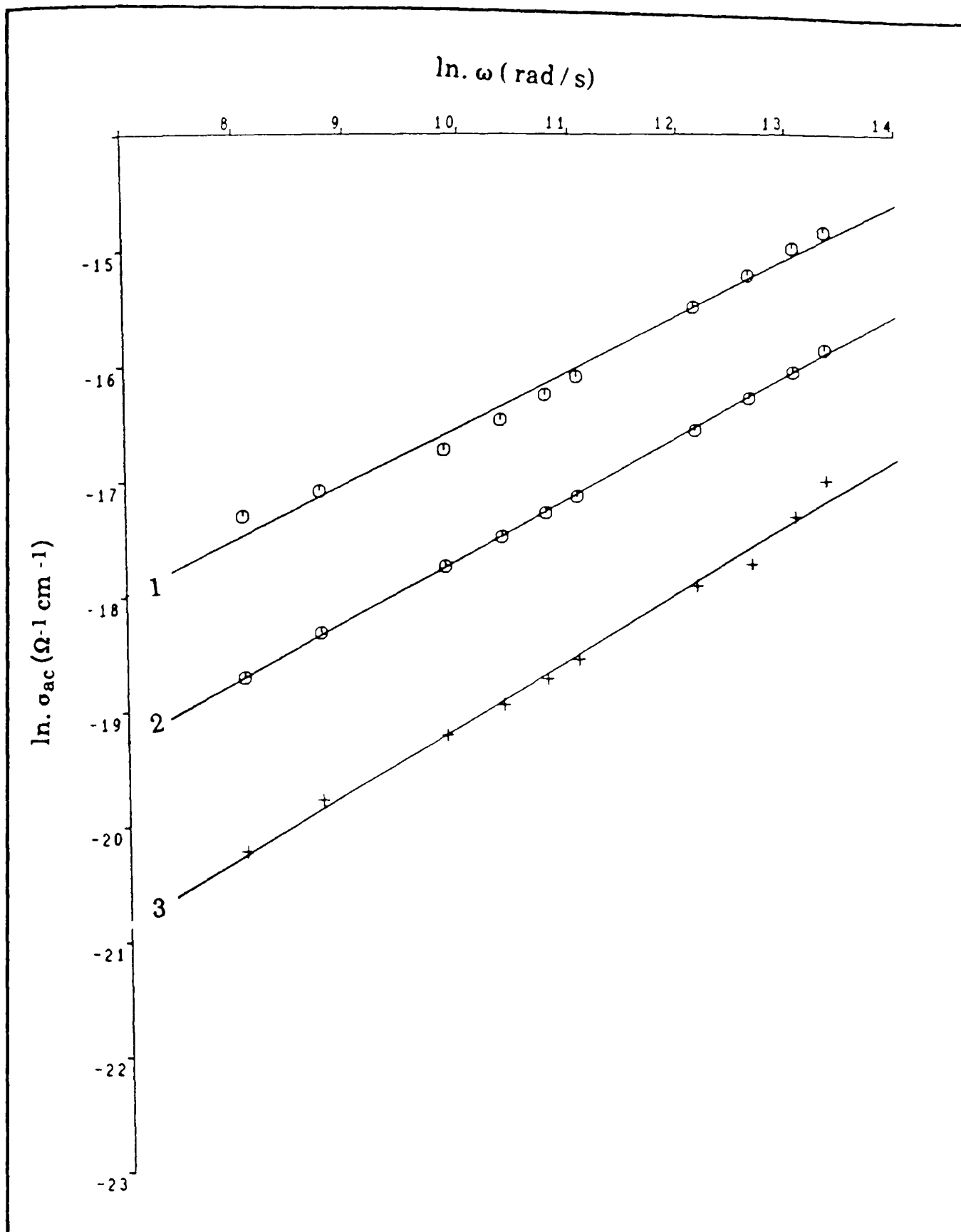


Figure 6.18: The variation of frequency dependend component of the conductivity at different temperatures for sandwich cell of AlPcF. 1(0°C), 2(-30°C), 3(-60°C).

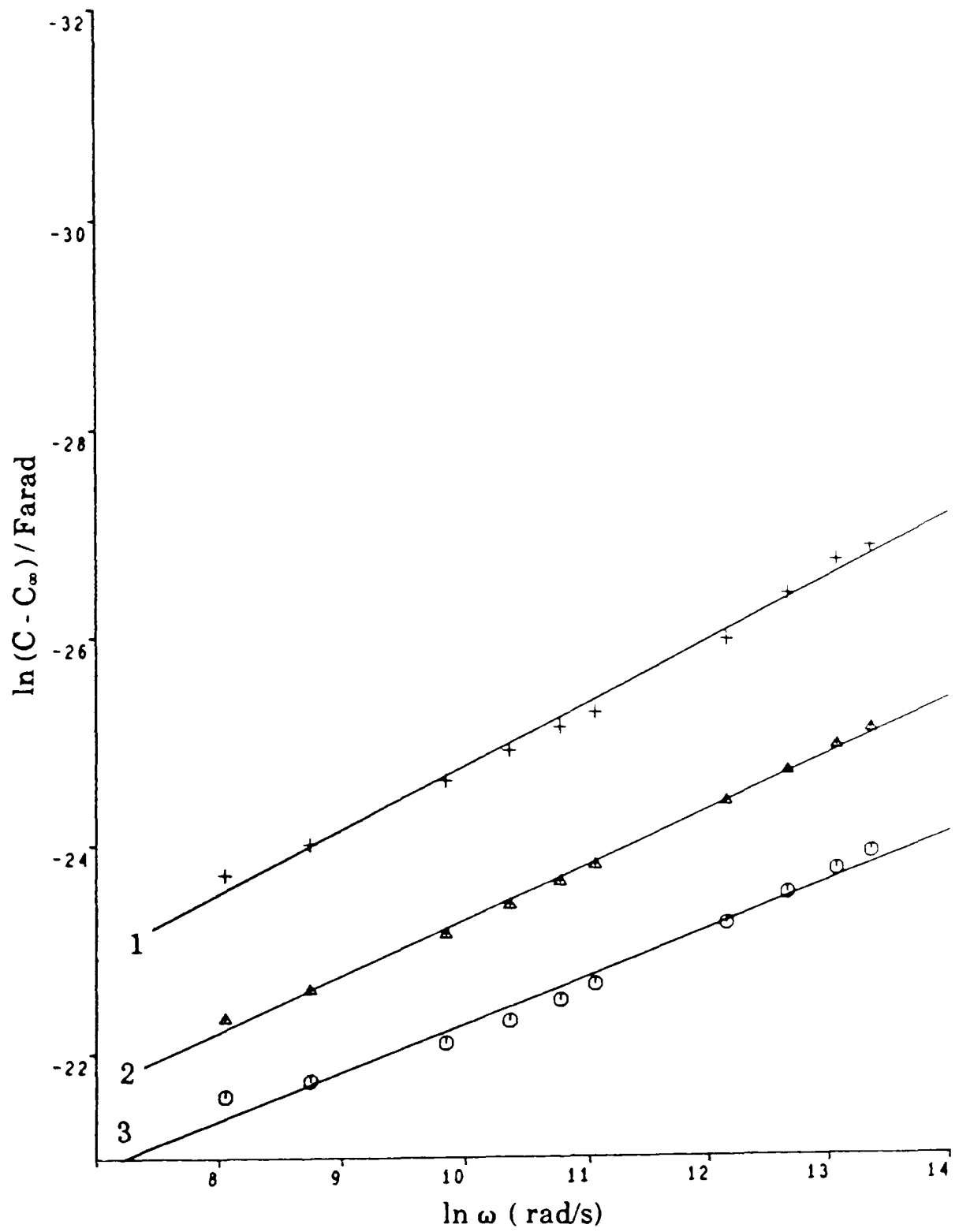


Figure 6.19: The variation of capacitance with angular frequency at different temperatures for sandwich cell of AlPcF. 1(-60 °C), 2(-30 °C), 3(0 °C).

Compound	Temperature °C	n from equation 6.33	n from equation 6.38
AlPcF	0	0.48	0.50
	-30	0.52	0.51
	-60	0.57	0.50
GaPcF	27	0.71	0.57
	0	0.77	0.62
	-33	0.83	0.74
Copolymer	26	0.88	0.60
	0	0.90	0.64
	-35	0.92	0.76

Table 6.3 Values of n for the sandwich cell

6.2.2) GaPcF:

a) Conductivity measurements:

Figures 6.20 and 6.21 show the variation of the measured a.c. conductivity (σ_T) for compaction and sandwich cell with frequency. Compared to the AlPcF cells, they are more frequency dependent which suggests that a hopping mechanism is dominant in both types of cells over the entire temperature range studied^(6.5), as a consequence of the fact that the d.c. conductivity is so much lower.

Figure 6.22 and 6.23 show the plots of the natural logarithm of the measured a.c. and d.c. conductivities against reciprocal temperature for the two types of cell, as an alternative to figures 6.20 and 6.21. Table 6.1 shows the activation energies for σ_{ac} AlPcF and GaPcF at three different frequencies. It shows that the temperature dependent hopping conduction is small compared to the apparent activation energy for d.c. conductivity and decreases with frequency in both types of cells for both materials.

The difference between figure 6.13 and 6.22 is that the compaction of AlPcF shows more temperature dependence than the GaPcF compacted disc at low frequencies and this dependence increases with temperature.

The sandwich cells for AlPcF and GaPcF as shown in figure 6.15 and 6.23 show nearly similar behaviour.

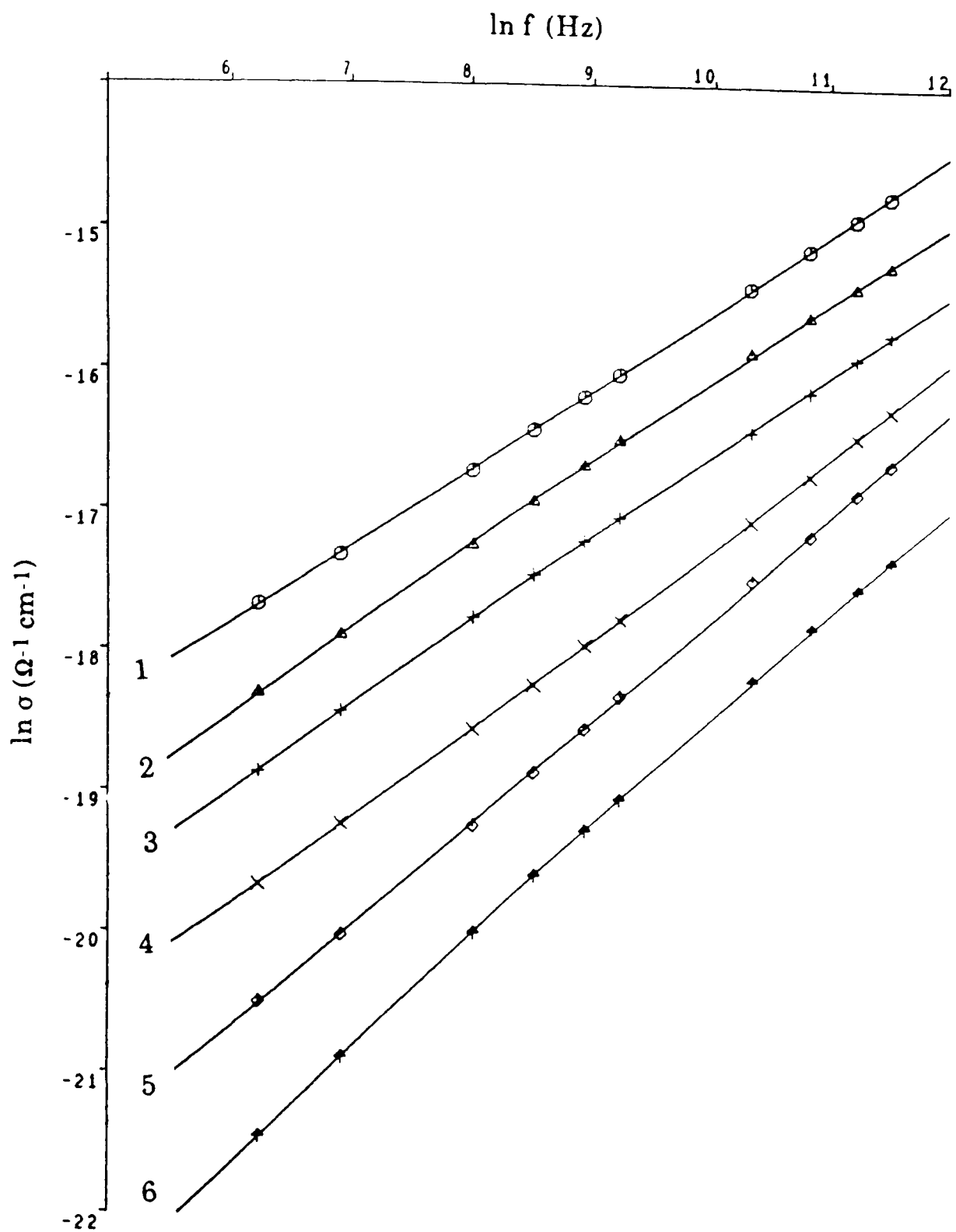


Figure 6.20: The frequency dependence of a.c. conductivity at a series of temperatures for compaction of GaPcF. 1(75), 2(500°C), 3(250°C), 4(0°C), 5(-60°C), 6(-90°C).

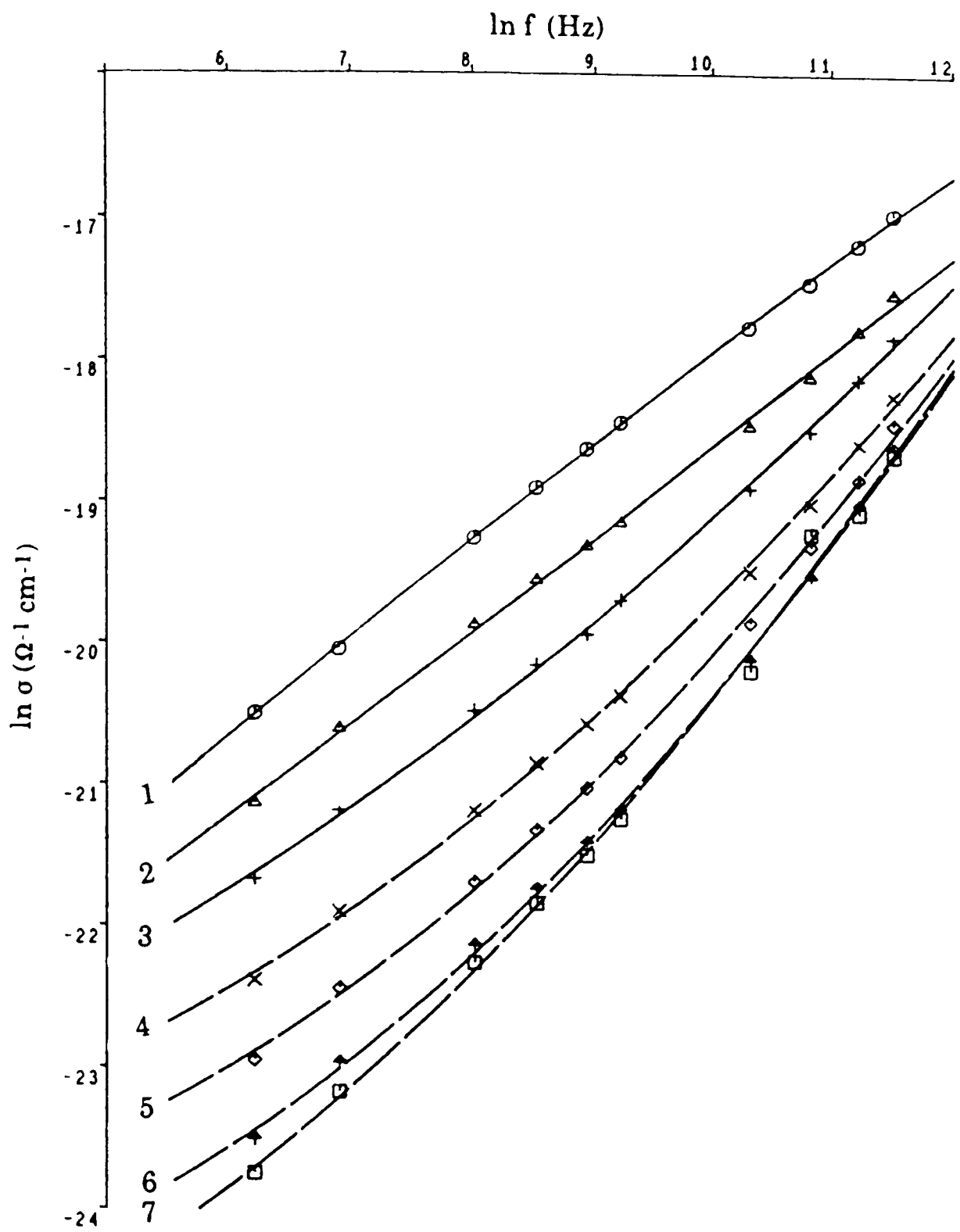


Figure 6.21: The frequency dependence of a.c. conductivity at a series of temperatures for sandwich cell of GaPcF. 1(90), 2(50°C), 3(25°C), 4(0°C), 5(-35°C), 6(-90°C).

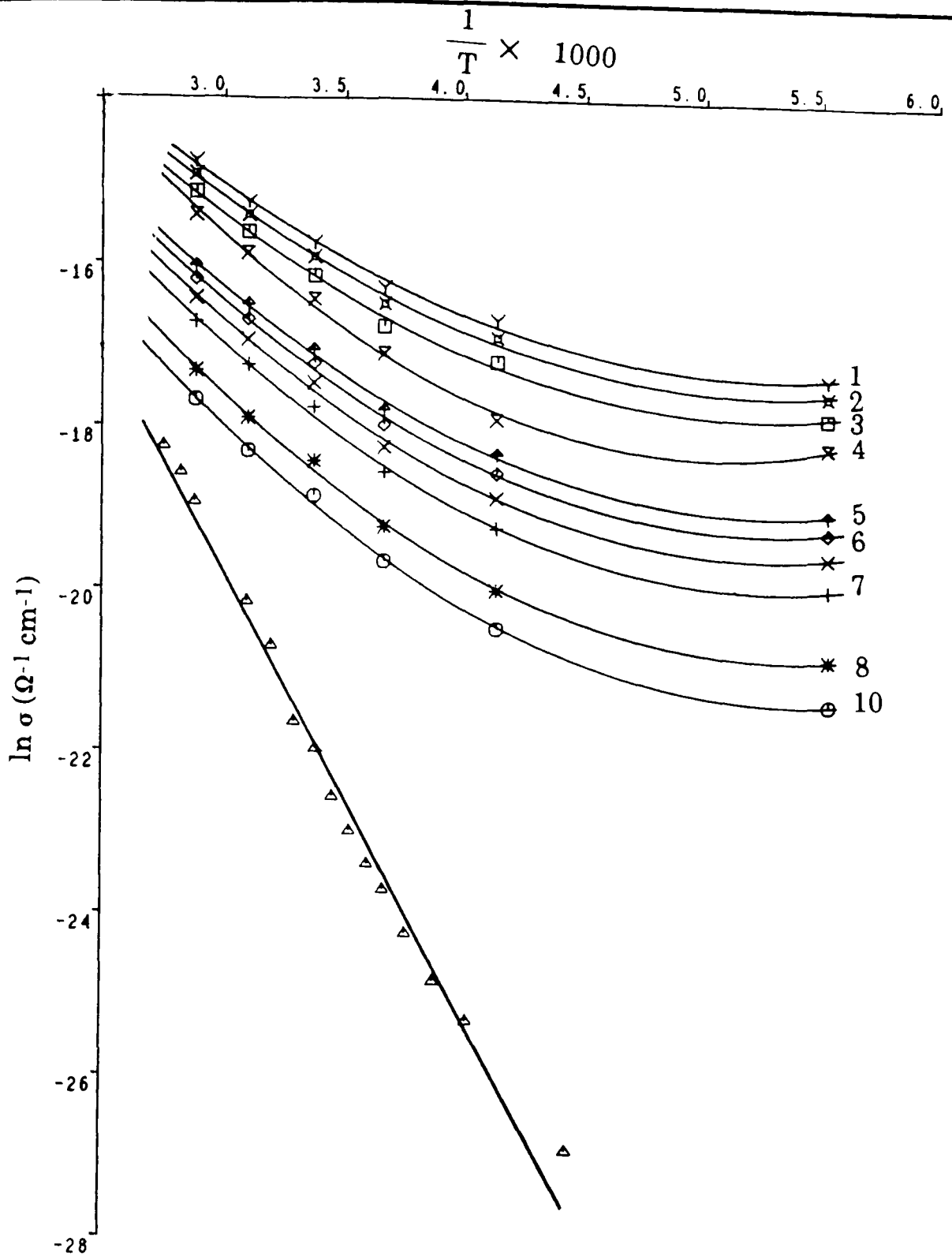


Figure 6.22: The d.c. conductivity and the temperature dependence of a.c. conductivity at a series of frequencies for compaction of GaPcF. 1(100Hz), 2(75Hz), 3(50Hz), 4(30Hz), 5(10Hz), 6(7.5Hz), 7(5Hz), 8(3Hz), 9(1Hz), 10(0.5Hz).

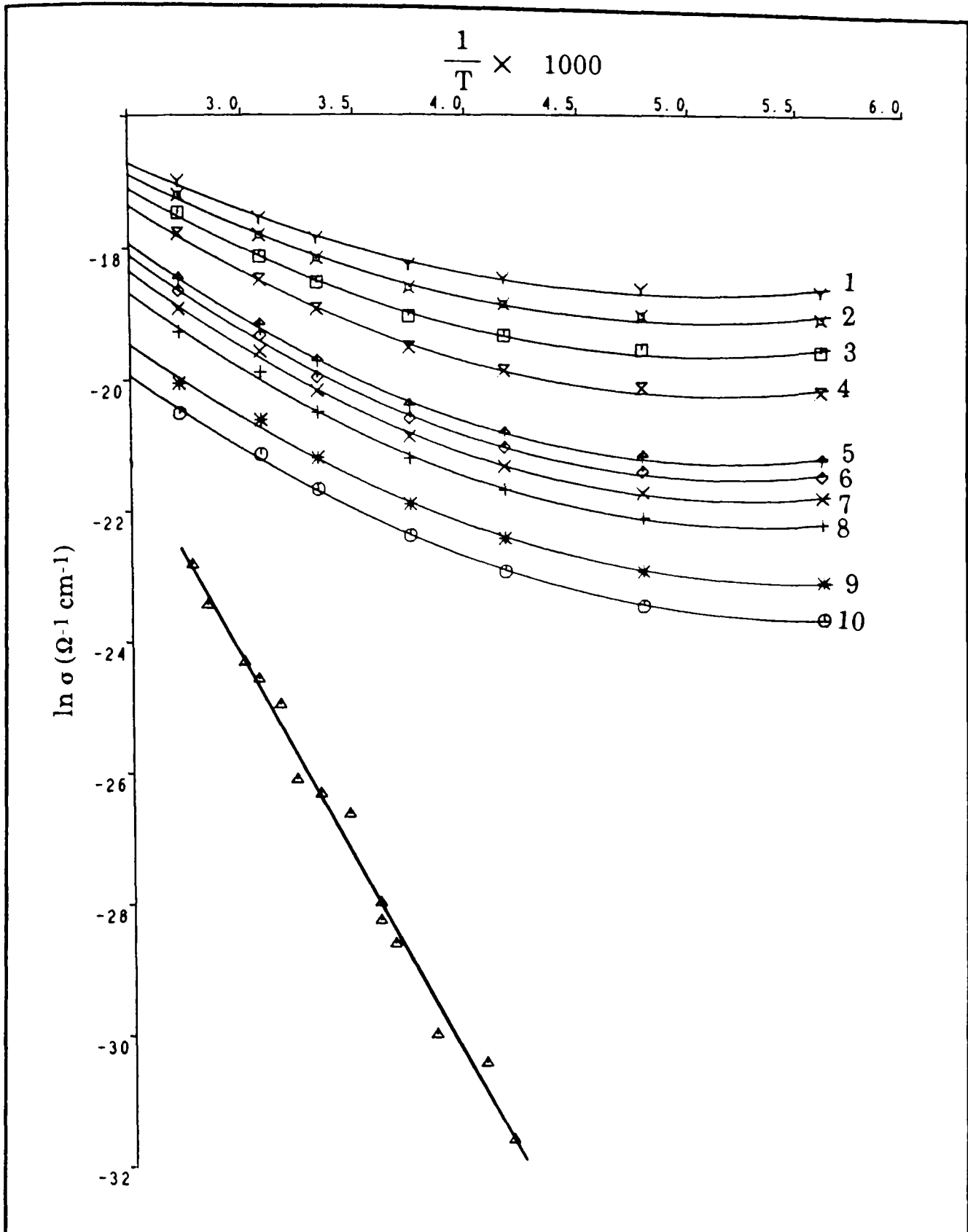


Figure 6.23: The d.c. conductivity and the temperature dependence of a.c. conductivity at a series of frequencies for sandwich cell of GaPcF. 1(100Hz), 2(75Hz), 3(50Hz), 4(30Hz), 5(10Hz), 6(7.5Hz), 7(5Hz), 8(3Hz), 9(1Hz), 10(0.5Hz).

b) Capacitance Measurements:

Capacitance measurements on GaPcF sandwich films show a similar behaviour to AlPcF films. The capacitance tends to a common value at high frequencies as shown in figure 6.24.

The values of n (table 6.3) were obtained from figure 6.25 using equation 6.33. The *Kramers-Kronig relation* was used to obtain the frequency dependence of the capacitance taking C_{∞} at 10^5 Hz obtained from figure 6.24 as 2.1×10^{-9} F, which corresponds to a *relative permittivity* of 9.5 which is in agreement with the *relative permittivity* of phthalocyanines (6.39).

From figure 6.26 it can be seen that equation 6.38 is closely obeyed, and from table 6.3, the values of n , obtained from the slopes of figure 6.25 and 6.26, are in good agreement which lead to the conclusion that GaPcF shows the expected consistency between conductivity and capacitance.

6.2.3) Copolymer:

a) Conductivity measurements:

Figures 6.27, 6.28 and 6.29 show the variation in the measured a.c. conductivity with frequency at different temperatures for the three kinds of cells (compaction, surface and sandwich cells). It shows that the frequency dependence increases as the temperature is reduced, which is similar behaviour to that observed for AlPcF and GaPcF.

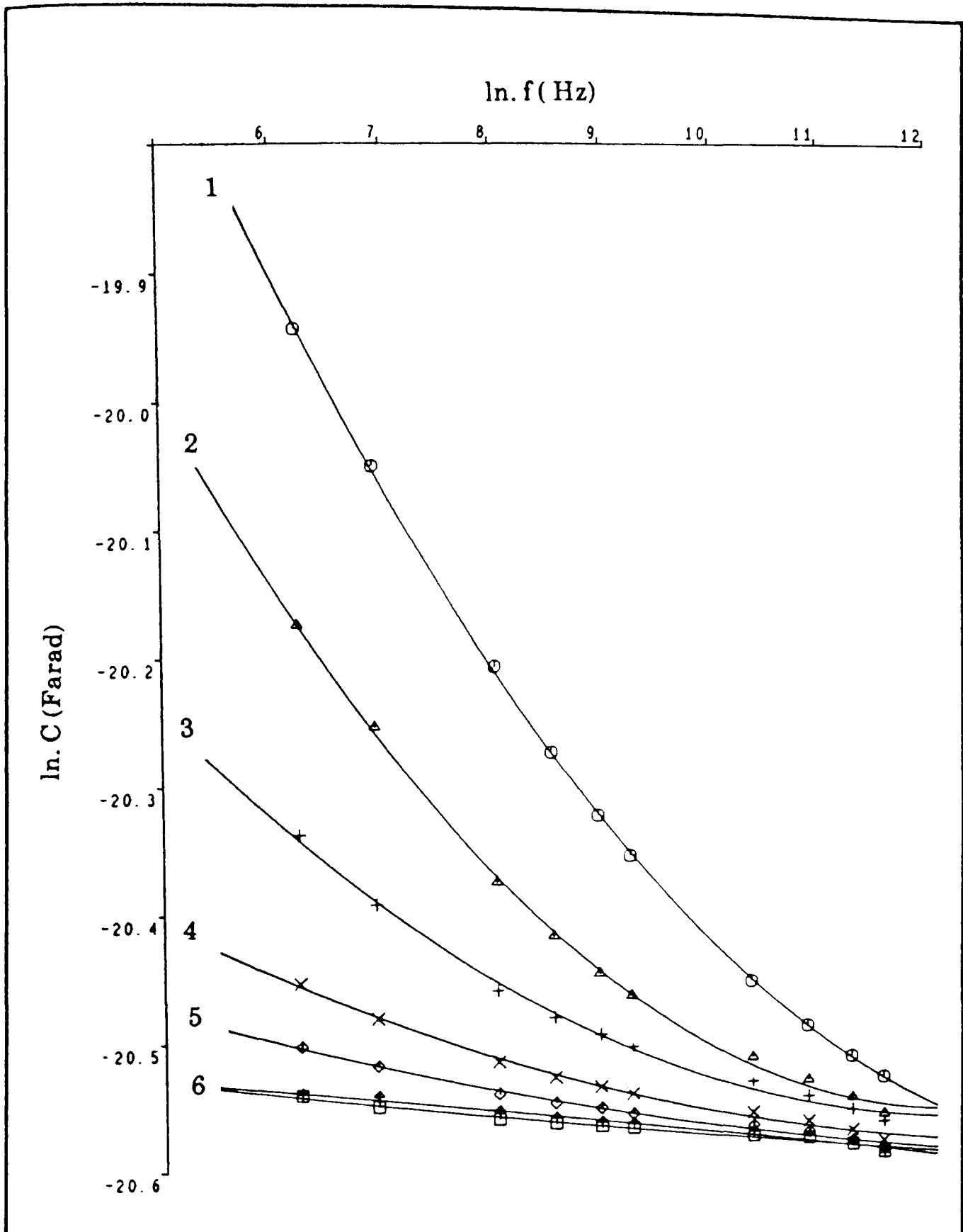


Figure 6.24: The variation of capacitance as a function of frequency at different temperatures for sandwich cell of GaPcF. 1(90°C), 2(50°C), 3(25°C), 4(0°C), 5(-9°C), 6(-90°C).

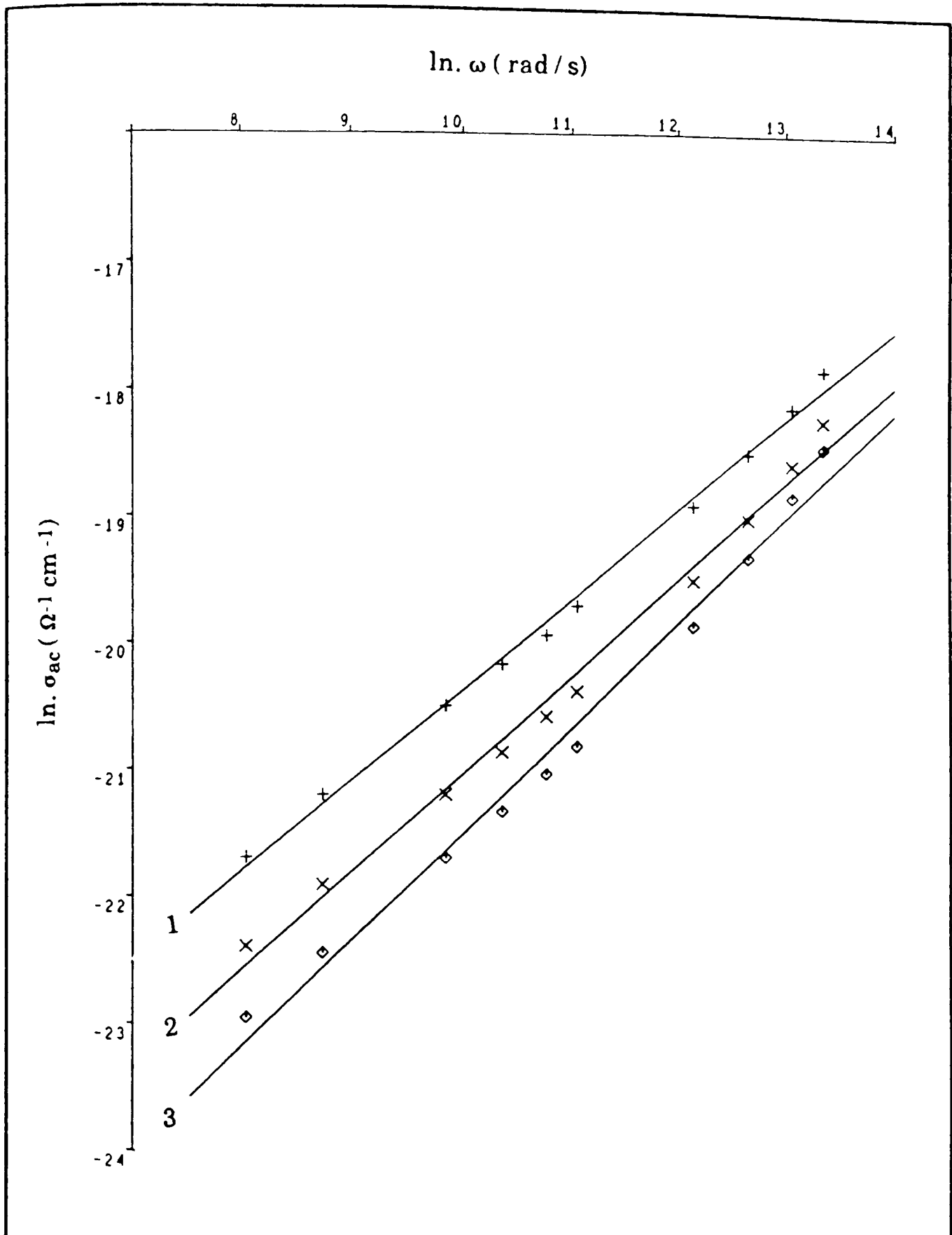


Figure 6.25: The variation of frequency dependent component of the conductivity at different temperatures for sandwich cell of GaPcF. 1(27°C), 2(0°C), 3(-33°C).

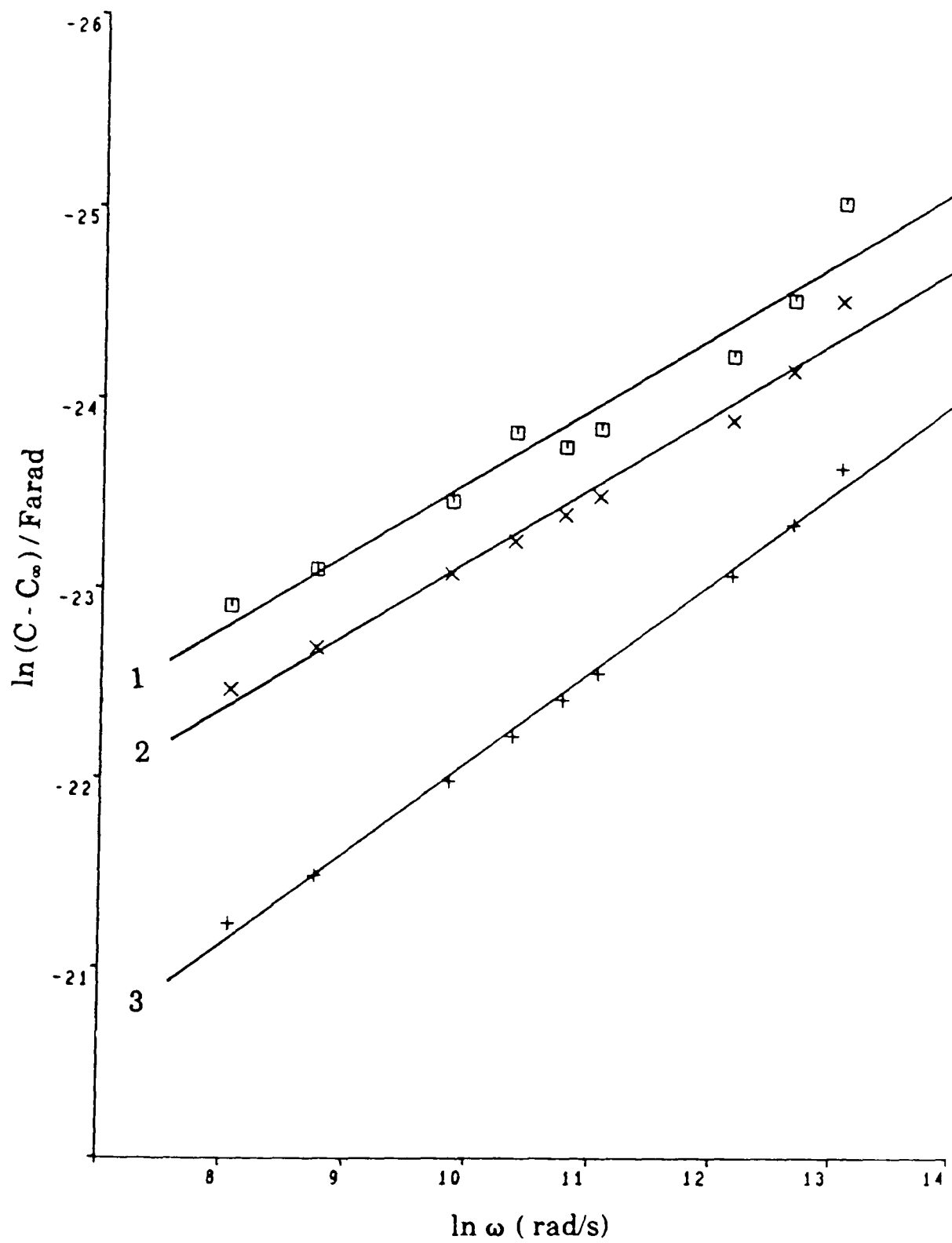


Figure 6.26: The variation of capacitance with angular frequency at different temperatures for sandwich cell of GaPcF. 1(-33 °C), 2(0 °C), 3(27 °C).

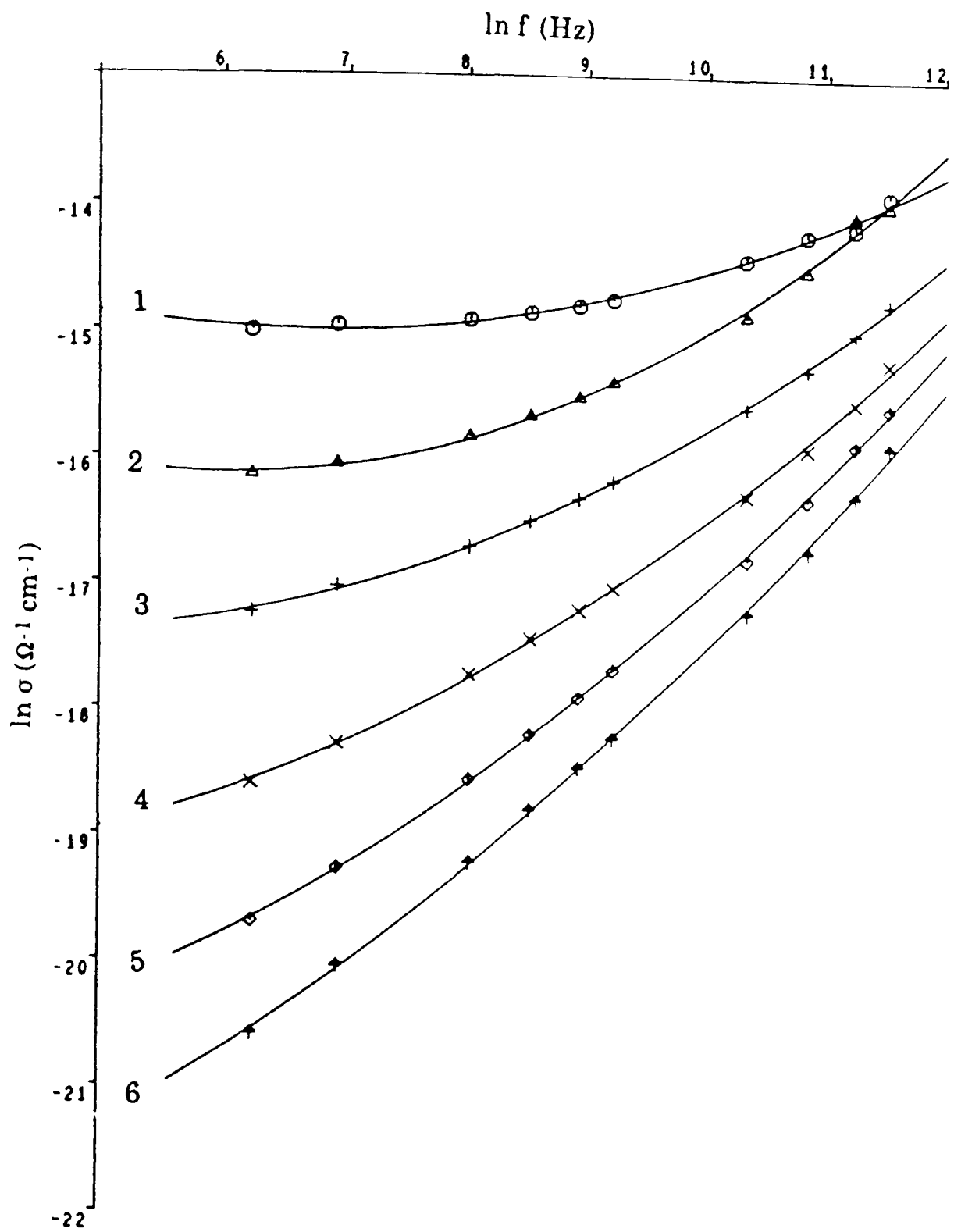


Figure 6.27: The frequency dependence of a.c. conductivity at a series of temperatures on compaction of the copolymer. 1(50), 2(250°C), 3(0°C), 4(-30°C), 5(-60°C), 6(-90°C).

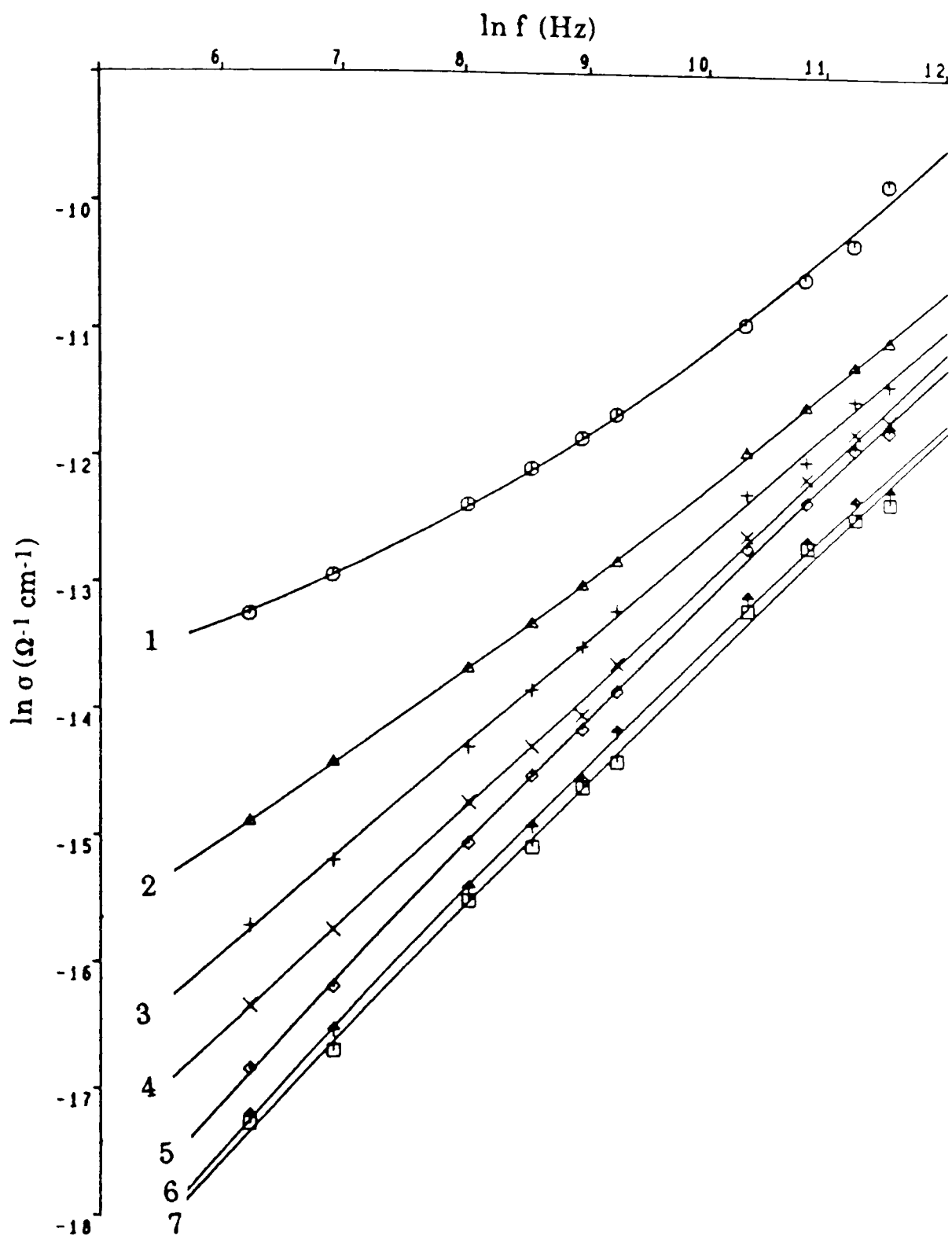


Figure 6.28: The frequency dependence of a.c. conductivity at a series of temperatures on surface cell of the copolymer. 1(90), 2(500°C), 3(240°C), 4(0°C), 5(-35°C), 6(-60°C), 7(-90°C).

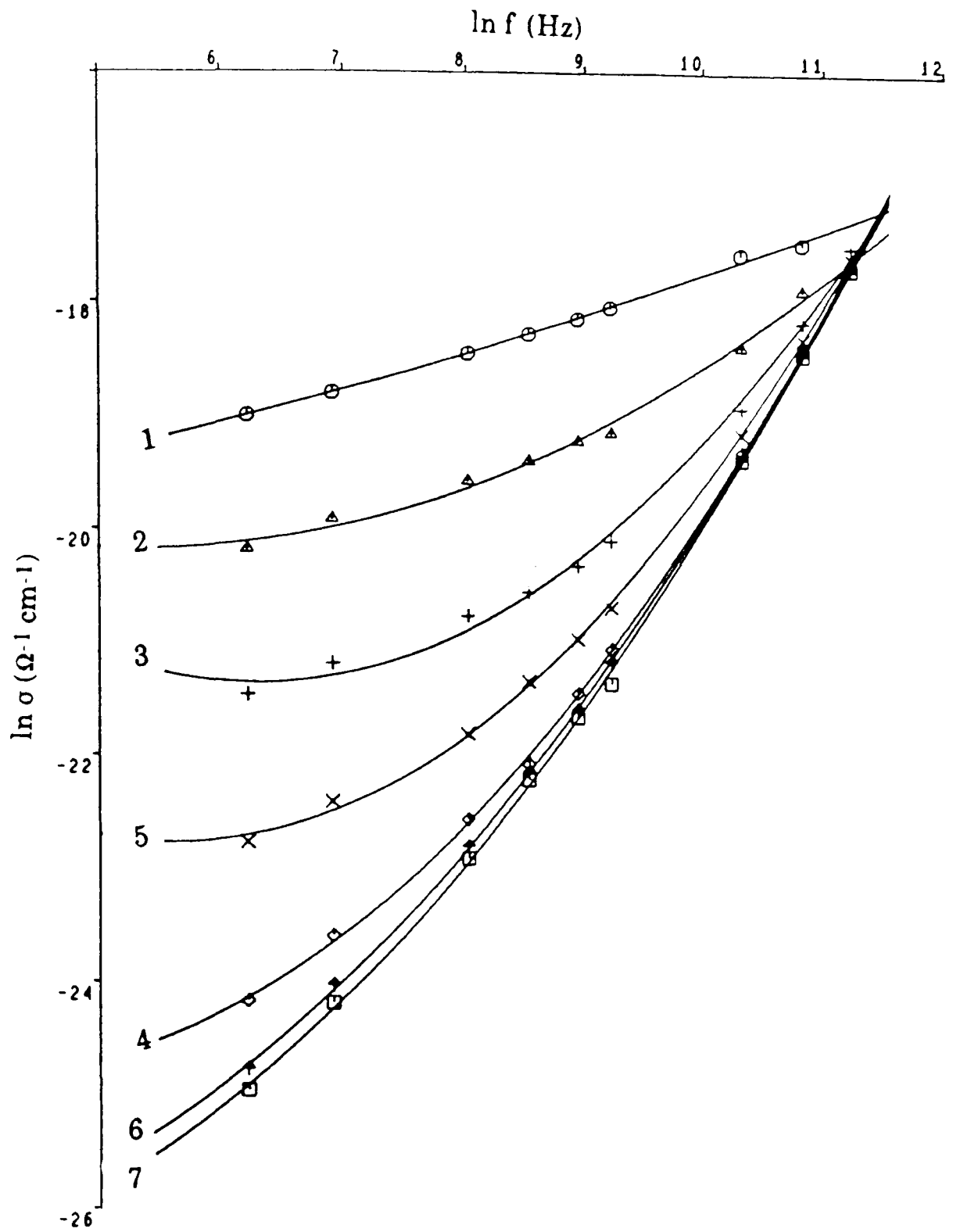


Figure 6.29: The frequency dependence of a.c. conductivity at a series of temperatures on sandwich cell of the copolymer. 1(90), 2(50°C), 3(24°C), 4(0°C), 5(-30°C), 6(-60°C), 7(-90°C).

Figures 6.30-32 show the variation in the measured a.c. and d.c. conductivities for the three kinds of cells as plotted against reciprocal temperature. They show a similar general behaviour. The compacted disc of the copolymer (figure 6.30) shows a greater frequency dependence than AlPcF at high temperature (24 °C and more), a case which is similar to the GaPcF compacted disc. The surface and sandwich cells for the copolymer (figure 6.31 and 6.32) show a general similarity in the frequency and temperature dependency to that of the AlPcF and GaPcF cells (figures 6.14, 6.15 and 6.23). Table 6.3 shows that activation energies for the hopping conduction are small and decrease with frequency for the three types of cells as was observed in AlPcF and GaPcF cells.

Figure 6.33 and 6.16 show the generally similar behaviour of the copolymer and AlPcF. They show that at low frequencies where the measured conductivity approaches the d.c. conductivity, the sequence of the conductivities tend to be as were found by d.c. measurement (equation 6.43). As the frequency increases the sequence changes as shown in equation 6.44, a case which is similar to that found for AlPcF samples. This can also be explained by the *Mott and Davis model*. The estimated density of states near the *Fermi level*, assuming the *Mott and Davis model* (6.29), and using data at 24 °C and 10^5 Hz, is summarised in table 6.1, which suggests a higher degree of disorder in the surface cell than in compacted disc and sandwich cells. The explanation for this behaviour is the same as that proposed for AlPcF.

b) Capacitance Measurements:

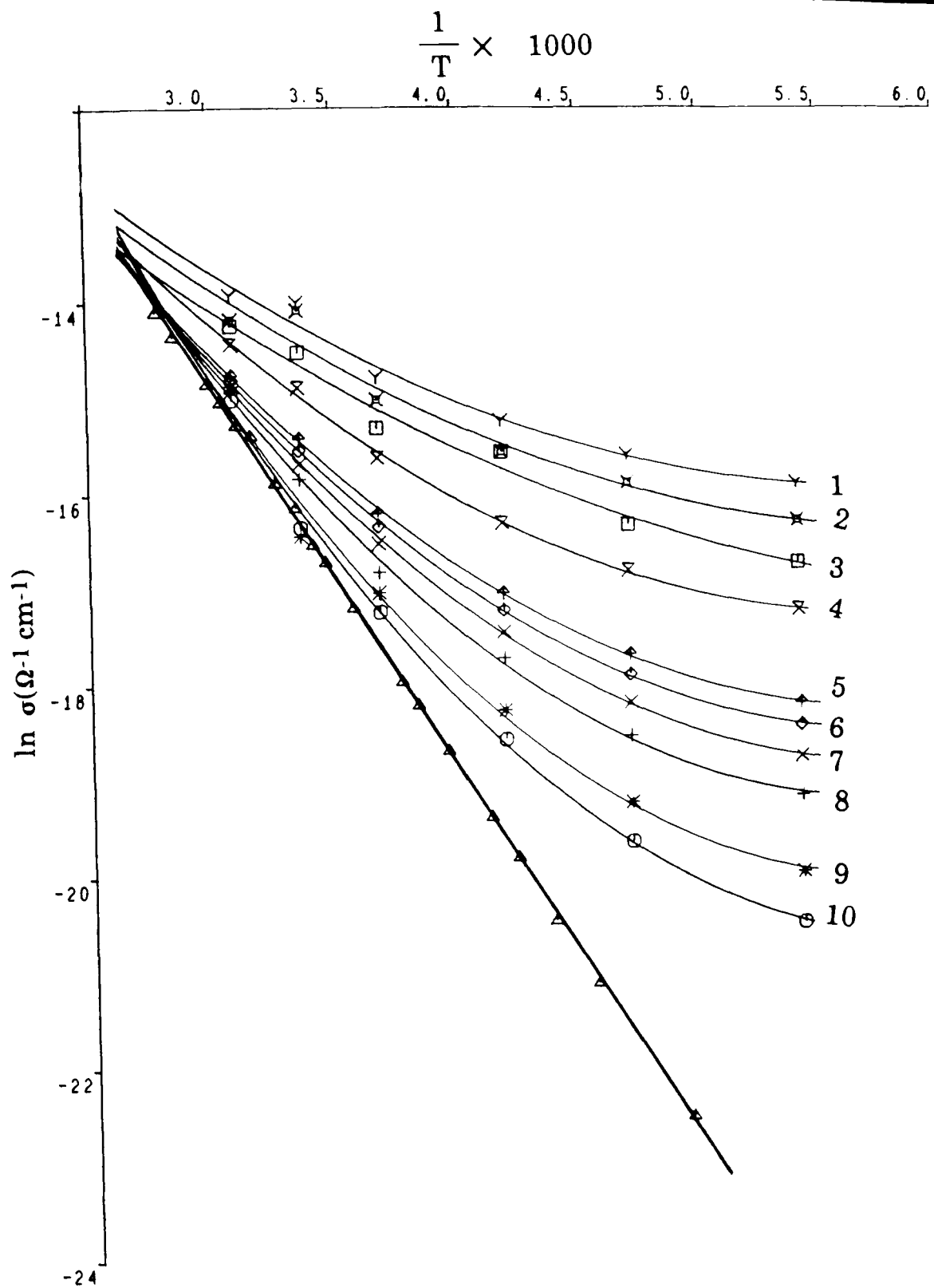


Figure 6.30: The d.c. conductivity and the temperature dependence of a.c. conductivity at a series of frequencies for compaction of the copolymer. 1(100Hz), 2(75Hz), 3(50Hz), 4(30Hz), 5(10Hz), 6(7.5Hz), 7(5Hz), 8(3Hz), 9(1Hz), 10(0.5Hz).

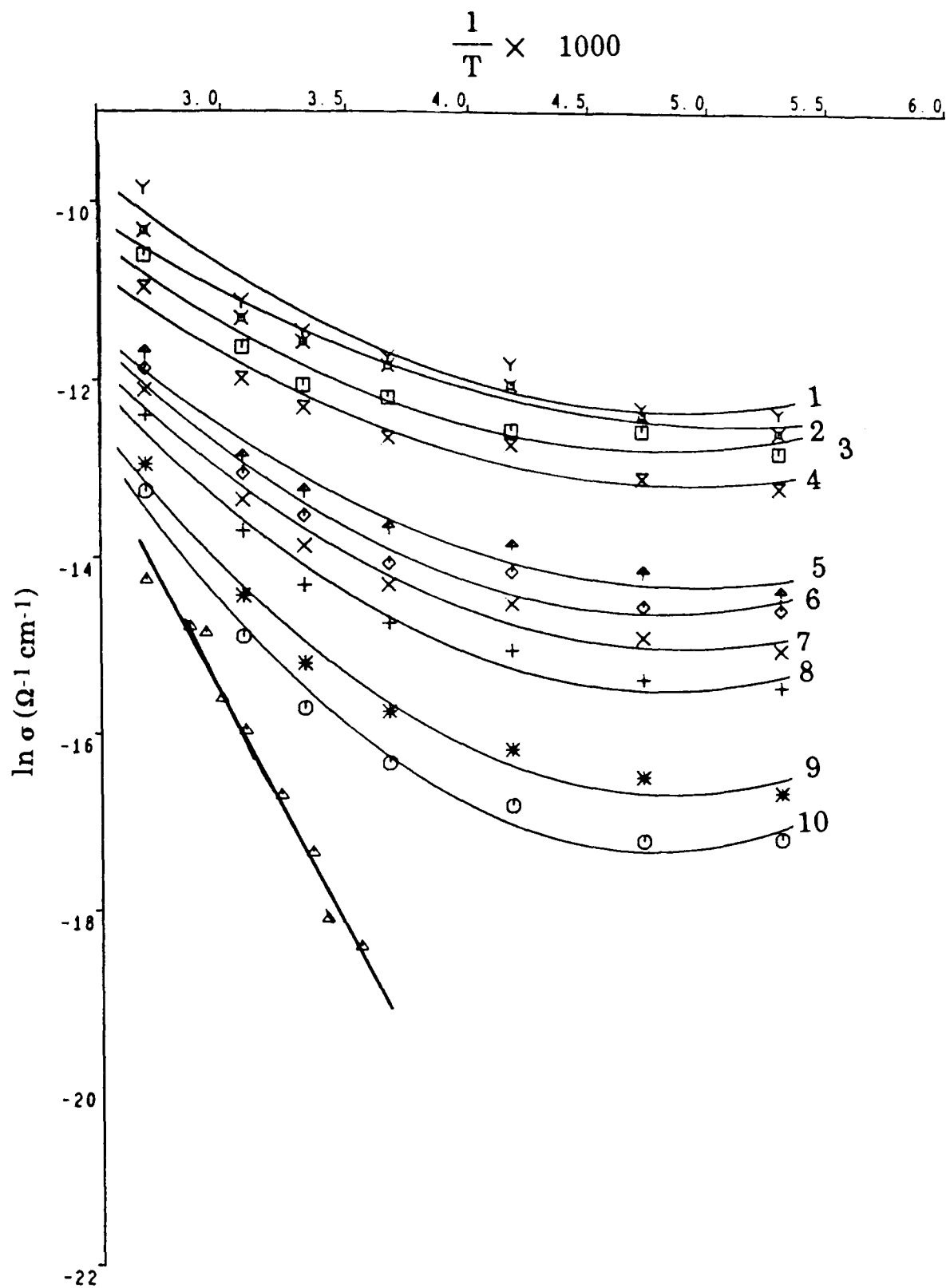


Figure 6.31: The d.c. conductivity and the temperature dependence of a.c. conductivity at a series of frequencies for surface cell of the copolymer. 1(100Hz), 2(75Hz), 3(50Hz), 4(30Hz), 5(10Hz), 6(7.5Hz), 7(5Hz), 8(3Hz), 9(1Hz), 10(0.5Hz).

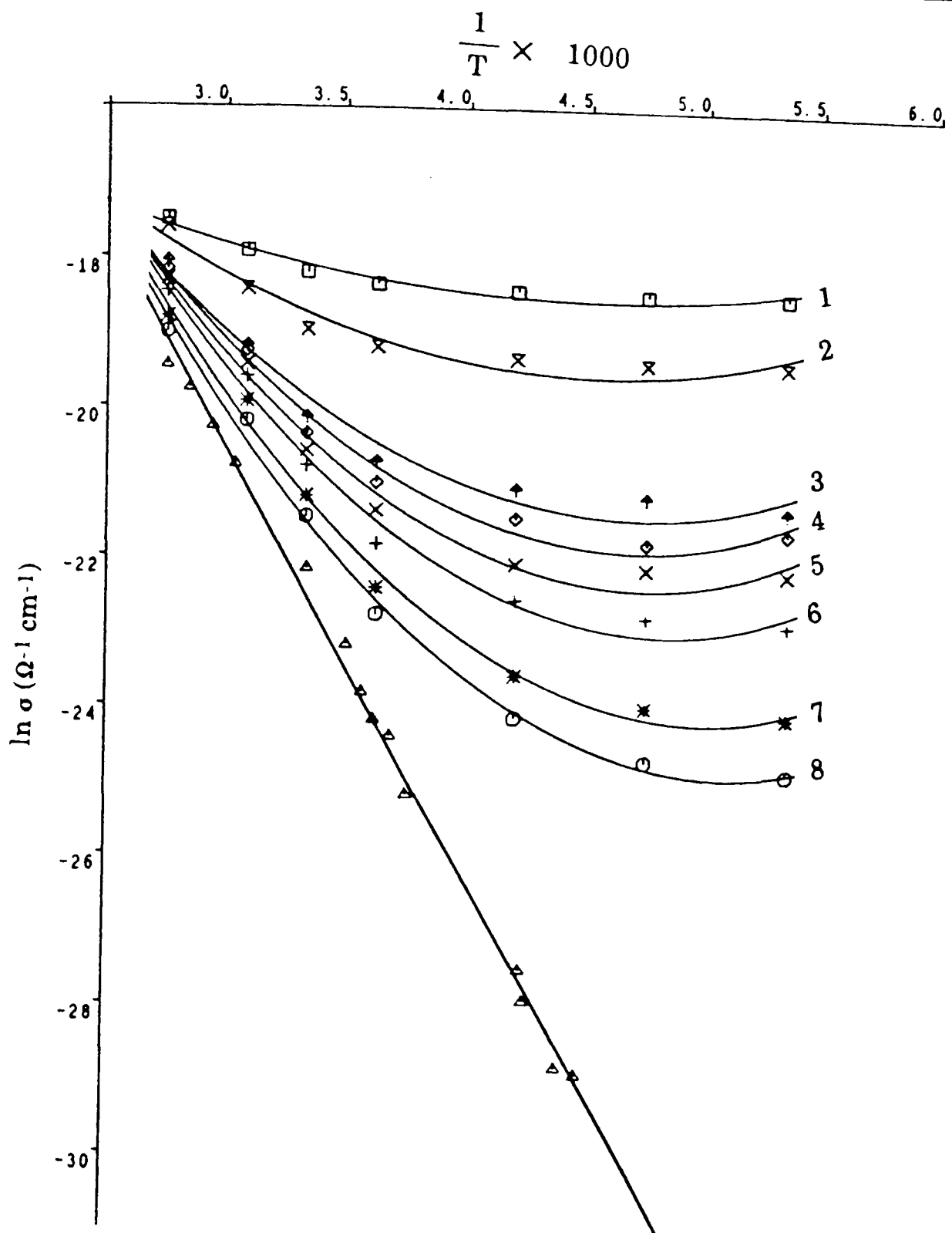


Figure 6.32: The d.c. conductivity and the temperature dependence of a.c. conductivity at a series of frequencies for sandwich cell of the copolymer. 1(50Hz), 2(30Hz), 3(10Hz), 4(7.5Hz), 5(5Hz), 6(3Hz), 7(1Hz), 8(0.5Hz).

The capacitance behaviour of the copolymer is qualitatively similar to that of the separate compounds. Figure 6.34 shows that the capacitance tends to a common value at high frequencies.

Using equation 6.33 the values of n were calculated from figure 6.35. The frequency dependence of the capacitance was calculated using the *Kramers-Kronig relation*, taking C_{∞} as 1.2×10^{-9} F at 10^5 Hz, which corresponds to *relative permittivity* of 5.5. From figure 6.36 it can be concluded that equation 6.38 is closely obeyed, and that the values of n obtained from the slopes of figures 6.35 and 6.36 are in a good agreement. Thus the material shows a consistency between conductivity and capacitance.

6.2.4) The Mixture:

Figure 6.37 shows the variation of measured a.c. conductivity with frequency and temperature for a compacted disc of a mixture of AlPcF and GaPcF (1:1 mole ratio) which shows, qualitatively similar behaviour to the AlPcF compacted disc. It shows little frequency dependence at high temperature. The dependency decreases as the temperature decreases. This can be presented alternatively in figure 6.38 which shows the variation of the measured a.c. and d.c. conductivities with inverse temperature at different frequencies. This figure shows that the mixture exhibits a frequency independent behaviour which is in agreement with the conduction. At lower temperatures it shows more frequency dependence due to the hopping mechanism. The activation energies for hopping conduction shown in table 6.1 suggest that the frequency dependent hopping conductivity is small and decreases with frequency, a case which is similar to the previous samples, AlPcF, GaPcF, and the copolymer.

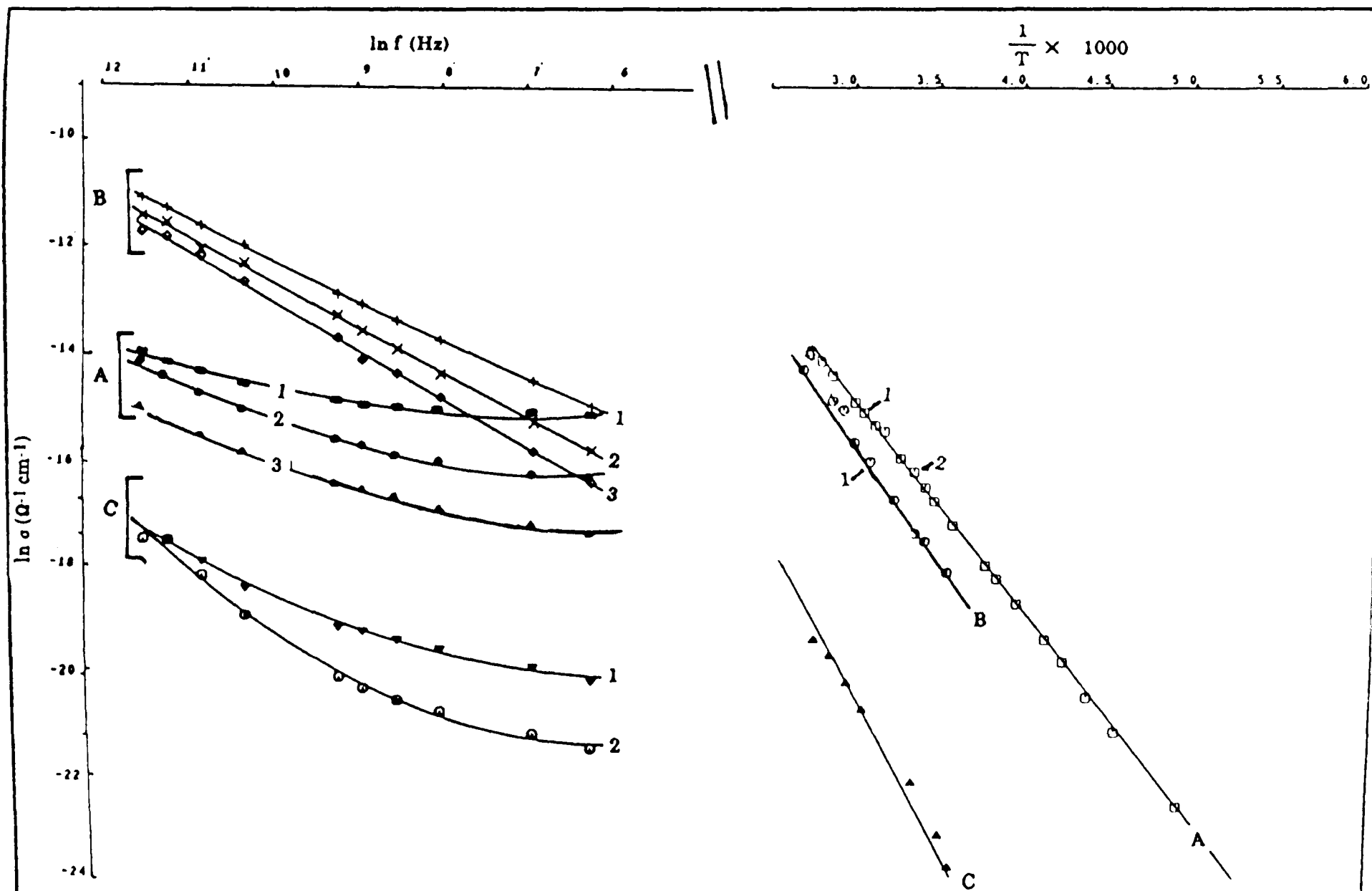


Figure 6.33: The a.c. and d.c. conductivities at different temperatures for the copolymer. (1 = 50 °C, 2 = 25 °C, 3 = 0 °C for compaction (A) and surface cell (B), and 4 = 0°C for sandwich cell (C)).

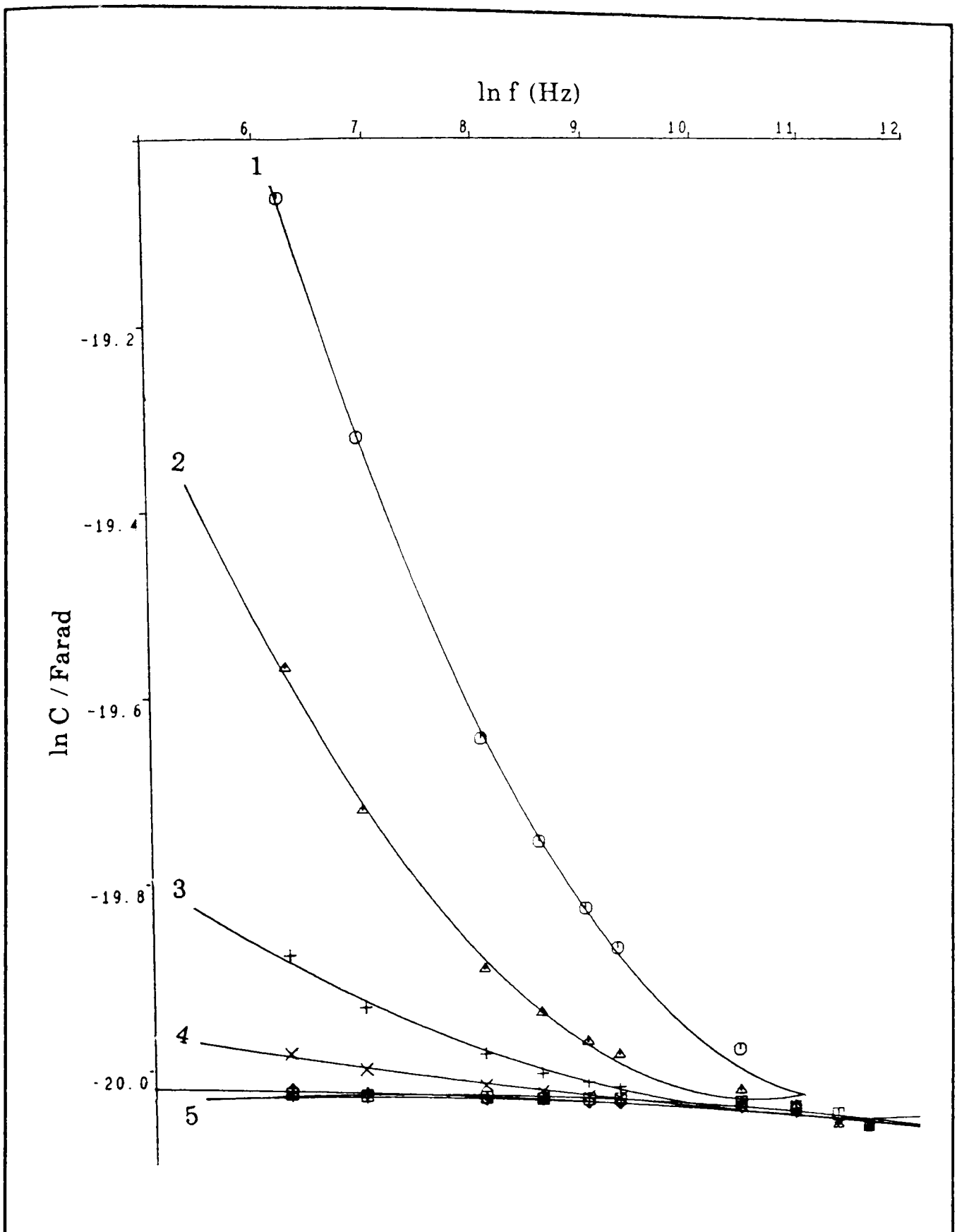


Figure 6.34: The variation of capacitance as a function of frequency at different temperatures for sandwich cell of the copolymer. 1(90°C), 2(50°C), 3(25°C), 4(0°C), 5(-90°C).

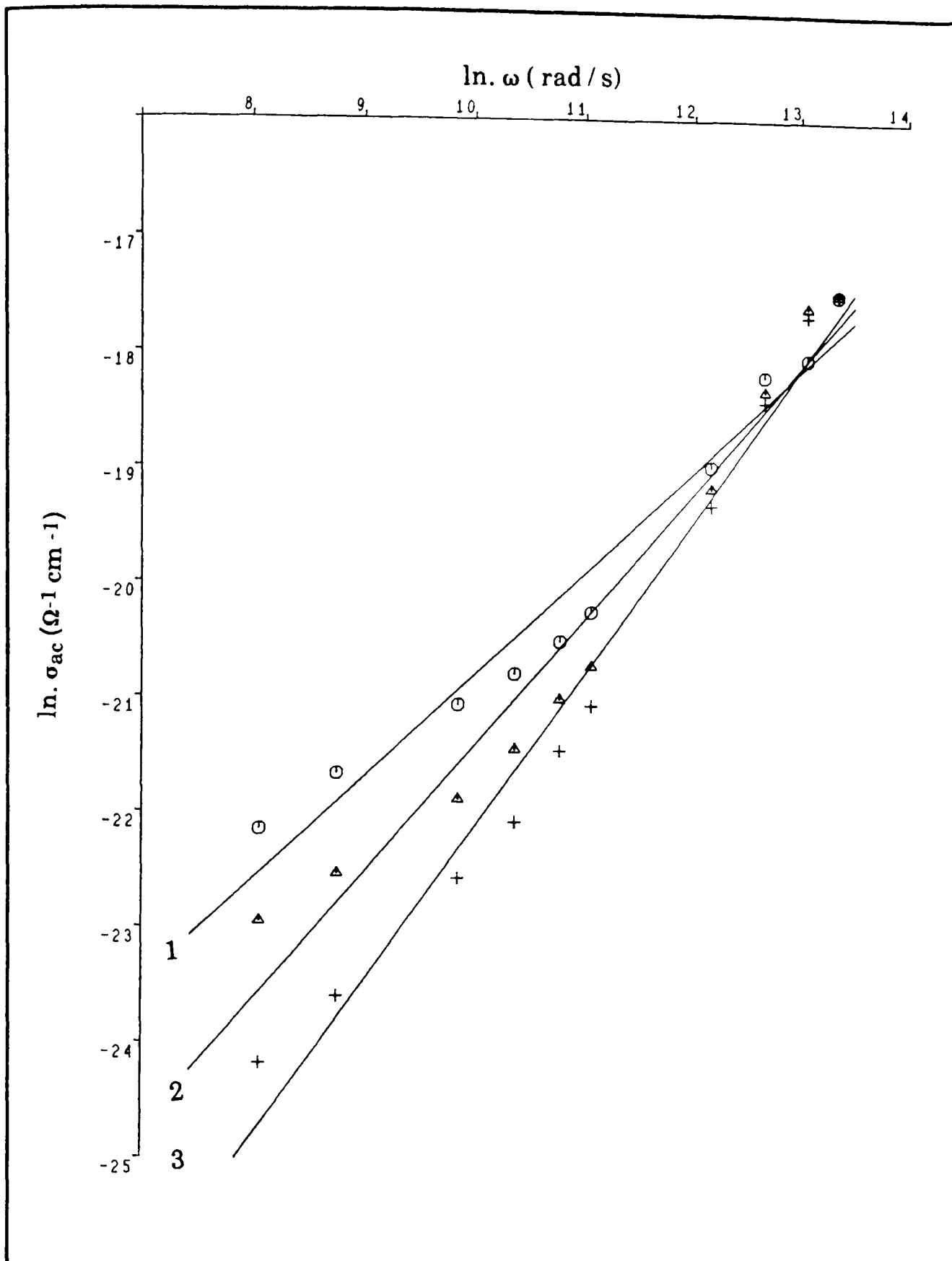


Figure 6.35: The variation of frequency dependent component of the conductivity at different temperatures for sandwich cell of the copolymer. 1(26°C), 2(0°C), 3(-35°C).

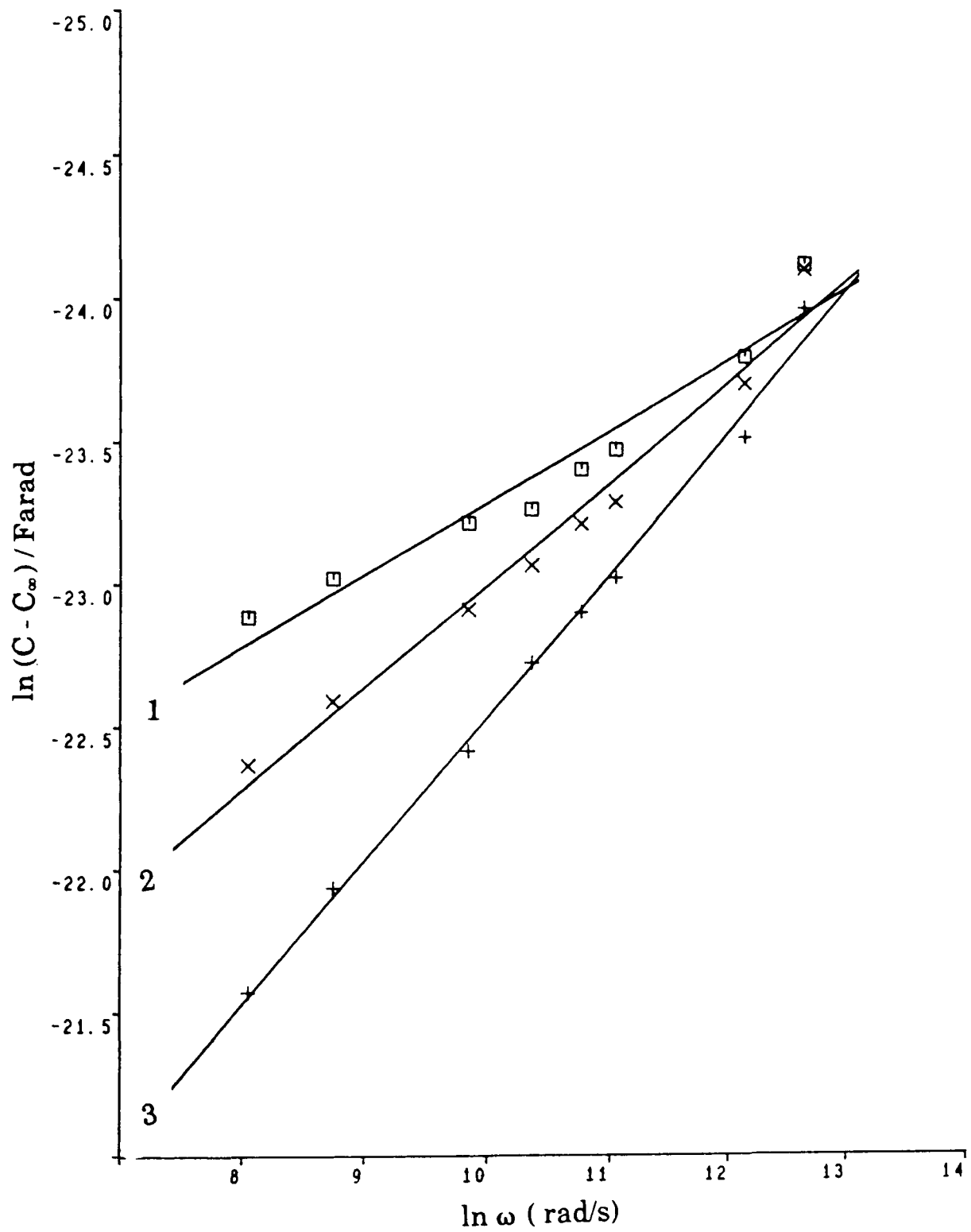


Figure 6.36: The variation of capacitance as a function of frequency at different temperatures for sandwich cell of the copolymer. 1(-35°C), 2(0°C), 4(26°C).

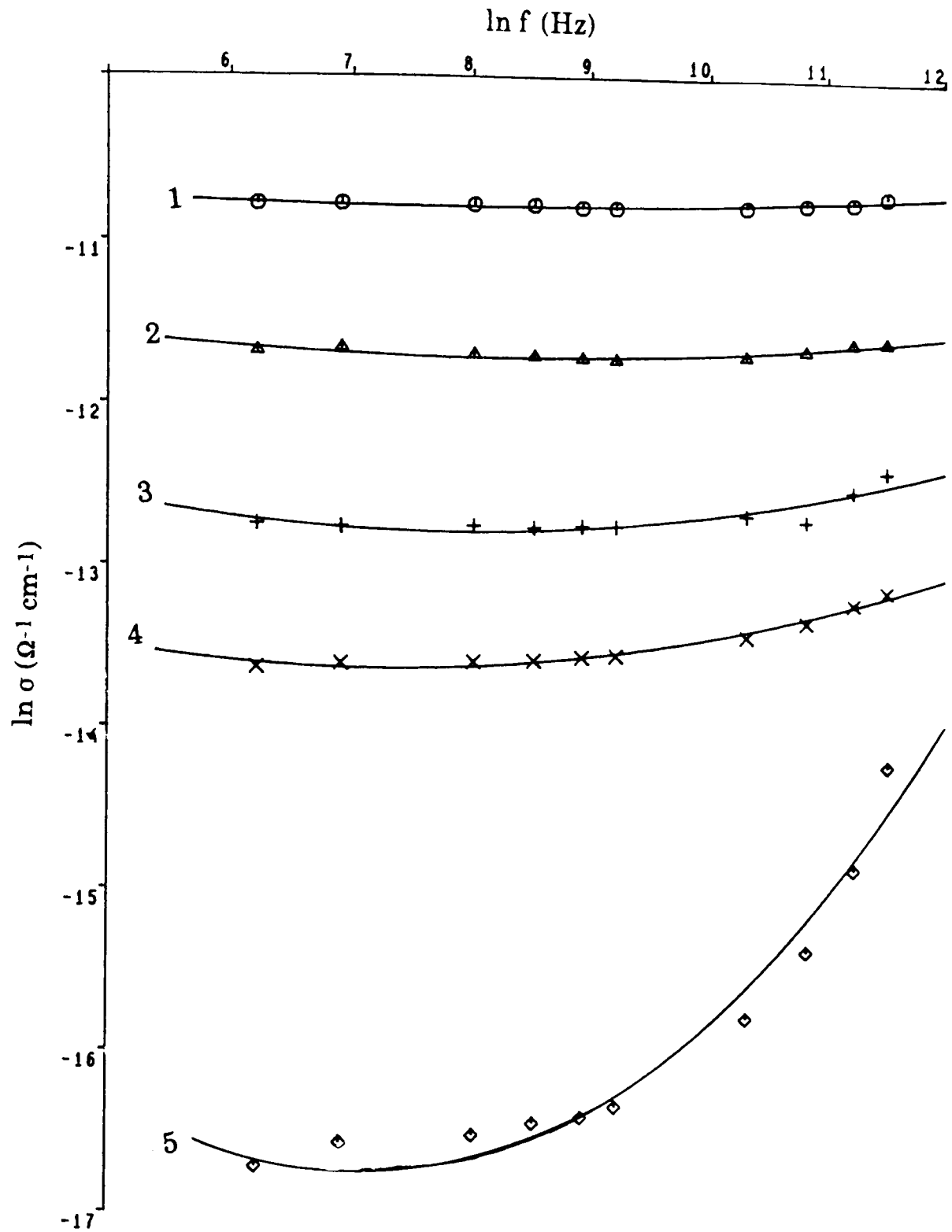


Figure 6.37: The frequency dependence of a.c. conductivity at a series of temperatures on compaction of the mixture. 1(30°C), 2(0°C), 3(-30°C), 4(-50°C), 5(-90°C).

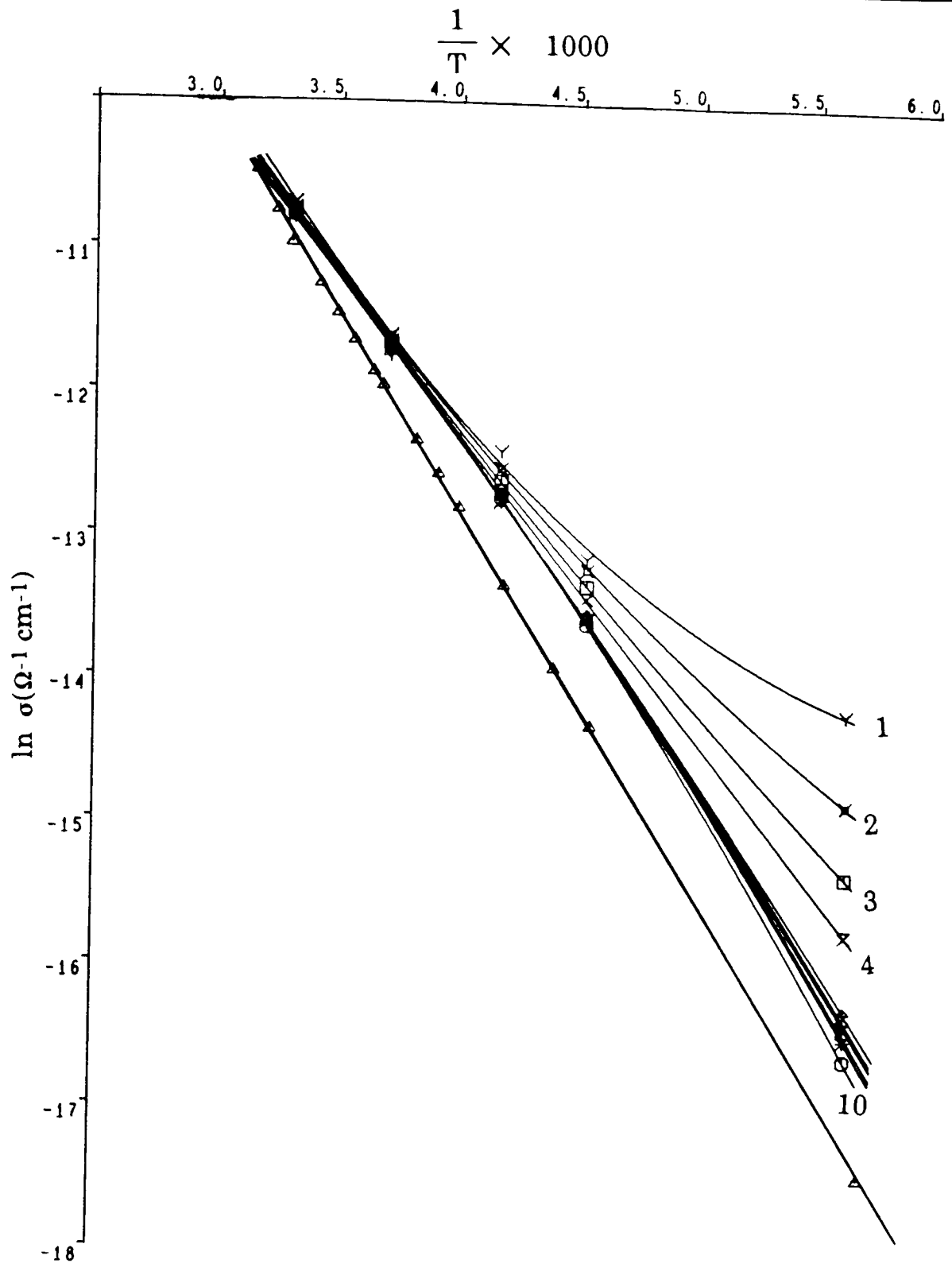


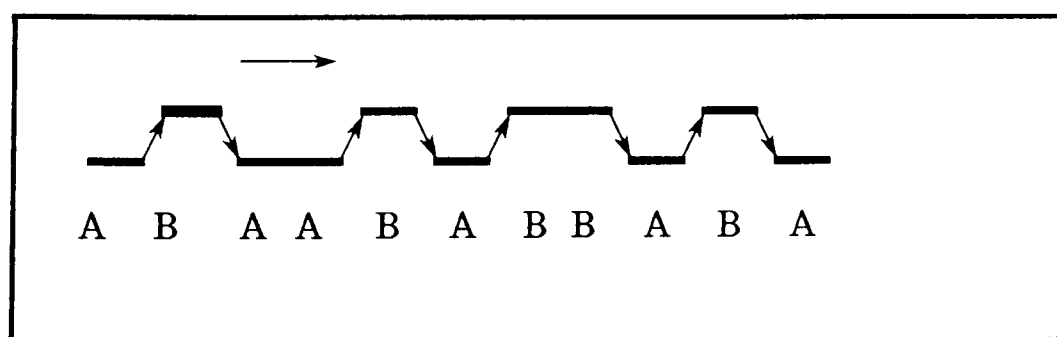
Figure 6.38: The d.c. conductivity and the frequency dependence of a.c. conductivity at a series of temperatures for compaction of AlPcF. 1(100Hz), 2(75Hz), 3(50Hz), 4(30Hz), 5(10Hz), 6(7.5Hz), 7(5Hz), 8(3Hz), 9(1Hz), 10(0.5Hz).

6.2.5) Conclusion:

The general purpose of the a.c. studies was to discover whether the creation of a copolymer, which is an important synthetic approach to the control of electrical properties by structural modification, inevitably creates additional trapping sites which would in turn reduce the carrier mobility and hence adversely affect device performance. Since mobility cannot be measured directly and reliably in polycrystalline films and powders, the study of trapping sites by a.c. is particularly valuable.

Copolymerisation might introduce new hopping sites which would manifest themselves as a.c. losses in one of two ways:

① Since the AlPcF and GaPcF molecules are different electronically it is to be expected that carriers located on them will have different energies. Thus for a random copolymer of A and B it might be expected that the energy path of a carrier would be



The recurrent activated hop $A \rightarrow B \rightarrow A$ would occur with a characteristic frequency and gives rise to a loss peak corresponding to hopping between pairs of identical sites.

② Allowing for the possibility of other hopping processes such as $A \rightarrow B \rightarrow B \rightarrow A$, and interchain hopping, as well as the disordered nature of the material, copolymerisation might merely increase the concentration of the random hopping sites and consequently increase the size of σ_{ac} .

Fortunately neither of the two above effects occur. There is no loss peak, and the value of σ_{ac} is intermediate between that of the two components. We must conclude that either the material is closer to a block copolymer in which the number of the above mentioned sites are small, or more likely, that the hopping sites involve electrons localised in the π -systems of molecules at random sites and the metal atom is not involved in any of the processes.

CHAPTER SEVEN

PHOTOCONDUCTIVITY

7.1) Introduction:

Photoconductivity is the enhancement of electrical conductivity in matter produced by the motion of carriers created by absorbed radiation. Photoconduction is either intrinsic or extrinsic. The term intrinsic photoconduction means the excitation of an electron into the conduction band by the absorption of energy from an incident photon. In the band model extrinsic photoconduction is when electrons are excited from a donor level into the conduction band (electron conduction) or from the valence band into the acceptor levels (hole conduction)(7.1).

The study of photoconductivity involves the investigation of both photogeneration and transport of carriers. Photogeneration involves the process of excitation leading to carrier formation. Transport under an applied electric field involves the processes of capture and release of carriers from shallow and deep traps and finally recombination (7.2-5).

When a photoconductor is illuminated, there is an increase in conductivity, $\Delta\sigma$, such that,

$$\Delta\sigma = e(\mu_n \Delta n + \mu_p \Delta p) \dots\dots\dots 7.1$$

$$\Delta\sigma_n = e \mu_n \Delta n \quad \text{for } n\text{-type photoconduction} \dots\dots\dots 7.2$$

$$\Delta\sigma_p = e \mu_p \Delta p \quad \text{for } p\text{-type photoconduction} \dots\dots\dots 7.3$$

where $\Delta\sigma_n$ and $\Delta\sigma_p$ are the increase in the electron and hole conductivities respectively. e , μ_n and Δn are the charge, mobility and increase in concentration of electrons respectively. p , μ_p and Δp are the hole charge, mobility and increase in concentration of hole respectively.

Light absorption may lead to a band-to-band transition and the creation of a mobile electron and a mobile hole. On the other hand it may lead to an intermediate state in which the electron and hole are still bound by Coulomb interaction. Such excitations are called excitons and may be tightly bound (*Frenkel* excitons) or loosely bound (*Wannier* excitons). In molecular systems the most important excitons are the molecular excitons, in which the excitation is largely localised in a single molecule, and the charge transfer excitons in which the electron and hole are on adjacent molecules.

Molecular excitons are highly mobile and may migrate rapidly through the crystal. The extra energy necessary to dissociate the excitons into carriers can be obtained in a number of ways:

- ①) Exciton-exciton interaction leading to an electron and hole.
- ②) Exciton-trap interaction leading to one trapped and one mobile carrier.
- ③) Exciton-surface interaction, again leading to a single mobile carrier.
- ④) Thermal dissociation of the exciton. In many systems this is unlikely for a molecular exciton but is more probable for a charge transfer exciton.

7.2) Examination of Photoconduction:

Photoconducting properties can be examined using a variety of techniques, such as steady state, pulsed light and chopped light. It has been found that chopping the light at a range of frequencies can give a true photocurrent and the slower heating contribution can be removed (7.6).

In this work the chopped light technique was used to study the photoconduction in sandwich cells of the GaPcF and the 1:1 mole ratio copolymer of AlPcF and GaPcF. AlPcF showed little photoconductive response.

In chopped light measurements the period of illumination is followed by an equal period of complete darkness. The method and theory were developed by *Ryukin*(7.7). By using chopped light, a peak-to-peak alternating photocurrent corresponding to the voltage is observed. The photoconductivity ($\Delta\sigma$) at a given chopping frequency (f) is related to the true stationary photoconductivity ($\Delta\sigma_{stat}$) by the *Ryukin equation*

$$\Delta\sigma = \Delta\sigma_{stat} \tanh\left(\frac{1}{4\tau f}\right) \dots\dots\dots 7.4$$

where τ is the charge carrier lifetime. Since the frequency, $f = 1/2t_1$, where t_1 is the time of interruption of the light, then

$$\Delta\sigma = \Delta\sigma_{stat} \tanh\left(\frac{t_1}{2\tau}\right) \dots\dots\dots 7.5$$

where $t_1 \gg \tau$ i.e, the duration of the pulsed light is considerably greater than the lifetime, τ , the value of $\tanh(t_1/2\tau)$ tends to unity, and hence becomes $\Delta\sigma_{stat}$, thus giving steady state conduction. τ and $\Delta\sigma_{stat}$ can be

determined by applying a least squares curve-fitting program to the equation 7.5.

Work using the chopped light method has been carried out to study the effects of external parameters such as wavelength, light intensity and voltage on τ and $\Delta\sigma$. One of the effects of using chopped light is the removal of a bolometric signal, leaving only a true photocurrent^(7.8). The theory being outlined by *Eldridge*^(7.9). He derived a relation which showed that since the bolometric effect involves the absorption of radiation by lattice vibration and other non-conductive mechanisms. It can be reduced, either if the chopping frequency is increased, or the resistance is enlarged by reducing the temperature.

7.3) External Effects on Photoconduction:

The observed photoconduction may depend on the temperature, the applied voltage, and the ambient atmosphere. Since these factors may influence the concentration or mobility of carriers, the study of their influence can give information on charge generation and decay, and carrier migration.

a) Temperature :

The photocurrent at constant voltage increases with temperature for most organic semiconductors^(7.10), and is given by

$$I_{ph} = A e^{\frac{-\Delta E_{ph}}{kT}} \dots \dots \dots 7.6$$

where I_{ph} is the photocurrent and ΔE_{ph} is the photoactivation energy. A plot of $\log I_{ph}$ vs. $1/T$ will yield a straight line of slope $\Delta E_{ph}/k$. ΔE_{ph} is usually small compared with the dark electric conduction activation energy. The difference in the photo and the dark activation energies is due to different processes being involved. A strong or weak temperature dependence is determined by the density and distribution of the traps and the position of the *Fermi level* (2.7). In some cases the dark and photoactivation energies have proved identical. *Tamamura et al* (7.11) suggested that for some organic salts the observed activation energies are indicative of a conduction mechanism in which carriers migrate from trap to trap, no activation energy being needed for carrier production. In other systems the similarity between dark and photoconduction activation energies is indicative of a heating (bolometric) effect rather than true photoconduction.

b) Voltage:

At low fields the photocurrent obeys *Ohm's law* and increases linearly with field. At higher fields a change to a superlinear dependence may be observed, which is characteristic of space charge limited current (SCLC). At high voltage the photocurrent can show saturation (7.10)

c) Light Intensity:

The light intensity and photocurrent are related(7.1)

$$I_{ph} \propto I^\alpha$$

..... 7.7

where I_{ph} is the light intensity and the constant α , is the intensity parameter. The value of α depends on the traps present within the samples, their distribution in energy, and the methods of carrier generation, transport and recombination^(7.9-11). Values of $0.1 \leq \alpha \leq 1$ are generally observed with organic photoconductors, but values as high as 4 are possible^(7.12,7.14). For α values greater than unity, the current displays what is called "superlinear region", where the photocurrent increases as a higher power of the light intensity. The model for this effect was introduced by *Rose* ^(7.14), in which two sets of centres, recombination and trapping, were considered. The movement of the *Fermi level* as the light intensity is increased changes the traps into recombination centres. This produce a change in carrier lifetime and hence a superlinear photocurrent.

Another model for $\alpha > 1$ considers the recombination of charge carriers which are produced by exciton auto-ionisation ^(7.13).

d) Wavelength:

In inorganic materials the threshold of light absorption usually corresponds to a band to band transition. In organic materials, where the visible-U.V. absorption spectrum is similar to that of the isolated materials, the onset of absorption corresponds to a molecular $n-n^*$ transition and the formation of a molecular exciton. In some cases the photocurrent follows the absorption spectrum (symbiotic behavior) and in other cases the photocurrent has peaks on either side of the absorption band (antibatic behaviour)^(7.14). The difference lies in the extent of penetration of the light and the region of the crystal where carrier generation is formed. Where surface generation is the dominant process, the photocurrent follows the

absorption spectra, since regions of highest absorption give excitons at the surface. Where bulk generation is dominant, antibatic behaviour is observed. Antibatic behaviour may also be observed when the field at the surface is neutralised by space charge.

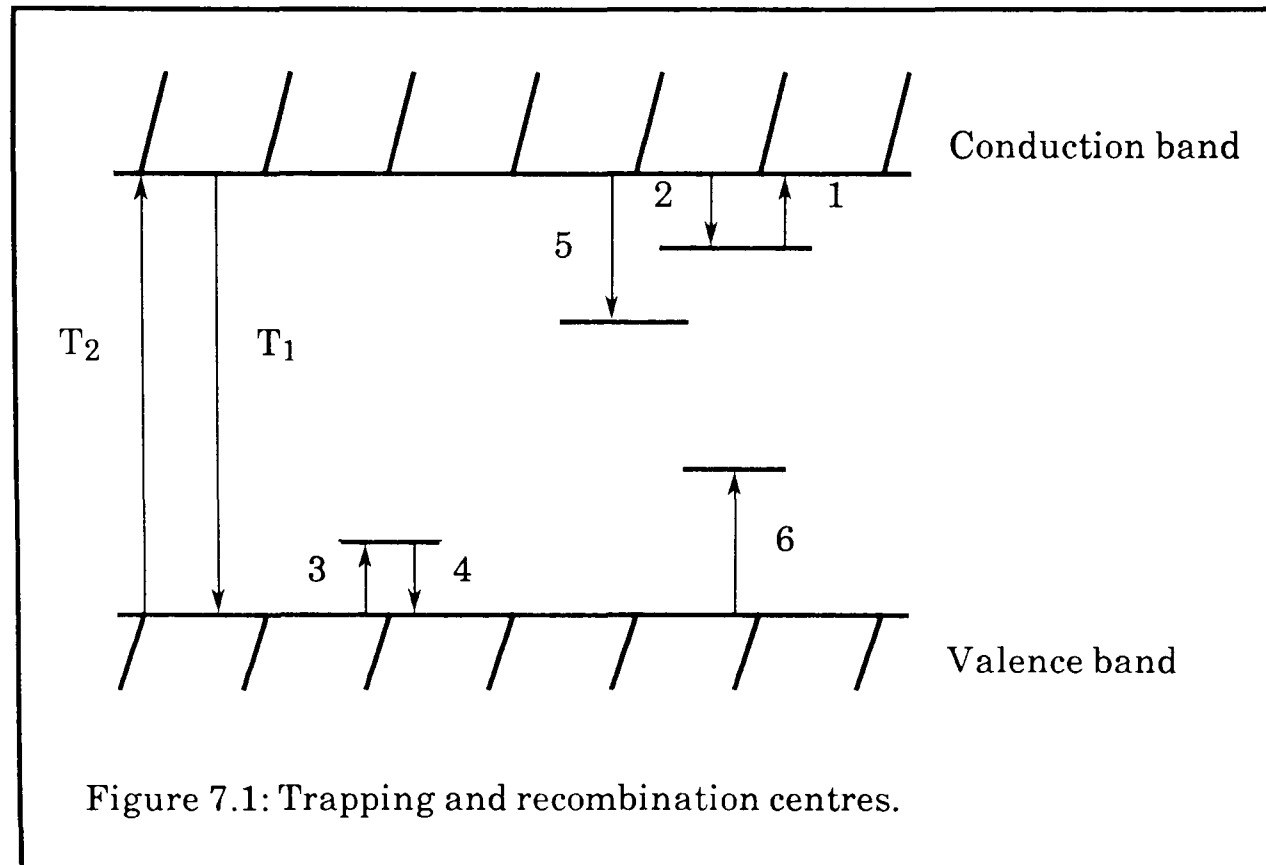
Gases have a large influence on photoconduction values, producing shifts in spectra and changes in magnitude^(7.15-16). The gases are responsible for trap formation on the surface of the sample, O₂ producing electron traps and H₂ producing hole traps

7.4) Trapping and Recombination:

Once electrons and holes have been freed by absorption of a sufficiently energetic photon (transition T2 in figure 7.1), they will remain free until they are captured by one of the capturing centres. These capturing centres can be divided into two groups:

- ① Trapping centres, at which the captured carriers have a greater probability of being thermally re-excited to the free state than of recombining with a carrier of opposite sign.
- ② Recombination centres, at which the captured carriers have greater probability of recombining with a carrier of opposite sign than of being re-excited to a free state.

Figure 7.1 shows the trapping and thermal release of electrons in electron traps (transition 1 and 2), trapping and thermal release of holes in hole traps (transition 3 and 4) and also capture of an electrons (transition 5) and capture of holes (transition 6) at recombination centres. These recombination centres are introduced in the forbidden energy zone, either by defects or by chemical impurities^(7.3). The free electron may recombine directly with a free hole according to transition T₁. The probability of this



transition is small(7.2). There could be either more than one set of discrete trapping and recombination centres or there could be a continuous distribution of traps and recombination centres(7.3). The capture cross section of a centre is determined by the potential variation in the neighbourhood of the centre ,i.e., a free carrier will be captured if it approaches sufficiently close to a centre so that the binding energy due to *Coulomb* attraction is equal to or greater than kT .

7.5) Kinetics of Recombination Processes:

In the case of intrinsic semiconductors, and if there are no collecting contacts, the excess carriers due to optical excitation are limited through recombination (7.10). Thus the rate of change of carrier density with generation rate, g , and recombination rate, R , can be written,

$$\frac{dn}{dt} = \frac{dp}{dt} = g - R \quad \dots\dots\dots 7.8$$

$$\frac{dn}{dt} = g - k_r n^2 \quad \dots\dots\dots 7.9$$

where k_r is the recombination rate constant of holes and electrons. In the steady state, and where the carrier density, n , due to optical excitation, is much higher than the thermal excitation, n_0 , i.e., $n_0 \ll n$ then

$$\frac{dn}{dt} = \frac{dp}{dt} = 0 = g - k_r n^2$$

Rate of decay is,

$$\frac{dn}{dt} = -k_r n^2, \quad \frac{dp}{dt} = -k_r p^2 \quad \dots\dots\dots 7.10$$

In the presence of recombination centres, the rate of decay becomes,

$$\frac{dn}{dt} = -k_r' N_r n \quad \dots\dots\dots 7.11$$

where N_r is the concentration of capturing centres (holes, traps, etc.), and k_r' is the recombination rate constant for these centres.

If τ is the lifetime of the charge carrier then (7.10,7.13),

$$\tau = \frac{1}{k_r' N_r} \quad \dots\dots\dots 7.12$$

Rate of decay is,

$$\frac{dn}{dt} = \frac{-n}{\tau} \quad \dots\dots\dots 7.13$$

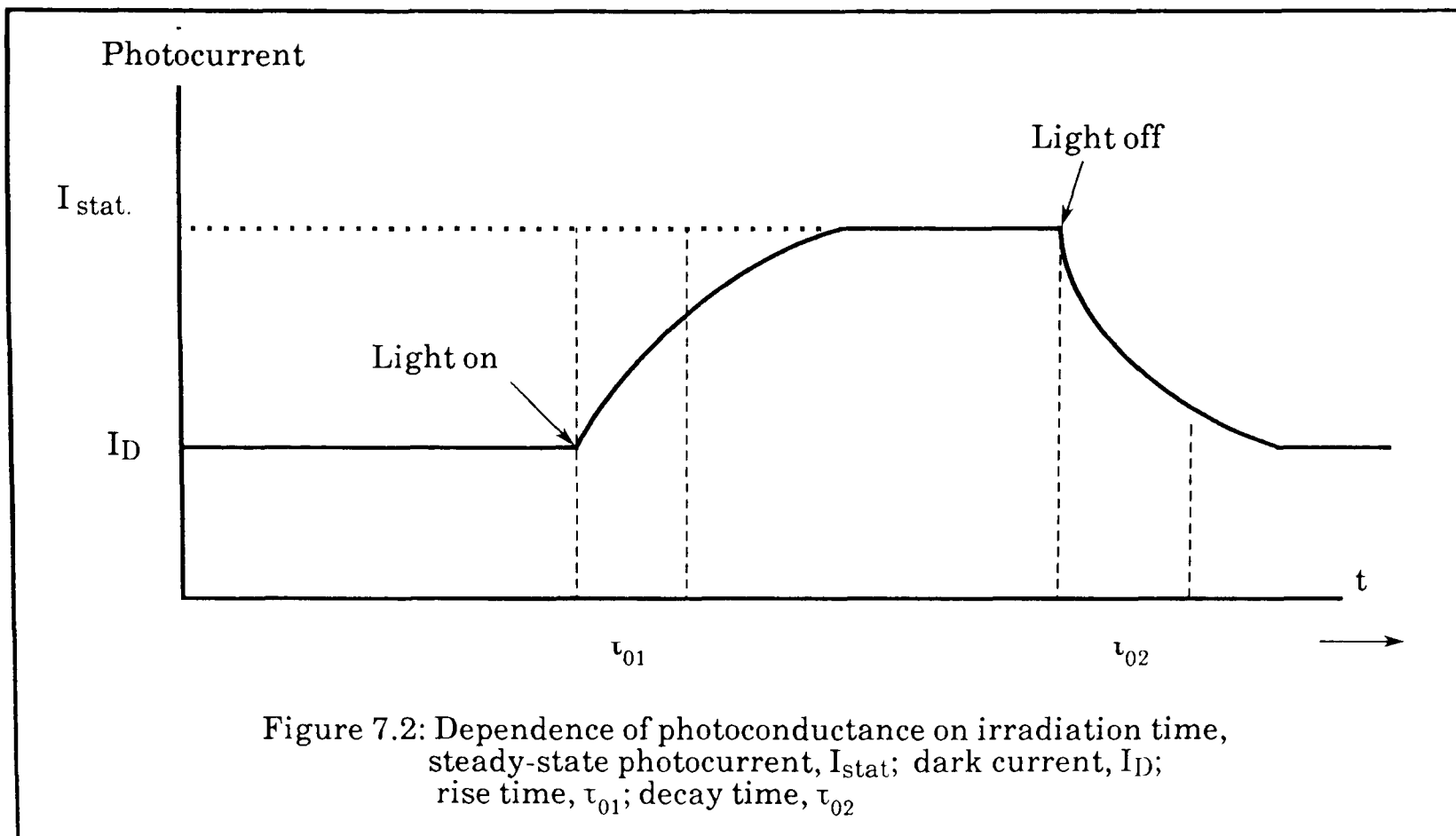
and rate of generation is,

$$\frac{dn}{dt} = g - \frac{n}{\tau} \quad \dots\dots\dots 7.14$$

7.6) Growth and Decay of Photocurrent:

Except in certain semiconductors where the effects of trapping can be neglected any analysis for the growth and decay of photoconductivity must include the contributions of trap filling and emptying (7.2). The presence of traps has an influence on the rise and decay of the photocurrent(7.12).

Figure 7.2 shows the dependence of photoconduction on irradiation time at constant light intensity. The differential equation describing these processes is obtained using the time constant for rise and decay τ_0 ,



$$\frac{dn}{dt} = g - \frac{n}{\tau_0} \quad \dots\dots\dots 7.15$$

From this equation we obtain

$$n = n_0 + n_{stat} (1 - e^{-\frac{t}{\tau_0}}) \quad \dots\dots\dots 7.16$$

where n_0 is the carrier density at the dark and n_{stat} is the steady-state carrier density.

Equation 7.16 describes the time dependence of the increase of carrier density when the light is switched on. At $t = \tau_0$ the density increases from $n = n_0$ to $n = n_0 + n_{stat} (1 - 1/e)$. The steady state photoconductance, i.e. $n = n_{stat}$, is established only when $t \gg \tau_0$.

When the light is switched off, the decay of the excess carrier is,

$$n = n_0 + n_{stat} e^{-\frac{t}{\tau_0}} \quad \dots\dots\dots 7.17$$

At $t = \tau_0$ the carrier density decays to $n_0 + n_{stat}(1/e)$ and to the dark carrier density when $t \gg \tau_0$.

A rise time is required for the steady state to be established between the new density of free carriers and the new occupancy of traps after an exciting light is switched on. Also a decay time is required for the trapped carriers to be thermally released after the excitation is terminated. The occurrence of the rise and decay times much greater than the carrier life time is caused by trapping of the carriers(7.17).

7.7) Results and Discussion:

The photoconductivity measurements were carried out by Mr. D. Petty, in a collaborative investigation. Sandwich cells were prepared on a glass slide substrate. The electrodes were evaporated gold films and the thickness of the phthalocyanine layer was $1\mu\text{m}$. The chopped light technique was employed and measurements were made as a function of light intensity, wavelength, and chopping frequency. The voltage applied was 1.5 V providing a field of $1.5 \times 10^4 \text{ V cm}^{-1}$.

In an investigation where there is a technological objective as well as a desire to explore fundamental principle, there is a dilemma over the best experimental conditions to employ. These experiments are directed towards developing materials suitable for photoconductive devices such as photocopiers where the photoreceptor must operate in air. On the other hand oxygen is known to complex with phthalocyanines, and so fundamental studies require conditions of ultra-high vacuum. In this study the object was to compare the properties of GaPcF and its 1:1 copolymer with AlPcF. It was felt that measurements at room temperature, in air, would suffice. Further studies, under vacuum, are in progress.

1) Light Intensity:

The photoconductivity response was measured as a function of light intensity, using monochromatic light (800 nm) chopped at a constant chopping frequency.

Figure 7.3 shows that the photoconductivity of GaPcF films varies with light intensity as

$$\sigma \propto I^\alpha \quad \dots\dots\dots 7.18$$

with $\alpha = 0.6$. A value of unity suggests a single photon process with a unimolecular carrier loss process, whereas a value of 0.5 suggests a bimolecular loss process (7.18). The observed value is therefore indicative of a bimolecular loss process, either direct or indirect electron-hole recombination or more likely recombination at a recombination centre (7.12,7.19).

The behaviour of AlPcF (7.20) which an extremely poor photoconductor is intensity dependent. In sharp contrast to GaPcF, the copolymer gives a value of $\alpha = 1.4$ (figure 7.4). Values greater than unity have been observed in phthalocyanines(7.21) and other compounds (7.12,7.14). It is usually taken as to indicate the involvement of two photons in the generation process, such as in an exciton exciton collision (7.4). The problem requires further investigation before any firm conclusions can be drawn. However, it may be worthwhile to speculate as to what the mechanism might be.

It is known that excitons are very mobile in molecular crystals(7.12). In these linear chain polymers it is to be expected that the exciton motion is largely confined to motion along the chain. If furthermore, excitons are long lived and localised, the probability of a two-photon collision leading to an electron and a hole is enhanced. Such a situation might arise in a fairly random copolymer containing some blocks of one component. The charge transfer (CT) exciton is likely to be formed where A and B are adjacent to each other.

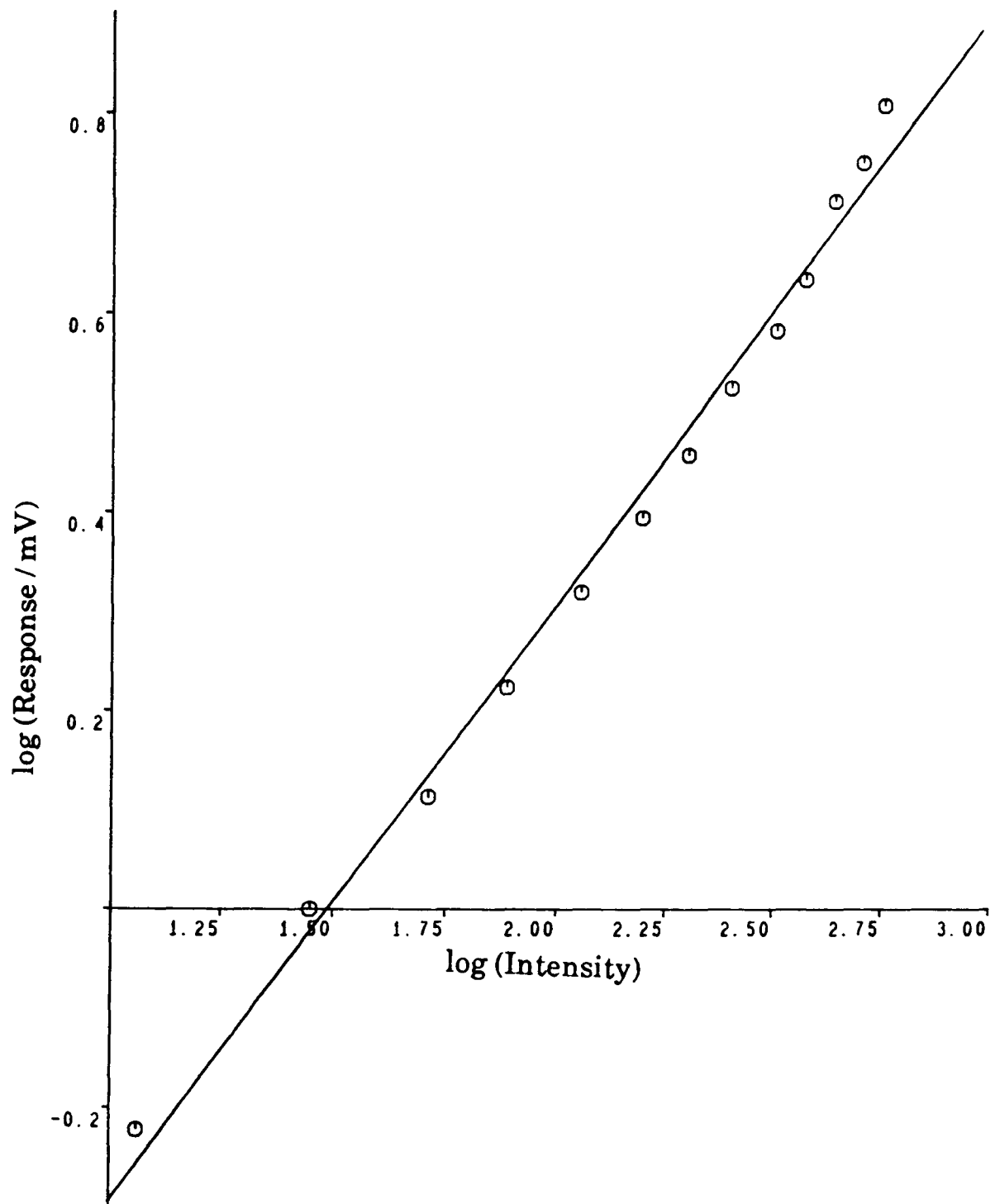


Figure 7.3: The photoconductivity response as a function of light intensity for GaPcF.

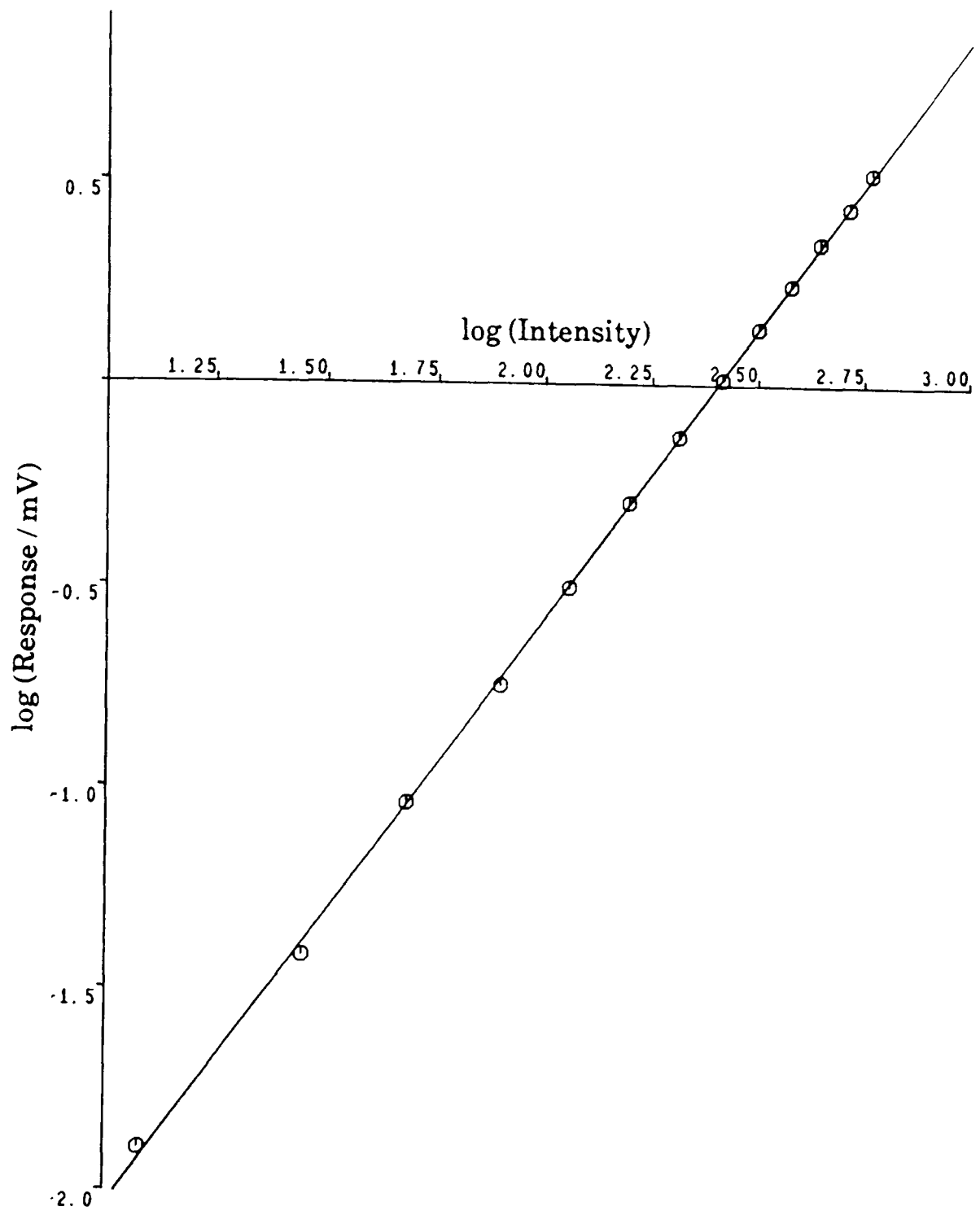
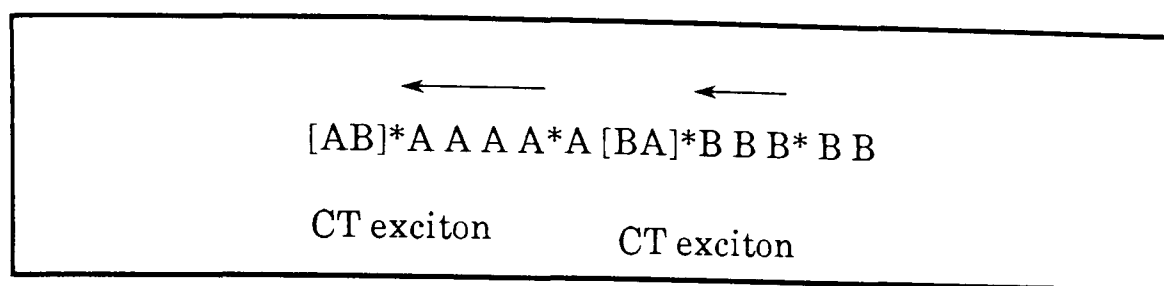


Figure 7.4: The photoconductivity response as a function of light intensity for the copolymer .



Normally the observaton of exciton-exciton effects requires very high light intensity. However, in phthalocyanines which have very strong light absorption the exciton density at the illuminated surface will be high.

II) wavelength:

The photoconductivity response was measured as a function of illumination wavelength at a constant chopping frequency and a constant light intensity. The GaPcF and the copolymer both show a peak at 520-530 nm and a broader peak around 800 nm (figure 7.5-6). Since the Q band of these materials in the solid state is 700 nm ^(7.5), the action spectrum is clearly antibatic. This contrasts with the much weaker photoconductor AlPcF, which shows symbiotic behaviour under similar conditions. This has been attributed to charge detrapping at the surface ^(7.20).

These results lead to two conclusions:

- ① The photoresponse is not due to heating, which is expected to follow the absorbance^(7.22).
- ② Bulk generation rather than surface generation appears to be the dominant processes.

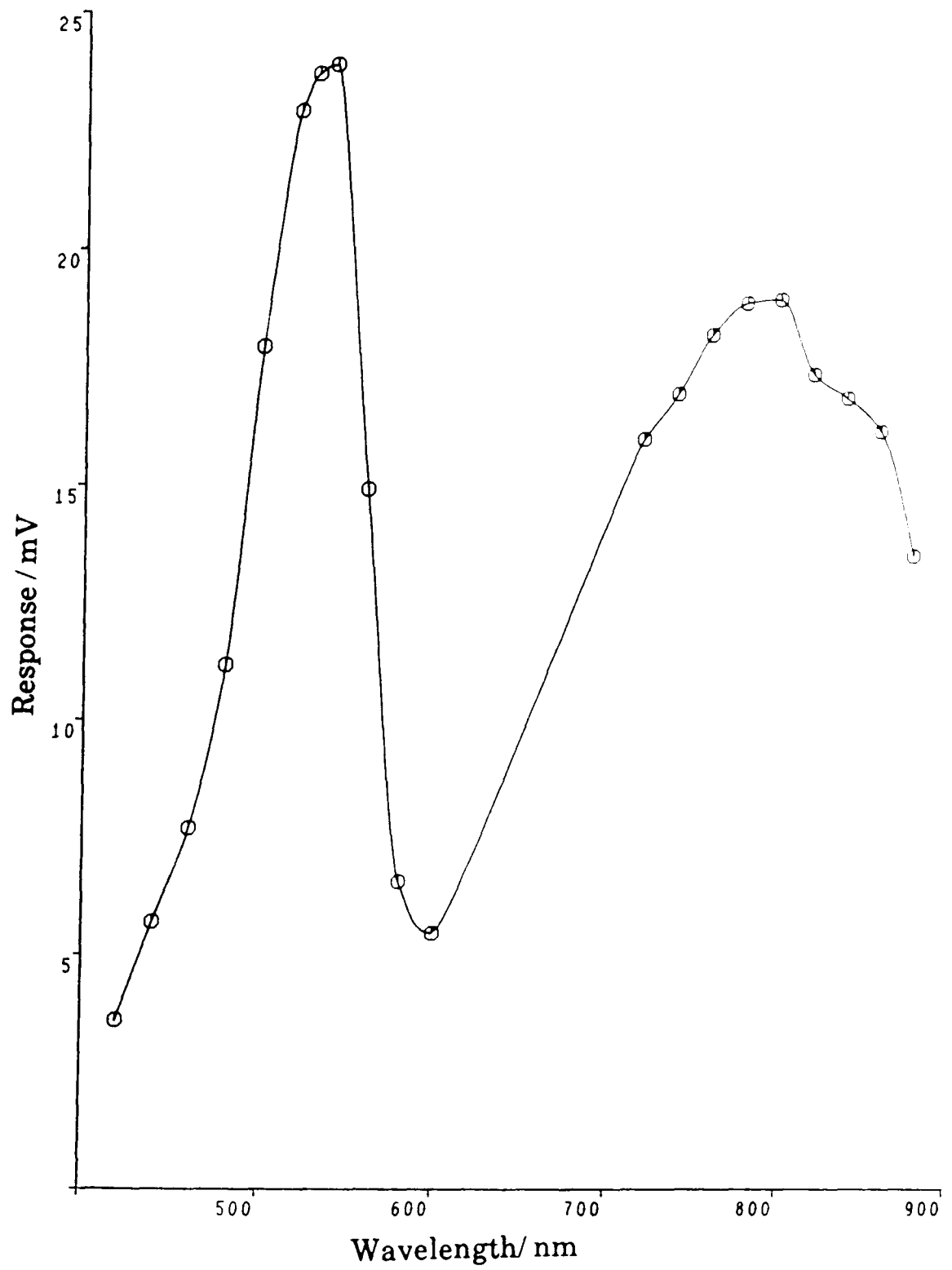


Figure 7.5: The photoconductivity response as a function of wavelength of illumination for GaPcF.

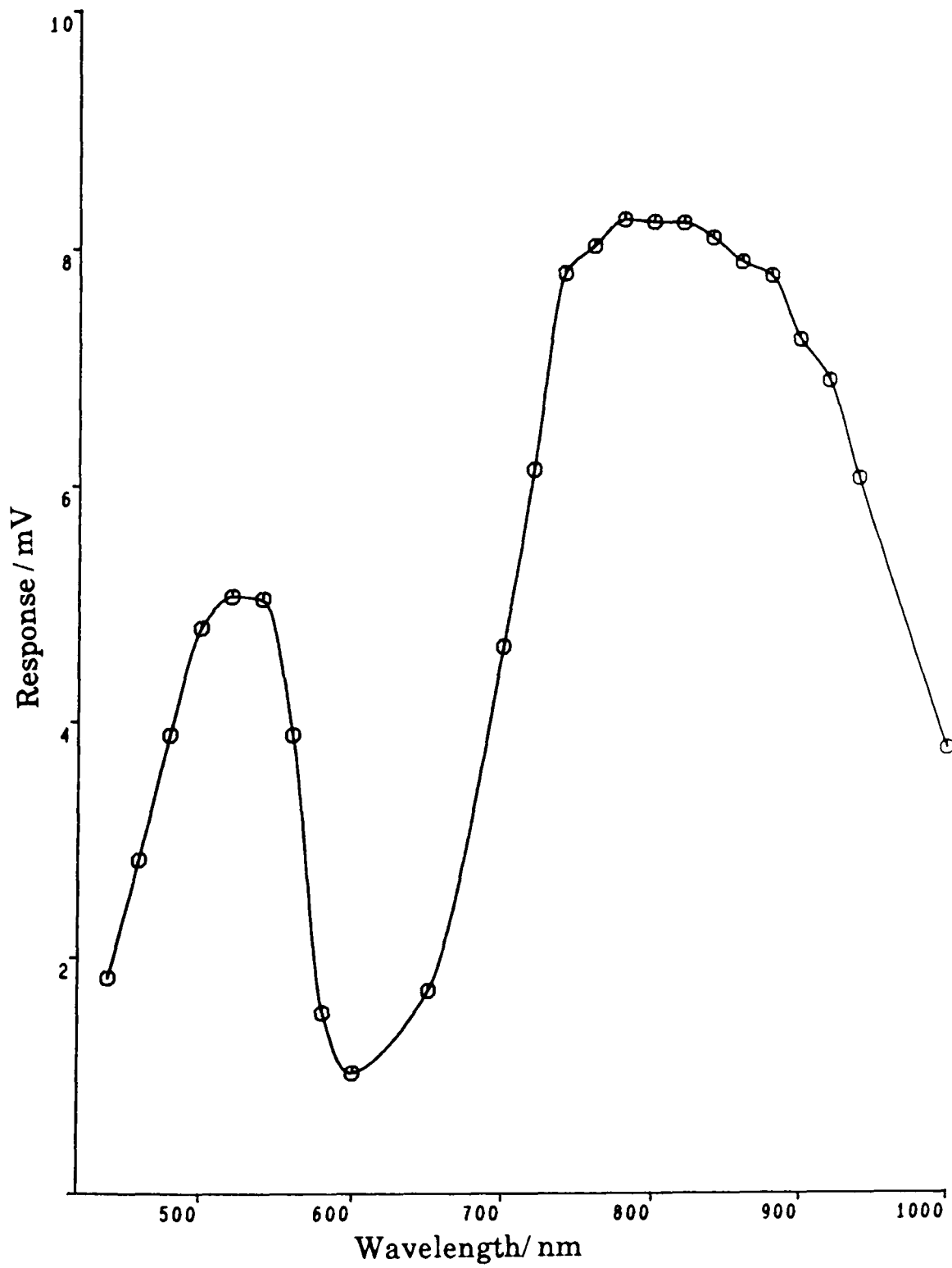


Figure 7.6: The photoconductivity response as a function of wavelength of illumination for the copolymer.

III) Chopping Frequency:

Films of GaPcF and the copolymer were studied under illumination corresponding to peak photoresponse as a function of chopping frequency. The results are shown in figures 7.7 and 7.8, and are presented as the signal from the phase sensitive detector, against the illumination period. Since the response does not reach a plateau it is not possible to assign the order unequivocally, but the data fits the *Ryvkina equation*, permitting the determination of lifetime, τ , and the extrapolated value of the steady state conductivity. The lifetimes were independent of wavelength as is the case for TCNQ (7.6). The results are tabulated below (measurements were taken at a wavelength of 800nm).

	τ (ms)	$\sigma_{\text{stat}}(\Omega^{-1} \text{ cm}^{-1}) \times 10^{-9}$
GaPcF	4	0.4
Copolymer	3	6.0

7.8) Conclusion:

The ability to prepare copolymers of predetermined composition offers a method for modifying the properties of the material in such a way as to optimise its photoconductive properties. There is good reason to expect that copolymers of AlPcF and GaPcF may show enhanced photoconductivity. In the *Noolandi and Hong model* (7.23) for the photogeneration, the excited molecule (*Frenkel exciton*) leads to the reversible formation of a bound charge pair, which may dissociate into free carriers

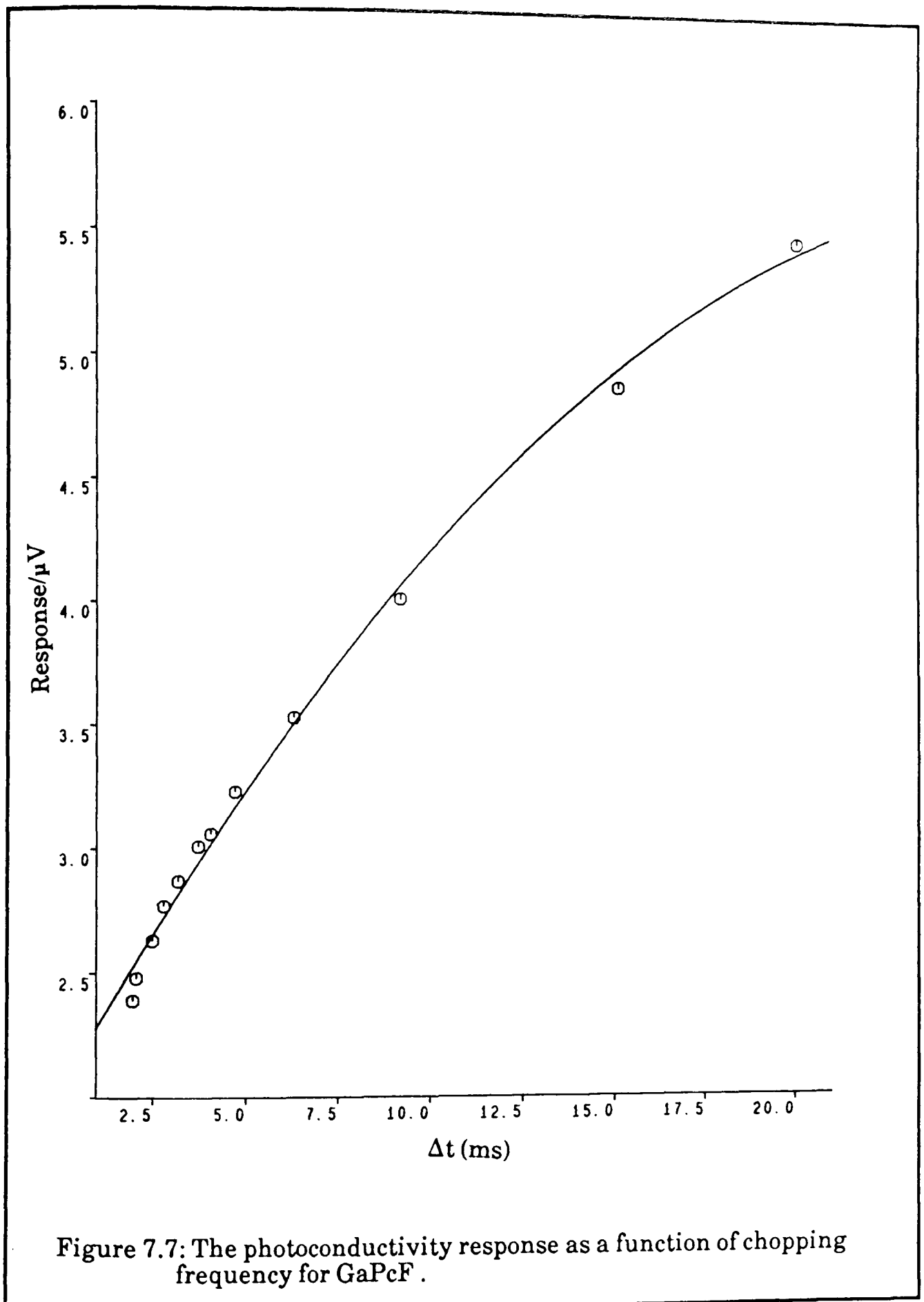


Figure 7.7: The photoconductivity response as a function of chopping frequency for GaPcF .

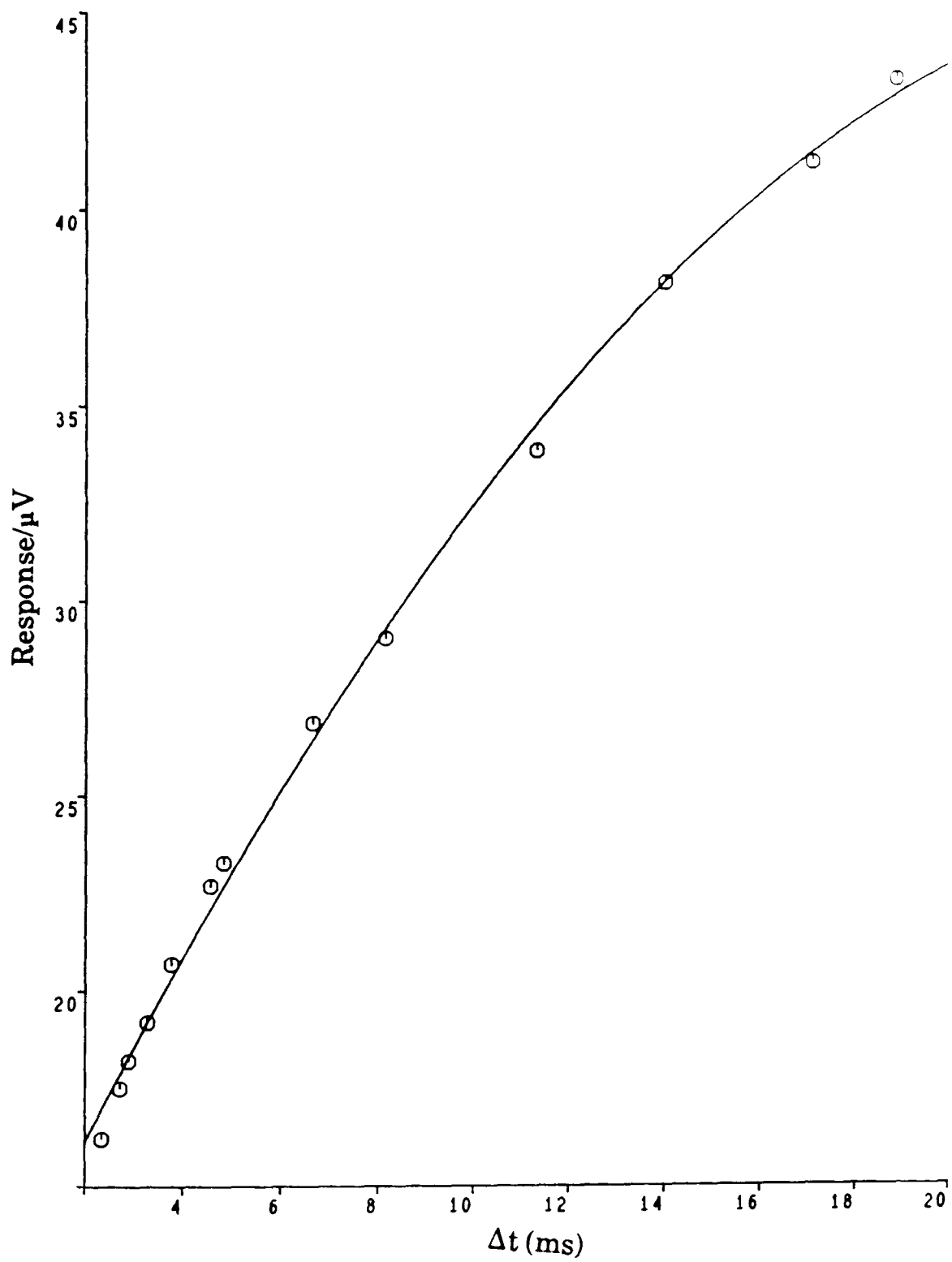
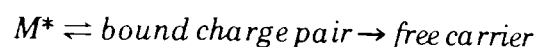


Figure 7.8: The photoconductivity response as a function of chopping frequency for the copolymer .



It follows that any structural change which favours the formation of the bound charge pair will enhance the concentration of photogenerated carriers. Provided that the mobility is unaffected, then the photoconductivity is increased proportionally. In these materials the bound pair may well be the charge transfer exciton. The difference in electron affinity of the two components will favour the formation of the CT exciton.

The results reported above seem to support this proposal. AlPcF is a very poor photoconductor, but its copolymer with GaPcF is a slightly better photoconductor than pure GaPcF. The photocurrent lifetime is, however, reduced suggesting an enhanced imperfection concentration in the copolymer.

CHAPTER EIGHT

GENERAL CONCLUSIONS AND SUGGESTIONS FOR FURTHER WORK

The principal objectives of this research project have been achieved. A successful synthesis of copolymers of the cofacially stacked phthalocyanines AlPcF and GaPcF has been achieved. The copolymer has been purified and characterised. It can be deposited as a sublimed film suitable for devices, without significant change in composition. The material has been characterised electrically and its properties are intermediate between those of its constituent monomers, offering a means of tailoring the properties of the material to the requirements of the device. The copolymer photoconducts better than either component, and thus offers an approach to maximising this property for applications of photoconductivity such as photocopying.

The copolymer, like the monomers, is dopable with iodine to give a highly conducting material. Furthermore the behaviour of the doped copolymers has much in common with classical alloys in that it obeys

Mathiessen's rule. This preliminary observation is worth repeating with highly purified material down to liquid helium temperatures.

One question still unanswered about the copolymer is whether it is a block or random copolymer. Experiments so far have been inconclusive. Infra-red studies on ordered films may be more informative, as may be the observation of the fluorine resonance by magic angle spinning NMR.

Now that the general principle of copolymerisation in these systems has been established, there are synthetic approaches to the control of electrical properties which could be attempted.

① Instead of using two rather similar phthalocyanines, one could be modified to give it acceptor properties (e.g. by the substitution of cyanide groups around the periphery) or donor properties (e.g. by the substitution of amino groups). The effect is expected to be analogous to the doping of silicon by boron and phosphorus.

② It may well be that the substituted phthalocyanines are insufficiently stable to sublime. In this case soluble polymers could be prepared by also substituting alkoxy groups in the periphery. Films may be deposited from solution by solvent evaporation or by spinning.

③ It may be possible to synthesize an alternating copolymer by the interaction of the difluorophthalocyanine of a tetravalent metal with a phthalocyanine of a divalent metal. Such a material may well favour formation of the charge transfer exciton, and hence be a good photoconductor.

REFERENCES:

CHAPTER ONE

- 1.1) Gutmann, F., and Lyons, L. E.: "Organic Semiconductors"
John Wiley and Sons, Inc., New York, 1967.
- 1.2) Wright, J. D.: "Molecular Crystals"
Cambridge University Press, Cambridge, 1987.
- 1.3) Skotheim, T. A.: "Handbook of Conducting Polymers" Vol.1
Marcel Dekker, Inc, New York, 1986.
- 1.4) Little, W. A.:
Phys. Rev., 134A, 1416 (1964).
- 1.5) Bechgaard, K., and Jerome D.:
Sci. American, 247, 50 (1982)
- 1.6) Kao, K. C., and Hwang, W.: "Electrical Transport in Solids" Vol.14
Pergmon Press, Oxford, 1981.
- 1.7) Smith, R.A.: "Semiconductors"
Cambridge University Press, Cambridge, 1978.
- 1.8) Sommerfeld, A.:
Z. Phys., 47, 1 (1928).
- 1.9) Kittel, C.: "Introduction to Solid State Physics"
John Wiley and Sons, Inc, New York 3rd Edition, 1966.
- 1.10) Bloch, F.:
Z. Phys., 52, 555 (1928).
- 1.11) Rosenberg, H. M.: "The Solid State "
Clarendon Press, Oxford, 2nd Edition (1978).
- 1.12) Simon, J., and Andre' J.J.: "Molecular Semiconductors"
Springer-Verlag, Heidelberg, Berlin, 1984.
- 1.13) Hannay, N. B.: "Semiconductors"
Reinhold Publishing Corporation, New York, 1959.
- 1.14) Hannay, N. B.: "Solid State Chemistry"
Prentice-Hall, Inc, New Jersey, 1967.

- 1.15) Weller, P.F.:" Solid State Chemistry and Physics" Vol.1
Marcel Dekker, Inc., New York, 1973.
- 1.16) Wright, H. C.:"Elementary Semiconductor physics"
Van Nostrand Reinhold Company, New York, 1979.
- 1.17) Heilmeyer, G. H.; Harrison S. E.:
Phys. Rev., 132,2010(1963).
- 1.18) West, A. R.:"Solid State Chemistry and its Applications"
John Willey and Sons, Chichester, 1985.
- 1.19) Meier, H.:"Organic Semiconductors"
Verlag Chemie,Germany, 1974.
- 1.20) Sukungara, M. and Nelson, R. C.:
Molecular Physics 17,387(1969).
- 1.21) Silbey, R., Jortner, J., Rice, S., and Vala, M. T.:
J. Chem. Phys., 43, 2925(1969).
- 1.22) Skotheim, T. A.:"Handbook Of Conducting Polymers"Vol.2
Marcel Dekker, Inc, New York, 1986.
- 1.23) Eley, D.D., Parfitt, G.D.:
Trans. Farad. Soc., 51, 1529(1955).
- 1.24) Eley, D. D., and Willis, M. R.:" Symposium on Electrical Conductivity
in Organic Solids"
Interscience Publ. New York, 1961, p.247.
- 1.25) Lyons, L. E.:
J. Chem. Soc., 5001(1957).
- 1.26. Devaux, P., and Schott, M.:
Physica Status Solidi, 27, 201, 1968.
- 1.27) Cusack, N. E.:"The Physics of Structurally Disorderd Matter"
Adam Hilger (University of Sussex Press), Bristol, 1987.
- 1.28) Burges, R. E.:
J. Polym. Sci., C17,51(1967).
- 1.29) Weaive, D. and Thorpe, M. F.:
Phys. Rev., 4,2508(1971).
- 1.30) Weaive, D. and Thorpe, M. F.:
Phys. Rev.,4, 3518(1971).

- 1.31) Bube, R. H.: "Photoconductivity in Solids"
John Wiley and Sons, Inc, London, 1960.
- 1.32) Siebrand, W.:
J. Chem. Phys., 41, 3574(1964).
- 1.33) Glarum, S. H.:
Physics and Chemistry of Solids, 24, 1577(1963).
- 1.34) Mott, N. F., and Davis, E. A.: " Electronic Processes in
Non-crystalline Materials"
Clarendon Press, Oxford (1971).
- 1.35) Kryszewski, M. and Szymanski, A.:
Macromol. Rev., 4, 245(1970).
- 1.36) Seanor, D. A.: "Elec. Props. polymers"
Technomic, 1972.

CHAPTER TWO

- 2.1) Moser, F. H., and Thomas, A. L.: "Phthalocyanine compounds"
Reinhold Publishing Corporation, New York, 1963.
- 2.2) Lever, A. B. P.: " Advances in inorganic chemistry and
Radioactivity" Vol.7
Academic Press, New York, 1965.
- 2.3) Metz, J., Schneider, O., Hanack, M.:
Inorg. Chem. 23, 1065(1986).
- 2.4) Achar, B. N., Fohlen, G. M., Parker, J. A.:
Polyhedron, 6, 1463(1987).
- 2.5) Simon, J., and Andre', J. J.: " Molecular Semiconductors"
Springer-Verlag, Berlin, 1985.
- 2.6) Iwatsu, F., Kobayashi, T., and Uyeda, N.:
J. Phys., Chem., 84, 3223(1980).
- 2.7) Sharp, J. H., Lardeon M.:
J. Phys. Chem., 72, 3230(1968).
- 2.8) Hartman, P., and Perdok, W. G.:
Acta Cryst., 8, 49(1955).

- 2.9) Gutmann, F., and Lyons, L. E.: "Organic Semiconductors"
John Wiley and Sons, Inc., New York, 1967.
- 2.10) Kloffo, T. J., Rieke, P. C., Linkous, C. A., Buttner, W. J.,
Nauthakumar, A., Mewborn, T. D., and Armstrong, N. R.:
J. Electrochem. Soc., 132, 2134(1985).
- 2.11) Kirin, I. S., Moskalev, P.N., Moskalev, Yu. A.:
Russ. J. Inorg. Chem., 10, 1065(1965).
- 2.12) Marks, T. J., Stojakovic, D. R.:
J. Am. Chem. Soc., 100, 1695(1978).
- 2.13) Meier, H.: "Organic Semiconductors"
Verlag Chemie, Germany, 1974.
- 2.14) Yudasaka, M., Nakanishi, K., Hara, T., Tanaka, M., and Kurita, S.:
Jap. J. Appl. Phys., 24, L887(1985).
- 2.15) Schoch, K. F., Kundalkar, B. R., and Marks, T. J.:
J. Am. Chem. Soc., 101, 7071(1979).
- 2.16) Linsky, T. P., Paul, T. R., Nohr, R. S., and Kenney, M. E.:
Inorg. Chem., 19, 3131(1980).
- 2.17) Futamata, M., Higuchi, S., Takahashi, S.:
Synth. Met., 30, 39(1989).
- 2.18) Datz, A., Metz, J., Schneider, O., Hanack, M.:
Synth. Met., 9, 31(1984).
- 2.19) Hanack, M., Leverenz, A.:
Synth. Met., 22, 9-14(1987).
- 2.20) Kobel, W., Hanak, M.:
Inorg. Chem., 25, 103(1986).
- 2.21) Hanack, M., Keppeler, U., and Schulze, H., J.:
Synth. Met., 20, 347(1987).
- 2.22) Kuznesof, P. M., Nohr, R. S., Wynne, K. J., and Kenny, M. E.:
J. Macromol. Sci. Chem., A16(1), 299(1981).
- 2.23) Stymne, B., Sauvage, F. X., and Wettermark, G.:
Spectrochimica acta 36A, 397(1980).
- 2.24) Uyeda, N., Kobayashi, T., Suito, E.:
J. Appl. Phys., 43, 5181(1972).

- 2.25) Djurado, D., Fabre, C., Hamwi, A., and Coussiens, J. C.:
Synth. Met., 22, 121(1987).
- 2.26) Nohr, R. S., Kuzuznesof, P. M., Wynne, K. J., Kenney, M. E., and
Siebenman, P. G.:
J. Am. Chem. Soc., 103,4371(1981).
- 2.27) Yoshihara, K., Kishimoto, M., Takahashi, M., Suzuki, S.,
Shiokaura, T. :
Radio. Chem. Acta, 21,148(1974).
- 2.28) Yoshihara, K., Wolf, G. K., Baumgartner T.:
Radio. Chem. acta, 21, 96(1974).
- 2.29) Yang, C. H., Lin, S. F., Chen, H. L., Chang, C. T.:
Inorg. Chem., 19,3541(1980).
- 2.30) Sugimoto, H., Mori, M., Hideki, M., and Taga, T.:
J. Chem. Soc. Chem. Commun., 962(1986).
- 2.31) Barrett, P. A., Dent, C. E., and Linstead, R. P.:
J. Chem. Soc., 1719(1936).
- 2.32) Elvidge, J. A.,and Linstead, R. P.:
J. Chem. Soc., 3536(1955).
- 2.33) Bellido, J., Cardoso, J., Akachi, T.:
Macromolecul. Chem., 182,713(1981).
- 2.34) Dolphin D., Sams, J. R., and Tsin, T. B.:
Inorg. Synth., 20, 155(1987).
- 2.35) Boas, J. F., Fielding P E., and Mackay A. G.:
Aust. J. Chem., 27,7(1974).
- 2.36) Elvidge, J. A.:
J. Chem. Soc., 869(1961).
- 2.37) Yamada, A., Shigehara K., Hara, M.:
Synth. Met., 18, 821(1987).
- 2.38) Berlin, A. A., Sherle, A. I.:
Inorg. Macromol. Rev., 1,37(1971).
- 2.39) Heilmeier, G. H., and Warfield, G:
J. Appl. Phys., 34, 2278 (1963).
- 2.40) Mathure, S. C., and Ramesh, N.:

- Chem. Phys. Lett., 37, 276(1976).
- 2.41) Chen, I.:
J. Chem. Phys. 51, 3241(1969).
- 2.42) Cox, G. A., and Knight, P. C.:
B50, K135(1972).
- 2.43) Cox, G. A., and Knight, P. C.:
J. Phys. C7, 146(1974).
- 2.44) Mathur, S. C., and Ramesh, N.:
Chem. Phys. Lett., 37, 276(1976).
- 2.45) Singh, J.:
Phys. Status Solidi, B82, 263(1977).
- 2.46) Mathur, Singh, J., Singh, D. C.:
J. Phys. C Solid State Physics, 4,3122(1971).
- 2.47) Sukigara, M., and Nelson, R. C.:
Molecular Physics, 17,387(1969).
- 2.48) Devaus, P., and Delacote, G.:
Chem. Phys. Lett., 2,337(1968).
- 2.49) Devaus, P., and Delacote, G.:
J. Chem. Phys., 52,4922(1970).
- 2.50) Rodof, M., Barbe, M., and Dixmier, J.:
Revue De Phys. App., 12,1223(1977).
- 2.51) Ture, P., Petit, P., Andre', J. J., Simon, J., Even, B.,
Boudjema G.,Guillaud, G., and Maitrot, M.:
J. Am. Chem. Soc., 109,5119(1987).
- 2.52) Doris, K. A., Ciliberto, E., Fragala, J., and Ratner, M. A.:
Isr. J., Chem., 27, 337(1986).
- 2.53) Schaffer, A. M., Gouterman, M., and Davidson, E. R.:
Theoret. Chem. Acta, 30, 9(1973).
- 2.54) Cox, G. A., and Knight, P. C.:
J. Phys. Chem. Solids, 34, 1655(1973).
- 2.55) Heilmeyer, G. H., and harrison, S., E.:
Phys. Rev. 132,2010(1963).
- 2.56) Hamann, C.:

- Phys. Status Solidi, 20,481(1967).
- 2.57) Devaux, P., Quedec, P.:
Phys. Lett., 28A,537(1969).
- 2.58) Kearns, D. R., Calvin, M.:
J. Chem. Phys., 34,2022(1961).
- 2.59) Lyons, L. E.:
J. Chem., 33,1717(1980).
- 2.60) Hamann, C.:
Phys. Status Solidi, 26,311(1968).
- 2.61) Willis, M. R.:
Mol. Cryst. Liq. Cryst., 17,217(1989).
- 2.62) Epstein, A., and Wilidi, B. S.:
J. Chem. Phys., 32,324(1960).
- 2.63) Whangbo, M. H., and Stewart, K. R.:
Isr. J. Chem., 23,133(1983).
- 2.64) Canadell, E., and Alvarez, S.:
Inorg. Chem. 23,573(1984).
- 2.65) Cox, P. A.: "The Electronic Structure and Chemistry of Solids"
Oxford University press, Oxford, 1987.
- 2.66) Inokuchi, H., and Akamatu, H.:
Solid state Phys., 12,108(1961).
- 2.67) Fielding, P. E., and MacKay, A. G.:
J. Chem. Phys., 38,2777(1963).
- 2.68) Harrison, S. E., and Assour, J. M.:
J. Chem. Phys., 40,365(1964).
- 2.69) Harrison, S. E., and Ludewig, K. H.:
J. Chem. Phys., 45,343(1966).
- 2.70) Bradley R. S., Grace, J. D., and Munro, D. C.:
Trans. Faraday Soc. 58,776(1962).
- 2.71) Onodera, A., Kawai, N., and Kobayashi, T.:
Solid state Communications, 17,775(1975).
- 2.72) Dann, A. J.: Ph.D thesis, Nottingham University, 1987.

- 2.73) Fahy, M.: Ph.D thesis, Nottingham University, 1988.
- 2.74) Kepler, R. G.:
Phys. Rev., 119, 1226(1960).
- 2.75) Kobayashi, T., Fujiyoshi, Y., and Uyeda, N.:
Acta Crys., A38, 356(1982).
- 2.76) Castongnay, G., and Theoret, A.:
Thin Solid Films, 69,95(1980).
- 2.77) Joyner, R. D., Kenney, M. E.:
Inorg. Chem., 1,717(1962).
- 2.78) Eley, D. D., and Parfitt G. D.:
Trans. Farady Soc., 51,1529(1955).
- 2.79) Sugimoto, H., Mori, M., Masuda, H., Taga, T.:
J Chem. Soc. Chem. Commun., 962(1986).
- 2.80) Usov, N. N., and Benderskii, V. N.:
Phys. Stataus Solidi, 37, 535(1970).
- 2.81) Morel, D. L., Berger, H.:
J. Appl. Phys., 46,863(1975).
- 2.82) Eley, D. D.:
Nature 162, 819(1948).
- 2.83) Vartanian, A. T.:
Zh. Fiz. Khim., 22, 769(1948).
- 2.84) Eley, D. D., Parfitt, G.D., Perry, M. J., and Taysum, D. H.:
Trans. Farad. Soc., 49, 79(1953).
- 2.85) Datz, A., Metz, J., Schneider, O., Hanack, M.:
Synth. Met., 9, 31(1984).
- 2.86) Martinsen, J Stanton, J. L., Greene, R. L., Tanaka, J., Hoffman, B. M., Ibers, J. A.:
J. Am. Chem. Soc., 107, 6915(1985).
- 2.87) Schramm, C. J., Scaringe, R. P., Stojakovic, D. R., Hoffman, B. M., Ibers, J. A., Marks, T. J.:
J. Amer. Chem. Soc., 102,6702(1980).
- 2.88) Kobayashi, T., Fujiyoshi, Y., and Uyeda, N.:
Acta. Cryst., A(38),356(1982).

- 2.89) Ingram, D. J. E., Bennett, J. E.:
Phil. Mag., 45,545(1954).
- 2.90) Yasunaga, H., Kojima, K., Yohdo, H., Takeya, K.:
J. Phys. Soc. Japan, 37,1024(1974).
- 2.91) Kearns, D., Calvin, M.:
J. Am. Chem. Soc., 83,2110(1961).
- 2.92) Briegleb, G.:
Angew. Chem. Int. Ed., 3,617(1964)
- 2.93) Djurado, D., Hamwi, A., Cousseins, J. C.:
Synth. Met., 11,109(1985).
- 2.94) Djurado, D., Fabre, C., Hamwi, A., and Cousseins, J. C.:
Synth. Met., 22, 93(1987).
- 2.95) Brant, P., Weber, D. C., Haupt, S. G., Nohr, R. S., and Wynne, K. J.:
J. Chem. Soc. Dalton. Trans., 269(1985).
- 2.96) Hamann C., Starke, M., Wagner, H.:
Phys. Stat. Solidi, A16,463(1973).
- 2.97) Skotheim, T. A.:" Handbook of Conducting Polymes"Vol.1
Marcel Dekker, Inc, New York, 1986.
- 2.98) Inoue, H., Kida, Y., and Imoto, E.:
Bull. Chem. Soc. Japan, 41, 684(1986).
- 2.99) van Ewyk, R.L., Chadwick, A. V., and Wright, J. D.:
J. Chem. Soc. Faraday 1, 76,2194(1980).
- 2.100) van Ewyk, R.L., Chadwick, A. V., and Wright, J. D.:
J. Chem. Soc. Faraday 1, 77,73(1981).
- 2.101) Bott, B., and Jones, J. A., Transducers'85 "International Conference
on solid-State Sensors and Actuators"(IEEE,1985) 128.
- 2.102) Wynne, K.J., and Nohr, R.S.:
Mol. Cryst. Liq. Cryst., 81,243(1982).
- 2.103) Nohr, R. S., Wynne, K.J.:
J. C. S. chem. Comm., 1020(1981)
- 2.104) Kreuger, P.C., and Kenney, M. E.:
J. Org. Chem., 28,3379 (1963)
- 2.105) Baret, P.A., Frye, D.A., and Linstead, R.P.:

J. Chem. Soc., 1157(1938).

CHAPTER THREE

- 3.1) Linsky, J. P., Paul, T. R., Nohr, R. S., Kenney, M. E.:
Inorg. Chem., 19, 3131(1980).
- 3.2) Djurado, D., Hamwi, A., and Cousseines, J. C.:
Synthetic metal, 11, 109(1985).
- 3.3) Brant, P., Weber, D. C., Haupt, S. G., Nohr, R. S., and Wynne, K. J.:
J. Chem. Soc. Dalto Trans. 269(1985).
- 3.4) Mcghie, A. R., Garito, A. F., and Heeger, A. J.:
Journal of crystal growth, 22, 295(1974).
- 3.5) Wagner, H. J., Loutfy, R. O., Hsiao, C. K.:
Journal of material science, 17, 2781(1982).
- 3.6) Instruction Manual, Meyrovac Coating Unit Type 12,
Associated Electrical Industries Limited.
- 3.7) Instruction Manual of Film Thickness Monitor, Model FTM4
Edward high vacuum, England.
- 3.8) Operation manual, Model 192, Keithely Instruments, Inc, USA, 1980.
- 3.9) Low level measurement, Keithley instrument, Inc, guide book, USA,
1984.
- 3.10) Instruction Manual Type 1621 Capacitance Measurement System,
General Radiocompany, Concord, USA, 1971.
- 3.11.) Instruction Manual Type 1316 Oscilator,
General Radio Company, Concord, USA, 1971.
- 3.12) Instruction Manual Type 1238 Detector,
General Radio Company, C oncord, USA, 1971.
- 3.13) Thomas H. E., and Clark C. A.:
"Handbook of Electronic Instrumens and Measurement Techniques"
Prentice-Hall, Inc, Englewood cliffs, N. J. page 36(1967).
- 3.14) Instruction Manual to Stanton Redcroft TG-770 Thermobalace.

- 3.15) Reed S. J. B.: "Electron Microprobe Analysis"
Cambridge University Press, 1975.

CHAPTER FOUR

- 3.1) Linsky, J. P., Paul, T. R., Nohr, R. and Kenney, M. E.:
Inorg. Chem. 19,3131(1980).
- 4.2) Simon, J and Andre, J.J.: "Molecular semiconductor"
springer-Verlag, Berlin, 1985.
- 4.3) Lever, A. B. P.:
Adv. Inorg. and radiochem. 7,27(1965).
- 4.4) Schaffer, A. M., Gouterman, G., and Davidson, E. R.:
Theoret. Chem. Acta. 30,9(1973).
- 4.5) Lever, A. B. P., Pickens, S. R., Minor, P. C., Licoccia, S.,
Ramaswamy, B. S., and Magnell, K.:
J. Am. Chem. Soc. 103,6800(1981).
- 4.6) Klofa T. J, Rieke P. C., Likous, Buttner, Nanthakumar. A, Mewborn
T. D. and Armstrong N. R.:
J. Electrochem. Soc. Electrochemical Science and Technilogy,
132, ,2134(1985).
- 4.7) Day, P., and Williams, R. J. P.:
J. Chem. Phys. 37, 567(1982).
- 4.8) Schaffer, A. M., Gouterman, M., and Davidson, E. R.,
Theor. Chem. Acta 30, 9(1973).
- 4.9) Hollebon, B. R., Stillman, M. J.:
J. Chem. Soc. Faraday Trans 11 , 74, 2107(1978).
- 4.10) Stillman, M. J., Thomson, A. J.:
J. Chem. Soc. Faraday Trans 11 , 70, 805(1974).
- 4.11) Brant, P., Weber, D. C., Haupt, S. G., Nohr, R. S. and Wynne, K. J.:
J Chem. Soc. Dalton. Trans., 269 (1985).
- 4.12) Djurado, D., Hamwi, A., Faber, C., Avignunt, D., and Cousseins, J. C.:
Synthetic Metals 11, 109(1985).

- 4.13) Eley, D. D., Hazeldine, D.J., and Palmer, T. F.:
J. Chem. Soc. Faraday Trans., 2, 1808(1973).
- 4.14) Barber, M., Bordoll, R. S., Elliott, G. J., Sedgwick, and Tyler, A. N.:
Anal. Chem., 54, 645A(1982).
- 4.15) Freas, R. B., and Campana, J. E.:
Inorg. Chem., 23, 4654(1984).
- 4.16) Miller, J. M.:
J. Organometal. Chem. 249,299(1983).
- 4.17) Davis, R. D., Groves, I. F., Durrant, J. L. A., Brooks, P., and Lewis, I.:
J. Organometallic chemistry, 241, C27(1983).
- 4.18) Simkin, D.: Ph.D thesis, Nottingham university(1984).
- 4.19) The Instrument Instruction Manual for Stanton Redcroft TG-750
Thermobalance,
Copper Mill Lane, London.
- 4.20) Newkirk, A. E.:
Anal. Chem., 32,1558(1960).
- 4.21) Coats, A. W., and Redfern, J. P.:
Analyst, 88, 906(1963).
- 4.22) Guiochon, G.:
Anal. Chem., 33, 1124(1961).
- 4.23) Diel, B. N., Inabe, T., Taggi, N. K., Lyding, J. W., Schneider, O.,
Hanak, M. K., newurf, C. R., Marks, T. J., and Schwartz, L. H.:
J. Am. Chem. Soc., 103,4371(1981).
- 4.24) Nohr, R. S., Kuznesof, P. M., Wynne, K. J., Kenney M. E., and
Siebenman P. G.:
J. Am. Chem. Soc., 103,4371(1981).
- 4.25) Djurado, D., Fabere, C., Hamwi, A., and Cousseins, J. C.:
Synthetic Metal, 22, 93(1987).
- 4.26) Brant, P., Nohr, R. S., Wynne, K. J., and Weber, D. C.:
Mol. Cryst. Liq. Cryst., 81, 255(1982).
- 4.27) Wynne, K. J., and Nohr, R. S.:
Mol. Cryst. Liq. Cryst., 81, 243(1982).
- 4.28) Djurado, D., Hamwi, A., and Cousseins, J. C.:
Synthetic Metals, 11, 109(1985).

- 4.29) Weber, D. C., Brant, P., Nohr, R. S., Haupt, S. G., and Wynne, K. J.:
Journal DE. Physique, C3, 1639(1983).
- 4.30) Brant, P., Weber, D. C., Haupt, S. G., Nohr, R. S., and Wynne, K. J.:
J. Chem. Soc. Dalton Trans, 269(1985).
- 4.31) Boas, J. F., Fielding, P. E., and MacKay, A. G.:
Aust. J. Chem., 27,7(1974).
- 4.32) Klug, H. P., and Alexander, L. E.: "X-Ray Diffraction Procedures"
John Willey and Sons, Inc. New York, 6th Edition, 1970.
- 4.33) " Powder Diffraction File, Joint Committee on Powder Diffraction
Standards",
1601, Park lane, Swarthmore Pa. 19081.
- 4.34) "International Tables for X-Ray Crystallography",
Vol.11(1959), Kynoch Press, Birmingham.
- 4.35) Woolfson, M. W.: " An Introduction to X-Ray Crystallography"
Cambridge, University Press, 1970.
- 4.36) "Tables for Conversion of X-Ray Diffraction Angles to Interplanar
Spacing, National Bureau of Standards. Applied Mathematics Series,
No. 10, September 20, 1950, U.S. Government Printing Office,
Washington, D.C.
- 4.37) Wynne, K. J.:
Inorg. Chem. 24,1339(1985).
- 4.38) Nohr, R. S., and Wynne, K. J.:
J. C. S. Chem. Comm., 1210(1981).
- 4.39) Wynne, K. J.:
Inorg. Chem., 4658(1984).
- 4.40) Lawes G., "Scanning Electron Microscopy and X-Ray Microanalysis"
John Wiley and Sons Chichester, 1987.
- 4.41) Golstein, J. I., Newbury, D. E., Echlin, P., Joy D. C., Fiori, C., and
Lifshin, E.: " Scanning Electron Microscopy and X-Ray Microanalysis",
Plenum Press, New York and London, 1981.
- 4.42) Sze, S. M.: "VLSI Technology" 2^{ed} Edition, 1988,
McGraw-Hill Book Company.
- 4.43) Nefedov, V. I.: "X-Ray Photoelectron Spectroscopy of Solid Surfaces"
VSP, Utrecht. The Netherlands, 1988.

- 4.44) West, A.R.: "Basic Solid State Chemistry"
John Wiley and Sons, Chichester, 1988.
- 4.45) Turner, N. H., Dunlap, B. I., and Cotton, R.J.:
Anal. Chem., 56,373R(1984).
- 4.46) Prutton, M.: "Surface Physics"
Clarendon Press. Oxford, 1975.
- 4.47) Dann, A.J: Ph.D thesis, Nottingham University, 1987.
- 4.48) Fahy, M.R: ph.D thesis, Nottingham University, 1988.
- 4.49) Wagner, C. D., Riggs, W. M., and Moulder, J. F.: "Handbook of X-Ray Photoelectron Spectroscopy"
Perkin-Elmer Corporation Physical Electronics Division, USA, 1979.

CHAPTER FIVE:

- 5.1) Eley, D. D.:
Nature, 162,819(1948).
- 5.2) Vartanyan, A. T.:
ZHUR. FIZ. KHIM, 22(1948).
- 5.3) Cox, G. A., Knight, P.C.:
J. Phys. Chem. Solids, 34,1655(1973).
- 5.4) Usov, N. N., Benderskii, V. A.:
Phys. Status Solidi, B37,535(1970).
- 5.5) Hamann, C.:
Phys. Status Solidi, 20,481(1967).
- 5.6) Barbe, D. F., and Westgate, C. R.:
J. Chem. Phys., 52, 4046(1970).
- 5.7) Kuznesof, P. M., and Wynne, K. J.:
J. C. S. Chem. Comm., 121(1980).
- 5.8) Nohr, R. S., Kusnesof, P. M. Wynne, K. J., Kenney, M. E. and Siebenman, P.G.:
J. Am. Chem. Soc., 103,4371(1981).
- 5.9) Brant, P. Nohr, R. S., Wynne, K. J. and Weber, D. C.:
Mol. Cryst. Liq. Cryst. 81,255(1982).

- 5.10) Dann, A. J.: Ph.D thesis, Nottingham univesity, 1987.
- 5.11) Keithely Instruction Manual, Digital Electrometer, Model 616.
Keithley Catalog and Buyers Guide, Electronic Measurement
Instrumentation.
- 5.12) Low Level Measurements, Keithely Instruments, 1984.
- 5.13) Waclawek, W., and Zabkowska, M.:
Acta Physica Academica Scientiarum Hungaricae, 49, 275(1980).
- 5.14) Hall, K. J., Bonham, J. S., and Lyons, L. E.:
Aust. J. Chem., 31,1661(1978).
- 5.15) Kanyama, S., Hiroi, M., Okuyama, N.:
Japanese J. Appl. Phys., 22, 348(1983).
- 5.16) Katz, W., Evans, Jr. C. A.:
J. Vac. Sci. Technol., 15(4), 1561(1987).
- 5.17) Shimorura, M., Toyoda, A.:
Japanese J. Appl. Phys., 23, 1462(1984).
- 5.18) Linsky, J. P., Paul, T. R., Nohr, R. S., and Kenney, M. E.:
Inorg. Chem. 19,3131(1980).
- 5.19) Meier, H.:"Organic Semiconductor"
Verlage Chemie, Germany, 1974.
- 5.20) Hamann, C., Stark, M., and Wagner, H.:
Phys. Stat. Solidi, (a)16,463(1973).
- 5.21) Simon, J., and Andre, J. J.:"Molecular Semiconductors"
Springer-Verlag Berlin, 1987.
- 5.22) Baddour, R. F., and Selvidge, C.W.:
Progress in Solid-State Chemistry, 3,45(1967).
- 5.23) Boas, J. F., Fiedly, P. E., Mckay, A. G.:
Aust. J. Chem., 27,7(1974).
- 5.24) Wayner, H. J., Loutfy, R. O., Hsiao, C. K.:
J. Material Science , 17, 2781(1982).
- 5.25) Kao, K. C. and Hwang, W.:
"Electrical transport in solids"
International Series in the Science of the Solid State, Vol.14
Pergamon press, Oxford, 1981.

- 5.26) Sawyer, D. T., Gibian, M. J., Morrison, M. M., Seo E. T.:
J. Amer. Chem. Soc., 100,627(1980).
- 5.27) Dahlberg, S. C., Musser, M. E.:
J. Chem. Phys. 72(12), 6706(1980).
- 5.28) Assure, J. M. and Harrison, S. E.:
J. Phy. Chem., 68,872(1964).
- 5.29) Van Ewyk, R. L., Chadwick, A. V., and Wright, J. D.:
J. C. S. Farady 1, 76, 2194(1980).
- 5.30) Heilmair, G. H., Harrison, S. E.:
Phys. Rev. 132,2010(1963).
- 5.31) Bradley, R. S., Grace, J. D., and Munro, D. C.:
J. Phys. Chem. Solids, 25,725(1964).
- 5.32) Yasunaga, H., Kojima, K., Yahda, H., and Takeya, K.:
J. Phys. Soc. Japan, 37,1024(1974).
- 5.33) Wright, J. D.: "Molecular Crystals"
Cambridge University Press, Cambridge, 1987.
- 5.34) Berthet, G., Blance, J. P., Germain, J. P., Larbi, A., Maleysson, C.,
and Robert, H.:
Synth. Met., 18, 715(1987).
- 5.35) Uyeda, N., Ashida, M., Suito, E.:
J. Applied physics, 36,1453(1965).
- 5.36) Kobayashi, T., Fujiyoshi, Y., Iwatsu, F. and Uyeda, N.:
Acta Cryst., A37,692(1981).
- 5.37) Hashi, H., Dann, A. J., Maruyama, Y., Inabe T. and Willis, M. R.:
Nihon Kagakukai 56(spring meeting, 1988) 3(2) B11.
- 5.38) Kobayashi, T., Kiyoshi y., and Uyeda, N.:
Acta Cryst., B40,263(1984).
- 5.39) Harrison, S. E., and Ludewig, K. H.:
J. Chem. Phys. 45,343(1966).
- 5.40) Andre, J. J., Simon, J., Even, R., Boudjema, B., Guiland, G. and
Maitrot, M.:
Synthetic metals, 18,683(1987).

- 5.41) Rose, A.:
Phys. Rev., 97,1583(1955).
- 5.42) Hamann, C.:
Phy. Stat. Sol.,26,311(1968).
- 5.43) Delacote, G M., Fillard, J. P. and Mareo, F. J.:
Solid State Commun., 2373(1964).
- 5.44) Ingnas, O., and Lundstrom, I.:
Synthetic Metals 10,5(1984/1985).
- 5.45) Twarowshi, J. A.:
J. Chem. Phys., 77(3),1458(1982).
- 5.46) Liou, K., Jacobsen, C. S., and Hoffman, B. M.:
J. Am. Chem. Soc., 111,6616(1989).
- 5.47) West, C. A.,and Thomson, R. M.: "Physics of Solids"
McGraw-Hill Book Company. Inc. New York, 1964.

CHAPTER SIX

- 6.1) Harrop, P. J.: "Dielectrics"
Butterworths, London, 1972.
- 6.2) Leaver, K. D. and Chapman, B. N.: "Thin Films"
The Wykeham Science Series, 17,
Wykeham Publications, London, LTD, 1971.
- 6.3) von Hippel, A. R.: "Dielectrics and Waves"
John Willey and Sons, Inc, New york, 1962.
- 6.4) Wright, J. D.: "Molecular Crystals"
Cambridge University Press, Cambridge, 1987.
- 6.5) David, V. V.: "Dielectric Relaxation"
Academic Press, London, 1967.
- 6.6) Zaky, A. A., and Hawley, R.: "Dielectric solids"
Solid State Series, Routledge and Kegan paul LTD, London, 1970.
- 6.7) Pethig, R.:
"Dielectric and electronic properties of biological materials"
John Wiley and Sons, Chichester, 1979.

- 6.8) Anderson, J. C.: "Dielectrics"
Chapman, and Hall, LTD, London, 1964.
- 6.9) Cole, K. S. and Cole, H. R.:
Journal of Chemical Physics, 9, 341(1941).
- 6.10) McCrum, N. G., Read, B. E., Williams, G.:
"Anelastic and Dielectric Effects in Polymeric Solid"
John Wiley and sons, London, 1967.
- 6.11) Hill, N., Vanghan, W. E., Price, A. H. and Davis, M.:
"Dielectric Properties and Molecular Behaviour"
van Nostrand, London, 1969.
- 6.12) Johnsher, A. K.:
Phys. Stat. Sol., B(83),585(1977).
- 6.13) Lewis, T. J.: "Dielectric and Related Molecular Processes"
Chemical Society Specialist Periodical Report 3, 186(1977).
- 6.14) Bottcher, C. J. F.:
"Theories of Electric Polarisation"
Vol. 1 "Dielectrics in Static Fields"
Elsevier Scientific Publishing Company, London, 1973.
- 6.15) Alfrey, T., and Gurnee, E. F.: "Organic Polymer"
Prentice-Hall, Inc., Englewood, 1967.
- 6.16) Long, A. R.:
Advances in Physics 31,553(1982).
- 6.17) Pollak, M., and Geballe, T. H.:
Phys. Review, 122,1742(1961).
- 6.18) Pollak M.: International Conference "The Physics of
Semiconductors", Institute of Physics and Physical Society, Exeter,
England,86(1962).
- 6.19) Argall, F., and Jonscher, A. K.:
Thin Solid Films, 2, 185(1968).
- 6.20) Anderson, P. W.:
Physical Review, 109,1492(1958).
- 6.21) Diaconu, I., Eley, D. D., and Willis, M. R.:
Phys. Stat. Sol. (a)85,283(1984).
- 6.22) Mott, N. F., :
Can. J. Phys., 34,1356(1956).

- 6.23) Pollak, M.:
Phil. Mag., 23, 519(1971).
- 6.24) Rockstad, H. K.:
J. Non-Crystalline Solids, 2, 192(1970).
- 6.25) Pike, G. E.:
Phys. Rev., 6, 1572(1971).
- 6.26) Gubanove, A. I.:
Soviet physics Solid State, 42104(1962).
- 6.27) Webb, J. B., Williams, D. F.:
J. Phys. C: Solid State Phys., 12, 3173(1979).
- 6.28) Rockstad, H. K.:
J. Non-Crystalline Solids, 2, 192(1970).
- 6.29) Davis, E. A., and Mott, N. F.:
Phil. Mag., 22, 9038(1970).
- 6.30) Mott, N. F., and Davis, E. A.:
"Electronic Processes in Non-Crystalline Materials", Oxford, 1971.
- 6.31) Sakai, Y., Sadaoka, Y., and Yokouchi, H.:
Bull. Chem. Soc. Jap., 47(8), 1886(1974).
- 6.32) Kao, K. C., and Hwang, W.: "Electrical Transport in Solids"
International Series in the Science of the Solid State, Vol.14
Pergamon Press, Oxford, 1981.
- 6.33) Vidadi, Y. A., Rozenshtein, L. D., and Chistyakov, E. A.:
Soviet Physics-Solid State, 11, 173(1969).
- 6.34) Abkowitz, M., Lakatos, A., and Scher, H.:
Phys. Rev. 9, 1813(1974).
- 6.35) Diaconu, I., Eley, D. D., and Willis, M. R.:
Phys. Stat. Sol. (a) 85, 283(1984).
- 6.36) Bradly, R. S., Grace, J. D., and Munro, D. C.:
J. Phys. Chem. Solids, 25, 725(1964).
- 6.37) Stauffer, D.: "Introduction to Percolation"
Taylor and Francis, London, 1985.
- 6.38) Dann, A. J.: Ph.D thesis, Nottingham University, 1987.

- 6.39) Hamon, B. Y.:
Australian J. Phys., 6, 304(1953).

CHAPTER SEVEN

- 7.1) Gorlich, p.: "Photoconductivity in solids"
Routledge and Kegan Paul LTD, London, 1967.
- 7.2) Bube, R.H.: "Photoconductivity in Solids"
John Wiley and Sons, Inc, New York, 1960.
- 7.3) Pai, D.M.: "Photoconductivity in Polymers"
An Interdisciplinary Approach, Technomic (1976).
- 7.4) Mort, J. and Pai, D.M.: "Photoconductivity and Related Phenomena"
Elsevier Scientific Publishing, Oxford, 1976.
- 7.5) Simon, J. and Andre', J.J.: "Molecular Semiconductors"
Springer-Verlag, Berlin, 1985.
- 7.6) Kinnear, S.: Ph.D thesis, Nottingham University (1981).
- 7.7) Ryvkin, S.M.:
J. Exp. Theor. Phys., 20(2), 139 (1950)
- 7.8) Eley, D.D., Kinnear, S. and Willis, M. R.:
Phys. Stat. Sol. (b) 677 (1981).
- 7.9) Eldridge, J.E.:
Solid State Comm., 21, 737 (1977).
- 7.10) Kao, K.C. and Hwang, W.: "Electrical Transport in Solids" Volume 14.
Pergamon Press, Oxford, 1981.
- 7.11) Tamamura, T., Yasuba, H., Okamoto, K., Imai, T., Kusabayashi, S.
and Mikawa, H.:
Bull. Chem. Soc. Jap., 47(2), 448 (1974).
- 7.12) Meier, H.: "Organic Semiconductors"
Verlag Chemie, Germany, 1974.
- 7.13) Hasegawa, K. and Yoshimura, S.:
Phys. Rev. letters 14, 689 (1965).
- 7.14) Pope, M. and Kallman, H.:
Symp. Elec. Cond. Org. Solids, Wiley (1960).

- 7.15) Maruyama, Y. and Inokuchi, H.:
Bull. Chem. Soc. Jap., 39,1419(1966).
- 7.16) Reucroft, D.J., Rudyi, O. N. and Labes, M. M.:
Mole. Cryst., 1,429(1966).
- 7.17) Rose, A.:
Phys. Rev., 97,322(1955).
- 7.18) Loferski, J. J.:
Phys. Rev.,93(4),707(1954).
- 7.19) Stockmann, F.:
Phys. stat. Sol., 34,741(1969).
- 7.20) Davis, C.: ph.D thesis, Nottingham Univesity, 1989.
- 7.21) Usov, N. N. and Benderskii, V. A.:
Phys. Stat. Sol.,37,535(1970).
- 7.22) Eley, D. D., Kinnear, S., Willis, M. R.:
Phys. Stat Sol.(b)108,373(1981).
- 7.23) Noolandi, J., Hong, K. M.:
J. Chem. Phys.,70, 3230(1979).

Appendix 1

The programme was used to measure the d.c. electrical conductivity up to four samples (for low resistance materials).

It is written in BASIC for the Commodore PET 3032.

```
3 DIMS0G(300,10),Q(300),T2(300)
5 REM*****COND MEAS*****
6 Q=1
7 REM***TEMP. READ***
8 DIMV(300),T(300):POKE59459,64:GOSUB400
10 OPEN7,7:PRINT#7,"00X":PRINT#7,"F0X"
21 INPUT#7,X1#:IFST=2THEN21
22 X1=1000*VAL(MID$(X1#,5,16)):X=X1:GOSUB300
23 T1=T:X1=X:PRINTX1,T1
24 TI#="000000":PRINT:PRINT"WAITING FOR TEMP STABILITY CHECK"
25 IFVAL(TI#)>100THEN25
26 INPUT#7,X2#:IFST=2THEN26
27 X2=1000*VAL(MID$(X2#,5,16)):X=X2:GOSUB300
28 X2=X:T2=T:IFABS(T1-T2)>1THEN21
29 PRINT"Q":PRINTX2,T2:PRINT
30 REM***SWITCHINGSECONDS***READY.
35 FORJ=7TO4STEP-1:K=J*8
40 FORI=7TO0STEP-1:L=I+K+192
50 POKE59459,L
60 FOR B=1TO100:INPUT#7,V1#:NEXTB:IFST=2THEN60
61 FORH=1TO50:INPUT#7,V1#:V=V+VAL(MID$(V1#,5,16)):NEXTH:V1=ABS(V,50)
62 IFV1>4.00RNDI>0THEN V=0:NEXTI
64 VXC(J)=V1:EC(J)=10-I:PS(J)=101-EC(J):I=0:NEXTI
80 M=L-64:POKE59459,M
90 FORB=1TO500:INPUT#7,V2#:NEXTB
91 FORB=1TO500:INPUT#7,V2#:V2=V2+VAL(MID$(V2#,5,16)):NEXTB:V5(J)=V2,50:V2=0
92 RX(J)=RS(J)*VXC(J)/V5(J):PRINT(8-J),"1E":EC(J):V5(J):VXC(J):RX(J)
95 NEXTJ
100 FORI=7TO4STEP-1:IFE(I)=0THENNEXTI
105 IFQ=1THEN INPUT"SCALE FACTOR":SL(I)
110 RH(I)=R(I)*SL(I):SG(I)=1, RH(I):NEXTI
115 REM***PRINTERINTERFERENCE***
120 POKE59459,64:OPEN4,4,0:OPEN1,4,1:OPEN2,4,2
130 PRINT#4," TEMP " :T2,T2+273.16,1/T2+273.16 : " VTC" :T2:PPRINT#4,
140 PRINT#4,"FILM RS VS VX RK PH":
150 PRINT#4," SG " :PRINT#4,
160 FORJ=7TO4STEP-1:G=8-J:IFE(J)=0THEN210
165 SG(Q,J)=LOG(ABS(SG(J)))
170 A#=" 9 AAA9 9.9999 9.9999 999999999999 99999999 9.999999999"
180 B#=" 999.9999 " :C#=A#+B#:PRINT#2,C#
190 PRINT#1,G,"1E"CHP$(29),EC(J),V5(J),VXC(J),RX(J),RH(J),SG(J),SG(Q,J)
200 GOTO220
210 PRINT#4," FILM":G:"TOO RESISTIVE"
220 NEXTJ
225 PRINT#4,"-----"
230 PRINT#4,:PRINT#1,:PRINT#2,:PRINT#7,
240 CLOSE1:CLOSE2:CLOSE4:CLOSE7
241 T2(Q)=T2:Q=Q+1:IFQ<300GOTO10
242 PRINT"Q":INPUT"NEW TEMP. (Y/N)":F#
```

```

243 IF(F#="N")THEN250
244 IF (F#="Y")THENQ=Q+1:PRINT"Q"
246 PRINT"PRESS SPACE BAR WHEN SATISFIED WITH TEMP STABILITY":WAIT59410,4,4
247 PRINT"Q":GOTO10
250 INPUT"DO YOU WANT THE DATA STORED ON DISC";F#
252 IF(F#="N")THEN280
254 PRINT"Q"
256 PRINT"PLACE FILE DISC IN DRIVE-0"
258 PRINT"PRESS SPACE BAR WHEN READY":WAIT59410,4,4
260 PRINT"Q"
262 INPUT"NAME OF FILE";W#
264 W#="0:"+W#+",SEQ,WRITE"
266 OPENS,8,2,W#
270 PRINT#5,0;CHR$(13);
272 FORI=1TOQ:T(I)=(1000*(1/(T2(I)+273.16))) :PRINT#5,T(I);CHR$(13);
275 PRINT#5,SQ(I,7);CHR$(13);SQ(I,6);CHR$(13);SQ(I,5);CHR$(13);
276 PRINT#5,SQ(I,4);CHR$(13);
278 PRINTT(I),SQ(I,7),SQ(I,6),SQ(I,5),SQ(I,4):NEXTI
279 PRINT#5,W#:CLOSE5
280 END
290 REMXXXXXXXXXXT/C CONV.XXXXXXXXXXXXXXXXXX
300 K=0:X=INT(X*1000+.5)/1000
310 IFK=40THENRETURN
320 IFX>V(K)ANDX>V(K+1)THENK=K+1: GOTO310
330 T=T(K)+(X-V(K))*(T(K+1)-T(K))/(V(K+1)-V(K))
340 T=INT(T*1000+.5)/1000:RETURN
390 REMXXXXXXXXXXCALIBXXXXXXXXXXXXXXXXXXXX
400 FORK=0TO40:READV(K):T(K)=K*10-200:NEXTK:RETURN
410 DATA-5.54,-5.38,-5.20,-5.02,-4.82,-4.60,-4.38,-4.14
420 DATA-3.89,-3.62,-3.35,-3.06,-2.77,-2.46,-2.14,-1.81
430 DATA-1.47,-1.11,-.75,-.38,0.0,.39,.79,1.19,1.61,2.03
440 DATA2.47,2.91,3.36,3.81,4.28,4.75,5.23,5.71,6.20,6.70
450 DATA7.21,7.72,8.23,8.76,9.29

```

Appendix 2

A general computer programme was used to plot different types of data.

```
PROGRAM NUZ
REAL T(5),C1(5),C2(5),C3(5),C4(5),C5(5),C6(5),C7(5),
*C8(5),C9(5),C10(5),C11(14),T11(14)
CHARACTER *20,ILAB
DATA T /3.367,3.663,4.115,4.739,5.464/
DATA T11 /2.747,2.778,2.899,2.967,3.058,3.175,3.247,
*3.333,3.425,3.610,3.676,3.788,3.906,4.016/
DATA C1 /-12.463,-13.493,-15.375,-17.987,-20.261/
DATA C2 /-12.461,-13.496,-15.345,-17.924,-20.007/
DATA C3 /-12.460,-13.492,-15.333,-17.615,-19.609/
DATA C4 /-12.458,-13.478,-15.309,-17.399,-19.285/
DATA C5 /-12.457,-13.465,-15.291,-17.226,-19.096/
DATA C6 /-12.454,-13.459,-15.274,-17.100,-18.984/
DATA C7 /-12.428,-13.399,-15.057,-16.657,-17.934/
DATA C8 /-12.401,-13.342,-14.884,-16.388,-17.373/
DATA C9 /-12.361,-13.271,-14.679,-15.774,-16.461/
DATA C10 /-12.323,-13.218,-14.563,-15.569,-15.869/
DATA C11 /-10.021,-10.137,-10.668,-10.991,-11.299,
*-11.767,-12.120,-12.448,-12.833,-13.614,-13.925,
*-14.407,-14.926,-15.430/

CALL DIG
CALL SIMBEG
CALL PAGE (21.0,29.7)
CALL PICSIZ(12.0,16.0)
CALL SCALES(2.5,6.0,1,-22.0,-11.0,1)
CALL AXES('1/T X 1000',10,'ln.Cond.(ohm.cm)',16)
CALL DRAWBX(0.0,0.0,0.2,0.0025)
CALL TITLE7('H','C','AlPcF, compacted disc')
CALL PEN(1)
DO 10 I=1,5
CALL CVTYPE(5)
CALL BRKNCV(T,C1,5,0)
CALL MARKPT(T(I),C1(I),1)
CALL BRKNCV(T,C2,5,0)
```

```
CALL MARKPT(T(I),C2(I),2)
CALL BRKNCV(T,C3,5,0)
CALL MARKPT(T(I),C3(I),3)
CALL BRKNCV(T,C4,5,0)
CALL MARKPT(T(I),C4(I),4)
CALL BRKNCV(T,C5,5,0)
CALL MARKPT(T(I),C5(I),1)
CALL BRKNCV(T,C6,5,0)
CALL MARKPT(T(I),C6(I),1)
CALL BRKNCV(T,C7,5,0)
CALL MARKPT(T(I),C7(I),1)
CALL BRKNCV(T,C8,5,0)
CALL MARKPT(T(I),C8(I),1)
CALL BRKNCV(T,C9,5,0)
CALL MARKPT(T(I),C9(I),1)
CALL BRKNCV(T,C10,5,0)
CALL MARKPT(T(I),C10(I),1)
10 CONTINUE
CALL PEN(2)
DO 20 I=1,14
CALL CVTYPE(4)
CALL BRKNCV(T11,C11,14,0)
CALL MARKPT(T11(I),C11(I),1)
20 CONTINUE
CALL ENDPLT
STOP
END
```

Appendix 3

The programme used to measure the temperature
(for high resistance materials).

It is written in BASIC for the Commodore Pet 3032.

```
3 DINT2(1000)
5 Q=1
7 REM:XXTEMP. READ:XXXXXXXXXXXXXXXXXXXX
8 DIM W(300),T(300):POKE59459,64:GOSUB400
10 OPEN7,7:PRINT#7,"00X":PRINT#7,"F0X"
21 INPUT#7,X1#:IFST=2THEN21
22 X1=1000*VAL(MID$(X1#,5,16)):X=X1:GOSUB300
23 T1=T:X1=X:PRINTX1,T1
24 TI#="000000":PRINT:PRINT"WAITING FOR TEMP STABILITY CHECK"
25 IFVAL(TI#)<100THEN25
26 INPUT#7,X2#:IFST=2THEN26
27 X2=1000*VAL(MID$(X2#,5,16)):X=X2:GOSUB300
28 X2=X:T2=T:IFABS(T1-T2)>0.5THEN21
29 PRINT"0":PRINTX2,T2:PRINT
30 PRINT"-----"
35 PRINT" | |"
40 PRINT" | TEMP. IS STABLE |"
50 PRINT" | |"
55 PRINT"-----"
56 POKE59459,64:OPEN4,4,0:OPEN1,4,1:OPEN2,4,2
57 PRINT#4," TEMP IS ":T2
58 CLOSE1:CLOSE2:CLOSE4
60 GOTO 21
280 END
290 REM:XXXXXXXXXXNTAO CONW. XXXXXXXXXXXXXXXX
300 F=0:X=INT(X*1000+.5)/1000
310 IFX=40THENRETURN
320 IFX<W(K)ANDX<W(K+1)THENX=W(K+1):GOTO310
330 T=(T*(K+X-W(K))+(T*(K+1)-T*(K))/2)/(W(K+1)-W(K))
340 T=INT(T*1000+.5)/1000:RETURN
390 REM:XXXXXXXXXXNCALIB:XXXXXXXXXXXXXXXXXXXX
400 FORK=0TO40:READW(K):T(K)=K*10-200:NEXTK:RETURN
410 DATA-5.54,-5.38,-5.20,-5.02,-4.82,-4.60,-4.38,-4.14
420 DATA-3.89,-3.62,-3.35,-3.06,-2.77,-2.46,-2.14,-1.81
430 DATA-1.47,-1.11,-.75,-.38,0.0,.39,.79,1.19,1.61,2.03
440 DATA2.47,2.91,3.36,3.81,4.28,4.75,5.23,5.71,6.20,6.70
450 DATA7.21,7.72,8.23,8.75,9.29
```